R. B. Lib.

The University of Sydney

Copyright in relation to this thesis*

Under the Copyright Act 1968 (several provisions of which are referred to below), this thesis must be used only under the normal conditions of scholarly fair dealing for the purposes of research, criticism or review. In particular no results or conclusions should be extracted from it and it should not be copied or closely paraphrased in whole or in part without the written consent of the author. Proper written acknowledgement should be made for any assistance obtained from this thesis.

Under Section 35(2) of the Copyright Act 1968–1976 (Commonwealth) the 'Author of a literary, dramatic, musical or artistic work is the owner of any copyright subsisting in the work'. By virtue of Section 32(1)(a) copyright 'subsists in an original literary, dramatic, musical or artistic work that is unpublished' and of which the author was an Australian citizen, an Australian protected person or a person resident in Australia.

The Act, by Section 36(1) provides: 'Subject to this Act, the copyright in a literary, dramatic, musical or artistic work is infringed by a person who, not being the owner of the copyright and without the licence of the owner of the copyright, does in Australia, or authorises the doing in Australia of, any act comprised in the copyright'.

Section 31(1)(a)(i) provides that copyright includes the exclusive right to 'reproduce the work in a material form'. Thus, copyright is infringed by a person who, not being the owner of the copyright and without the licence of the owner of the copyright, reproduces or authorises the reproduction of a work, or of a substantial part of the work, in a material form, unless the reproduction is a 'fair dealing' with the work 'for the purpose of research or private study'.

Kenneth W. Knight
Registrar

* 'Thesis' includes 'treatise', 'dissertation' and other similar productions.

THIN-WALLED STRUCTURAL SYSTEMS

by

Andrew H. Baigent

Thesis presented for the Degree of
Doctor of Philosophy

Volume II

School of Civil Engineering
The University of Sydney

June, 1980.

CONTENTS

VOLUME II

CHAPTER 6 SIMULATION OF THE ELASTIC BEHAVIOUR OF THE TEST FRAMES

6.1 INTRODUCTION

In Chapter 3, a linear elastic analysis was presented which enabled the prediction of the response of a thin-walled structure. In Chapters 4 and 5, tests on thin-walled channel section portal frames were described. The frames were representative of thin-walled structural frames that are presently used. The test frames contained eccentrically applied loads and were restrained eccentrically by simulated purlins and girts. Hence, the object of this Chapter is to use the analytical methods to predict the behaviour of the test frames. The simulation of the behaviour of the test frames in this Chapter, will be confined to the elastic response.

The first response to be predicted was the in-plane behaviour. The in-plane response consisted of the horizontal and vertical deflections as well as in-plane rotations of the frame. The second response to be predicted was the out-of-plane behaviour. This behaviour consisted of the rotations about the longitudinal axis of each member. These rotations were the result of two different components. Firstly, the elastic rigid-body rotation resulting from a matrix displacement analysis and secondly, the distortion of the cross-section were determined. The overall rotation of the top flange could be

obtained from the superposition of the two rotations. The third response to be predicted was the longitudinal stress distribution. The stress distribution is useful as it permits the major-axis bending moment distribution to be calculated. Obtaining the stress distribution is also important in the region of local buckling in order to determine the buckling load for the member. Hence, this Chapter will investigate the in-plane and out-of-plane response and the longitudinal stress distribution for each of the frames tested in the experimental study.

6.2 THEORETICAL ELASTIC ANALYSIS

A general program in which a linear elastic analysis was performed for thin-walled frames was developed in Chapter 3. The analysis of the experimental frames by the general thin-walled program is discussed in this Chapter. The overall and cross-section geometry of the frames was given in Chapter 4. The four members of the frame were subdivided into a further four elements for the discrete element analysis. The eave and apex joints were considered as separate members and they were subdivided into a further two elements each. Hence, to describe the geometry of the frame, a total of twenty four elements and twenty five nodes were required.

The global axis system used to describe the frame geometry was orientated such that the Y-axis

was horizontal and the Z-axis was vertical. A total of seven constraints could be applied at each of the nodes. The constraints consisted of displacement restraints in the direction of the three global axes, rotation restraints about the same three axes and a warping restraint. In each frame, the X-axis or out-of-plane displacement was constrained at each of the purlin and girt positions as well as at the base joints. Horizontal and vertical displacement in the Y-axis and Z-axis respectively was constrained only at the base joints. However, when analysing the internally braced Frames 5, 6 and 7 in which rotation about the longitudinal axis was effectively prevented at the point of attachment of the bracing, appropriate rotation constraints were included. In all the frames tested the in-plane or X-axis rotations were not prevented at any position. Warping displacement was also not constrained at any point around each frame.

The analysis required data in the form of the elastic and shear moduli, the area, major-axis and minor-axis moments of inertia and the torsion and warping constants for each discrete element. The member axis system, as described in Chapter 3, was located such that the origin of the axis system was at the centre of the web of the channel and the member x-axis passed through both the centroidal and shear centre positions. Centroidal and shear centre axis eccentricities with respect to the member axis system were required to

describe the position of the cross-section.

The bolted joints shown in Fig. 4.3 were designed to transmit moments and forces from the web of one channel member to the neighbouring channel member without any slip occurring in the bolted connections. The analytical representation of the joints is shown in Fig. 6.1. Since the plate thickness of the joints including the cover plate was 25 mm and the plate thickness of the channel section was 1.86 mm, the joints were regarded as effectively being rigid bodies linking the webs of two adjacent channel sections. In the analysis, they were treated as prismatic members with their shear centre and centroidal axes coinciding along the centreline of the plate. They were considered as having no warping torsion capability but transmitted all torque by Saint Venant torsion. Hence, they could not transmit a bimoment. Consequently, the bimoment on the end of the channel was zero calculated with respect to the X', Y' and Z' axes. Equation (3.46) has shown that for this condition the bimoment (B_z) calculated with respect to the shear centre of the channel is simply equal to the major-axis bending moment multiplied by the distance from the shear centre to the channel web. Therefore, this value of bimoment was applied to the end of the channel.

The points of restraint, simulating the purlins and girts were eccentrically placed with respect to the member axis system. Hence, the

restraint eccentricities in the X', Y' and Z' directions were specified in the data. In the out-of-plane direction, the eccentricity was equal to half the flange width. The in-plane eccentricity was equal to half the depth of the section added to a constant 50 mm which was the distance that the restraint was located from the outside flange. The horizontal and vertical forces were applied to the restraint points around the frame in the same ratios as the experimental loading patterns.

6.3 IN-PLANE DEFORMATION PREDICTION

The elastic thin-walled program (FEETA) was used to analyse each of the seven test frames. The in-plane deformations were obtained from the analysis. A comparison could then be made with the results of the experimental study.

6.3.1 Elastic Deformations

In-plane deflections were predicted at the stanchion mid-point, eave joint, rafter mid-point and the apex joint for the left hand side of each frame. The deflections are shown in Table 6.1. In-plane rotations were predicted at the base joint and eave joint for the left hand side of each frame. The rotations are shown in Table 6.2. The deformations are based upon a linear extrapolation at a load equivalent to the experimental ultimate load of each frame.

6.3.2 Comparison Between Experimental and Theoretical Analysis

To enable a comparison to be made between the theoretical in-plane predictions and the experimental readings, frame flexibilities have been produced. These flexibilities were calculated by obtaining the linearly extrapolated deformation at the ultimate load and dividing by the ultimate load. The experimental in-plane flexibilities are given in Table 6.3. The corresponding theoretical elastic flexibilities are given in Table 6.4.

The stiffening of the in-plane response due to the additional braces has been highlighted in the experimental results. The analytical model accurately predicts the stiffer response of the braced frames. The stiffening effect was evident when comparing the displacement and rotation flexibilities shown in Table 6.4, for frames with corresponding load cases. For example, the flexibilities for Frame 1 and 2 may be compared with the flexibilities for Frame 5 since these frames were subjected to Load Case 1. Similarly, Frame 3 and Frame 6 may be compared as well as Frame 4 and Frame 7 since Load Cases 2 and 3 were used respectively. Hence, it is possible to calculate the flexibility reduction for Frames 5, 6 and 7 with their corresponding frames for each load case. The lateral movement of the eave

joint, E Δ_y and the vertical movement of the apex joint, A Δ_z in Table 6.4, show the effect of the additional bracing. For the eave joint, the predicted flexibility was decreased by amounts ranging from 17.9 per cent, 24.3 per cent and 17.8 per cent for the three load cases. The apex joint showed a corresponding decrease in flexibility ranging from 16.8 per cent, 25.1 per cent and 14.9 per cent for the three load cases. The corresponding results for the experimental analysis shown in Table 6.3 indicated a stiffening at the eave joint ranging from 8.0 per cent 24.0 per cent and 11.0 per cent respectively. The stiffening at the apex joint ranged from 10.0 per cent, 20.8 per cent and 14.9 per cent for the three load cases. The additional bracing was added to reduce the out-of-plane deformations including the rotation of the members about their longitudinal axis. However, the results indicate the marked effect of the bracing on the in-plane deformations.

The prediction of the in-plane flexibilities was reasonably accurate, considering the variations that may occur between frames used for a comparitive experimental study. Discrepancies do occur as indicated by the in-plane rotation at the eave joint, however, in this case the flexibilities are of a very small magnitude. The non-symmetrical behaviour of the test frames is also evident from a comparision between the apex lateral deformations shown in

Table 6.3 and Table 6.4.

A linear elastic prediction for each frame assuming "prismatic members" was performed. The results, expressed as flexibilities, are given in Table 6.5. The effects of cross-section monosymmetry and thin-walled torsion theory are not accounted for in the prismatic member analysis. Intuitively, the results from this analysis should reflect a much stiffer response from each frame because of the absence of thin-walled effects. The results shown in Table 6.5 can be compared with the experimental results in Table 6.3 and the theoretical results in Table 6.4. The prismatic member analysis has predicted deflection flexibilities which are as much as forty per cent lower than the theoretical thin-walled predictions. The deflections are consistently lower than the experimentally measured values. Because of the smaller deflections, the in-plane rotation flexibilities were smaller than those measured or predicted from the thin-walled analysis. The comparison indicated the inadequacies of a prismatic member analysis when used for a problem which included thin-walled members.

A graphical comparison between the accuracy of the thin-walled in-plane deformation predictions and the experimental response is shown in Fig. 6.2. The figure shows the response of the vertical apex deflection for Frame 2. Plotted on

this figure is the linear elastic prediction for a frame composed of prismatic members with a major-axis moment of inertia identical with the cold-formed channel. Also plotted is the prediction of the linear elastic behaviour including the effects of thin-walled torsion theory and cross-section monosymmetry. Their effect upon the elastic prediction for the apex joint movement is clearly shown. The elastic prediction for the frame at loads up to half ultimate is very close to the measured experimental response.

In general, the agreement between the experimental and thin-walled analytical model was favourable for all the frames. However, the experimental results shown in Table 6.3 had a tendency to indicate a slightly more flexible response that the theoretical results shown in Table 6.4. The tendency was more pronouced especially for the apex joint results. The discrepancy between the theoretical model and the experimental flexibilities was of the order of a few per cent. The consistency of the difference in the flexibilities indicated an influence that was present in each of the test frames. An explanation for the greater flexibility could be in the behaviour of the joint system used in the experimental frame study. The stiffened plate joint to which the web of the cold-formed channel members were attached, could result in a more flexible connection than that modelled analytically. This may be caused by the presence

of shear straining of the cold-formed channel at the member to joint interface. The shear straining is brought about by the presence of discrete connections which transfer the stress resultants from the joint plate into the channel member. A study was made of the problem and the results are given in Section 6.4.

6.4 THE EFFECT OF SHEAR STRAINING

The in-plane deformations of each test frame were found to be of the order of a few per cent more than the theoretical predictions. The greater flexibility could be associated with shear straining at the joint plate to channel member connection. The problem could be studied analytically by modelling the connection and using the finite strip and finite element methods to investigate the effect of shear straining. The joint was simplified by assuming that each bolt exerted a concentrated axial force on the channel member. The aim was to study the effect upon the longitudinal stress distribution that concentrated loading of this type would produce. Concentrated loads raise the magnitude of stress near the point of application and this was enunciated by Saint Venant (1855). The problem of localised stress concentrations has become a major concern in the field of prestressed concrete. Many reserachers have investigated the problem, including Coker et. al. (1921), Tesar (1932), Guyon (1951) and Som and Ghosh (1964).

6.4.1 Thin Beam Problem

In order to study the effect of shear straining, the simple problem of a deep rectangular beam subjected to a similar loading condition to the one outlined above was chosen. The rectangular beam was used so that firstly it would be simple to understand and secondly it would enable the evaluation of the accuracy of the numerical methods of analysis. The beam had a span of 1000 mm and cross-section dimensions of 200 mm by 5 mm. Point loads were located at each end and 25 mm from the outside edges of the beam. The loads were equal in magnitude and were equivalent to an in-plane moment about the centroidal axis. A diagram of the beam is shown in Fig. 6.3.

The thin beam was studied using three different approaches, namely the finite strip method, the finite element method and an analytical solution developed by Guyon (1951). In the finite strip analysis, the beam was subdivided into sixteen equal longitudinal strips. For the finite element study, the mesh used is shown in Fig. 6.4. The elements used for the study were eight node, linear strain, isoparametric elements (Zienkeiwicz [1977]). The finite element program used for the analysis was developed by Campbell (1978). The solution derived by Guyon is for the case of a prism of rectangular base and finite

length subjected to the action of forces parallel to the axis of the prism. An approximate solution is obtained by the use of a double Fourier series. The results from the three analyses have been non-dimensionalised. The notation used in the non-dimensional study is shown in Fig. 6.5. The results of the three analyses have been shown in Figs. 6.6 to 6.8. The non-dimensional variation of longitudinal stress using the finite strip analysis is shown in Fig. 6.6. A total of sixteen longitudinal strips modelled the beam and enabled the longitudinal stress distribution to be obtained. To achieve a sufficient accuracy from the finite strip method a large number of Fourier terms is required. Analyses were performed with increasing numbers of Fourier terms until a satisfactory convergence level was obtained. Hence, it was found that fifty Fourier terms, starting from the first harmonic and ending with the one hundred and first harmonic, were required for the analysis giving a convergence for the longitudinal stress of less than 1.2 per cent at a distance of 25 mm from the point of load application. A level of convergence smaller than the value achieved is difficult to obtain because of the nature of the loading case considered. A point load applied to the end of the beam will produce a value of infinite longitudinal stress at the point of application. Hence, for small distances in the longitudinal direction from the applied load, the solution will be very inaccurate for a low number of Fourier terms. The

longitudinal stress for the top half of the beam shown in Fig. 6.6 is identical but opposite in sign for the stresses in the lower half of the beam. The longitudinal stress distribution behaves according to the principle of Saint Venant in that at a distance from the end of the beam, equal to the depth of the beam, the stress distribution becomes linear and can be predicted by simple bending theory. The finite element solution is shown in Fig. 6.7 and the solution derived from Guyon's approach in shown in Fig. 6.8. The three methods produce approximately equivalent results.

6.4.2 Lipped Channel Problem

The thin beam problem demonstrated that the variation in longitudinal stresses could be predicted using numerical techniques. The aim now was to determine the variation in the longitudinal stress of the lipped channel. The channel is shown in Fig. 6.9. The section had a depth of 152 mm, a flange width of 76 mm and a thickness of 1.86 mm. The depth of the lip stiffener was 15 mm. Equal and opposite concentrated loads, idealising the bolts of the joint, were positioned 40 mm on either side of the neutral axis. The figure shows the subdivision of the channel into a total of eighteen longitudinal strips for the finite strip analysis.

The longitudinal stress distribution

according to simple bending theory is easily calculated for this loading. It simply consists of a major-axis bending moment and a bimoment and is shown in Fig. 6.10. The finite strip analysis was used to obtain the stress distribution along the longitudinal axis of the channel. As before, a total of fifty Fourier terms were used for the analysis giving convergence for the longitudinal stress of 3.0 per cent at a distance of 10 mm from the point of load application and 1.1 per cent at a distance of 150 mm. The longitudinal stress distributions for distances of 10 mm, 50 mm and 100 mm from the end of the channel are shown in Fig. 6.11. For a distance as close as 100 mm from the end, the stress distribution had almost approached the theoretical distribution. The variation in the longitudinal stress for five points around the cross-section is shown in Fig. 6.12. Even for such a complex cross-section as a lipped channel, the principle of Saint Venant appears to be correct. At a distance of 150 mm from the end of the channel, the stress distribution has become constant except for the lip stiffener which takes considerably longer to reach the theoretical stress. The problem was also solved using the finite element method. The element subdivision for the channel is shown in Fig. 6.13. The elements in the web were 200 mm long and the width varied from 26.6 mm to 35 mm. In the flange the elements were 200 mm long and 25.3 mm wide. A similar variation in the longitudinal stress distribution of the channel

cross-section was obtained using the finite element method and the results are shown in Fig. 6.14. Hence, for the purpose of analysis it is possible to assume that the shear straining which is taking place, occurs over a small length at the end of the member. The length of the stress disturbance is equivalent to the depth of the channel.

The results of the finite element method were used to produce diagrams for the deformed shape of the channel member. The channel, loads and element subdivision are shown in Fig. 6.14. A magnified view of the deformation for the channel in the same orientation as Fig. 6.14, is shown in Fig. 6.15. The figure shows the twisting and distortion that was similar to the observed behaviour of the stanchions and rafters in the test frames. The opening and closing of the cross-section can be seen from the movement of the lip stiffeners. The cross-sectional distortion is shown in an end view of the beam in Fig. 6.16. Only half the length of the beam has been shown in this view.

The relative rotation of the web in its own plane was calculated over the shear strain affected zone. The relative rotation was obtained from the difference of the rotation at the end of the channel and the rotation at a distance along the beam, equal to the depth of the section. The rotation at the end of the channel was calculated

from the longitudinal deformation of the two flange to web junctions. The relative rotation was also calculated over the same length of beam for the simple bending theory equivalent stress resultants acting on the beam. The ratio between the rotation resulting from the concentrated loading and the rotation calculated from simple engineering bending theory was found to the 3.6. Hence, a 3.6 increase in the rotation of the channel member over a length of 150 mm would influence the in-plane theoretical prediction of the behaviour of the frame. The effect of the increased rotation becomes more significant when it is multiplied by the six member to joint connections. However, the jointing system used for the test frames consisted of plates clamped onto the end of the web of the channel. Hence, in the test frames the load would not be applied to the end of the member as point loads but more as a continuous loading along the web with a concentration of loading at the bolt positions. The continuous loading effect would actually reduce the relative rotation at the end of the channel, however, for the purpose of this study, the loading was idealised by two point loads.

An analytical method for determining the effect of shear straining on the in-plane deformations of the frame was obtained by reducing the flexural stiffness of the 150 mm long element and performing an elastic analysis on the whole frame. It was found that a ten per cent reduction

in the major-axis stiffness resulted in a 2.6 per cent increase in the in-plane deformations. Similarly, twenty per cent and thirty per cent reductions in the stiffness increased the in-plane deformations by 6.0 and 10.0 per cent respectively. However, the scatter of the experimental readings prevented an accurate figure for the amount of reduction in flexural stiffness to be ascertained. It appeared that the greater flexibility was the result of shear straining, however, the increase in flexibility was of such a small magnitude that it was unimportant for engineering calculations. Moreover, it has been shown that a thin-walled frame analysis was sufficiently accurate for the prediction of the in-plane response of the frame.

6.5 OUT-OF-PLANE DEFORMATION PREDICTION

The general thin-walled analysis described in Chapter 3 was used to analyse each of the seven test frames. The out-of-plane deformations were obtained from the analysis. A comparison could then be made with the results of the experimental study.

6.5.1 Elastic Deformations

The out-of-plane deformations were predicted at the stanchion mid-point, eave joint, rafter mid-point and the apex joint. The out-of-plane load-rotation results are shown in Table

6.6. The rotation about the longitudinal axis of the stanchion and the rafter measured at the mid-length was a combination of the elastic free body rotation and the cross-sectional distortion as shown in Fig. 6.17. However, the rotations measured at the eave joint and the apex joint were not influenced by the cross-sectional distortion, because the displacement transducers were located on the rigid joints.

6.5.2 Cross-Sectional Distortion

Although very many studies have been performed on local and lateral buckling modes separately, very few studies have been made on cross-sectional distortion and distortional buckling. Early methods of analysing web distortion (Goodier and Barton [1944]) were based on the assumption that the web could be regarded as a series of thin vertical beams with a corresponding reduction in the Young's Modulus of the material. The bending analysis of these led to the prediction that the variation of the out-of-plane displacements down the web could be represented by a cubic polynomial. A closely related folded plate method of analysis (Suzuki and Okumura [1968]) has also been used, whilst a more refined folded plate analysis which accounts for the plate torsion actions in the web has been developed by Kollbrunner and Hajdin (1968).

In later methods, exact plate bending

theory was used (Timoshenko and Woinowsky-Krieger [1959]) and in some cases exact solutions were obtained (Goldberg et. al [1964]). More often, however, approximate solutions were obtained by using energy and variational methods with assumed displacement functions (Fischer [1967], Schmied [1967] and Bartels and Bos [1973]). Some of these methods involved the use of a cubic polynomial for the web displacement and so were closely related to the early beam bending approximation of web distortion.

More recently, finite element methods have been used. Rajasekaran and Murray (1973) presented a study of coupled local buckling in wide-flange beam columns. They used the finite element method of thin-walled line elements and included deformational modes associated with distortion of the cross-secton. The distortional deformation modes assumed in the analysis were limited and the model was only accurate in the case where the web restrained the flanges. Johnson and Will (1974) presented a study of lateral torsional buckling of I-beams including the effect of cross-sectional distortion. They used the finite element method and subdivided the beam into a large number of rectangular elements. A more recent study by Akay et. al. (1977) isolated the out-of-plane buckling from the in-plane stress analysis. Consequently, less equations were involved in the buckling analysis.

In this thesis the problem of the cross-sectional distortion of the member was studied by means of the finite strip method of structural analysis. As described earlier, the measured longitudinal rotations were a combination of the elastic rigid body rotation of each member and the distortional rotation of the loaded flange of the channel. Hence, by assuming that the flange rotations were a superposition of the two components, a simple model for the out-of-plane deformations was determined.

The finite strip method is a recent variation of the finite element method as described by Zienkiewicz (1977) and it was developed initially by Cheung (1976). The finite strip method differs from the finite element analysis in the manner in which the structural element is sub-divided for analysis. The finite strip method involves the sub-division of the element into longitudinal strips. The displacement function in the longitudinal direction of the strip is assumed to be a Fourier series. In the finite element method, each strip would be further sub-divided into a series of rectangular elements. The displacement function in the transverse direction of the strip is a polynomial. The general mathematical formulation of the displacement functions is presented by Cheung. The specific formulation used in this thesis is presented by Hancock (1977B).

The stiffness matrix of a strip is established in the same way as for a finite element. A stiffness matrix used in the finite element method for the analysis of thin plates in bending was established by Melosh (1961). Each strip in the finite strip analysis is subjected to in-plane or membrane stresses and to transverse bending forces. Because these two types of forces are not coupled, it is convenient to establish the characteristic stiffnesses separately in two phases and then combine them into a comprehensive stiffness matrix. In the formulation of the stiffness matrix for the strip, orthotropic plate theory is assumed. When the strip stiffnesses have been computed and the conditions of equilibrium have been imposed on the forces at each nodal line, it is necessary to work in terms of a common system of co-ordinates. This is necessary as the elements are very often not coplanar. Hence a transformation matrix as given by Cheung (1969) is used to transform the forces and displacements. Once the stiffness matrix has been transformed into the common co-ordinate system, it is possible to assemble the overall stiffness matrix for the whole cross-section in the conventional manner. The stiffness matrix for the finite strip analysis of folded plate structures is given by Cheung (1969).

The cross-sectional distortion was determined for the stanchions and rafters of each frame. In order to carry out the analysis, the

channel cross-section was sub-divided into a number of longitudinal strips. The two flanges and the web were sub-divided into two strips each and the reinforcing lip on each flange was represented by a further strip, making a total of eight longitudinal strips. Each member analysed was considered to be simply supported at each end. The loads which were applied to the stanchions and rafters of each frame, were applied to the particular element for analysis. Lateral restraint simulating the restraining action of the purlins and girts was also applied to the member in the analysis. However, the finite strip analysis does not allow discrete points of restraint along the member and for this reason nodal lines were fixed in position against lateral movement. For the external restraints, the centreline of the loaded flange was restrained, however, for the internal and external restraints, the centrelines of both flanges were restrained.

The distortional component of rotation was calculated from the difference between the rotation of the loaded flange, measured at the top of the web and the rotation of the unloaded flange, measured at the base of the web. The distortional rotations are shown in Table 6.7. The importance of the cross-sectional distortion can be gauged by the magnitude of the rotations given in Table 6.7.

6.5.3 Comparison Between Experimental and Theoretical Analysis

Out-of-plane frame flexibilities have been tabulated for the comparison between the experimental and theoretical analyses. The experimental flexibilities are given in Table. 6.8. The corresponding theoretical flexibilities are given in Table. 6.9 and include the combination of the elastic rigid body rotation and the cross-sectional distortion.

For the eave and apex joints where cross-sectional distortion is not a consideration, the agreement between the out-of-plane rotation flexibilities is of the same order of magnitude. In three cases the theoretical flexibility is of opposite sign, however, considering the small magnitude of the flexibilities, the predictions were reasonably accurate. For the analytical prediction at the stanchion and rafter mid-points, the influence of the distortional rotation is very significant in each of the frames. For Frames 5, 6 and 7, the simulated fly bracing has almost eliminated the rigid body rotation and hence the total rotation is a measurement of the cross-sectional distortion. The out-of-plane distortional model is thus quite accurate in the prediction of the distortional rotation. The

agreement, however, is not as precise for the frames without the internal restraints. For the rafter mid-point, the disagreement is more significant for Frame 3 than for Frames 1, 2 and 4. For Frame 3, the rigid body rotation accounts for a considerable proportion of the total rotation. The larger rotation of the rafter is a consequence of the nature of Load Case 2 in which a large positive bending moment occurs at the eave joint. The large bending moment produces a large bimoment on the end of the rafter which increases the rigid body rotation of the rafter. However, the simulated dead and live loading applied to Frames 1 and 2, induce negative bending moment at the eave joint which tends to have a restoring effect on the rigid body rotation of the rafter thus resulting in a greater contribution of the distortional component.

In general, the prediction of the out-of-plane flexibilities was reasonably good. The results were not as accurate as the in-plane predictions. However, the out-of-plane model was more complex as a result of the cross-sectional distortion being taken into account.

6.5.4 Non-Linear Out-of-Plane Response

The effect of load eccentricities can have a considerable influence on the behaviour of thin-walled structures, especially structures composed of asymmetrical or monosymmetrical cross-

sections. A thin-walled section deflects laterally, twists and warps when the loading plane does not contain the shear centre. As the distance between the shear centre and the loading plane increases with the twisting of the section, a non-linear effect arises. The effect is shown in Fig. 6.18. The load eccentricity of a thin-walled section for an angle of twist θ is given by Eq. (6.1)

$$e = a_{Y'} . \cos \theta + h. \sin \theta \quad .. \quad .. \quad .. \quad (6.1)$$

where $a_{Y'}$ is the distance between the loading plane and the shear centre and h is the perpendicular distance from the horizontal plane containing the shear centre to the point of load application. The effect of load eccentricity for lipped channel cross-sections has been investigated by Reis and Branco (1979). However, their work was aimed at the influence of lateral instability effects on the collapse of structures.

The out-of-plane rotation for the test frames was found to have a tendency to become non-linear at relatively small loads. This behaviour was particularly evident for the rafters which were subjected to large eccentric loadings. The long length of the rafters also enabled the effects of load eccentricity to be more pronounced. The rotation about the longitudinal axis of the rafter at the mid-point for Frame 1 is shown in Fig. 6.18. The figure shows that at a

load of 6 kN or forty per cent of the ultimate load, the load-rotation curve becomes distinctly non-linear.

An attempt was made to model the non-linear behaviour of the out-of-plane rotation with the use of Eq. (6.1). The theoretical solution for the non-linear load-rotation response is shown in Fig. 6.18 and is compared with the experimentally measured values of rotation. The elastic prediction is also shown in Fig. 6.18. The non-linear solution produces a response which is slightly more accurate than the elastic prediction. However, the modelling in the regions of higher load, very much underestimates the experimental response. For the test frame, the value of rotation at a load of 14 kN was 0.256 radians whilst the non-linear rotation at a similar load was 0.168 radians. The comparison has shown that the experimentally observed out-of-plane rotations reflect more than merely the effect of load eccenticity. Other effects which may have contributed to the non-linear response are firstly, possible yielding of the material which results in a reduction of the elastic properties of the cross-section and secondly, member non-linearity.

6.6 PREDICTION OF LONGITUDINAL STRESSES

An analytical model presented in Chapter 3 was used to obtain theoretical in-plane and out-

of-plane deformations. The model was also used for the prediction of longitudinal stresses around the cross-section. As previously stated, the longitudinal stresses are calculated from the axial force, the major-axis and minor-axis bending moments and the bimoment. The analytical model determined these stress resultants at any point of the structure and hence enabled a prediction to be made of the longitudinal stresses.

In the experimental study each frame was instrumented with two groups of strain gauges which were used to study local buckling in the regions of maximum major-axis bending moment. Each group consisted of eleven strain gauges. The gauges enabled an experimental comparison to be made with the longitudinal stress distributions calculated from the analytical model. The comparisons are shown in Fig. 6.19 to Fig. 6.26.

In each test the theoretical longitudinal stress distribution has been calculated for the loading increment at which yielding was first noticed at one of the strain gauge locations. The comparison for Frame 2 is shown in Fig. 6.19. First observed yield occurred at a load of 0.67 of the ultimate load. For Frame 3, the comparisons are shown in Fig. 6.20 and Fig. 6.21. Yielding occurred at an ultimate load factor of 0.79. The measured distribution of the two flanges in the right hand rafter location (Fig. 6.21) does not compare favourably with the theoretical

prediction. Considering the very good agreement for all the other frames, the result is puzzling. However, the out-of-plane analysis has already shown that the longitudinal rotation of the rafter for Frame 3 (shown in Tables 6.8 and 6.9) displayed a similar behaviour. It appears that whilst the frame generally gave good agreement with theoretical predictions, the rafters produced results which departed significantly from expectations. The comparison for Frame 4 is shown in Fig. 6.22 at an ultimate load factor of 0.55. Frames 2, 3 and 4 were the unbraced series and the results indicated small variations between the theoretical prediction and the experimentally measured stresses. The three internally braced frames, Frame 5, 6 and 7, had first yield factors of 0.74, 0.65 and 0.57 respectively. The comparisons for each of the three frames are shown in Fig. 6.23 to Fig. 6.26. In each of the three frames, the agreement between the theoretical prediction and the experimentally measured stress distribution is extremely good.

Except for the right hand rafter for Frame 3, the results generally showed that the prediction of the stress resultants was very good. This is supported by the close agreement between the experimental and longitudinal stress distribution for all seven frames.

6.7 SUMMARY

1. The thin-walled analysis presented in Chapter 3 has been used to predict the in-plane and out-of-plane deformations for each of the seven test frames. The analysis has also been used for the prediction of the stress resultants which are essential for the calculation of stresses in thin-walled structures.

2. The in-plane response of each of the test frames was compared with a theoretical model. The effect of shear straining on the in-plane response was investigated.

3. The out-of-plane response of each of the test frames was compared with a theoretical model. Cross-sectional distortion was found to be important in the theoretical model and the procedure for the calculation of the distortion was shown. An attempt was made to model the non-linear nature of the out-of-plane response.

4. The longitudinal stresses were predicted for various positions around the test frames and compared with experimental readings.

	DISPLACEMENT					
Frame No.	S Δ_y mm	E Δ_y mm	R Δ_y mm	R Δ_z mm	A Δ_y mm	A Δ_z mm
1	-10.7	-11.1	-5.1	-18.1	0.0	-33.0
2	-10.7	-11.1	-5.1	-18.1	0.0	-33.0
3	51.0	83.3	87.7	-11.5	81.2	8.2
4	15.8	17.0	7.6	29.1	0.0	50.4
5	-9.7	-10.4	-4.8	-17.1	0.0	-31.6
6	47.6	76.4	79.6	-9.8	73.6	8.2
7	13.3	14.9	6.7	25.0	0.0	45.6

TABLE 6.1 IN-PLANE LOAD-DEFLECTION THEORETICAL RESULTS

S = Stanchion Mid-Point
E = Eave Joint
R = Rafter Mid-point
A = Apex Joint

	ROTATION	
Frame No.	B θ_x rad.	E θ_x rad.
1	0.0116	-0.0068
2	0.0116	-0.0068
3	-0.052	-0.024
4	-0.017	0.010
5	0.0109	-0.0055
6	-0.050	0.021
7	-0.015	0.0075

TABLE 6.2 IN-PLANE LOAD-ROTATION THEORETICAL RESULTS

B = Base Joint

E = Eave Joint

	DISPLACEMENT FLEXIBILITIES						ROTATION FLEXIBILITIES	
Frame No.	$S\Delta_y$ mm/kN	$E\Delta_y$ mm/kN	$R\Delta_y$ mm/kN	$R\Delta_z$ mm/kN	$A\Delta_y$ mm/kN	$A\Delta_z$ mm/kN	$B\Theta_x$ rad/kN	$E\Theta_x$ rad/kN
1	-0.760	-0.653	0.020	-1.460	-0.020	-2.320	0.00067	-0.00031
2	-0.727	-0.627	0.067	-1.267	0.000	-2.233	0.00060	-0.00042
3	2.747	4.447	4.789	-0.848	4.342	-0.147	-0.00379	0.00337
4	0.400	0.418	0.039	0.796	0.113	1.453	-0.00044	0.00099
5	-0.659	-0.600	-0.006	-1.256	0.082	-2.088	0.00044	-0.00048
6	2.061	3.370	3.409	-0.533	3.435	-0.139	-0.00287	0.00113
7	0.403	0.372	-0.028	0.726	-0.062	1.236	-0.00039	0.00022

TABLE 6.3 EXPERIMENTAL IN-PLANE FLEXIBILITIES

	DISPLACEMENT FLEXIBILITIES						ROTATION FLEXIBILITIES	
Frame No.	$S\Delta_y$ mm/kN	$E\Delta_y$ mm/kN	$R\Delta_y$ mm/kN	$R\Delta_z$ mm/kN	$A\Delta_y$ mm/kN	$A\Delta_z$ mm/kN	$B\Theta_x$ rad/kN	$E\Theta_x$ rad/kN
1	-0.714	-0.743	-0.339	-1.205	-0.000	-2.201	0.00078	-0.00045
2	-0.714	-0.743	-0.339	-1.205	-0.000	-2.201	0.00078	-0.00045
3	2.687	4.386	4.614	-0.616	4.273	0.429	-0.00271	-0.00127
4	0.434	0.467	0.210	0.800	0.000	1.386	-0.00046	0.00027
5	-0.571	-0.610	-0.280	-1.008	-0.000	-1.861	0.00064	-0.00032
6	2.070	3.320	3.461	-0.427	3.198	0.357	-0.00215	-0.00092
7	0.344	0.384	0.174	0.647	0.000	1.180	-0.00038	0.00193

TABLE 6.4 THEORETICAL ELASTIC IN-PLANE FLEXIBILITIES

	DISPLACEMENT FLEXIBILITIES						ROTATION FLEXIBILITIES	
Frame No.	$S\Delta_y$ mm/kN	$E\Delta_y$ mm/kN	$R\Delta_y$ mm/kN	$R\Delta_z$ mm/kN	$A\Delta_y$ mm/kN	$A\Delta_z$ mm/kN	$B\Theta_x$ rad/kN	$E\Theta_x$ rad/kN
1	-0.446	-0.421	-0.182	-0.733	0.000	-1.291	0.00051	-0.00027
2	-0.446	-0.421	-0.182	-0.733	0.000	-1.291	0.00051	-0.00027
3	1.699	2.681	2.828	-0.443	2.599	0.240	-0.00176	-0.00075
4	0.267	0.262	0.113	0.464	0.000	0.814	-0.00029	0.00016
5	-0.446	-0.421	-0.182	-0.733	0.000	-1.291	0.00051	-0.00028
6	1.699	2.681	2.828	-0.443	2.599	0.240	-0.00176	-0.00075
7	0.267	0.262	0.113	0.464	0.000	-0.814	-0.00029	0.00016

TABLE 6.5 THEORETICAL ELASTIC PRISMATIC MEMBER IN-PLANE FLEXIBILITIES

	ROTATIONS				
Frame No.	$S\Theta_z$ rad.	$E\Theta_y$ rad.	$E\Theta_z$ rad.	$R\Theta_y$ rad.	$A\Theta_y$ rad
1	-0.177	-0.005	0.002	0.061	0.033
2	-0.177	-0.005	0.002	0.061	0.033
3	0.037	0.006	0.018	0.105	0.003
4	0.023	0.007	-0.004	-0.107	-0.055
5	-0.001	0.000	0.001	0.002	-0.002
6	0.005	0.000	-0.001	0.002	0.000
7	-0.001	0.000	-0.001	-0.004	0.003

TABLE 6.6 OUT-OF-PLANE LOAD-ROTATION THEORETICAL RESULTS

	ROTATIONS	
Frame No.	$S\,\theta_z$ rad.	$R\,\theta_y$ rad.
1	-	0.051
2	-	0.051
3	0.053	0.032
4	-0.051	-0.096
5	-	0.059
6	0.061	0.039
7	-0.062	-0.099

TABLE 6.7 OUT-OF-PLANE DISTORTIONAL ROTATION

	ROTATIONAL FLEXIBILITIES				
Frame No.	$S\theta_z$ rad/kN	$E\theta_y$ rad/kN	$E\theta_z$ rad/kN	$R\theta_y$ rad/kN	$A\theta_y$ rad/kN
1	0.00093	-0.00027	0.00100	0.00973	0.00340
2	0.00080	-0.00027	0.00093	0.00853	0.00340
3	0.00279	0.00047	0.00232	0.00484	0.00074
4	-0.00149	-0.00003	-0.00061	-0.00556	-0.00173
5	0.00065	-0.00018	0.00035	0.00365	0.00047
6	0.00196	0.00013	-0.00041	0.00187	0.00057
7	-0.00168	-0.00005	-0.00011	-0.00186	-0.00013

TABLE 6.8 EXPERIMENTAL OUT-OF-PLANE FLEXIBILITIES

	ROTATIONAL FLEXIBILITIES				
Frame No.	S θ_z rad/kN	E θ_y rad/kN	E θ_z rad/kN	R θ_y rad/kN	A θ_y rad/kN
1	-0.00118	-0.00033	0.00013	0.00744	0.00218
2	-0.00118	-0.00033	0.00013	0.00744	0.00218
3	0.00476	0.00034	0.00095	0.00721	0.00017
4	-0.00076	0.00020	-0.00012	-0.00558	-0.00153
5	-0.00003	-0.00000	0.00003	0.00358	-0.00011
6	0.00285	-0.00001	-0.00005	0.00179	0.00001
7	-0.00162	0.00000	-0.00002	-0.00266	0.00008

TABLE 6.9 THEORETICAL ELASTIC OUT-OF-PLANE FLEXIBILITIES

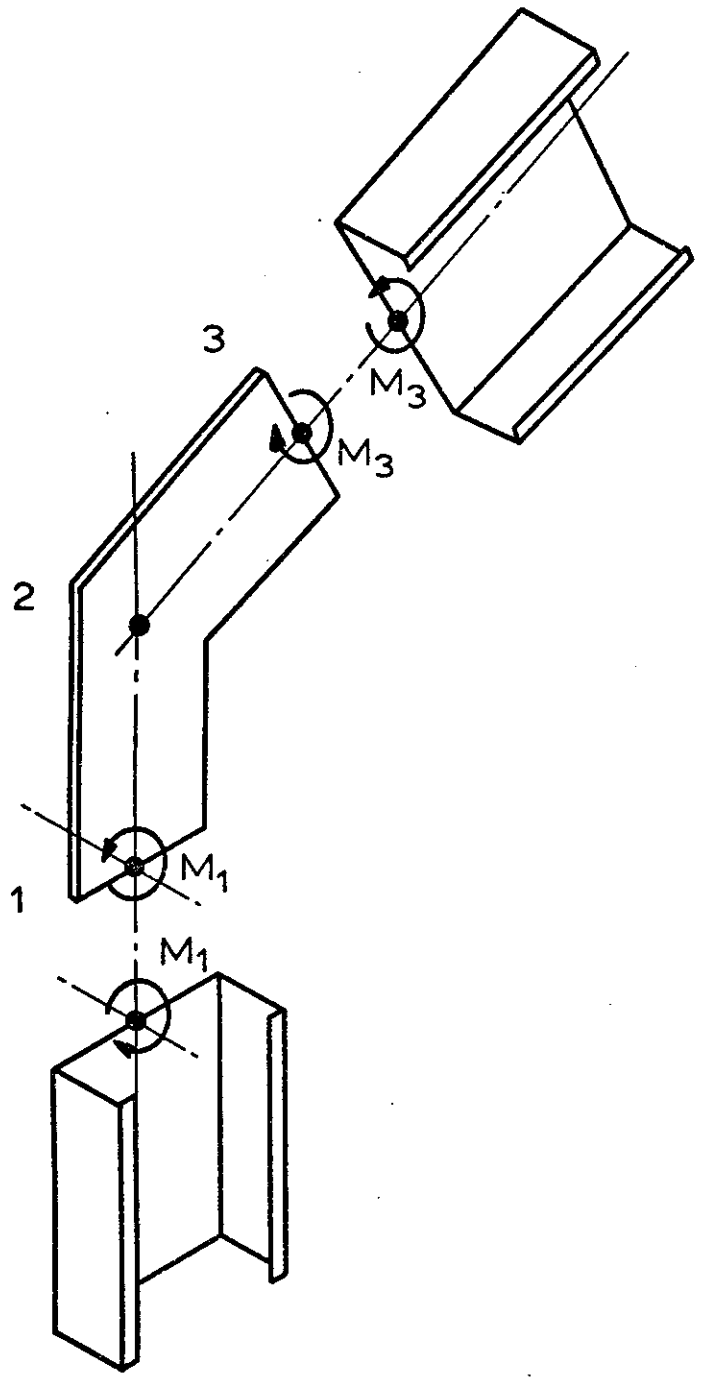

FIG.6.1 TRANSMISSION OF MAJOR AXIS MOMENT THROUGH JOINT.

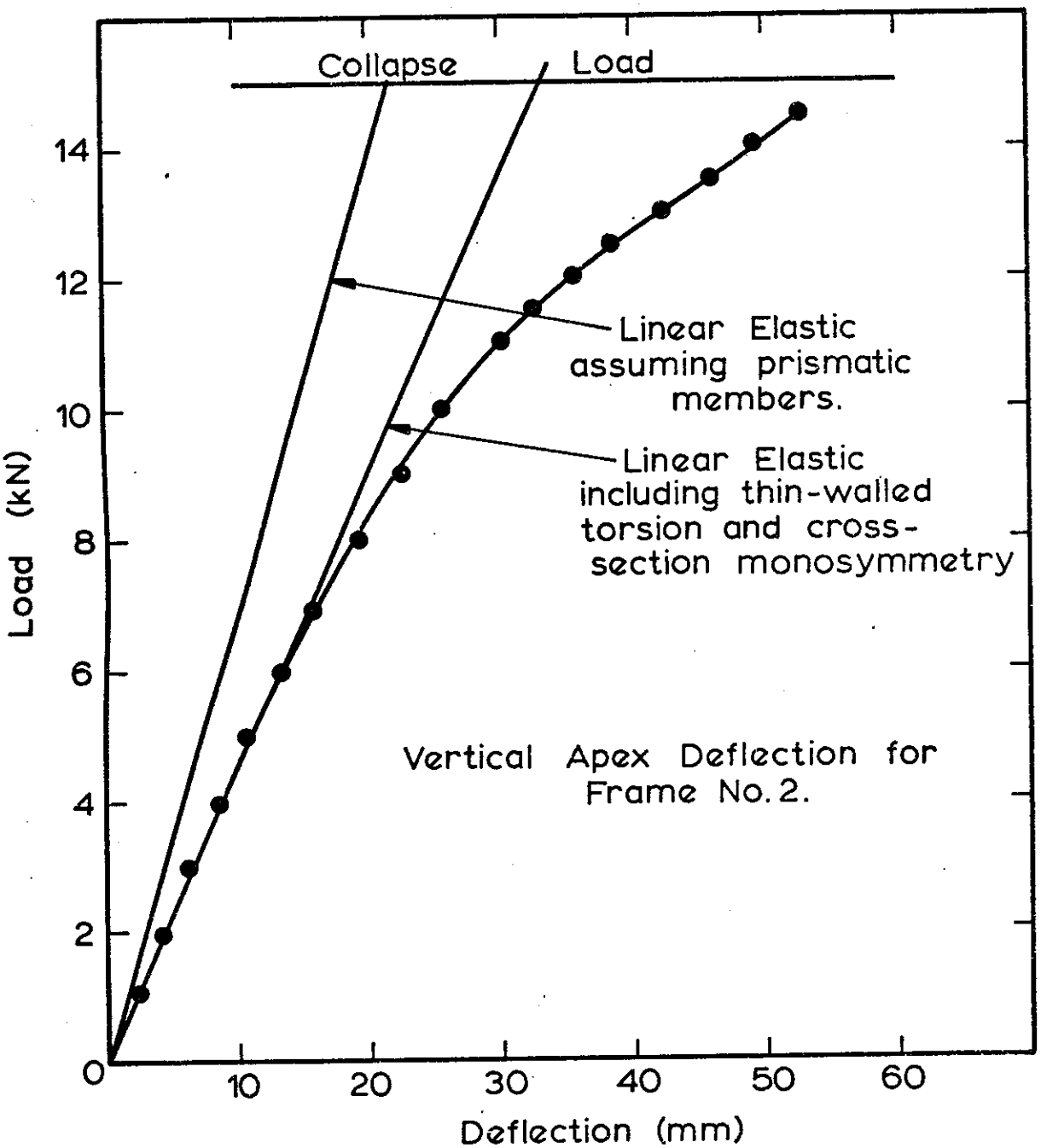

FIG.6.2 COMPARISON BETWEEN THEORETICAL MODEL AND FRAME TESTS.

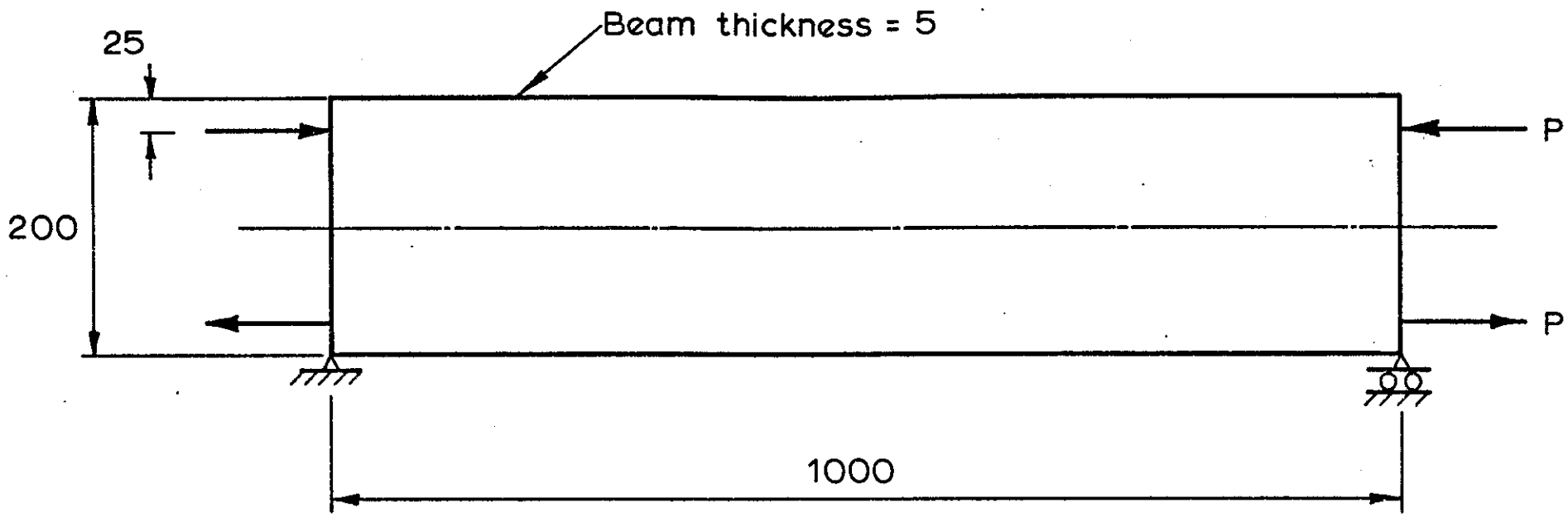

All dimensions in mm

Beam subdivided into sixteen equal longitudinal strips

FIG.6.3 THIN BEAM PROBLEM

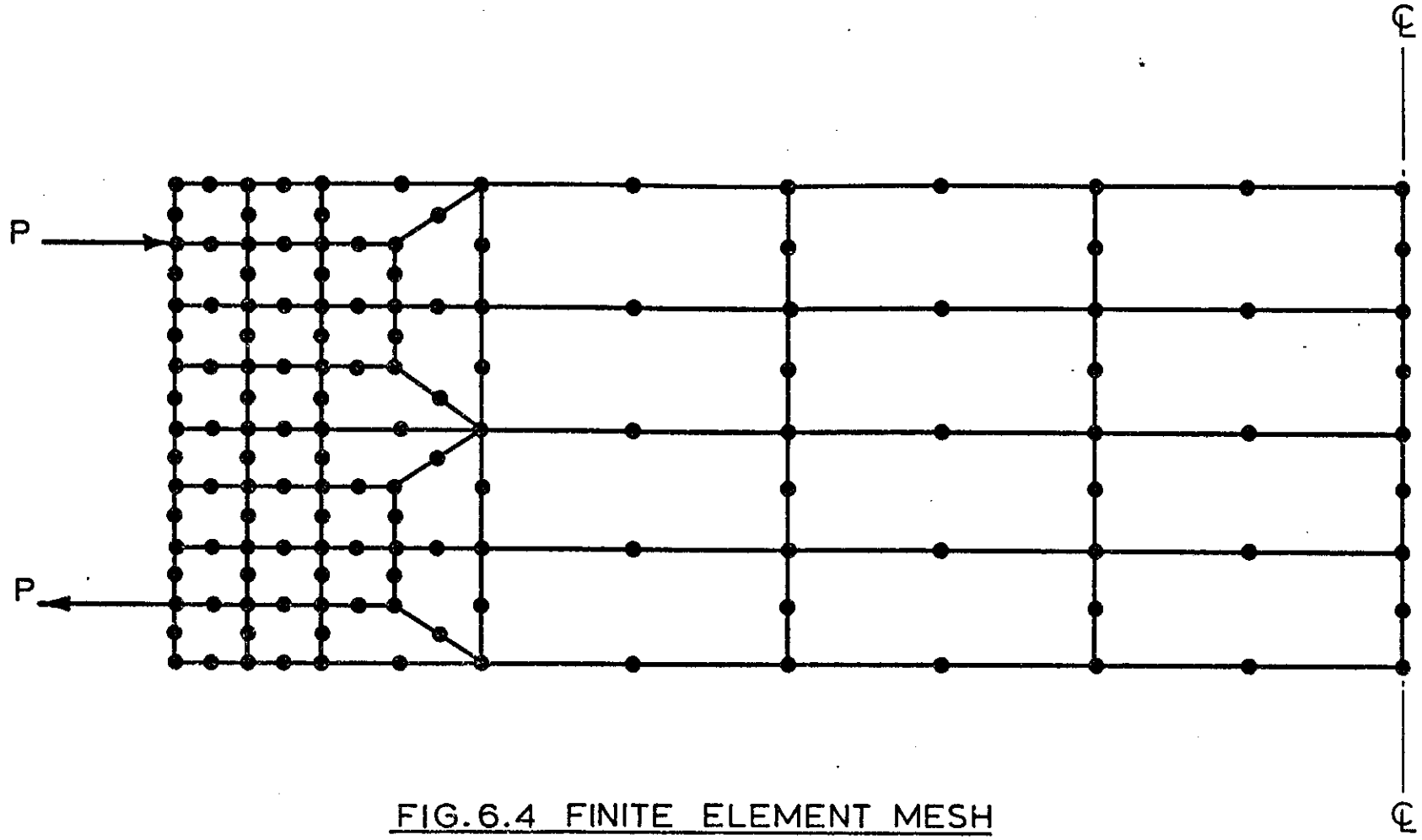

FIG.6.4 FINITE ELEMENT MESH

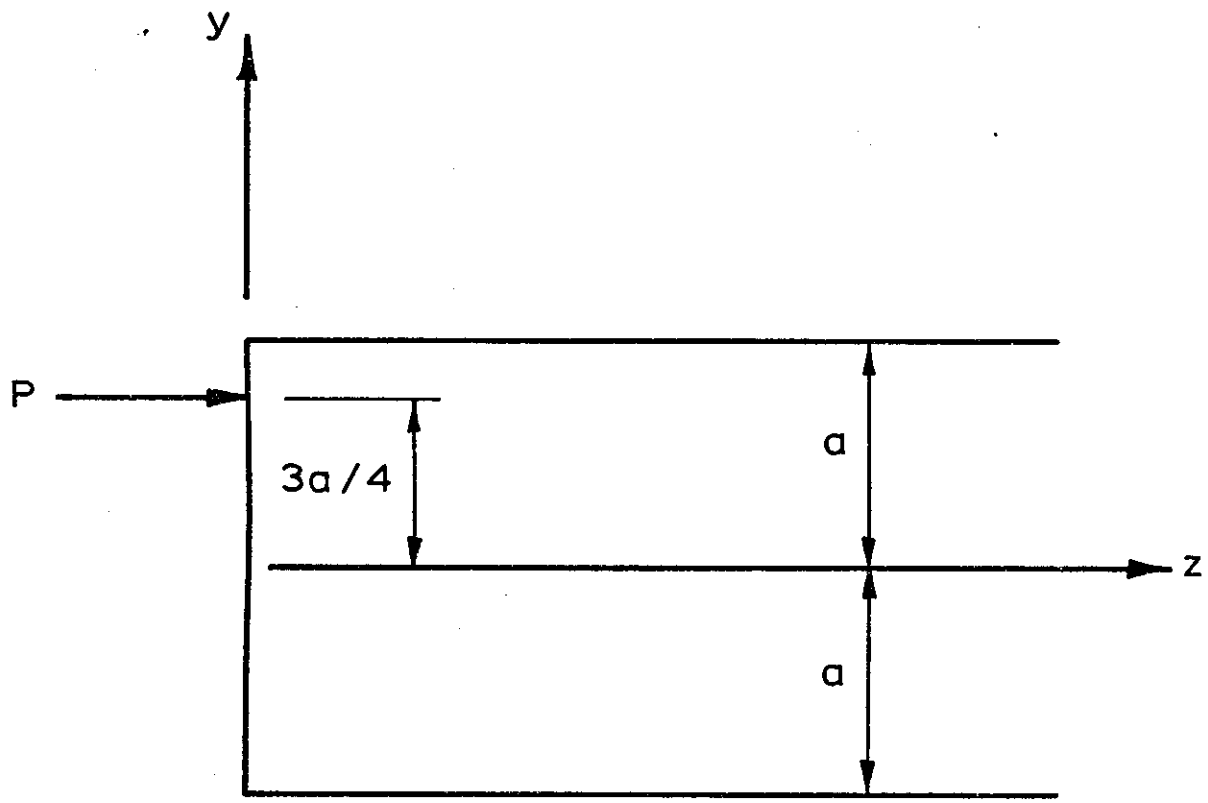

Stress Multiplying Factor $q = P/4ab$

b = beam thickness

FIG.6.5 GUYON'S THIN BEAM PROBLEM

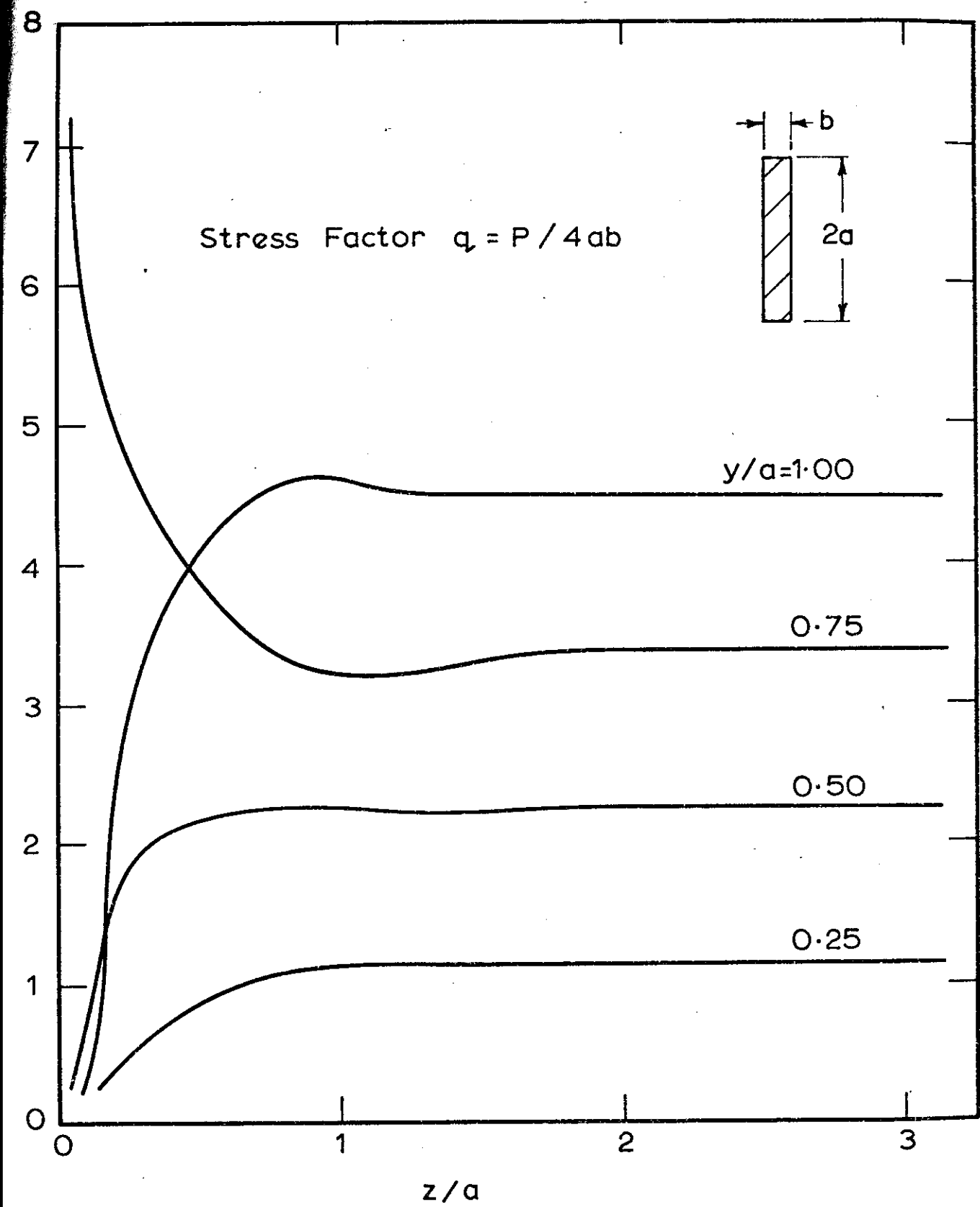

FIG.6.6 NON-DIMENSIONAL VARIATION OF LONGITUDINAL STRESS-FINITE STRIP SOLUTION

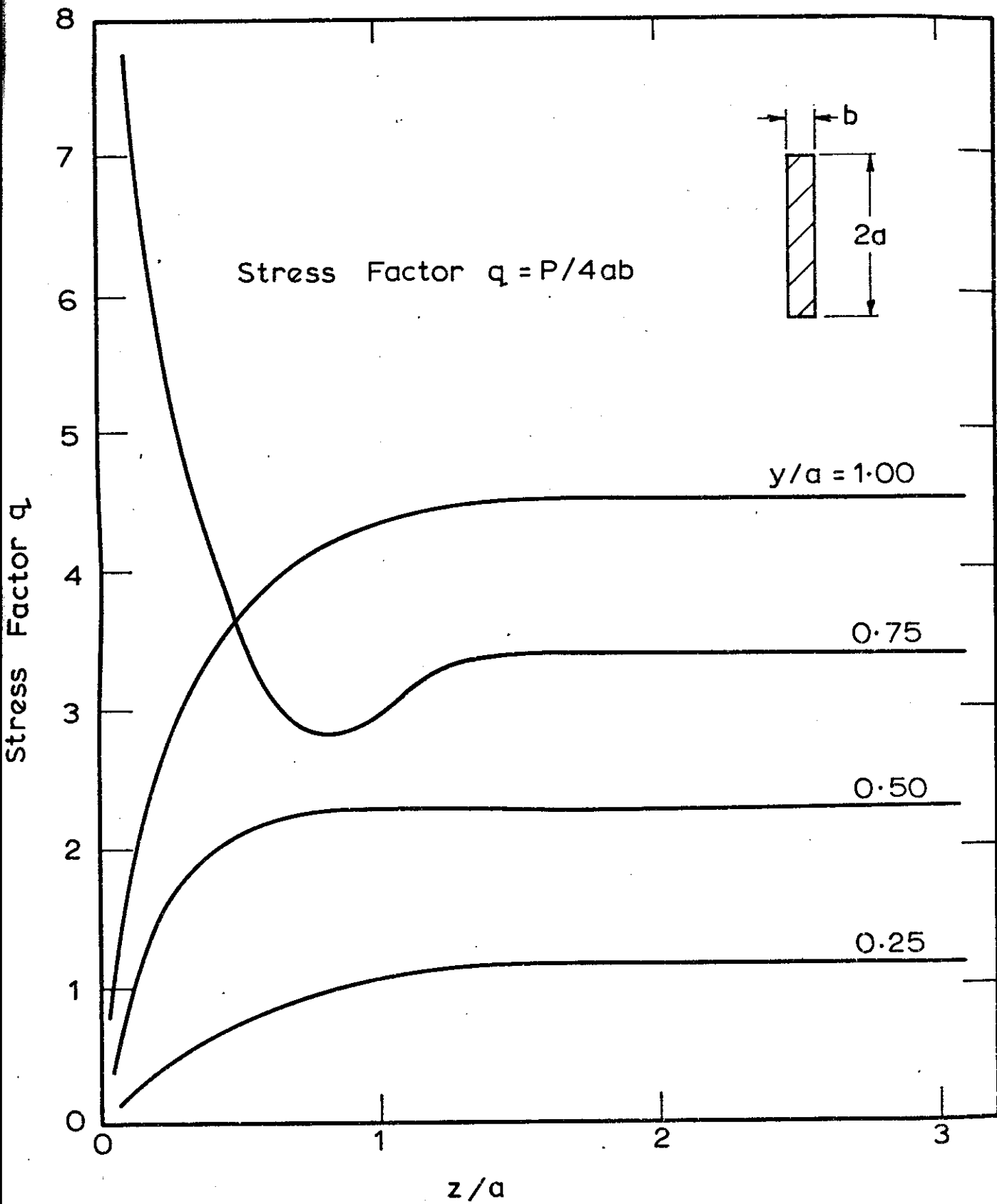

FIG.6.7 NON-DIMENSIONIAL VARIATION OF LONGITUDINAL STRESS - FINITE ELEMENT SOLUTION

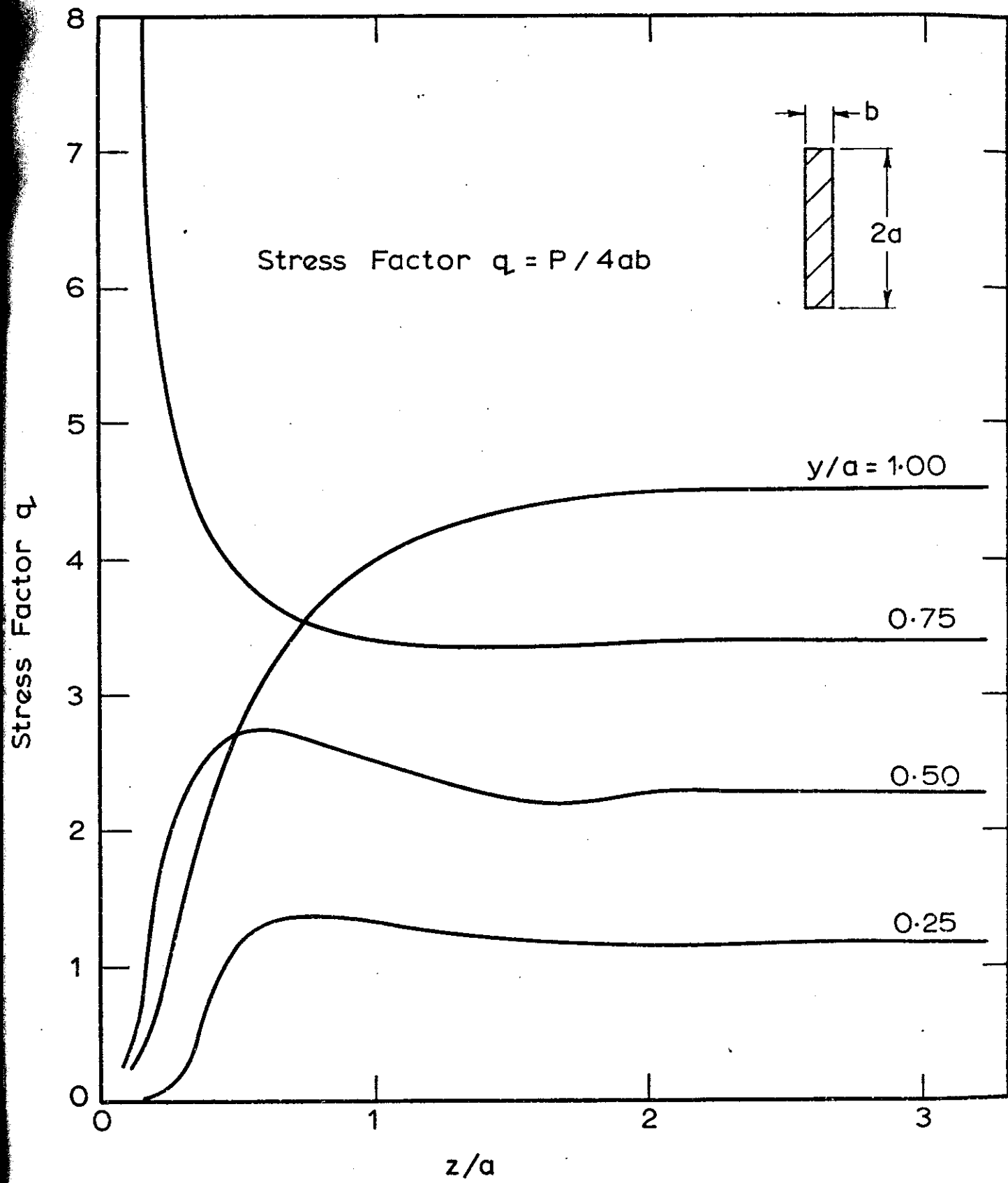

FIG. 6.8 NON-DIMENSIONAL VARIATION OF LONGITUDINAL STRESS - GUYON'S SOLUTION

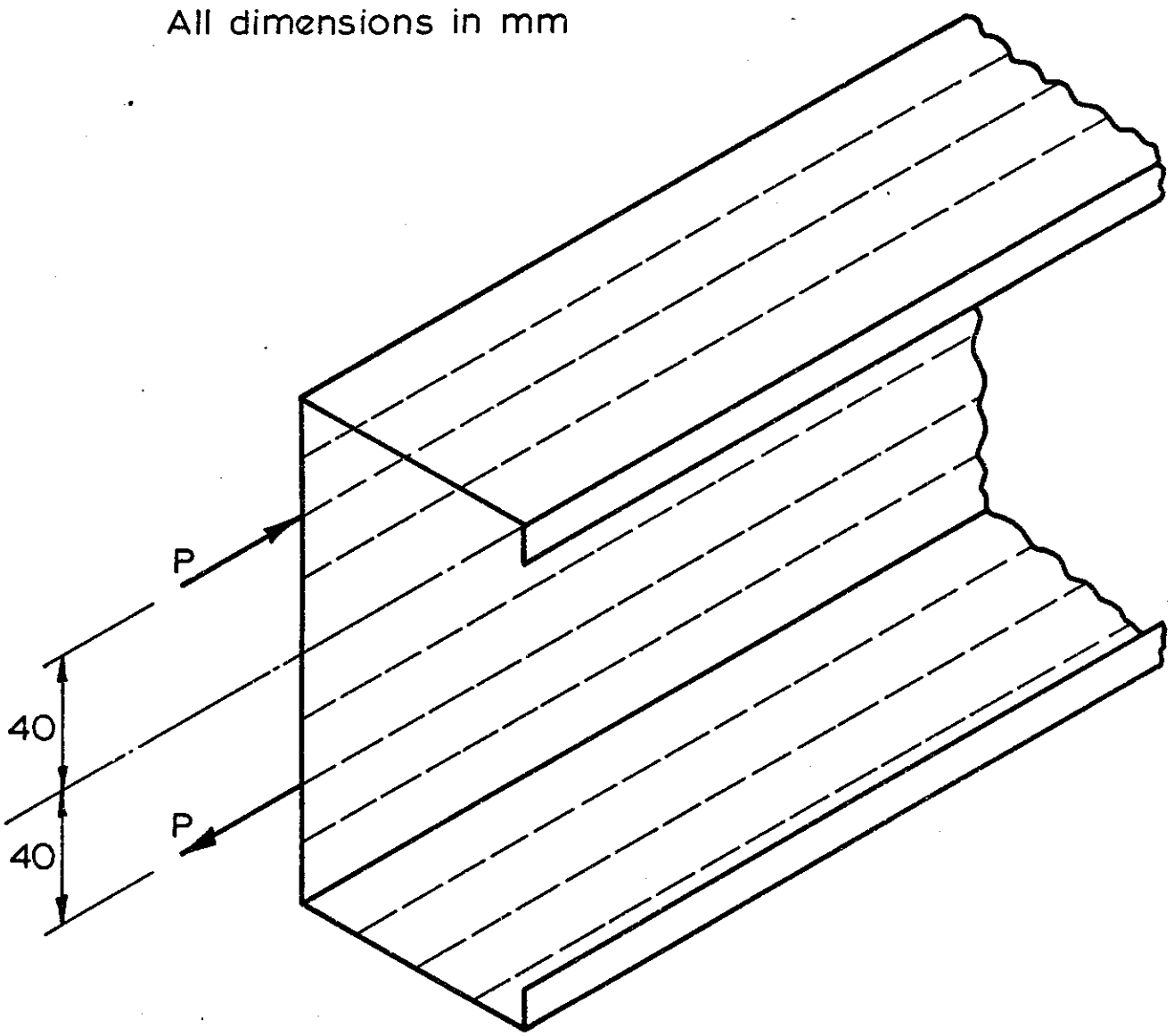

FIG.6.9 FINITE STRIP SUBDIVISION OF CHANNEL CROSS - SECTION

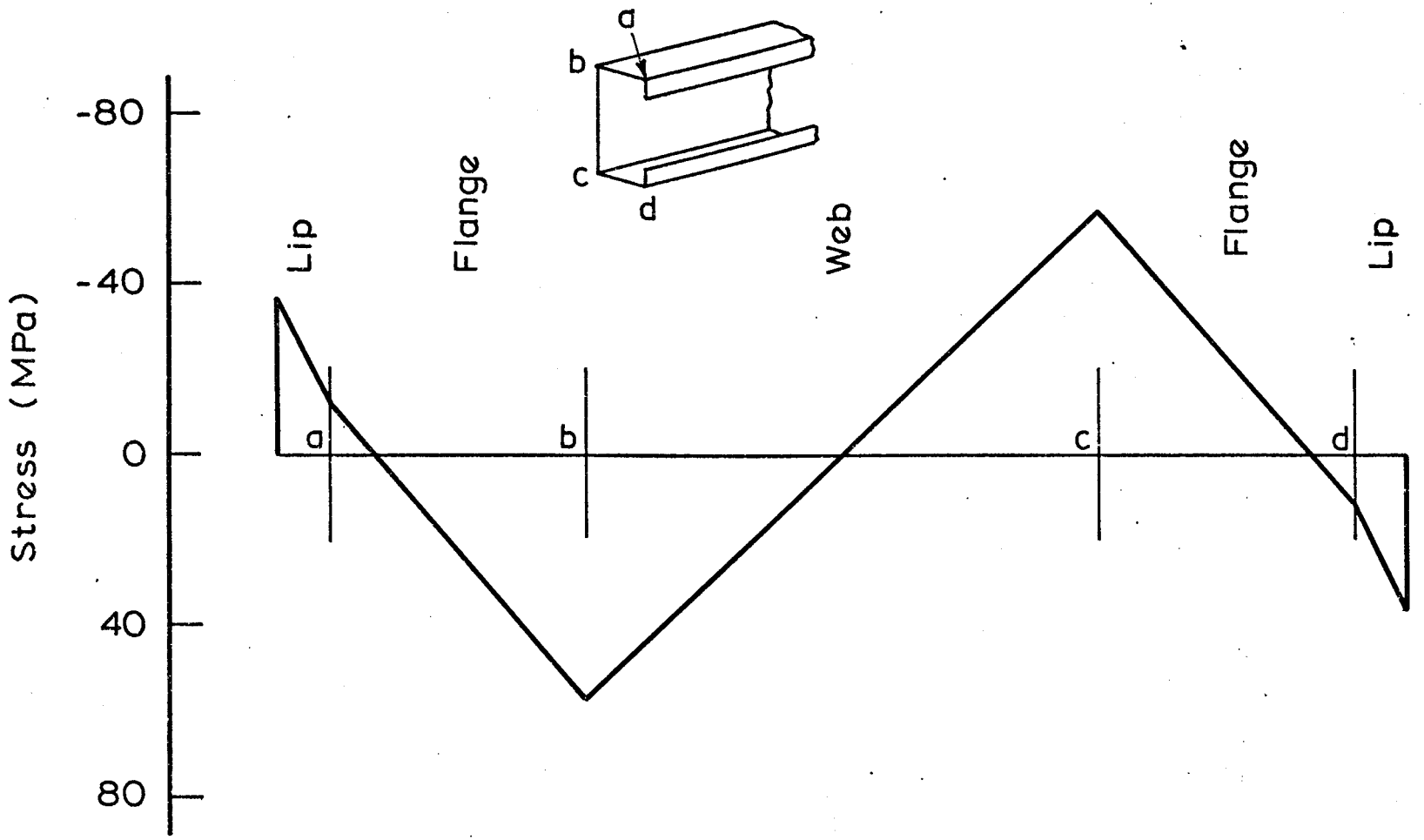

FIG.6.10 THEORETICAL LONGITUDINAL STRESS DISTRIBUTION

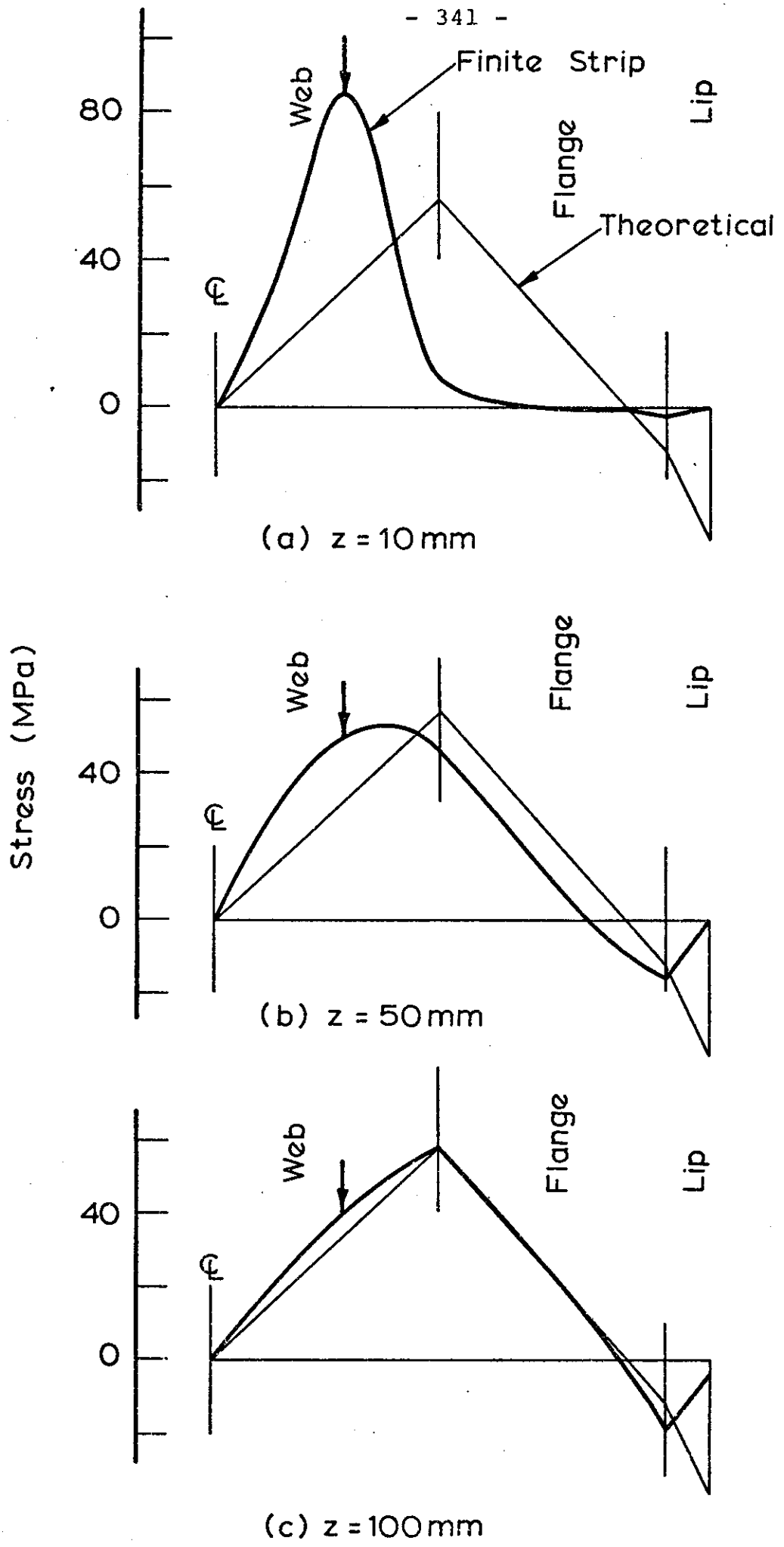

FIG.6.11 FINITE STRIP LONGITUDINAL STRESS DISTRIBUTIONS

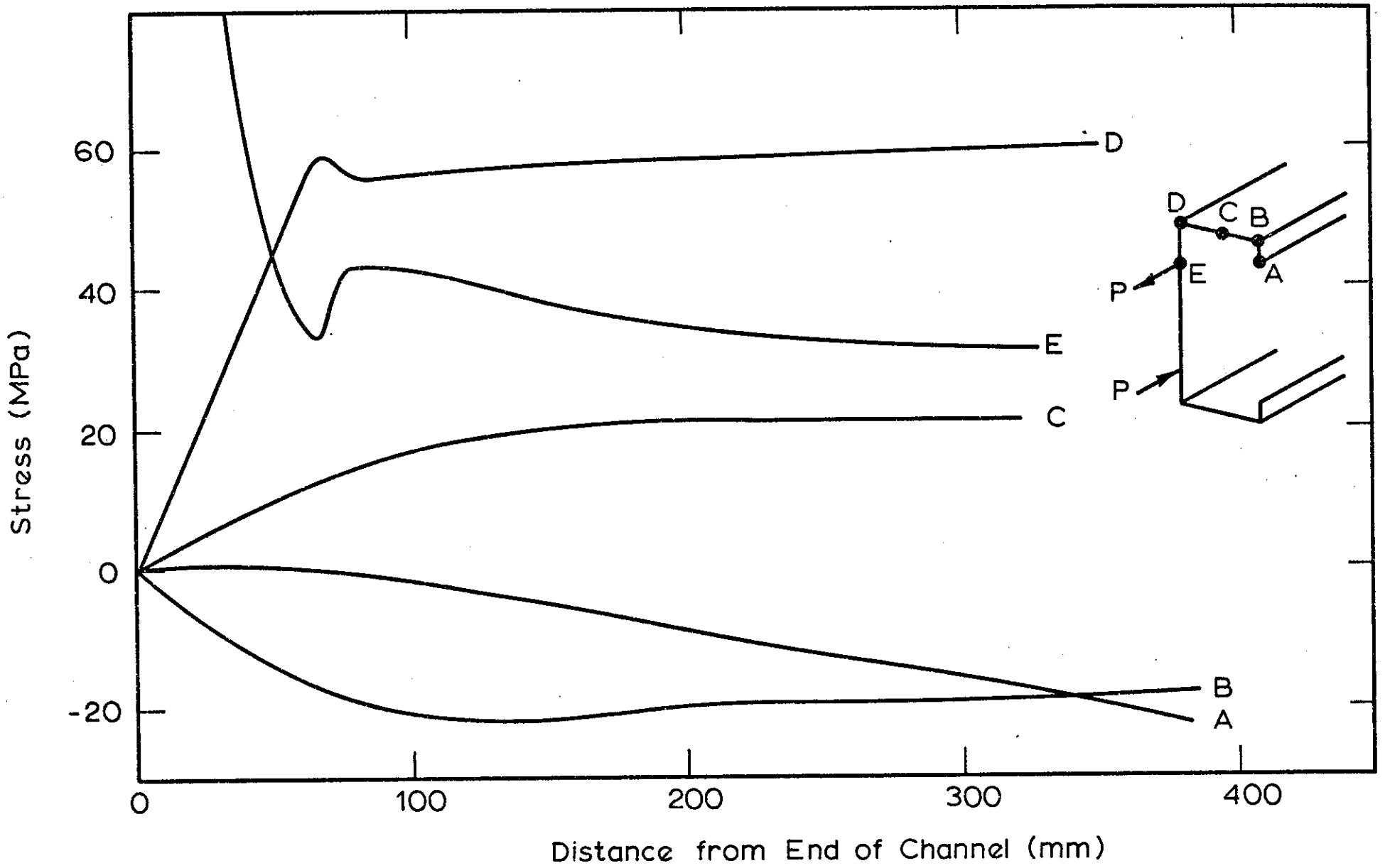

FIG.6.12 CHANNEL SECTION - VARIATION OF LONGITUDINAL STRESS USING FINITE STRIP METHOD

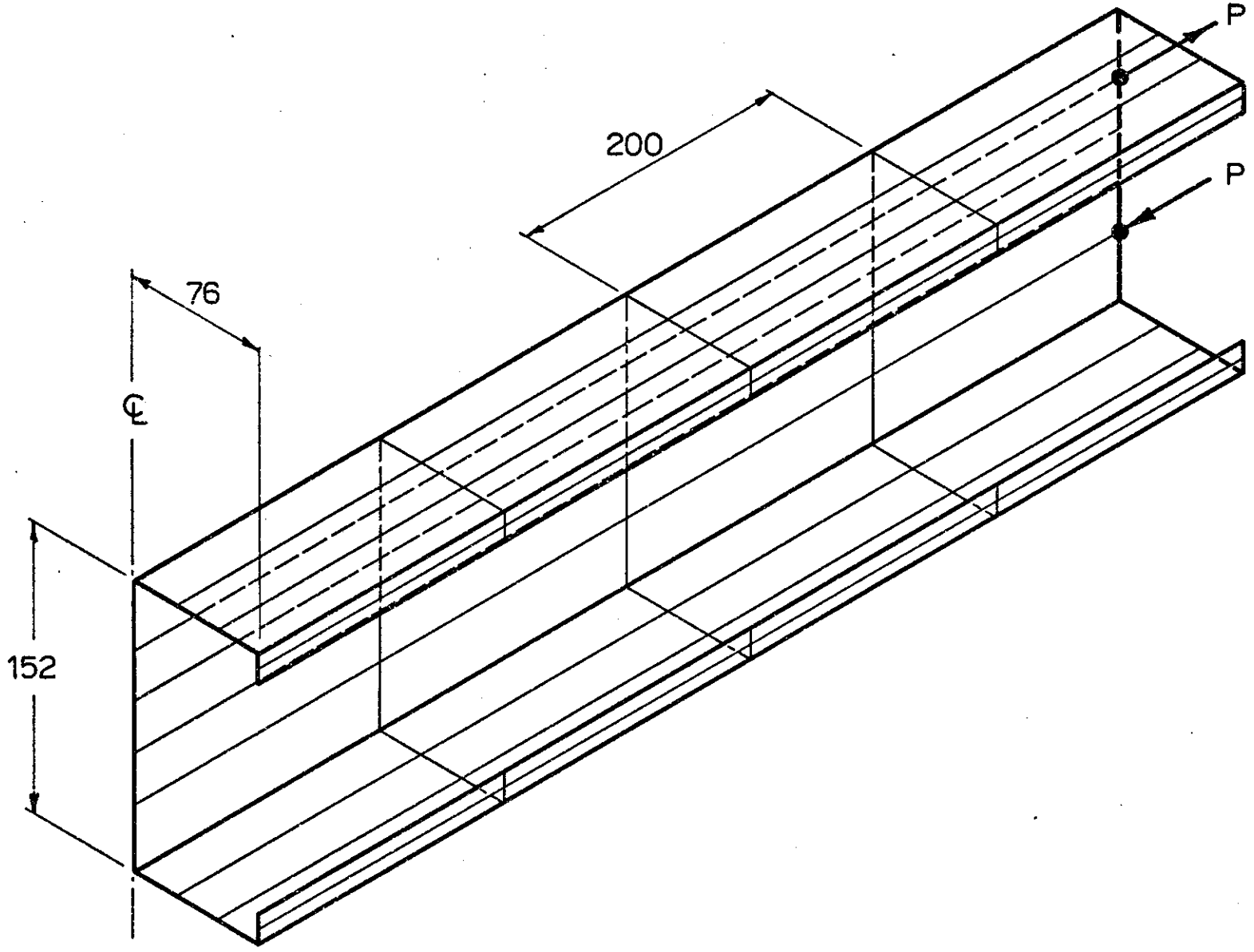

FIG.6.13 FINITE ELEMENT MESH

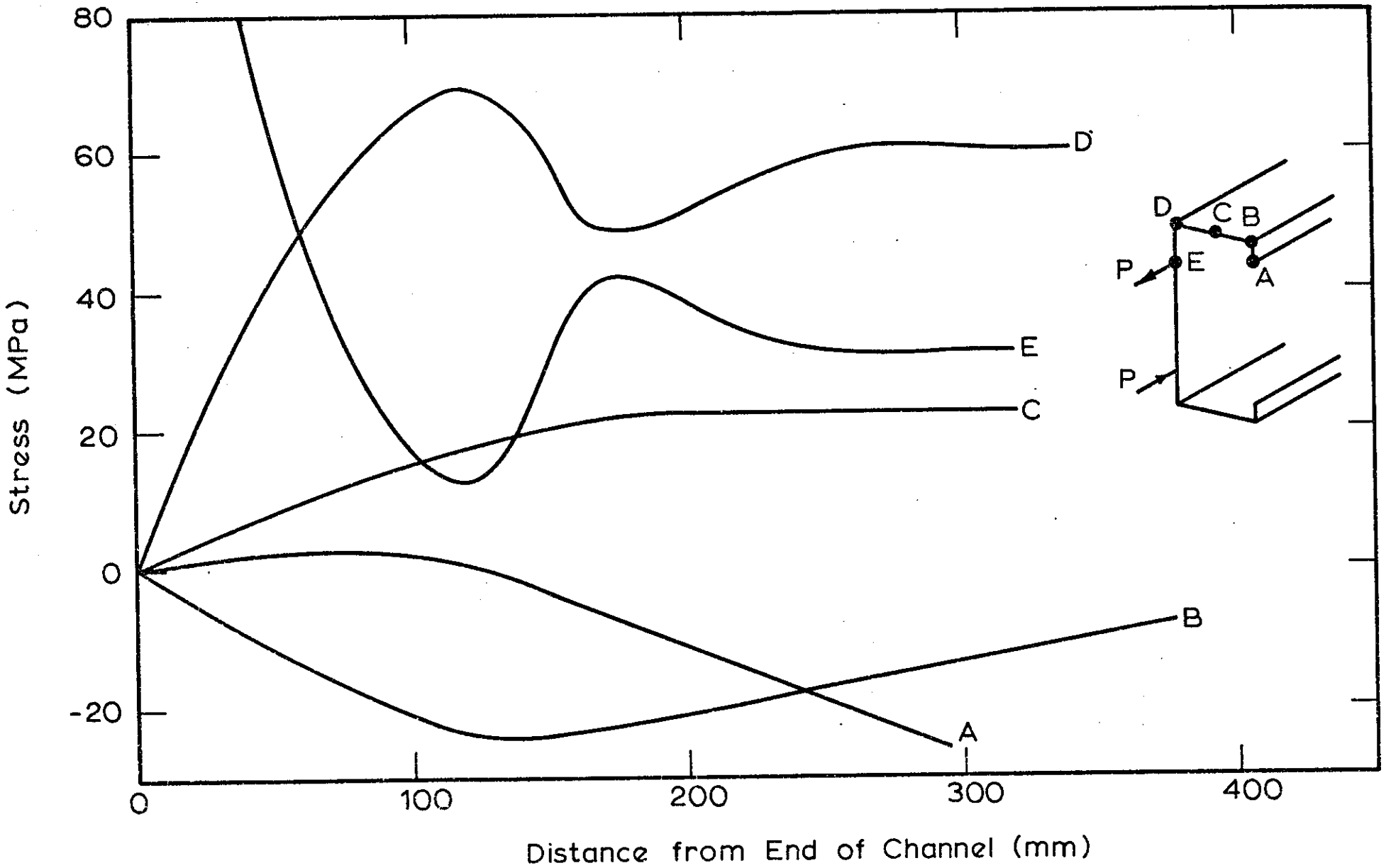

FIG.6.14 CHANNEL SECTION - VARIATION OF LONGITUDINAL STRESS USING FINITE ELEMENT METHOD

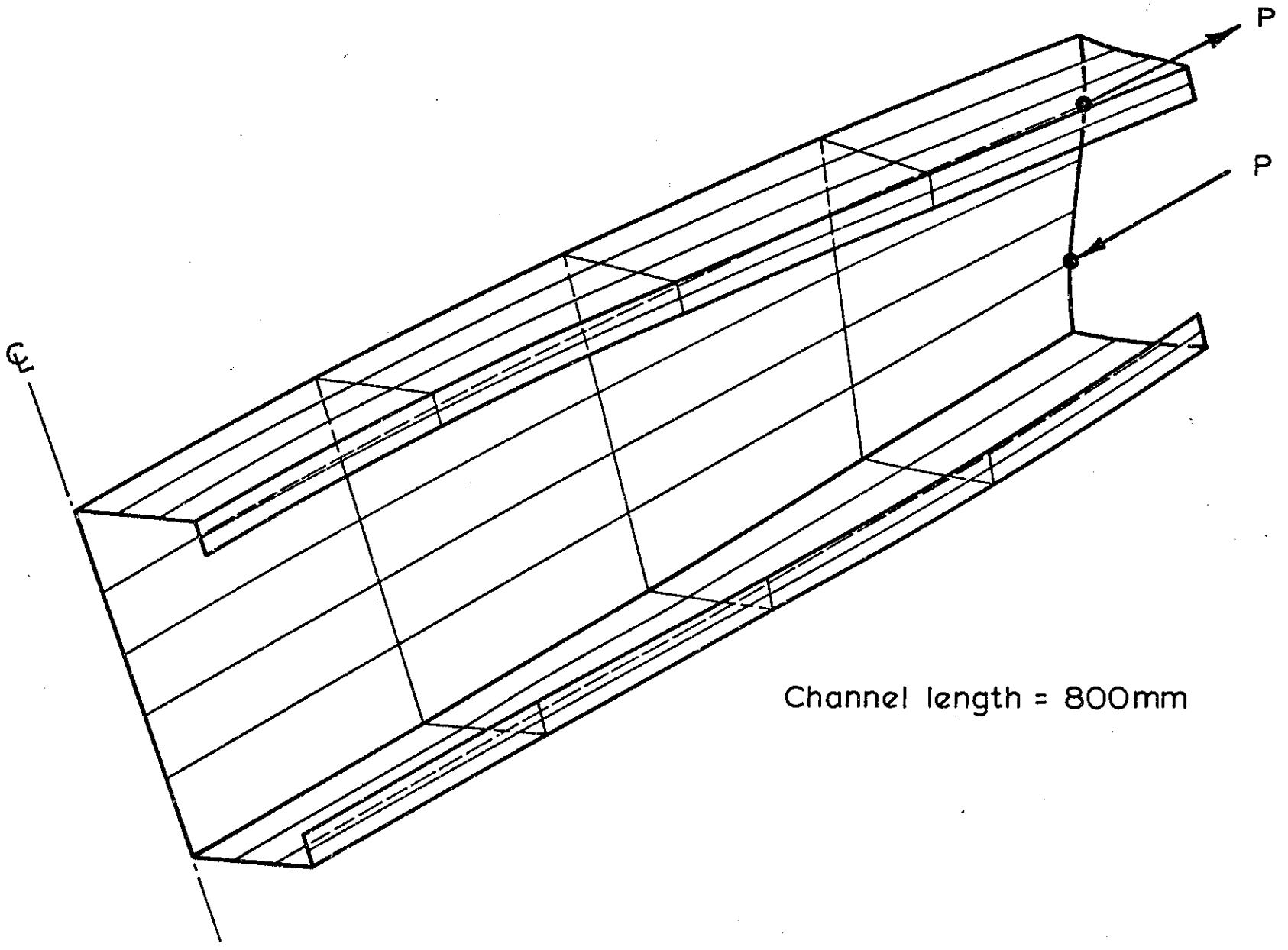

FIG.6.15 DEFORMED SHAPE OF CHANNEL

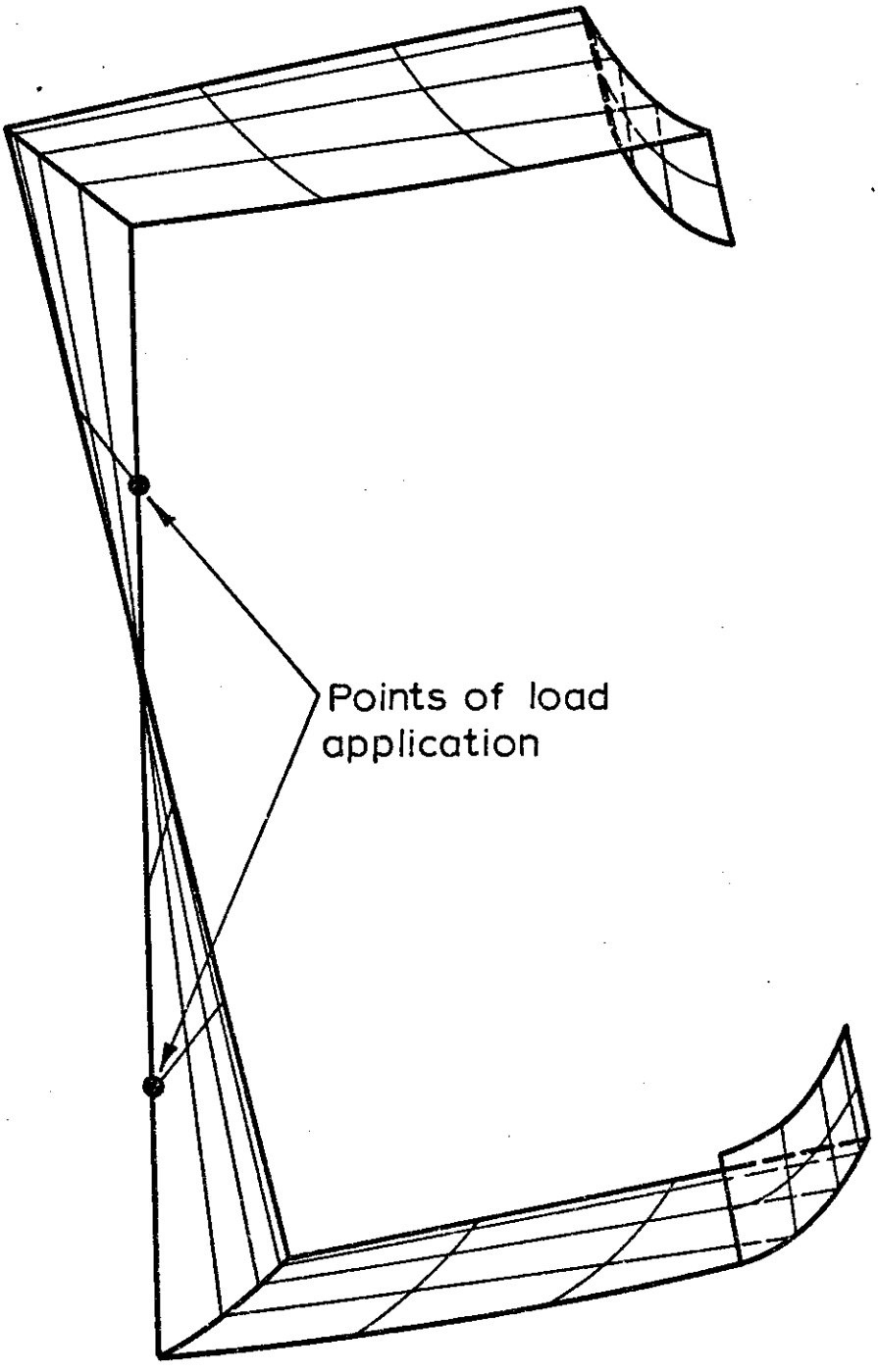

FIG. 6.16 DEFORMED SHAPE OF CHANNEL

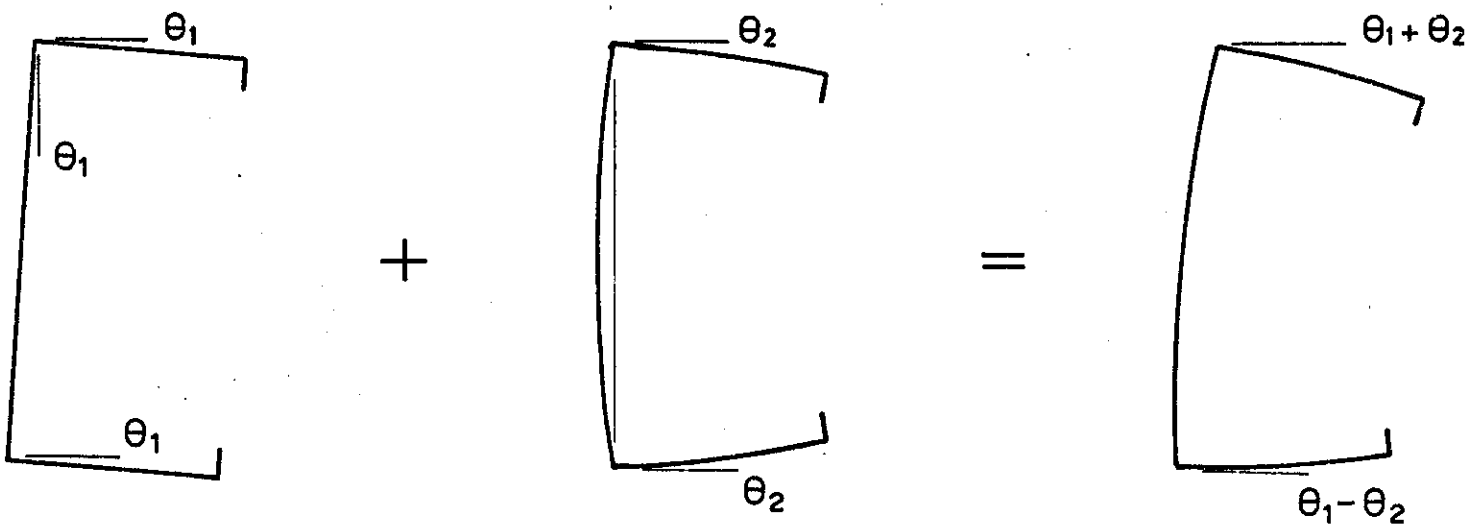

FIG. 6·17 ROTATION COMPONENTS FOR AN OPEN CROSS-SECTION

Collapse Load

Non-linear

Linear

Experimental Rafter Rotation
Frame 1

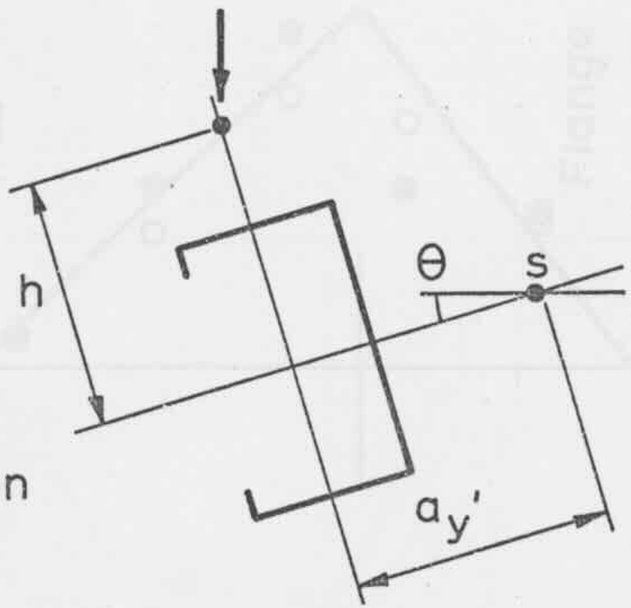

Load Eccentricity = $a_y' \cos\theta + h \sin\theta$

Load (kN)

16
12
8
4
0

0
0·04
0·08
0·12
0·16
0·20
0·24

Rotation (Rad)

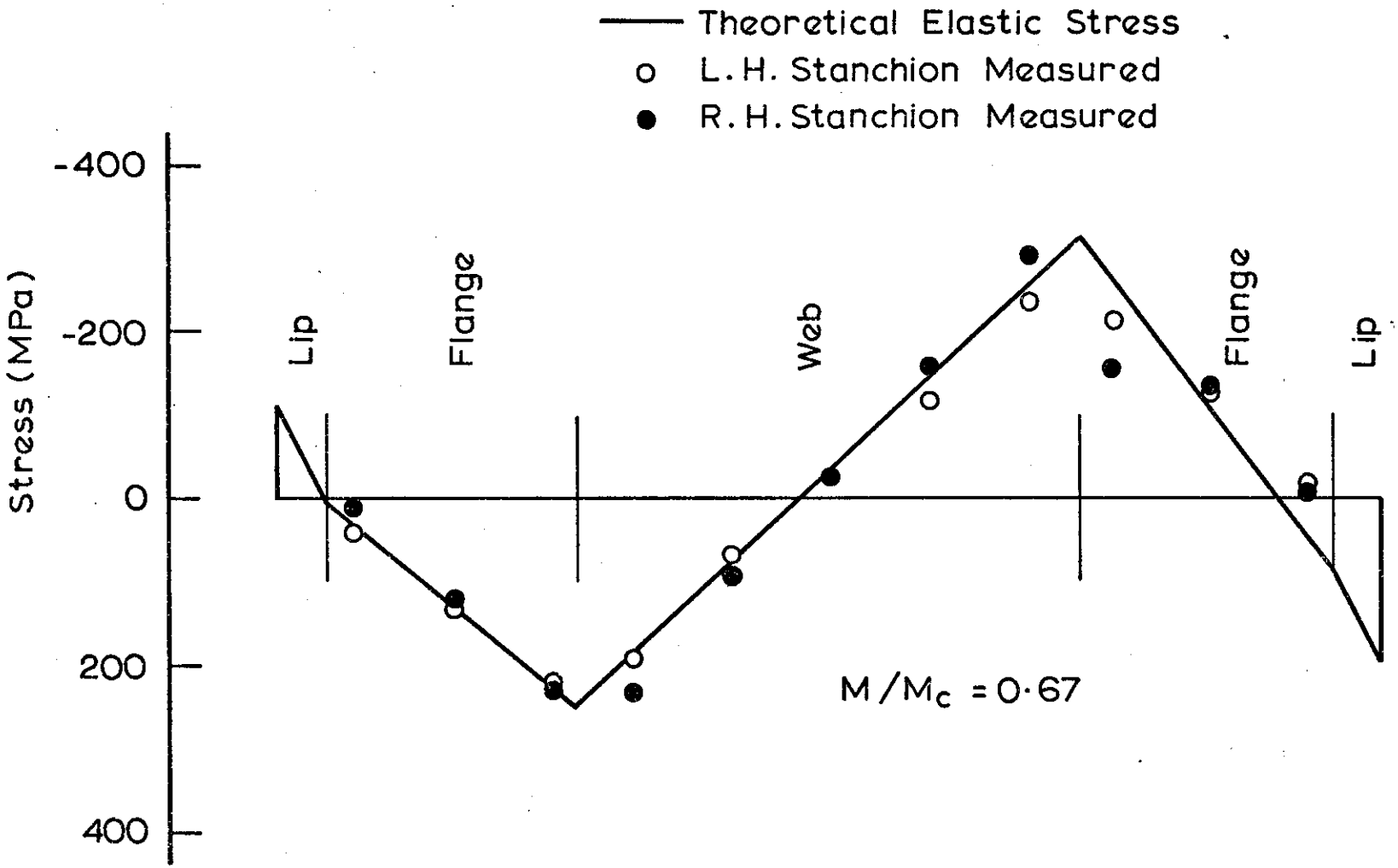

FIG.6.19 FRAME 2 - MEASURED STRESS DISTRIBUTION AT FIRST OBSERVED YIELD

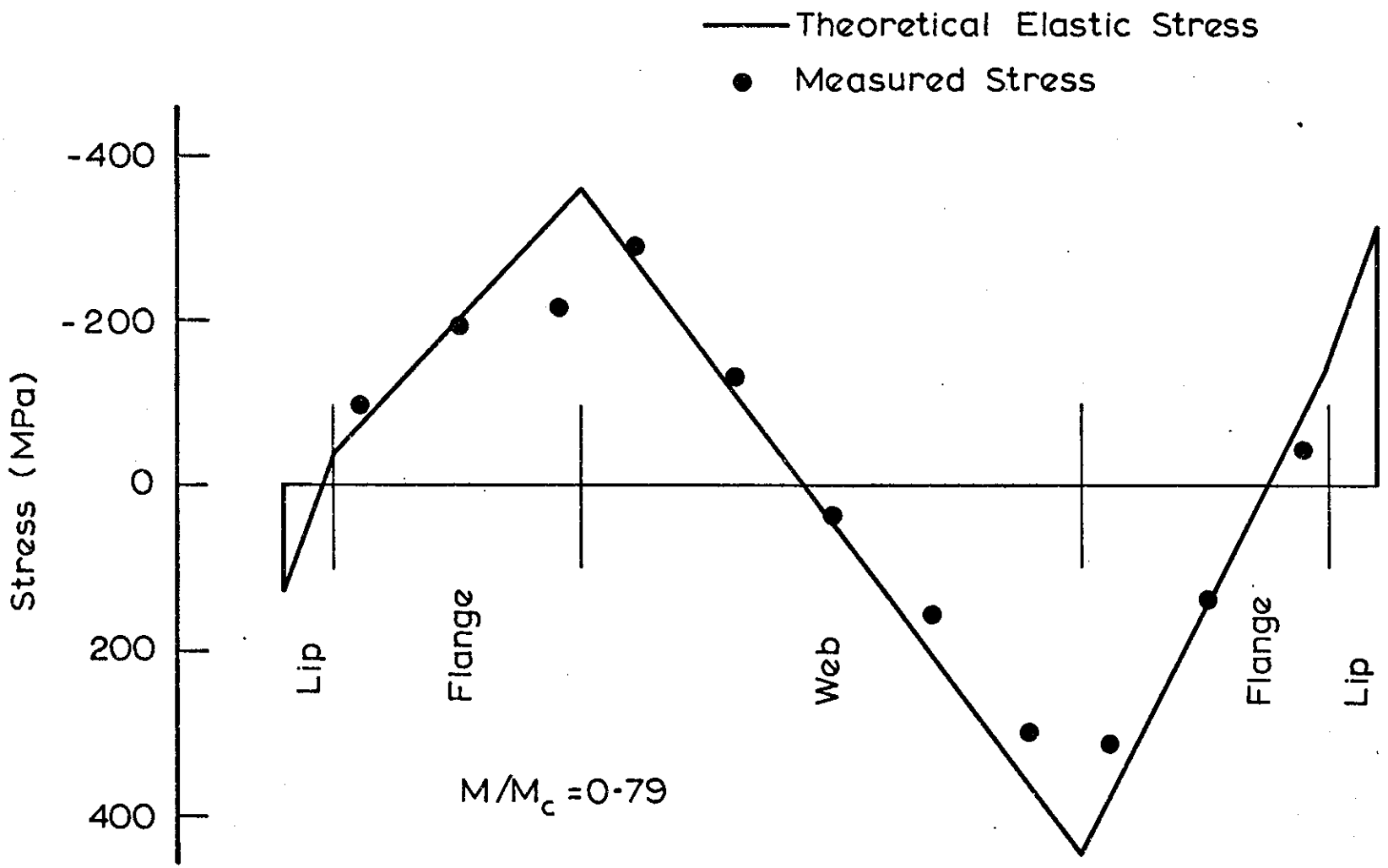

FIG.6.20 FRAME 3 - MEASURED STRESS DISTRIBUTION AT FIRST OBSERVED YIELD - L. H. STANCHION

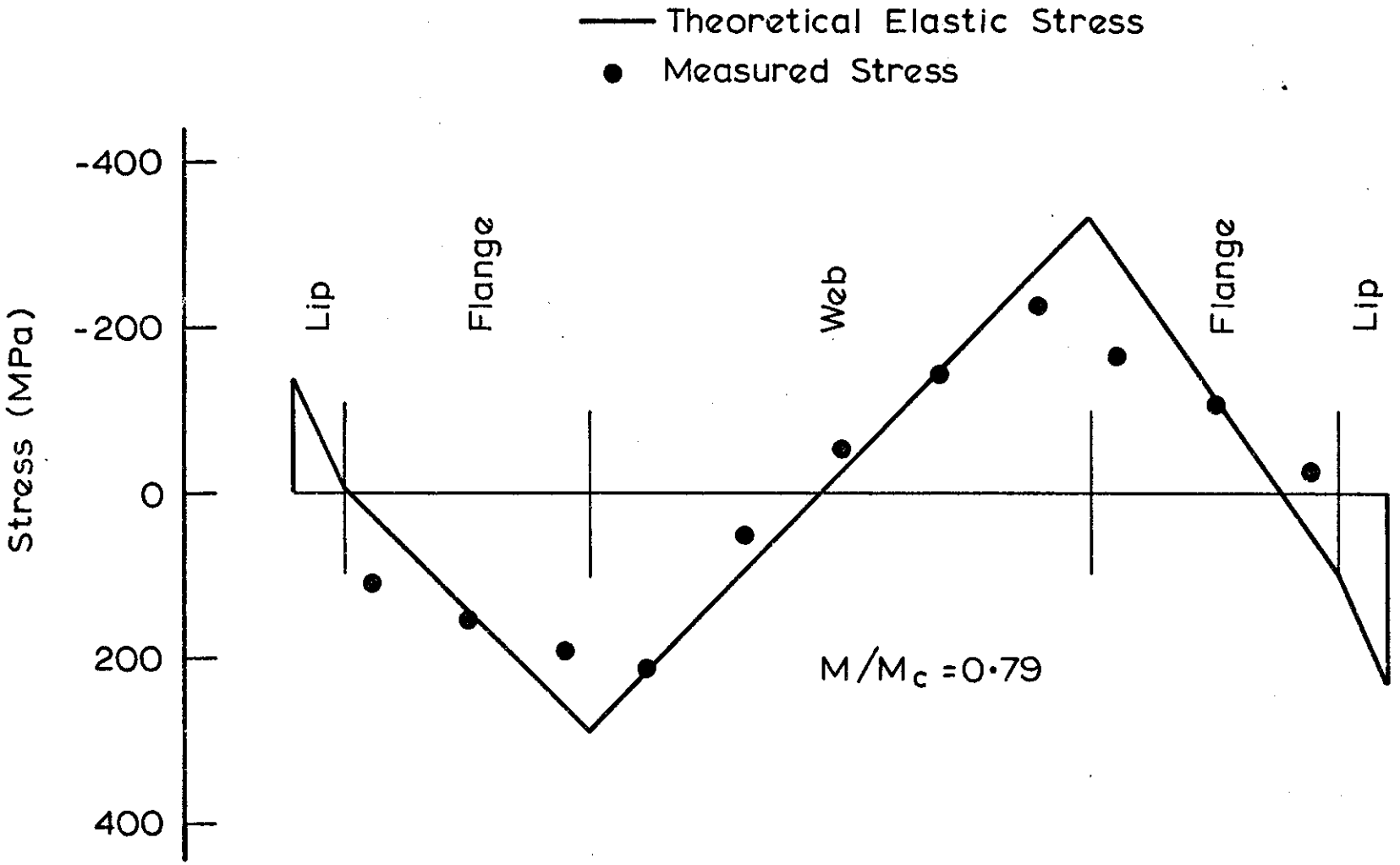

FIG. 6. 21 FRAME 3 - MEASURED STRESS DISTRIBUTION AT FIRST OBSERVED YIELD - R. H. RAFTER

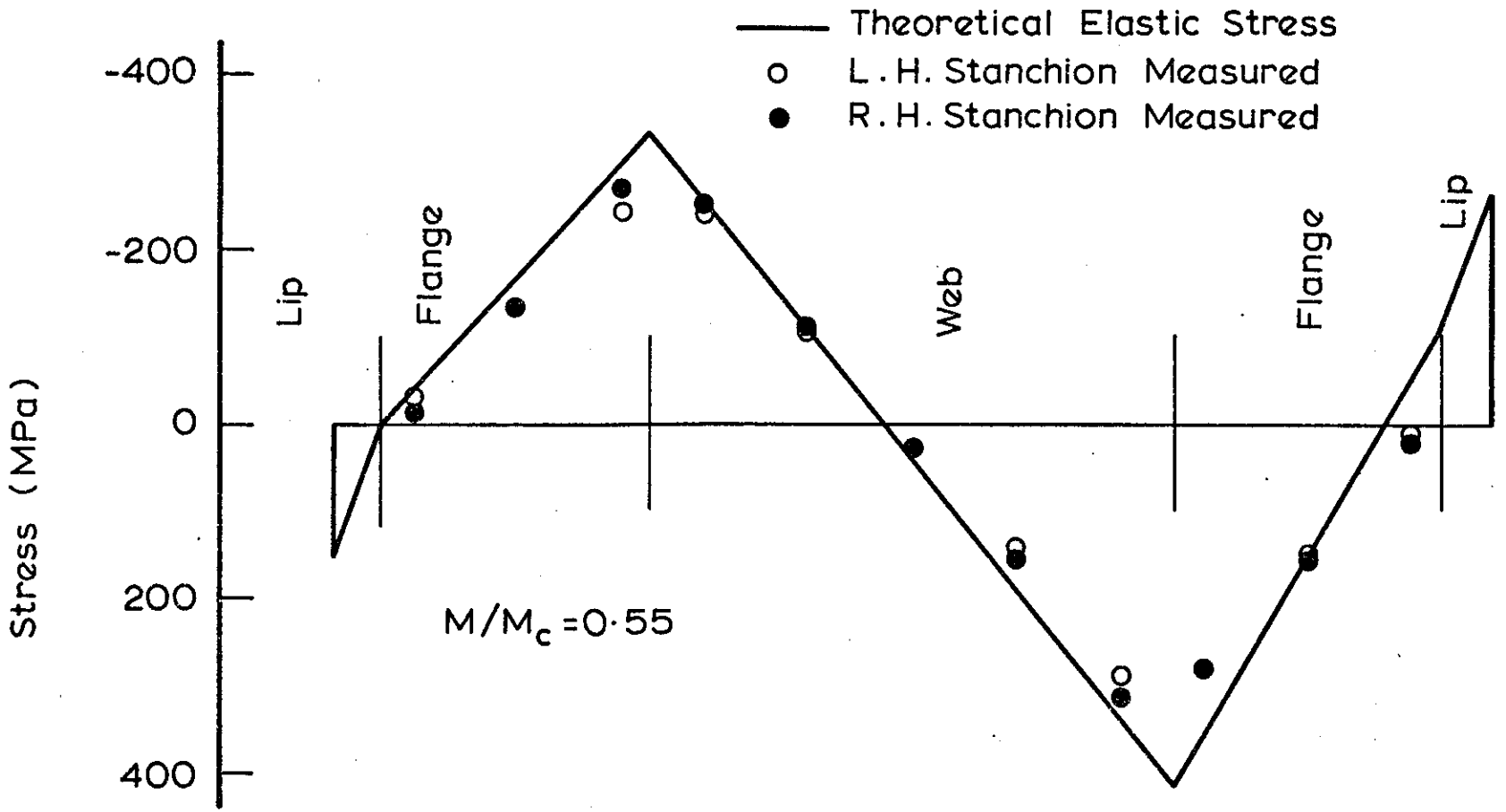

FIG. 6.22 FRAME - 4 MEASURED STRESS DISTRIBUTION AT OBSERVED FIRST YIELD

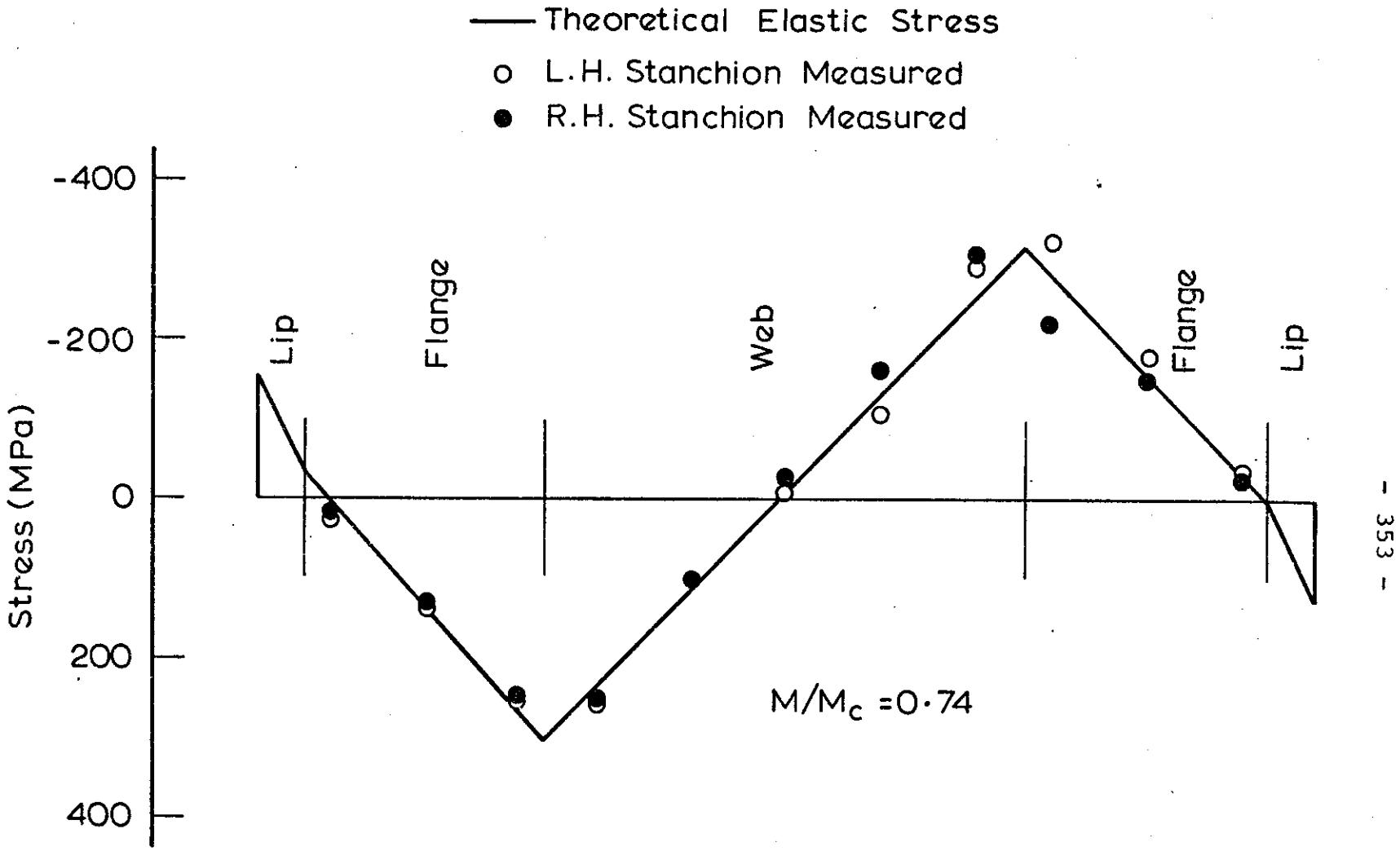

FIG.6.23 FRAME 5 - MEASURED STRESS DISTRIBUTION AT FIRST OBSERVED YIELD

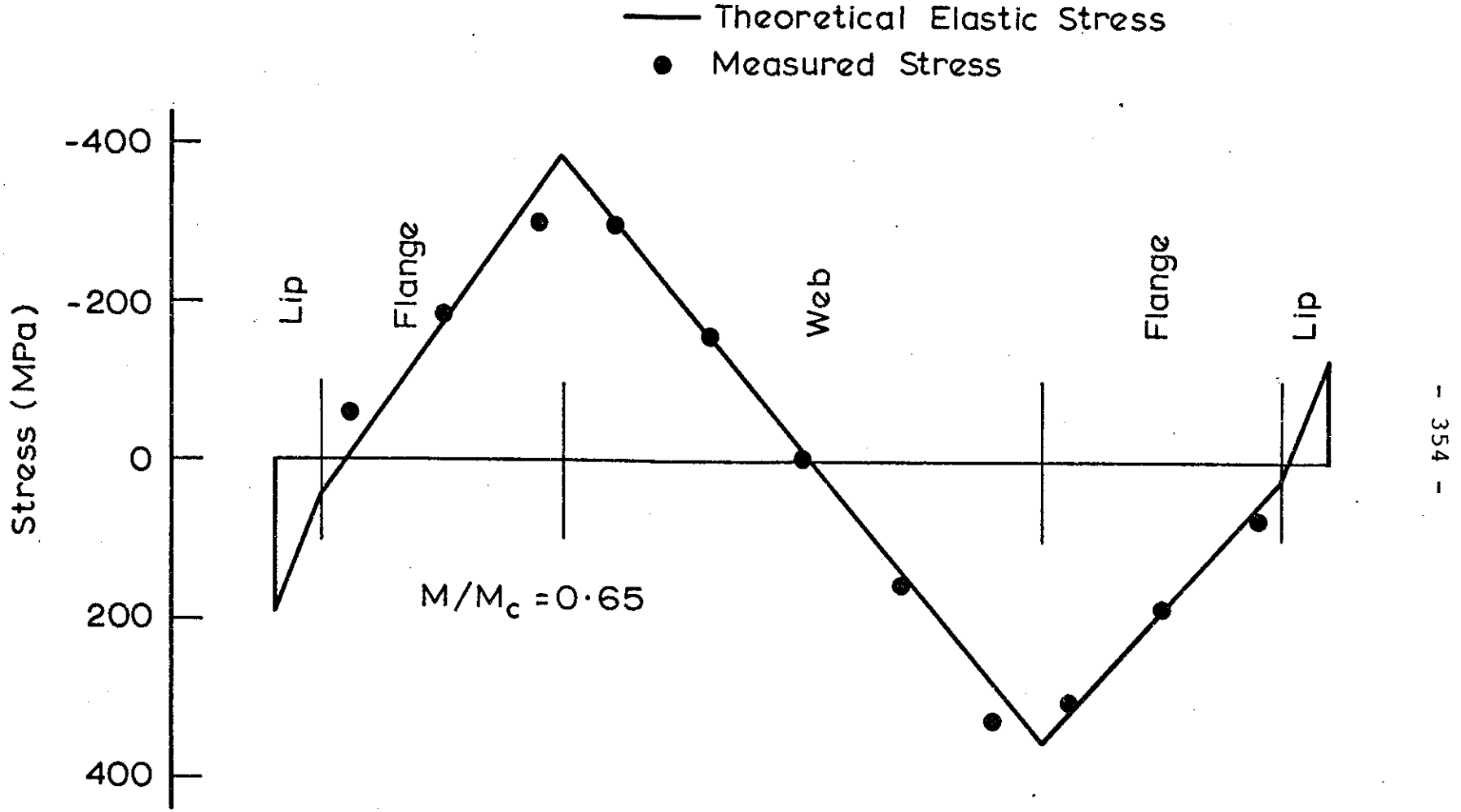

FIG. 6. 24 FRAME 6-MEASURED STRESS DISTRIBUTION AT FIRST OBSERVED YIELD - L. H. STANCHION

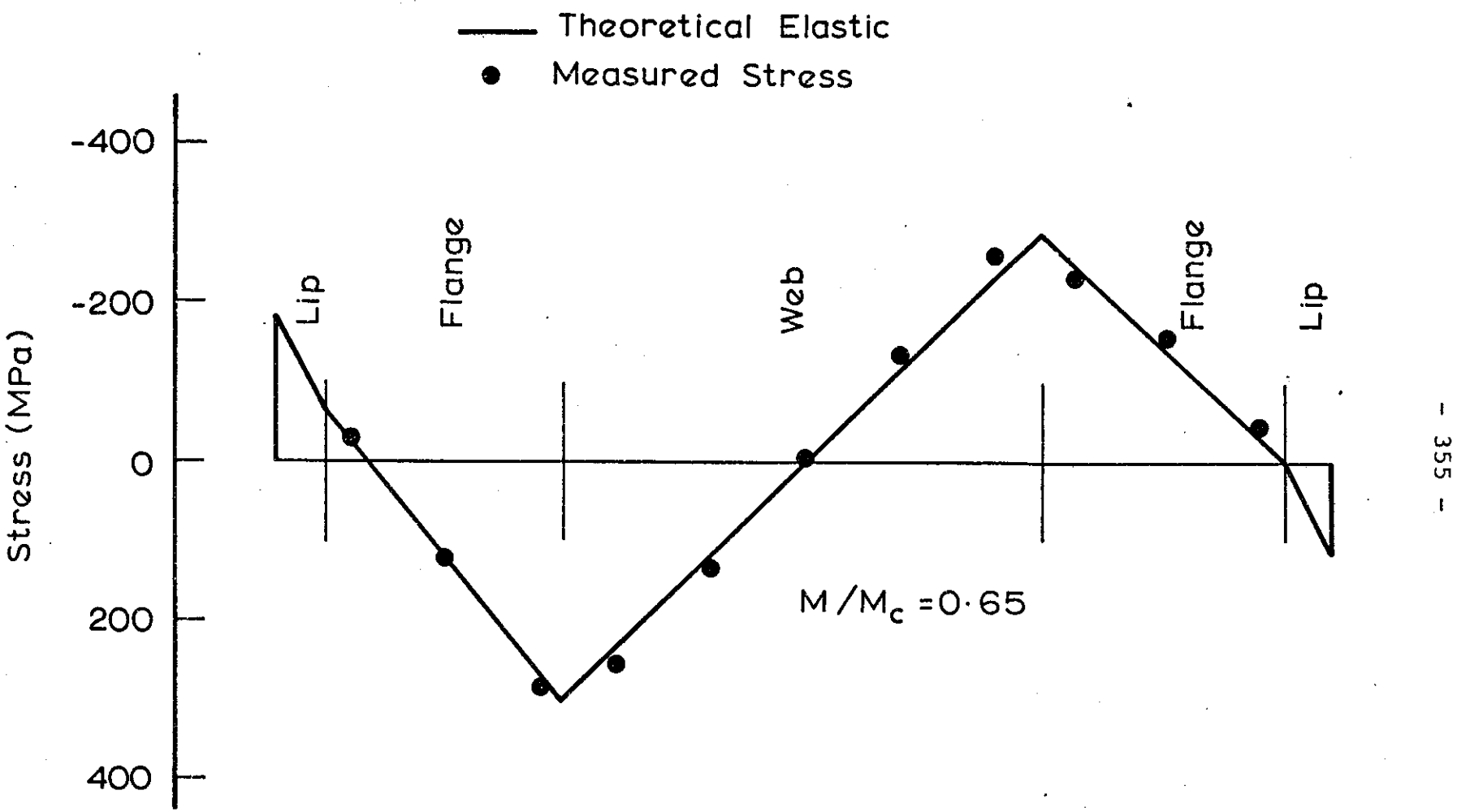

FIG.6.25 FRAME 6 - MEASURED STRESS DISTRIBUTION AT FIRST OBSERVED YIELD-R.H.RAFTER

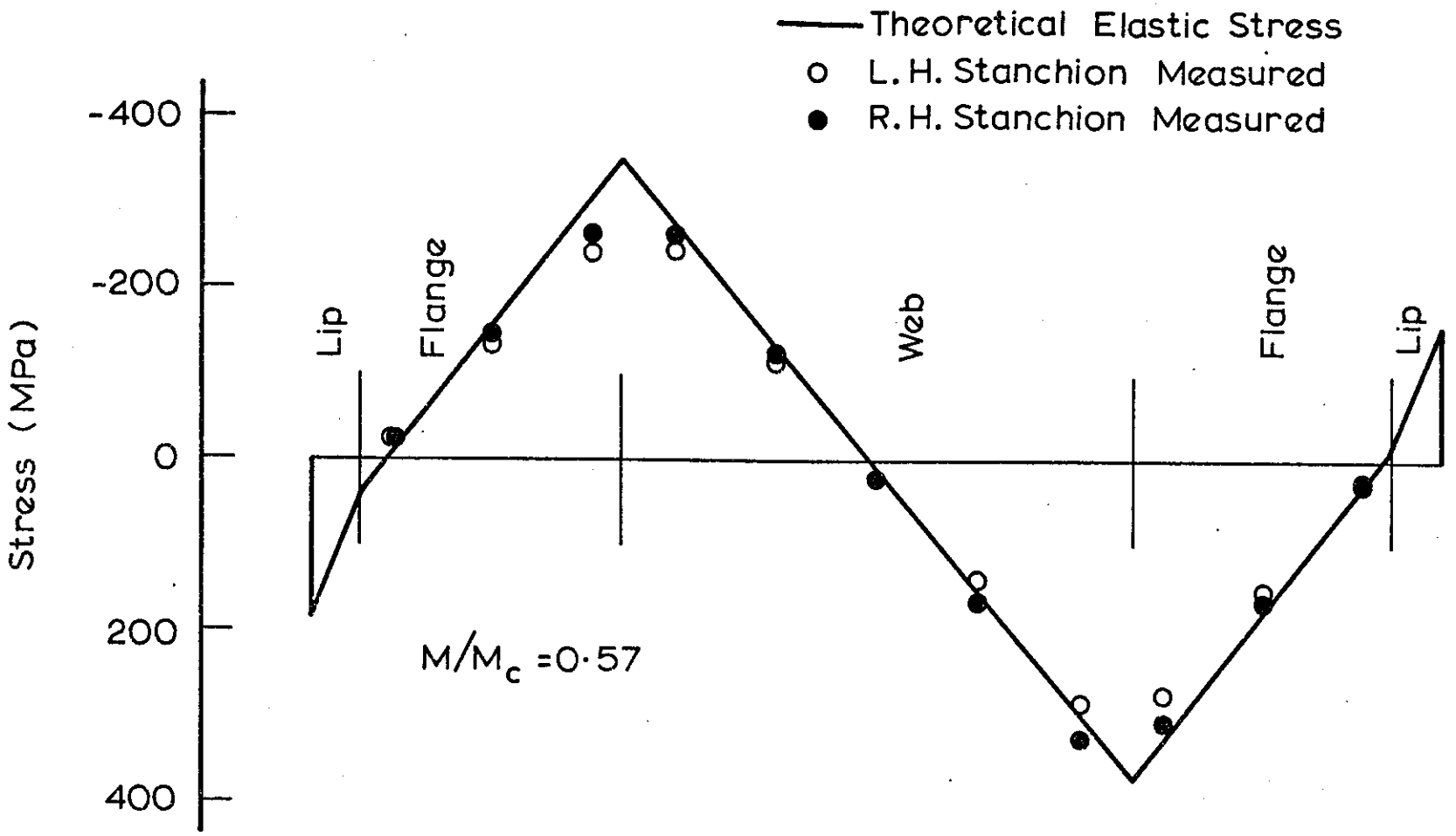

FIG.6.26 FRAME 7 - MEASURED STRESS DISTRIBUTION OBSERVED FIRST YIELD

CHAPTER 7 - BUCKLING AND INELASTIC BEHAVIOUR

7.1 INTRODUCTION

The tendency to buckle is a prominant characteristic of thin metal structures. The need to control buckling is one of the strongest factors which dominate structural form. In heavy steel construction, the chief forms of buckling which are considered in design are column buckling and lateral buckling. Column buckling governs the allowable axial stress which depends upon the slenderness ratio of the member, while lateral buckling of unbraced beams governs the allowable bending stress. Local buckling of the various plate-shaped components of which heavy structural sections consist, rarely needs to be considered because the plates are usually stocky. This means that the plates have such small width to thickness ratios that they will not buckle at stresses below the yield point. There are exceptions to this situation, such as thin webs of plate girders. In contrast, in cold-formed construction, the individual components of the section are frequently so thin that they will buckle at stresses below the yield point. It is necessary, therefore, to design such members so that at design loads, adequate safety exists against failure by local buckling.

Another form of buckling which must be considered in design is that which occurs when the cross-section is weak in torsion. This applies usually to open sections such as angles and

cruciforms in which the thickness of the plate is small. In this situation, the section may undergo purely rotational deformation about the longitudinal axis which will remain essentially straight. This type of deformation produces an instability known as torsional buckling. More commonly, where the section does not have two axes of symmetry, the cross-section will undergo translational and rotational movement. This is known as flexural-torsional buckling.

The onset of buckling in a structure is not necessarily the end of its load-carrying capacity. Indeed, the structure will often possess considerable post-buckling strength which may be used economically. This is used to advantage in light gauge steel design and makes it necessary to use more complex methods of analysis.

This Chapter will firstly be concerned with the problem of local buckling of thin-walled structures. Previous work will be reviewed. The development of local buckling theory will be presented, together with the effects of such concepts as effective width and lip reinforcement. The interaction between local and overall buckling will also be examined. Next, the inelastic behaviour of cross-sections will be presented. Finally, a buckling analysis will be presented for the prediction of inelastic local buckling.

7.2 LOCAL BUCKLING

It is well established that a geometrically perfect flat plate subjected to longitudinal compressive force remains unbuckled until the initial load is reached, at which stage it assumes a stable deflected equilibrium configuration (Bryan [1890], Cox [1933] and Hu et. al [1946]). The interchange between the two stable forms is characteristic of plate structures and leads to what is appropriately called a stable post-local-buckling strength. In practice, the presence of unavoidable imperfections will cause deflections to grow from the first application of load, the rate of growth becoming larger as the critical load is approached (Coan [1951]). The load deflection curves for both geometrically perfect and imperfect plates are shown in Fig. 7.1.

The fundamental differential equation for the deflection w of a plate subjected to forces in its middle plane under ideal conditions, was first derived by Saint Venant (1883) and is given by Eq. (7.1).

$$\frac{\partial^4 w}{\partial^4 x} + \frac{2\partial^4 w}{\partial^2 x \partial^2 y} + \frac{\partial^4 w}{\partial^4 y} = \frac{t}{D}\left(\sigma_{xx} \cdot \frac{\partial^2 w}{\partial^2 x} + 2\tau_{xy} \cdot \frac{\partial^2 w}{\partial x \partial y} + \sigma_{yy} \cdot \frac{\partial^2 w}{\partial^2 y} \right) \quad \ldots\ldots\ldots (7.1)$$

where $D = \frac{Et^3}{12\ (1-\nu^2)}$

and σ_{xx} is the normal stress in the x-direction, σ_{yy} is the normal stress in the y-direction, τ_{xy} is the shear stress and t is the thickness of the plate. If the loading is uniaxial, then σ_{yy} and τ_{xy} will be zero.

Bifurcation of the equilibrium position is indicated by the lowest value of the parameter σ_{xx}, called the critical stress or the local buckling stress, F_{cr}. Bryan (1890) presented the analysis for the rectangular plate, simply supported on all four edges and subjected to uniform compression on two edges. For this particular case, F_{cr} can be derived and is shown in Eq. (7.2).

$$F_{cr} = \frac{k.\pi^2.E}{12.(1 - \nu^2).(b/t)^2} \qquad .. .. .. (7.2)$$

where b/t is the thinness ratio of the plate and k is the local buckling constant.

For design purposes and particularly for establishing the load factors or the safety factors, the local buckling stress is useful as it indicates the loading values at which the deflections are still moderate and the structural elements still have a reserve of strength. Also,

near this stress significant deformations are initiated which eventually lead to the failure of the member.

The buckling coefficient k is determined by Eq.(7.3) (Bleich [1952]).

$$k = (L/mb)^2 + 2 + (mb/L)^2 \qquad .. .. .. (7.3)$$

where L and b are the length and breadth of the plate and m is the number of halfwaves in the longitudinal direction. For long narrow plates, k can be assumed to be equal to a constant value of 4.0 when the unloaded edges are simply supported. When the edges are fixed, k reaches a value of 6.97. In the case of plate components such as the web of a channel, the value of k will be between the two values due to the presence of mutual restraint at the longitudinal junctions of the flange components.

An unstiffened plate element may be defined as a plate which is simply supported along the transverse edges and one longitudinal edge, with the other longitudinal edge free. If this plate is subjected to the same stress conditions as the plate previously discussed, the differential equation of equilibrium is the same as Eq. (7.1). The solution for the elastic critical stress can still be expressed in the general form

of Eq. (7.2) in which the buckling coefficient is now approximated by (Chwalla [1940])

$$k = 0.425 + (b/L)^2 \qquad .. .. .. (7.4)$$

For the long plate elements which are used in most cold-formed members, the buckling coefficient is close to the minimum value of 0.425.

The solution to the problem of a single plate under compression and bending in its own plane, has been obtained by Schuette and McCulloch (1947). Johnson and Noel (1953) have published charts for plates subjected to bending in their own plane and suggested that their results be used with the tables published by Kroll (1943) in order to arrive at buckling loads. Walker (1966) studied plates and channel sections subjected to eccentric compression by means of an approximate solution using the Galerkin method.

In engineering design of thin-walled sections, it is not uncommon for the resultant load to be either applied eccentrically or combined with an applied moment so that non-uniform stresses are set up across the widths of some or all of the individual plate components. Rhodes and Harvey (1971 A) utilised the principle of minimum potential energy to obtain the local buckling stresses of plain channels under combined compression and bending.

The determination of the critical load for local buckling of thin-walled sections under concentric compression has been studied by a number of investigators including Kroll et. al. (1943), Hu and McCulloch (1947), Bleich (1952), Chilver (1953), Van der Maas (1954), Becker (1957), Divakaran (1966) and Bulson (1967). All the procedures disregard the out-of-plane deformation due to initial imperfection and the consequent partial plastification of elements which occurs prior to the theoretical local buckling. The case of eccentric compression has been studied by Venkataramaish and Roorda (1978).

Hence, the analysis of a thin-walled column such as a channel section as a complete unit is very complex. Therefore, one of the important simplifications is to consider a thin-walled member as a composite of individual plate elements. This simplification is ideally suited to the approximate methods of analysis which are readily solved by computer.

7.2.1 Post-Buckling Behaviour

Post-buckling behaviour is important in plate structures because of the additional load-carrying capacity which is available after initial buckling takes place. The analysis previously mentioned has been concerned with the elastic buckling and implies that the elastic critical load will be smaller than the squash load as shown in Fig. 7.2. The squash load is defined as the

product of the area of the cross-section and the material yield stress. Provided that the elastic critical load is less than the squash load, a plate can support loads in excess of the critical load (Walker [1975]) as is shown in Fig. 7.2. The thinner the plate for a given width the greater will be the excess. A simple model to explain the phenomenon has been devised by Winter (1947) and consists of the deflected plate being composed of a grid of longitudinal and transverse stiffeners as shown in Fig. 7.3 (a).

The analysis of a post-buckled plate is a complicated process. Von Karman (1910) was responsible for the formulation of the post-buckling differential equation given in Eq.(7.5). The equation is derived by considering the equilibrium of an element of the plate in the directions perpendicular to the plate. The normal and shear forces of the plate depend not only on the external forces applied in the plane of the plate but also on the strain of the middle plane of the plate due to bending. These considerations result in two force equilibrium equations and a third equation resulting from the strain components in the middle surface of the plate during bending. The solution of these three equations is greatly simplified by the introduction of a stress function, F (Timoshenko and Goodier [1970]).

$$\frac{\partial^4 F}{\partial x^4} + \frac{2\partial^4 F}{\partial x^2 \partial y^2} + \frac{\partial^4 F}{\partial y^4}$$

$$= E.\left[\left(\frac{\partial^2 w}{\partial x \partial y}\right)^2 - \frac{\partial^2 w}{\partial x^2} \cdot \frac{\partial^2 w}{\partial y^2}\right] \qquad \ldots\ \ldots\ \ldots\ (7.5)$$

Walker (1969) has developed an approximate expression which describes the variation of the deflection at the centre of a plate forming a cold-formed member, with an applied load greater than the critical load.

After the attainment of the critical load, the stresses in the plate redistribute as the plate buckles. The maximum direct stress occurs midway along the unloaded edge. Again, because of the mathematical complexity of the problem, no exact expression has been derived relating the applied load to the maximum edge stress. However, an approximate solution has been derived by Dawson and Walker (1972B). Graves-Smith (1969) has demonstrated that the occurrence of the maximum load closely coincided with the load at which the maximum edge stress reached the yield stress.

7.2.2 Effective Width

A plate axially loaded as shown in Fig. 7.3.(a), develops distinct wave-like distortions after the critical stress has been exceeded and the most highly stressed portions of the plate are those regions closest to the unloaded supported

edges. One way to account for the non-uniform stress distribution is to assume that the maximum edge stress acts over a certain portion of the plate width. The portion over which this stress acts is called the "effective width", b_e, of the plate and is shown in Fig. 7.3 (b). The total compression force in the element is equal to the area under the stress distribution curve times the thickness of the element. The same total force is obtained if the actual element is replaced by one of reduced effective width, b_e, and with uniform stress distribution of magnitude f_{max}. In this manner, the central portion of the compression element is thought of as removed and the element of actual width, b, is replaced by one of effective width, b_e.

The concept of effective width was first proposed by von Karman (1932). He suggested that the effective width could be calculated with the use of Eq.(7.6).

$$b_e = b\sqrt{\frac{F_{cr}}{F_y}} \qquad \ldots\ldots\ldots (7.6)$$

The effective width concept was introduced for design purposes by a number of researchers including Marguerre (1937), Hu et. al. (1946), Winter (1947), Argyris and Dunne (1952), Jombock and Clark (1961) and Abeld-Sayed (1969). The most well known approach has been the empirical

adjustment to von Karman's formula developed by Winter in 1947. Using the results of some 150 tests, he derived the formula given by Eq. (7.7)

$$\frac{b_e}{t} = 1.9\sqrt{\frac{E}{f_{max}}}\cdot\left(1-\frac{0.475}{b/t}\sqrt{\frac{E}{f_{max}}}\right) \quad .. .. .. (7.7)$$

It has been found that failure loads and deflections at service loads of thin-walled beams are safely and conservatively predicted on the basis of Eq. (7.7). The equation has been modified by Winter (1968) to eliminate some of the conservatism and the expression shown as Eq. (7.8) has been adopted by the AISI Cold-Formed Steel Design Specification (1968) and the SAA Cold-Formed Steel Structures Code (1974).

$$\frac{b_e}{t} = 1.9\sqrt{\frac{E}{f_{max}}}\cdot\left(1-\frac{0.415}{b/t}\sqrt{\frac{E}{f_{max}}}\right) \quad .. .. .. (7.8)$$

Using the effective width concept, the post-local-buckling behaviour has been investigated by Wang and Tien (1973, 1977) and others. Recently, Horne and Narayanan (1976) used large deflection theory to obtain the effective width formula for an initially imperfect plate with its longitudinal edges held straight. This was further extended by Tien and Wang (1978) for the case of the longitudinal edges free to wave.

7.2.3 Edge Stiffeners

One way to enhance the local buckling strength of thin-walled members is to add longitudinal stiffeners to the flat plate components. The purpose of the lip is to hold the edge of the element straight when the element has buckled locally, thus imposing a condition similar to that of a simple support. To achieve this purpose, the lip itself must be of sufficient depth (Kenedi and Harvey [1950]) to avoid the formation of out-of-plane waves. The buckling strength of a section will increase as the lip depth increases. However, the buckling strength of the section will only continue to rise until the width to thickness ratio of the lip reaches a value of approximately ten. At this ratio the buckling strength will decrease as the lip stiffener will itself buckle.

Two related but fundamentally different buckling modes characterise the behaviour of edge stiffened elements. One is the stiffener buckling mode, where instability is initiated by buckling of the stiffener in a direction perpendicular to the plane of the plate. For this mode, instability of the stiffener will induce simultaneous local buckling of the plate. The critical buckling equation for the stiffener buckling mode has been given by Chilver (1953B). The second mode is the local plate buckling mode, where instability is initiated by local buckling

of the flat plate elements. The critical buckling equation for this mode is given by Van der Maas (1954).

The effect of edge stiffeners has received many experimental investigations. Extensive research has been carried out recently by Winter (1968), Desmond (1977) and Desmond et. al. (1978). Their work has shown that the ultimate strength of a plate element with an adequate edge stiffener is equal to that of an element of similar dimensions and material properties but supported by a web at the stiffener location. Hasegawa and Maeno (1979) have also investigated edge stiffeners and edge stiffened elements.

7.2.4 Buckling of Sections

The local instability of thin-walled sections consisting of assemblies of flat plates occurs when the individual plate elements buckle simultaneously with a common wavelength. For channel and I-sections, the elastic initial buckling stress is influenced considerably by the width and thickness of the flanges and the ratio of the flange width to web width. The performance may be improved with the addition of edge stiffeners.

In considering the buckling of sections, the critical load is the important quantity to know. For a section, the critical load is a function of the geometry of the complete section and it may be

derived from a knowledge of the critical loads of the component plates having rotational restraint along the edges and matching the restraints at the mutual corners (Rhodes and Harvey [1971B]). Alternatively, a more mathematically complex method may be used in which the critical load for the whole section is calculated in a similar manner to that for a single plate. The mathematical solution has been researched by Harvey (1951), Chilver (1953B) and Walker (1966).

Provided the value for the coefficient k is known, the buckling load for any structural section may be found by using Eq. (7.9).

$$P_{cr} = \frac{k.\pi^2.E.A}{12\,(1-\nu^2)\,(b_w/t)^2} \qquad .. .. .. (7.9)$$

where b_w is the width of one of the component plates. The buckling coefficient for a channel section is shown in Fig. 7.4 (Walker [1975]). A variation in the buckling coefficient occurs because of the different cross-section geometries. The ratio of the flange width to web width also influences the value of k for a particular cross-sectional shape. Bulson (1970) has collated the critical loads and wave lengths for a wide variety of structural shapes.

7.3 FLEXURAL BUCKLING

Flexural buckling or Euler buckling is common to cold-formed and hot-rolled sections alike. Because of the large variety of section shapes which can be manufactured by rolling or pressing, it is necessary to treat a more general form of buckling than that of doubly-symmetric pin-ended struts. It is necessary to consider the situation where no axis of symmetry exists and the section twists as well as buckles sideways. This torsional-flexural behaviour is less prevalent in hot-rolled sections because of the higher torsional rigidity and also because they usually have at least one axis of symmetry. A very full presentation of the theory of torsional-flexural buckling has been presented by Timoshenko and Gere (1961), Chajes et. at. (1966), Galambos (1968), the Column Research Council (1976) and Trahair (1977).

The stress at which flexural buckling occurs, depends on the tangent modulus (Shanley [1947]) and the length and geometry of the member. Most members in cold-formed construction show a gradual yielding stress-strain curve which depends upon the steel and upon the effects of cold-work in the forming process. When the buckling stress is reached, the member fails about is axis of least resistance.

7.4 LOCAL AND OVERALL BUCKLING INTERACTION

A concentrically compressed section which is subjected to neither flexural-torsional nor torsional buckling and for which local plate buckling occurs prior to material yielding, fails in one of three patterns. Firstly, for low column slenderness ratios, local plate buckling occurs followed by the development of post-buckling strengthening, with failure occurring when the compressive strength of the component plates is reached. Secondly, for the moderate slenderness ratios, local plate buckling occurs followed by the development of post-buckling strength, with failure precipitated by overall flexural column buckling. Thirdly, for large slenderness ratios, failure occurs by overall buckling with no prior local plate buckling.

The theoretical problem of determining the behaviour of a strut which is experiencing local and overall deformations is very difficult. Research has been limited in the area of the interaction of plate buckling, including the post-buckling behaviour, with overall column buckling. Graves-Smith (1968) developed a large deflection analysis which used the pattern of local imperfections and non-linear behaviour of the material properties. He obtained very good comparisons with tests on aluminium tubes, however, the rigorous and complex analysis was not practical for the wide range of cold-formed steel shapes. Bijlaard and Fisher (1953), Scidenfaden

(1954) and Kloppel and Schubert (1971) have attempted theoretical analyses, although they have made assumptions limiting their work to elastic plate behaviour or to plates with small deflections only. Jombock and Clark (1961), Uribe (1969) and Skaloud and Zornerva (1970) have incorporated test results into their analyses. The semi-emperical approaches are simpler in application and because they are based upon test results, usually give good results. De Wolf et. al (1974) have developed an analytical approach which accounts for the combined effects of local buckling, column buckling and non-uniform material properties for compression members. The method was based upon the tangent modulus concept and utilised the effective width expression developed by Winter. The model satisfactorily predictd the ultimate strength of a series of column tests in which both the local buckling loads and the overall column buckling loads were varied.

7.5 INELASTIC BEHAVIOUR

The usual elastic design criterion regards the initiation of yielding in the outer fibres as defining failure. However, it is known that the actual maximum moment of the cross-section exceeds the initial yield moment and may only be attained when yielding spreads almost over the entire cross-section. Hence, the carrying capacity of continuous compact beams and frames exceeds that calculated from the initial yield criterion. This is because of firstly, the higher carrying

capacity of the cross-section and secondly, the inelastic moment redistribution.

Cold-formed sections do not generally fall into the category of compact sections whilst most hot-rolled sections do. This should cause a reduction in a cold-formed member's inelastic reserve strength. However, the neutral axis of cold-formed sections is quite often located eccentrically. Frequently, the neutral axis is so located that initial yielding takes place in tension. In addition, the ratio of the web area to the total area is generally larger for a cold-formed member. Both of these factors tend to increase the inelastic reserve strength of cold-formed sections (Reck et. at. [1975]).

The inelastic reserve strength of a beam cross-section can be defined as the ratio of the ultimate moment to the yield moment. The reserve strength is a result of inelastic stress redistribution across the depth of the section. The redistribution is associated with web plastification. In general, failure is initiated by failure of the web or of the compression flange or of interaction of the behaviour of these two elements. To determine the ultimate moment as influenced by the behaviour of the compression flange, it is necessary to know not only the ultimate strength but also the capacity to undergo axial plastic deformations prior to failure.

Compression flanges which are thin possess significant post-buckling strength but fail when yielding is initiated. Therefore, members with such compression flanges have no inelastic reserve capacity if yielding takes place in the compression rather than the tension flange. However, stocky compression flanges continue to carry their compression load after yielding. In this case, yielding will spread into the web, resulting in inelastic reserve strength. Inelastic reserve strength through partial web yielding is obtained also when the neutral axis is so located that yielding begins in the tension flange.

Consequently, two important parameters determine the extent of the inelastic stress distribution. They are firstly, the amount of additional strain beyond initial yielding which can be sustained by the compression flange and secondly, the cross-section geometry.

7.5.1 Effect of Yielding

As yielding progresses through the cross-section, the ability of the member to resist the applied forces diminishes. This is because of a reduction in the effective area of the cross-section and a reduction in the material properties. The material properties which are affected by yielding are the elastic Young's and shear moduli and the Poisson's ratio.

When the longitudinal stress in a plate loaded in one direction exceeds the proportional limit, the tangent modulus, E_t, applies in the longitudinal direction. This concept has been supported by the results of a great number of tests performed by Bleich (1924). However, in the analysis of plates, the value of the modulus in the transverse direction has been debated by many researchers.

Ros and Eichinger (1932) pointed out that a plastic material is isotropic and hence is yielded in all directions. Therefore, the elastic modulus in the transverse direction should be replaced with the reduced modulus, $\bar{E}$. The reduced modulus is a function of the elastic and tangent moduli and the second moment of area of the elastic and inelastic regions of the cross-section.

In the study of inelastic buckling a rational theory was developed by Ilyushin (1947) and Stowell (1948). Ilyushin based his solution on the concept that the concave side of the plate was in a plastic state of deformation whereas the other side of the plate behaved elastically. He assumed the plate to be incompressible and took Poisson's ratio to the 0.5. However, predictions of Ilyushin's theory do not show satisfactory agreement with test results. Stowell simplified Ilyushin's theory by assuming the material to be inelastic in the longitudinal direction with the tangent modulus being used for the definition of stiffness, and elastic in the unloaded transverse

direction. The solution to the resulting differential equation may be readily obtained. Successful attempts to apply such solutions to the buckling analysis of plates have been made recently by Swartz and Rosebraugh (1974) who compared them with experimental results. It was found that good correlation was achieved when isotropic plate behaviour based upon a tangent modulus in both directions was assumed. These results have led Popov and Medwadowski (1979) to conclude that the refinements introduced by Stowell do not appear to be necessary.

The determination of the inelastic shear modulus has resulted in as much conjective as for the inelastic modulus used for the definition of stiffness. Experimental studies carried out by Morrison and Shepperd (1950), Peters et. al. (1950), Budiansky et. al. (1952) and Feigen (1954) have shown that the shear modulus remains at or near the elastic value. The experiments support the proposal by Neal (1950) that the shear modulus of a yielded beam remains constant. However, Haaijer (1957) pointed out that these experimental results do not correctly predict the behaviour of mild steel under torsion in the strain hardening range. He found from a series of experiments that the shear modulus was much smaller than the elastic value. Lay (1965) derived a theoretical value for the shear modulus G_y in the yielded and strain hardened regions. The result is given in Eq. (7.10).

$$\frac{G_y}{G} = \frac{2}{1 + \frac{E/E_t}{4(1+\nu)}} \qquad .. .. .. (7.10)$$

When applied to mild steel where E/E_t is approximately equal to 33 then, G_y/G is approximately equal to 0.25. Nishimo et. al. (1968) in their studies of inelastic torsional buckling used the reduced shear modulus to obtain good correlation with test results. Massey (1963) also found that the torsional rigidity was reduced for plastic sections.

In this thesis it is assumed that isotropic plate behaviour is valid for inelastic buckling. The ratio of elastic to tangent modulus, E/E_t, is taken as 33 and the shear moduli ratio, G_y/G is taken as 0.25. Poisson's ratio has been assumed to be 0.3 in the elastic region and 0.5 for the inelastic material.

7.5.2 A General Inelastic Cross-Section Analysis

A method of analysis for determining the effect of yielding on thin-walled cross-sections is presented. The basis for this method is the general analysis of stresses in open sections described in Chapter 3. The method of inelastic analysis is similar to that described by Santathadaporn and Chen (1972) and extended by Hancock (1977) to include the stress resultant of

bimoment. The method includes the effect of the movement of the instantaneous shear centre within any general inelastic cross-section. The instantaneous shear centre is defined as the shear centre of the elastic core. All stress resultants, including the bimoment which is derived from the normalised unit warping pattern based upon the original shear centre position, are related to the original reference axes, x' and y' shown in Fig. 7.5.

There are four stress resultants which produce longitudinal stresses. These are the moments about the x and y axes (M_x, M_y), the axial tension (F_z) and the bimoment (B_z). The corresponding generalised strains are the curvatures about the x and y axes (ρ_x, ρ_y), the axial strain (ε_z) and the negative rate of change of twist ($-\phi''_z$) respectively. For an elastic cross-section they can be related to the stress resultants using Eq. (7.11).

$$F_z = EA.\ \varepsilon_z$$

$$M_x = EI_x.\ \rho_x$$

$$M_y = EI_y.\ \rho_y$$

$$B_z = EI\ .\ (-\phi''_z) \qquad \ldots\ \ldots\ \ldots\ (7.11)$$

Eq (7.11) can be expressed as a diagonal rigidity matrix and can be represented in matrix notation by Eq. (7.12)

$$\{W_{x,y}\} = [k] \cdot \{\varepsilon_{x,y}\} \quad .. .. .. (7.12)$$

At the onset of yield, the instantaneous shear centre and centroid occupy new positions S, C as shown in Fig. 7.5, depending upon the configuration of the new elastic core. Hence, it is necessary to define a new set of principal axes ξ , η which are associated with the new cross-section (Fig. 7.5). When yielding takes place, incremental changes in actions about the principal axes of the elastic core can still be applied using an incremental rigidity matrix. The incremental rigidity matrix is represented in matrix notation by Eq (7.13).

$$\{dW_{\xi,\eta}\} = [k^*] \cdot \{d\varepsilon_{\xi,\eta}\} \quad .. .. .. (7.13)$$

The (*) signifies that the properties are based upon the elastic core for an elastic-plastic cross-section. Similarly, the force and displacement transformations for incremental forces and displacements can be applied providing that the cross-section parameters used in the transformation are those of the elastic core. The force and displacement transformations are

expressed in matrix notation by Eq. (7.14) and Eq.(7.15) respectively.

$$\{dW_{x,y}\} = [G^*] \cdot \{dW_{\xi,\eta}\} \quad .. .. .. (7.14)$$

$$\{d\varepsilon_{\xi,\eta}\} = [G^*]^T \cdot \{d\varepsilon_{x,y}\} \quad .. .. .. (7.15)$$

Again eliminating $\{dW_{\xi,\eta}\}$ and $\{d\varepsilon_{\xi,\eta}\}$ produces Eq.(7.16).

$$\{dW_{x,y}\} = [G^*] \cdot [k^*] \cdot [G^*]^T \cdot \{d\varepsilon_{x,y}\} \quad .. .. .. (7.16)$$

The matrix triple product allows the calculation of the changes in the generalised strains resulting from changes in the stress resultants applied to a partially yielded cross-section. The rigidity matrix [k*] and the transformation matrices [G*] and $[G^*]^T$ are given in Appendix VII.

When yielding has occurred,the approach is to insert a node at the yield boundary. The partially yielded panel is therefore broken into two panels, one of which is yielded along its full length, whilst the other remains elastic as shown in Fig. 7.6. Since the yield boundary moves as loading increases, the additional node moves

during the analysis and is termed a floating node. The pattern of yielding and hence the floating node positions can be calculated once the strain pattern in the cross-section is known. The strain is calculated by summing the strain resulting from flexure, axial load and bimoment with a residual strain pattern if residual strains are present.

As a result of yielding, the stress resultants change and differ from the original set. The differences are calculated and the adjustments to the generalised strains are determined. The adjustments are added to the original strain set and the process repeated until a required degree of accuracy is obtained. The process is a tangent or Newton-Raphson correction procedure. The tangents result from the use of the section properties based on the transformed section.

A computer program named CAFOP has been written to carry out the analysis. The program calculates the centroidal position of the cross-section and locates the origin axes at this location. Hence, the stress resultants acting on the cross-section are defined relative to an axis system which is located on the centroid of the cross-section. The maximum strain in the cross-section is set to the yield strain and the stress resultants are incremented until failure or non-convergence takes place.

7.5.3 Example of General Inelastic Cross-Section Analysis

In order to evaluate the general inelastic cross-section analysis, a simple problem involving an unequal channel was solved. The dimensions of the channel are shown in Fig. 7.7 and the properties of the section are given in Table 7.1. The channel was subjected to a major-axis and minor-axis bending moment, an axial compression and a bimoment. The non-dimensional ratios of the stress resultants are given in Table 7.2. The mild steel had a yield strength of 312 MPa and the bilinear stress-strain curve used in the analysis had the properties described in Section 7.5.1.

From the analysis the ultimate major-axis bending moment for the channel was 8.99×10^6 Nmm. The major-axis and minor-axis curvatures and the rate of change of twist have been plotted against the major-axis moment in Fig. 7.8. First yield occurred in the section at the outstand of the bottom flange at a major-axis moment of 4.91×10^6 Nmm. It was at this value of bending moment that the three curves in Fig. 7.8 became non-linear. As the panels of the section yielded, the effective area of the cross-section decreased, resulting in the increased rates of curvature and twist. The rate at which the panels yield is shown in Fig. 7.9. The major-axis bending moment at which the panels began to yield is shown as a ratio of the first yield moment. Yielding began

at the bottom flange extremity (point E in Fig. 7.9) and continued until the load factor reached a value of 1.29. At this load, yielding began at the bottom flange and web junction (points C and D). The third onset of yielding occurred at a load factor of 1.80. At this level of load, yielding occurred at the web and top flange junction (points A and B). The section failed when the load factor reached a value of 1.83.

The effect of the panel yielding upon the properties of the cross-section is shown in Fig. 7.10. As the load factor increases to unity, there is no yielding and the section properties are obviously constant. As the load factor increases further the effective section properties are reduced. In the figure, the load factor is plotted against the moments of inertia about the x and y axes respectively and the slope of the neutral axis. The slope of the neutral axis is a function of the moments of inertia. The effect of the yielding at the bottom flange and web junction at a load factor of 1.29 is clearly shown in the response of the slope of the neutral axis.

7.6 INELASTIC BUCKLING OF MEMBERS

A finite strip analysis is presented for determining the initial buckling stresses of any structural element consisting of a series of thin flat plates rigidly connected together at their longitudinal edges. The buckling analysis is applicable to sections in which the load to cause

yielding lies well below the buckling load. This is shown as the inelastic buckling range in Fig. 7.2. Hence, the analysis enables a deteriorated critical load of a partially yielded section to be evaluated. The finite strip inelastic buckling method is not applicable to slender plate elements in which post-local-buckling occurs followed by yielding at the edges of the plate.

7.6.1 A General Analysis

The finite strip method of analysis was presented by Cheung (1976) and has been discussed in Chapter 6. Przemieniecki (1973) has shown how the method can be used to predict the initial local buckling stresses of plate assemblies under biaxial compression. His analysis was applicable to a wide range of structures and was based upon the assumption that in a local buckling mode, all line junctions between component plates remain perfectly straight. However, this is invalid for longer wavelength modes. Wittrick (1968A and 1968B) has solved the buckling differential equations to determine the stiffness matrix. However, Plank and Wittrick (1974) have used an energy method to determine the stiffness matrix. The former approach results in a continuous eigenvalue problem whereas the latter results in a linear eigenvalue problem. Hancock (1978) has used the latter approach to study the local, distortional and lateral buckling of beams. As part of the present thesis the method has been extended to allow an inelastic analysis to be

performed, with the inelastic material properties replacing the elastic properties in the yielded regions of the section.

Each component plate element is treated as a single element and it is assumed that all three components of displacement vary sinusoidally along any longitudinal line when buckling occurs. In this way the partial differential equations governing the in-plane and out-of-plane deformations of the component plates are reduced to ordinary differential equations which can then be solved. The stiffness matrices are derived relating the amplitude of the sinusoidally varying forces and displacements on the longitudinal edges of the plate. Each edge has therefore four degrees of freedom, consisting of a rotation and three translations. Two assumptions are required in the derivation of the stiffness matrix for the method. The first is that the plate behaves according to plate theory. The second assumption concerns the displacement fields used in the analysis of a strip. The plate theory and the displacement fields used are the same as those presented by Cheung. The plate theory used by Cheung is the orthotropic theory derived by Timoshenko and Woinowsky-Krieger (1959).

The method for the calculation of the stability matrix from the potential energy resulting from the longitudinal in-plane forces also has been presented by Cheung. The stability matrix for flexural displacements was first

presented by Przemieniecki (1973) and the stability matrix for membrane displacements was first developed by Plank and Wittrick (1974).

The buckling analysis can be represented in matrix format as a linear eigenvalue problem by Eq. (7.17).

$$[K] \cdot \{\delta\} - \lambda [G] \cdot \{\delta\} = \{0\} \quad \ldots (7.17)$$

where [K] and [G] are the stiffness and stability matrices, λ is a load factor and $\{\delta\}$ is the vector of nodal line displacements. The values of λ for which the determinant of the coefficients of $\{\delta\}$ in Eq. (7.17) vanishes are the eigenvalues. The corresponding values of $\{\delta\}$ are the eigenvectors.

The eigenvalue problem is solved by using the direct methods set out by Bishop et. al (1965). These methods involve the reduction of Eq. (7.17) to the standard eigenvalue problem set out in Eq. (7.18).

$$[A] \cdot \{\delta^*\} - \lambda^* [I] \cdot \{\delta^*\} = \{0\} \quad \ldots (7.18)$$

where $[A] = [L]^{-1} \cdot [G] \cdot [L]^{-T}$

$$[K] = [L] \cdot [L]^T$$

$$\{\delta^*\} = [L]^T \cdot \{\delta\}$$

$$\lambda^* = 1/\lambda$$

Householder's tridiagonalisation (Wilkinson [1960]) and Sturm's sequence property (Bishop et. al. [1965]) are used to extract the lowest eigenvalue from the matrix [A]. A method is used for the calculation of the corresponding eigenvector of the tridiagonal matrix derived from [A] (Wilkinson [1958]). The mathematical analysis for the method is set out in Hancock (1977B).

7.6.2 Inelastic Buckling Analysis Examples

A computer program named BFINST has been used to study the buckling behaviour of thin-walled members. A stress distribution corresponding to the action of one or to a combination of stress resultants can be applied to the cross-section and the load factor determined for a particular buckle half wavelength. Alternatively, the program can be used to determine the inelastic buckling load for a cross-section in which the stiffness of the yielded portions has been deteriorated. For the examples presented in this Section the material will be given an infinite value of yield stress and hence the inelastic capabilities of the program will not be tested. An analysis which involves the stress distribution reaching the inelastic region with subsequent panel yielding will be investigated in the following Section 7.7.

The program has been used to study the buckling behaviour of simply supported channel members. The channel analysed was the Armco 1572

section shown in Fig. 4.1. Each channel was divided into a series of ten longitudinal strips. The web consisted of four strips, the flanges consisted of two strips each and each lip constituted another strip. A total of six different stress conditions were investigated. Five of the stress conditions consisted of a concentric axial force, a major-axis bending moment, a minor-axis bending moment about both the strong and weak axis and a bimoment. The sixth stress condition, referred to as Load Case 1, was identical to the problem considered in the analysis of shear straining investigated in Chapter 6. The loading pattern consisted of equal and opposite forces applied to the web, 80 mm apart and symmetrically placed about the web centreline.

The buckle half wavelength and the corresponding buckling stress of each beam were investigated. In general, a beam of given length may buckle in a number of half waves. In this analysis, the buckling stress of the beam has been calculated using only one term of the Fourier series. The number of the particular Fourier terms used is equal to the number of half wavelengths of buckle over the length of the beam. The buckling stress versus buckle half wavelength for the channel section under axial compression has been plotted in Fig. 7.11. The buckling stress has been calculated for a large number of buckle half wavelengths. The buckling modes for the channel have been shown in Fig.

7.12. The modes are shown for buckle half wavelengths of 120 mm, 600 mm and 5000 mm. The three locations corresponded to the minimum values of buckling stress of the two troughs shown in Fig. 7.11 and a position on the elastic lateral buckling curve shown in the right hand side of the diagram. The first buckling mode shown in Fig. 7.12 corresponded to a local buckle of the web of the channel. The second location demonstrated the significant distortion that took place. The third position corresponded to a flexural-torsional buckle with no distortion of the cross-section. Hence, the complete curve shown in Fig. 7.11 demonstrated a continuous transformation from local through distortional to lateral buckling. Distortional buckling occurred at intermediate wavelengths when the beam was not long enough for cross-sections to displace as rigid bodies but where the line junctions between plate elements do not remain straight as in local buckling.

The curve shown in Fig. 7.11 is for a single buckle half wavelength. Similar curves may be calculated assuming that the beam buckles in two, three or more half wavelengths. The family of curves can simply be determined by moving the complete curve to the right. The new positions of the curves must produce identical values of buckling stress at beam lengths twice, three, etc., times larger than the original beam. The transformation is possible since the buckle length in the stiffness and stability matrices always occurs divided by the number of half

wavelengths. The envelope of the lowest points on the family of curves defines the minimum buckling stress versus beam length.

The buckling curve for the channel subjected to a major-axis bending moment is shown in Fig. 7.13. The buckling modes for the channel are shown in Fig. 7.14. At a buckle half wavelength of 75 mm the buckling mode corresponded to a local buckle. The section buckled as a result of a compression flange and web interaction. As in the previous analysis, a distortional buckle developed at the intermediate range of half wavelength. Finally, a lateral-torsional buckling mode developed for the longer wavelengths.

The next stress distribution investigated was caused by a minor-axis bending moment in which the web of the channel was in compression. This was the stronger of the two types of minor-axis bending. Fig. 7.15 and Fig. 7.16 show the buckling curve and the buckling modes for the stress distribution respectively. The buckling modes differ from the previous two examples in that there is no minimum on the curve at a distorional mode of buckling. However, a local buckling mode involving the web of the channel and a lateral-torsional mode were still the characteristic failure modes. For a channel subjected to a minor-axis bending moment in which the flanges were in compression, the buckling curve and buckling modes are shown in Fig. 7.17 and Fig. 7.18 respectively. This loading

condition produced the more severe bending stress distribution. This was evident in the buckling curve in which the buckling stresses were lower for the equivalent buckle half wavelengths than in the previous example. The local buckling mode showed the lip and compression flange interaction failure occurring at low half wavelengths.

The fifth example consisted of a stress distribution resulting from the application of a bimoment. The buckling curve is shown in Fig. 7.19 and the buckling modes are shown in Fig. 7.20. The buckling curve displayed a characteristic very different from that of the other examples. Instead of the lateral-torsional buckling stress decreasing with an increase in the half wavelength, the stress increased appreciably. At low half wavelengths, the local buckle consisted of a web buckle whilst at medium wavelengths the distortional mode became evident.

The final example considered was Load Case 1 referred to earlier in Section 6.4.2. The arrangement of the loads resulted in the channel being subjected to a major-axis bending moment and a bimoment. The buckling curve for the resulting stress distribution is shown in Fig. 7.21. The curve is similar to that resulting from a major-axis bending moment alone. Again, the buckling modes passed from a local buckle to a distortional buckle and finally to a lateral-torsional buckle. The buckling modes for the channel are shown in Fig. 7.22.

7.7 INELASTIC BUCKLING OF STRUCTURAL SYSTEMS

The inelastic buckling behaviour of structural systems is a complex problem. Most approaches rely upon the analysis of the overall behaviour of the structure. However, these types of analyses have limitations because of their complexity. For structural systems which are composed of cold-formed members in which sufficient lateral bracing is provided to prevent an overall member failure, the most likely mechanism of collapse will result from local buckling. In this Section, a method for estimating a lower bound to the collapse strength of thin-walled structural systems will be presented. The method performs discrete inelastic buckling analyses at locations around the structural system. The locations are the critical regions in the system where local buckling is likely to occur. However, any location along any member may be examined.

7.7.1 A General Analysis

The matrix displacement analysis presented in Chapter 3 is used to perform an elastic analysis of the particular thin-walled structure. This analysis enables the determination of the four stress resultants essential for the calculation of the longitudinal stress distribution. These are the moments about the major and minor axis, the axial force and the bimoment. The accuracy with which the thin-walled

analysis was able to predict the longitudinal stress distribution was studied in Section 6.6. A comparison between the experimentally measured stress distributions and the theoretical values indicated the accuracy of the analysis. Hence, for any general structure, the four longitudinal stress resultants could be found for any location. The ratios of the stress resultants with respect to the major-axis bending moment provided the data for an inelastic cross-section analysis which was reported earlier in this Chapter. Such an analysis enabled firstly, the determination of the moment-curvature relationship of the member at the particular cross-section location and secondly, the amount of yielding that had taken place for a particular load. The width of the yielded regions in the panels of the cross-section was essential for the use of the finite strip buckling analysis presented earlier in Section 7.6.

A load factor having the value of 1.0 when first yielding of the cross-section occurred, was used to quantify the strength reserve of the cross-section. Hence, a buckling analysis was performed for a load factor equal to unity. Subsequent analyses were performed for increasing values of load factor with the increase in panel yielding being taken into account. A family of local buckling curves were produced as shown in Fig. 7.23. The approach involved obtaining the load factor of a particular buckling curve whose minimum eigenvalue was equal to the load factor

and ensuring that the buckle half wavelength corresponding to the minimum value of eigenvalue lay within the local buckling region. For example, referring to Fig. 7.23, the curves A, B and C were calculated using yielded regions determined at load factors of 1.0, 1.25 and 1.5 respectively. The minimum value of eigenvalue for each curve is 1.46, 0.90 and 0.42 respectively. Hence a curve D is required whose load factor (1.13) is equal to the minimum eigenvalue (1.13). The load factor for curve D may be found from extrapolating the results of the three previous curves and the procedure will be presented in the following example. Once the load factor was obtained the magnitude of the stress resultants which caused local instability could also be calculated. Hence, knowing the ultimate stress resultants, the failure load of the cross-secton was obtained. However, the accuracy of the method would be enhanced if the actual stress resultants at the ultimate load were known. Once yielding has taken place, a redistribution of the stress resultants occurs around the structure. For simplicity the ratios of the stress resultants are assumed constant until failure. For light-gauge structures, the load factor to cause collapse is usually not more than 1.4 and hence the accuracy of the method relies upon the premise that little redistribution has occurred.

7.7.2 Example of Buckling Analysis

The constant moment beam tests described in Chapter 4 involved the testing of thin-walled lipped channel beams with a span of approximately 1.9 m. The particular beam that will be used to demonstrate the ability of the method is the Armco 1572 specimen. The channel profile for this section was identical to the channel used for the frame members in the experimental study. The beam was restrained to prevent the application of minor-axis bending moment. An elastic analysis was used to determine the major-axis bending moment, axial force and bimoment. A small axial force and bimoment were present as a consequence of the testing apparatus. The value of each of the longitudinal stress resultants was verified from the strain readings recorded during the testing of the beam. The ratios of the stress resultants are shown in Table 7.3.

An inelastic cross-section analysis was performed for the channel cross-section. The theoretical major-axis moment-curvature relationship for the cross-section is shown in Fig. 7.24. The analysis showed that the channel had very little reserve of strength from the first yield bending moment to the moment for failure. The small amount of reserve of strength was also demonstrated in the constant moment beam tests. The tests revealed that under almost pure major-axis bending moment, failure occurred shortly after the first strain gauges indicated yielding

of the material. This is clearly shown in the test results plotted earlier in Fig. 4.15 and Fig. 4.16.

The yielded widths of the panels of the cross-section were also calculated from the inelastic cross-section analysis and are shown in Fig. 7.25. Yielding initially occurred at the web to flange connection (points B and C in Fig. 7.25) in the compressive region. Yielding spread rapidly along the compression flange because of the dominance of the major-axis bending moment. Almost the whole compression flange had yielded before yielding occurred in the tension flange. The rapid spread of yielding throughout the compression flange was another indication that the cross-section would have a small reserve of strength after the onset of yield.

Inelastic buckling analyses were performed for load factors of 1.0, 1.01, 1.02 and 1.03. The resulting local buckling curves are shown in Fig. 7.26. The buckle half wavelength for the minimum value of eigenvalue for each buckling curve is approximately equal to the width of the plate. When the minimum eigenvalue of each buckling curve was plotted against the load factor, the critical load factor was obtained when the eigenvalue was equal to the load factor. From the analysis the critical load factor was 1.015. The load factor corresponded to a major-axis bending moment of 9.771×10^6 Nmm. The experimental determination of the buckling moment for the 1572 beam produced

a value of 9.727×10^6 Nmm. Hence, the buckling moment prediction was a 0.45 per cent overestimate of the experimental buckling moment. In a loading case where the major-axis bending moment dominated the stress resultants, the inelastic buckling analysis accurately predicted the collapse loads. The beam analysed was subjected to a uniform bending moment over the entire length. However, the more general type of loading would be that of a moment gradient.

An approximate local buckling load for the channel may also be obtained. For a simplification of the compression flange, it may be assumed that the flange is built in at the junction with the web and simply supported at the lip stiffened edge. If it is also assumed that the buckle half wavelength is of the order as the width of the flange, as is shown in Fig. 7.26, the Column Research Committee of Japan (1971) gives the value of the buckling coefficient k as 5.65. Using this coefficient to determine the critical stress in the inelastic range of buckling (Bleich [1952]), a critical moment of 9.164×10^6 Nmm was produced. This value of critical moment is six per cent below the experimentally obtained value.

7.8 SUMMARY

1. A summary of local buckling behaviour and theory was presented. The effects of edge stiffeners and the effective width concept were mentioned. The interaction between local and overall buckling was also discussed.

2. A matrix method of analysis of inelastic *thin-walled open cross-sections of general* geometry has been presented. The analysis included longitudinal stresses resulting from restrained warping (bimoment). The method also took account of the effect of the moving instantaneous shear centre.

3. The analysis was applied to a thin-walled unequal channel. The channel was subjected to the four stress resultants producing longitudinal stresses. The ultimate moment was calculated and the effect of yielding upon the section properties was investigated.

4. A matrix method of analysis for determining the buckling loads of thin-walled open cross-section members has been presented. The buckling analysis assumed either an

infinite material yield stress or a finite value of yield stress with subsequent panel yielding leading to a decreased effective cross-section. The method utilised the finite strip analysis. With the stress distribution applied to the cross-section, the analysis sets up and solves an eigenvalue problem to find the buckling stress.

5. The method was applied to a lipped channel section. The channel was subjected to different stress distributions resulting from the application of six different loading cases. Panel yielding was not taken into account. The buckling stress and buckle mode were investigated for different buckle half wavelengths of the beam.

6. A method for determining the lower bound for the collapse strength of a structural system assuming a local buckling failure mode was described. The method utilised the elastic displacement analysis as well as the inelastic cross-section and finite strip buckling analyses.

7. A structural system consisting of a simply supported beam was analysed. The theoretical collapse load compared well with the measured collapse load.

A	=	$1800\ mm^2$
I_{xx}	=	$6.4714 \times 10^6\ mm^4$
I_{yy}	=	$1.4714 \times 10^6\ mm^4$
J	=	$2.160 \times 10^4\ mm^4$
I_w	=	$2.5739 \times 10^9\ mm^6$

TABLE 7.1 UNEQUAL CHANNEL SECTION PROPERTIES

$\frac{M_{y'}}{M_{x'}}$	=	-0.100
$\frac{B_{z'}}{M_{x'}.d}$	=	0.167
$\frac{F_{z'}.d}{M_{x'}}$	=	-0.300

TABLE 7.2 UNEQUAL CHANNEL STRESS RESULTANT RATIOS

$\frac{M_{Y'}}{M_{X'}}$	=	0.0
$\frac{B_{Z'}}{M_{X'}.d}$	=	0.0067
$\frac{F_{Z'}.d}{M_{X'}}$	=	0.106

TABLE 7.3 RATIOS OF STRESS RESULTANTS FOR SIMPLE BEAM PROBLEM

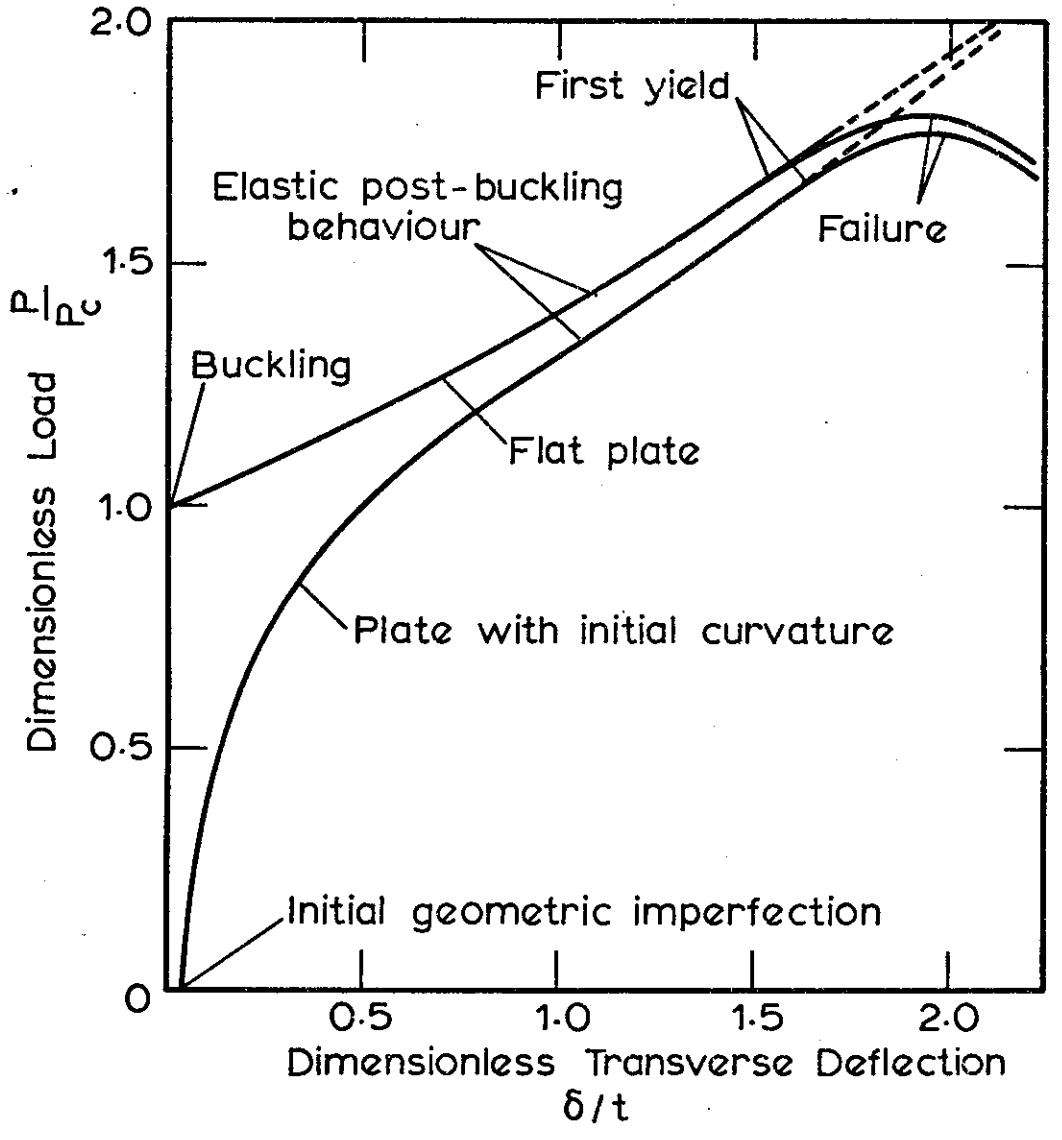

FIG. 7.1 POST-BUCKLING BEHAVIOUR OF THIN PLATES.

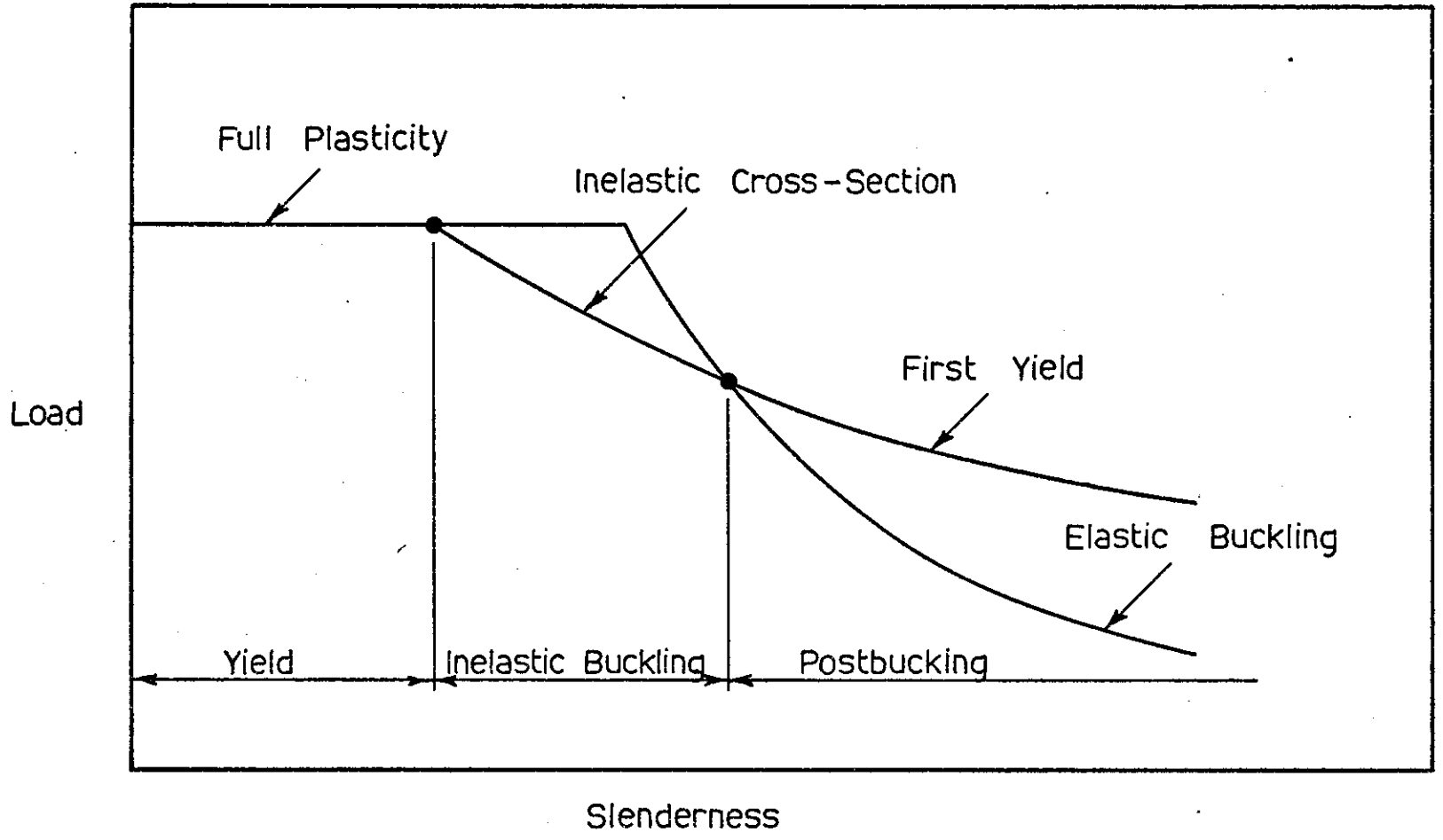

FIG. 7·2. ULTIMATE STRENGTH OF PLATES IN COMPRESSION

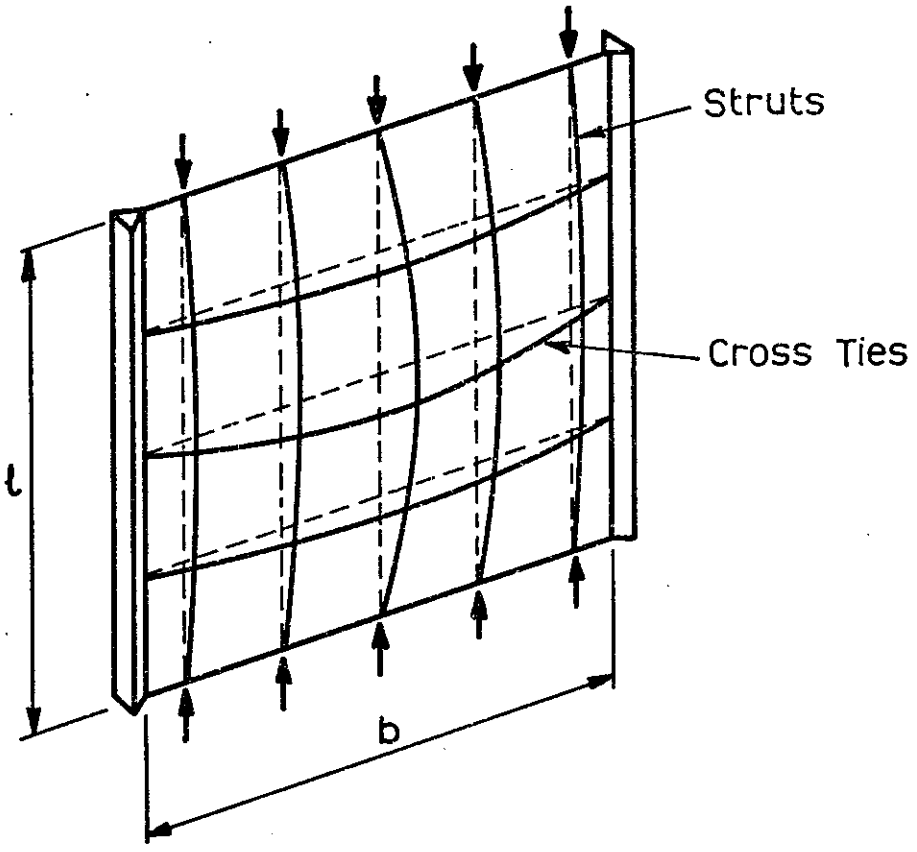

FIG. 7. 3 a POST BUCKLING BEHAVIOUR

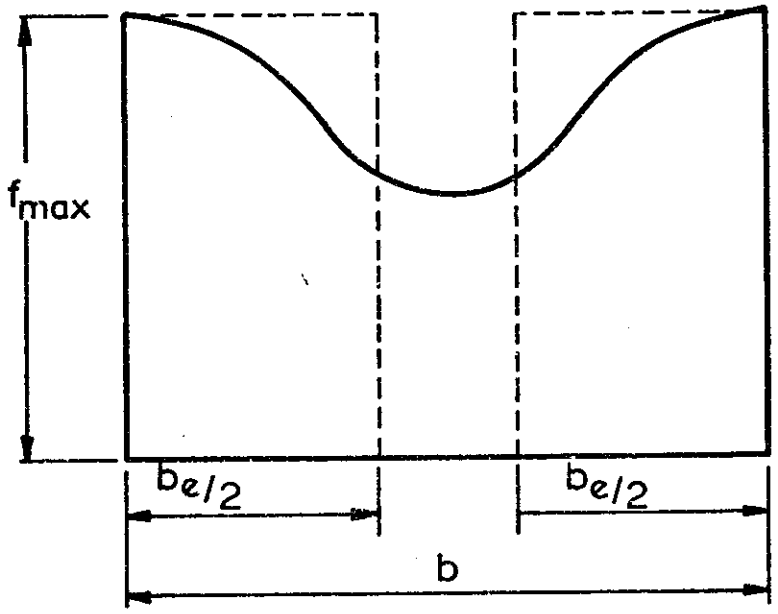

FIG.7.3 b EFFECTIVE WIDTH CONCEPT.

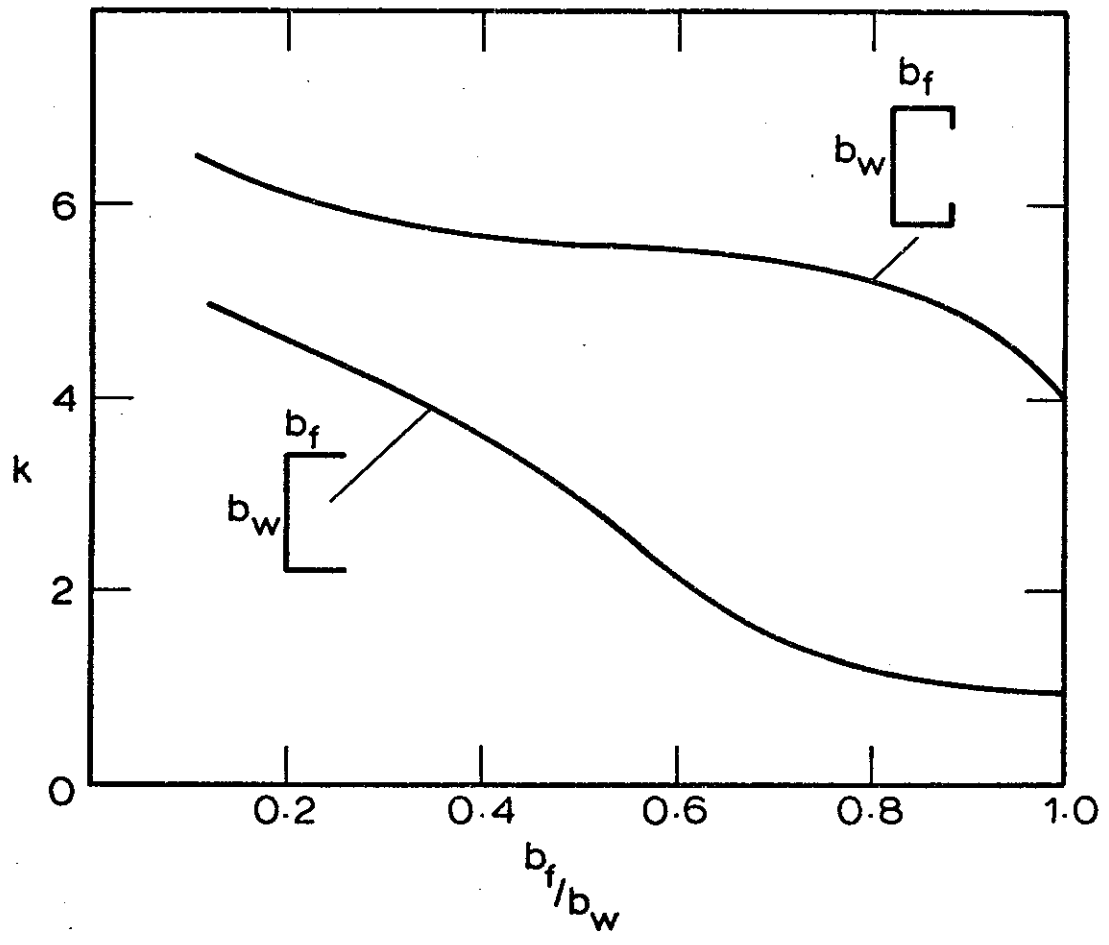

FIG. 7.4 BUCKLING LOAD COEFFICIENTS.

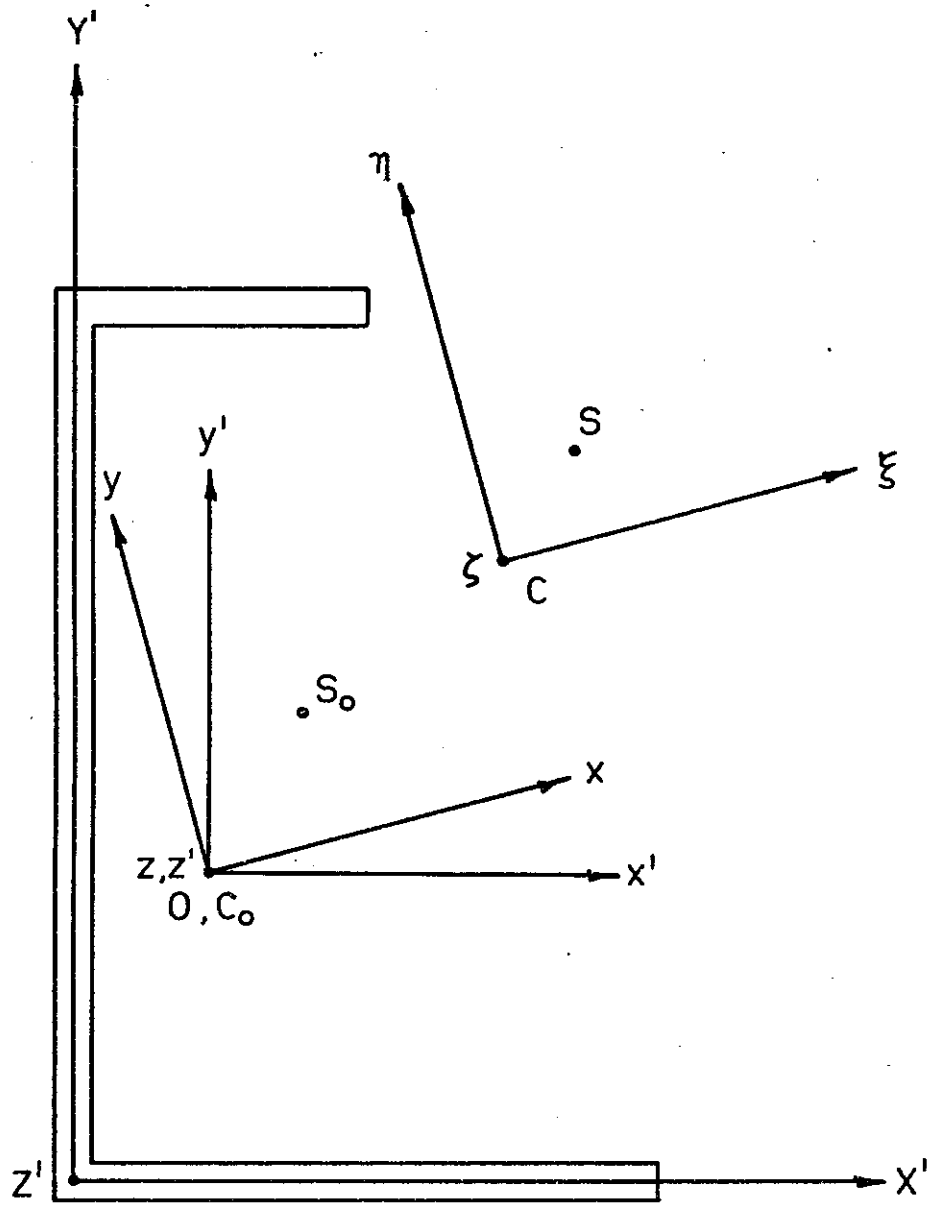

C_o, S_o = Original Positions

C , S = Position After Yield

FIG. 7·5. AXIS TRANSFORMATIONS

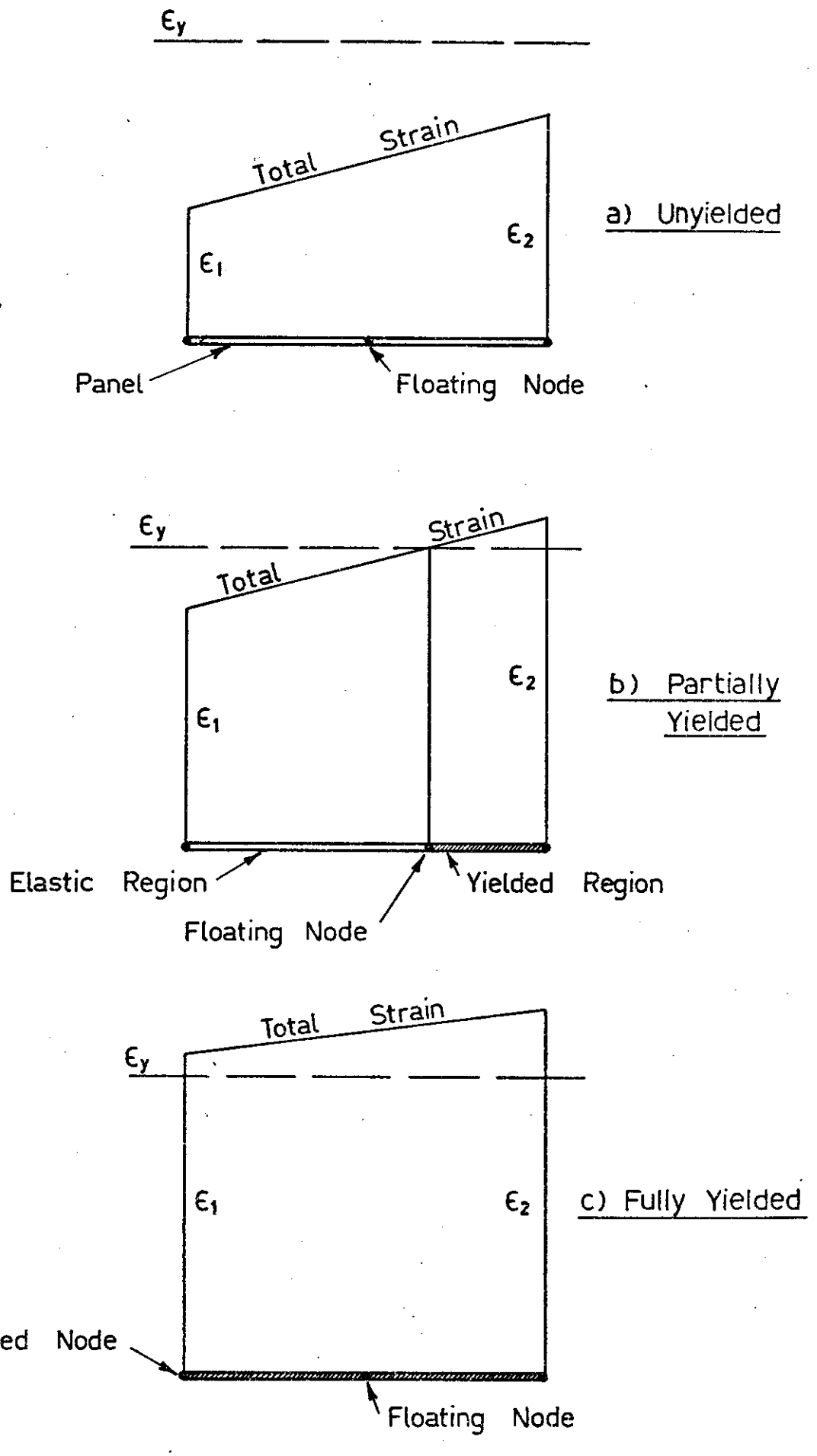

FIG. 7·6. PANEL YIELDING

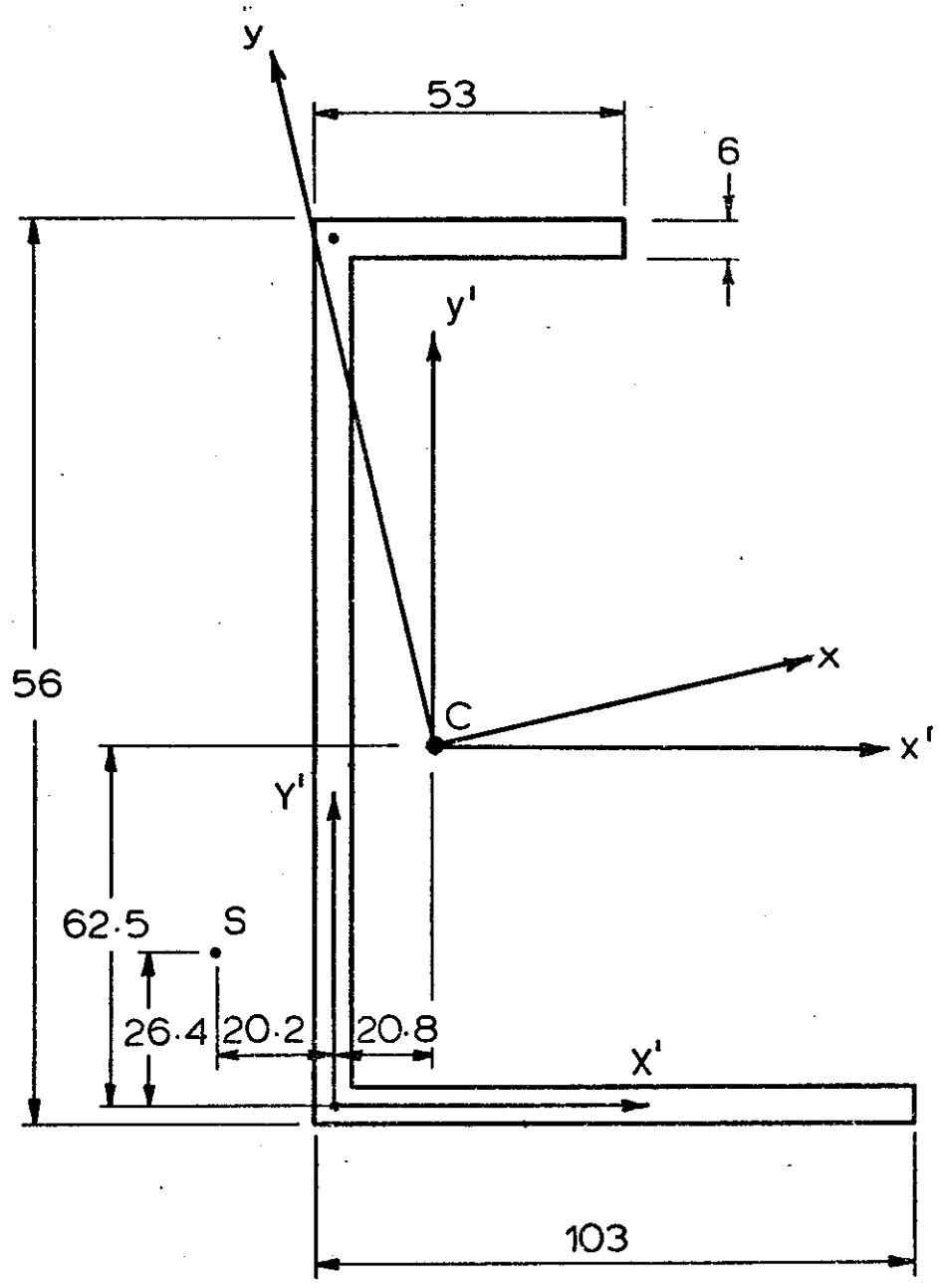

Dimensions in mm.

FIG. 7. 7 UNEQUAL CHANNEL DIMENSIONS.

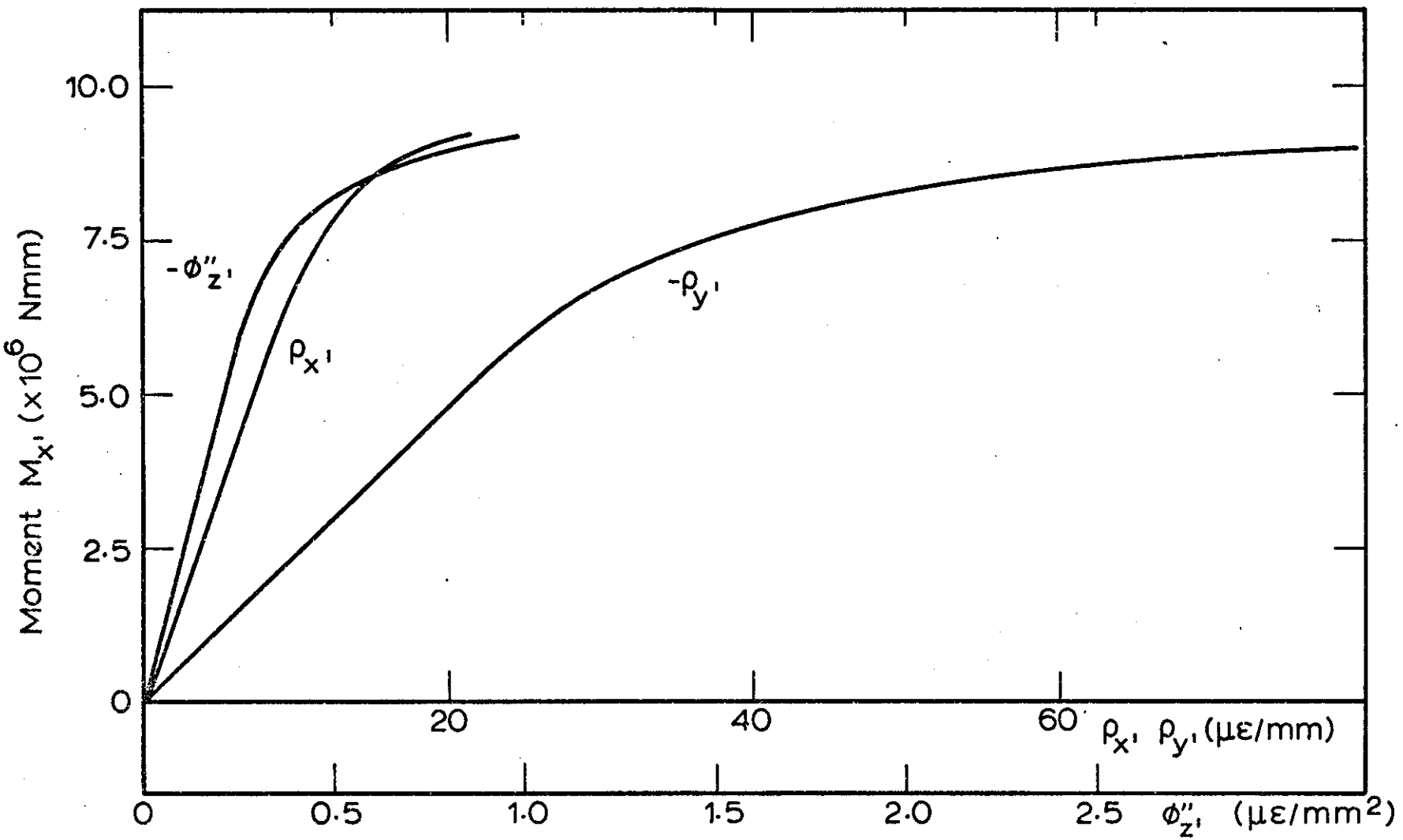

FIG. 7.8 UNEQUAL CHANNEL - MOMENT CURVATURE RELATIONSHIPS.

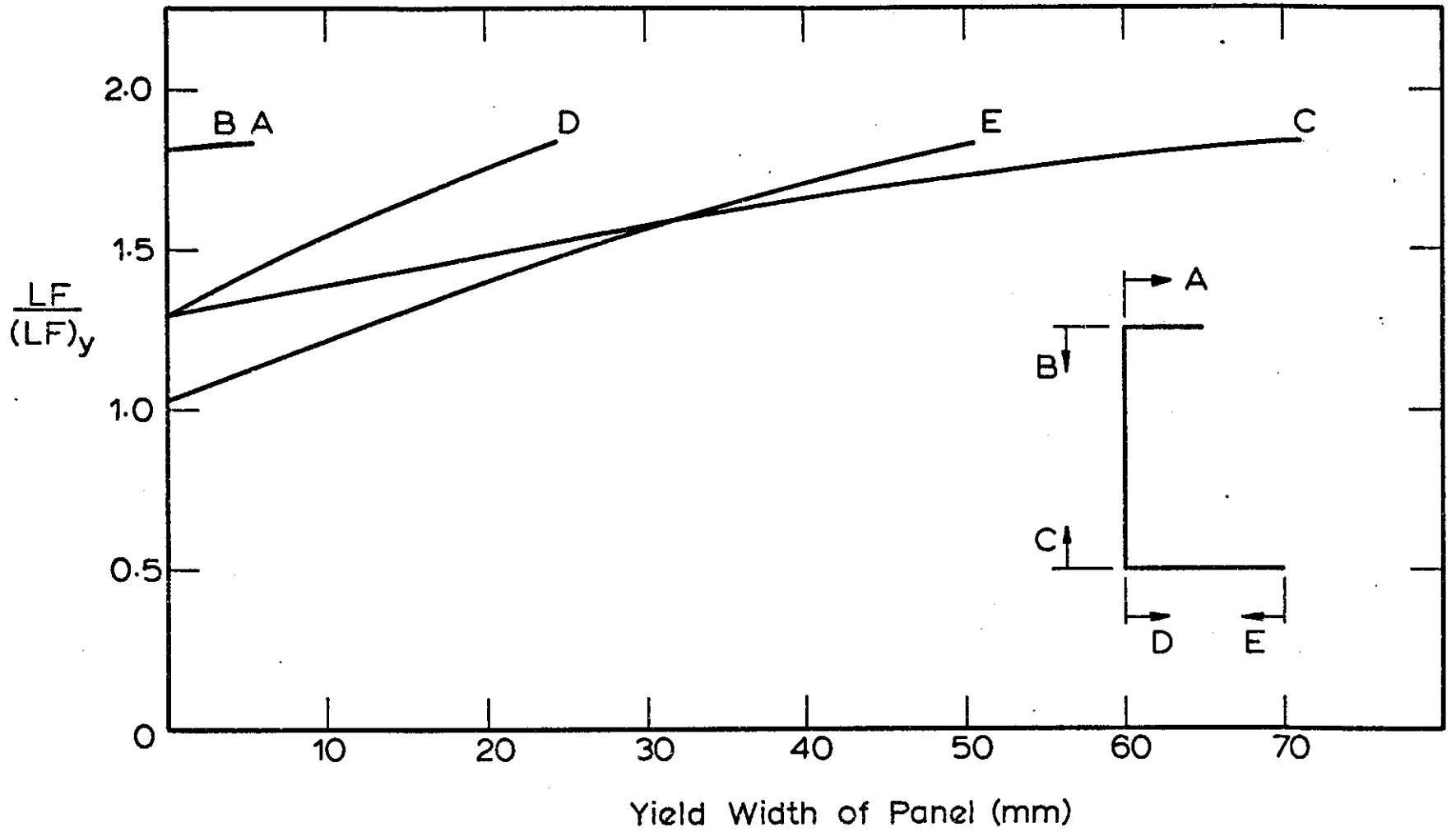

FIG. 7.9 UNEQUAL CHANNEL - PANEL YIELDING.

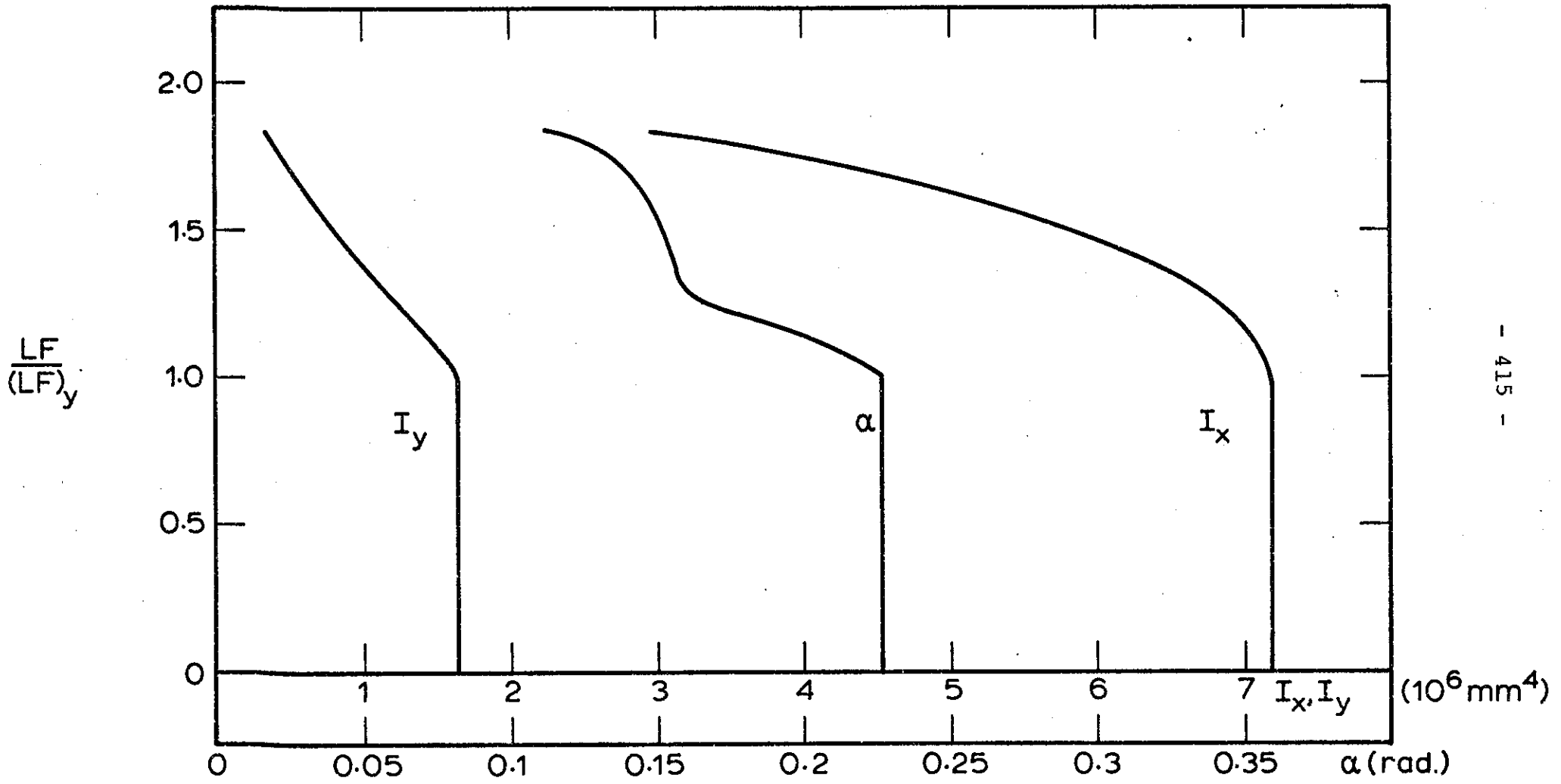

FIG. 7.10 UNEQUAL CHANNEL - EFFECT OF YIELDING UPON CROSS-SECTION PROPERTIES.

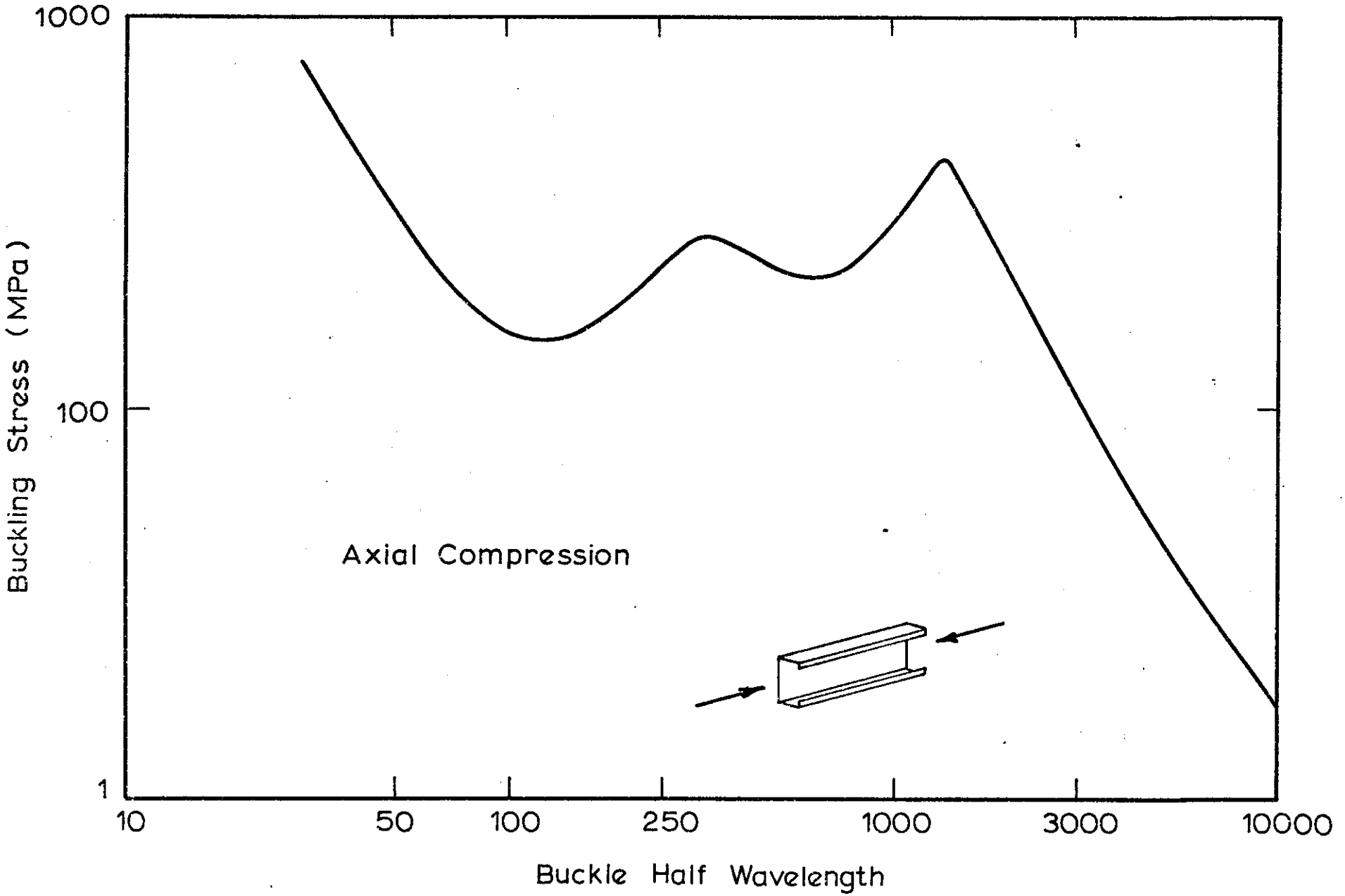

FIG. 7-11 AXIAL COMPRESSION BUCKLING STRESS VERSUS HALF-WAVELENGTH

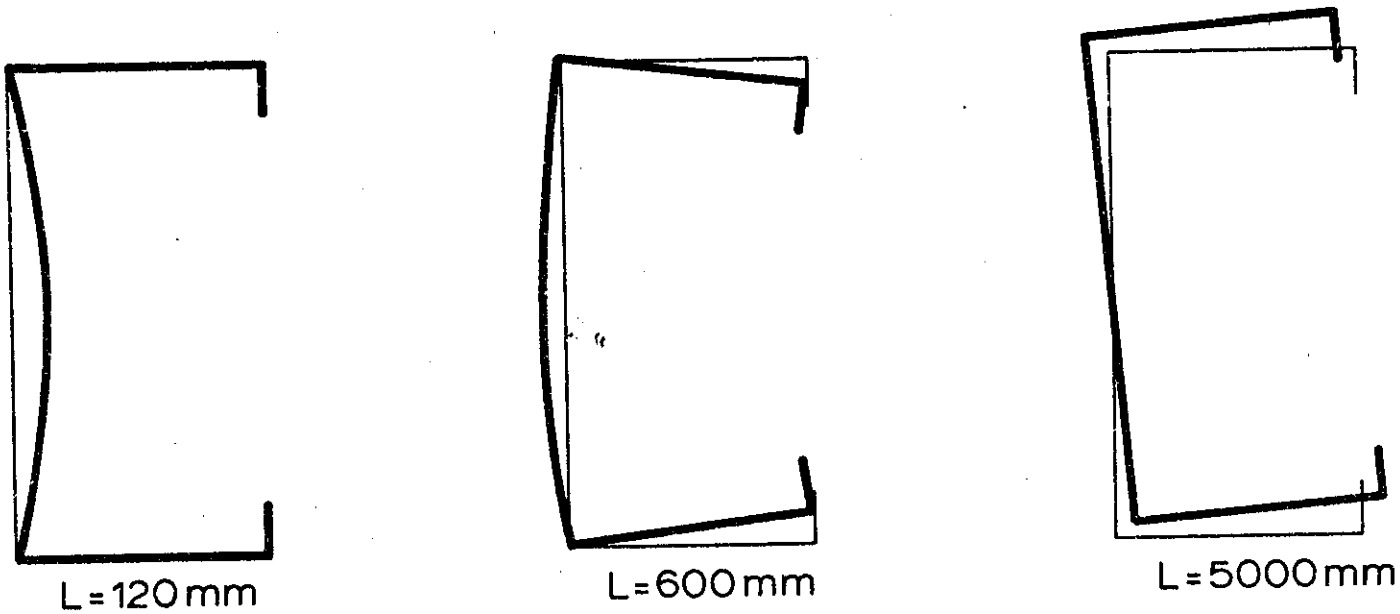

FIG.7.12 BUCKLING MODES OF CHANNEL UNDER AXIAL COMPRESSION.

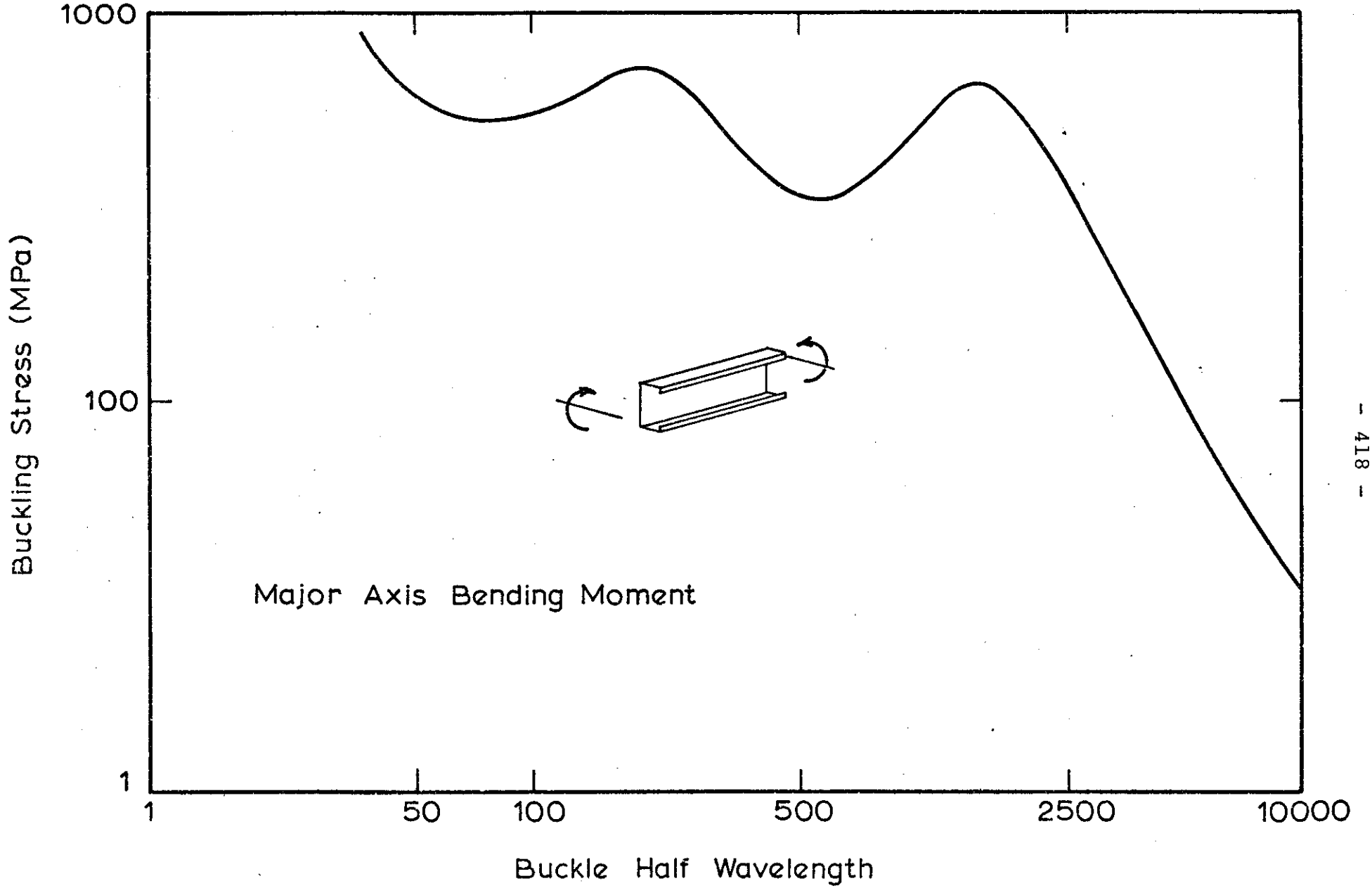

FIG.7.13 MAJOR AXIS BENDING MOMENT BUCKLING STRESS VERSUS HALF-WAVELENGTH FOR A CHANNEL

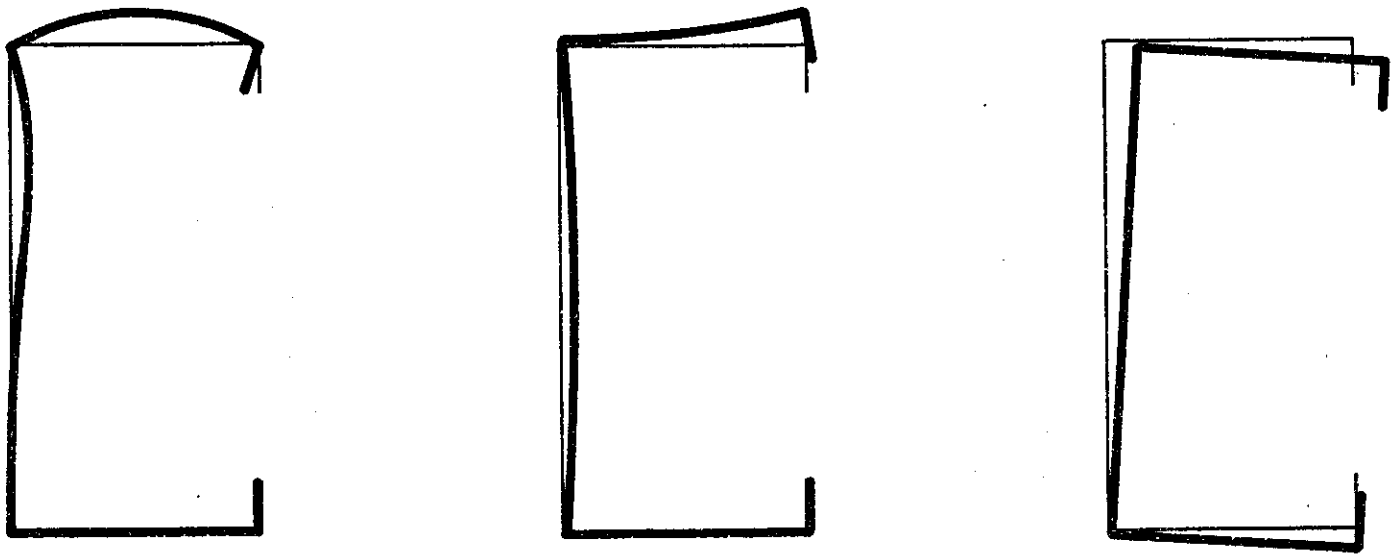

FIG.7·14 BUCKLING MODES OF CHANNEL UNDER MAJOR AXIS BENDING MOMENT.

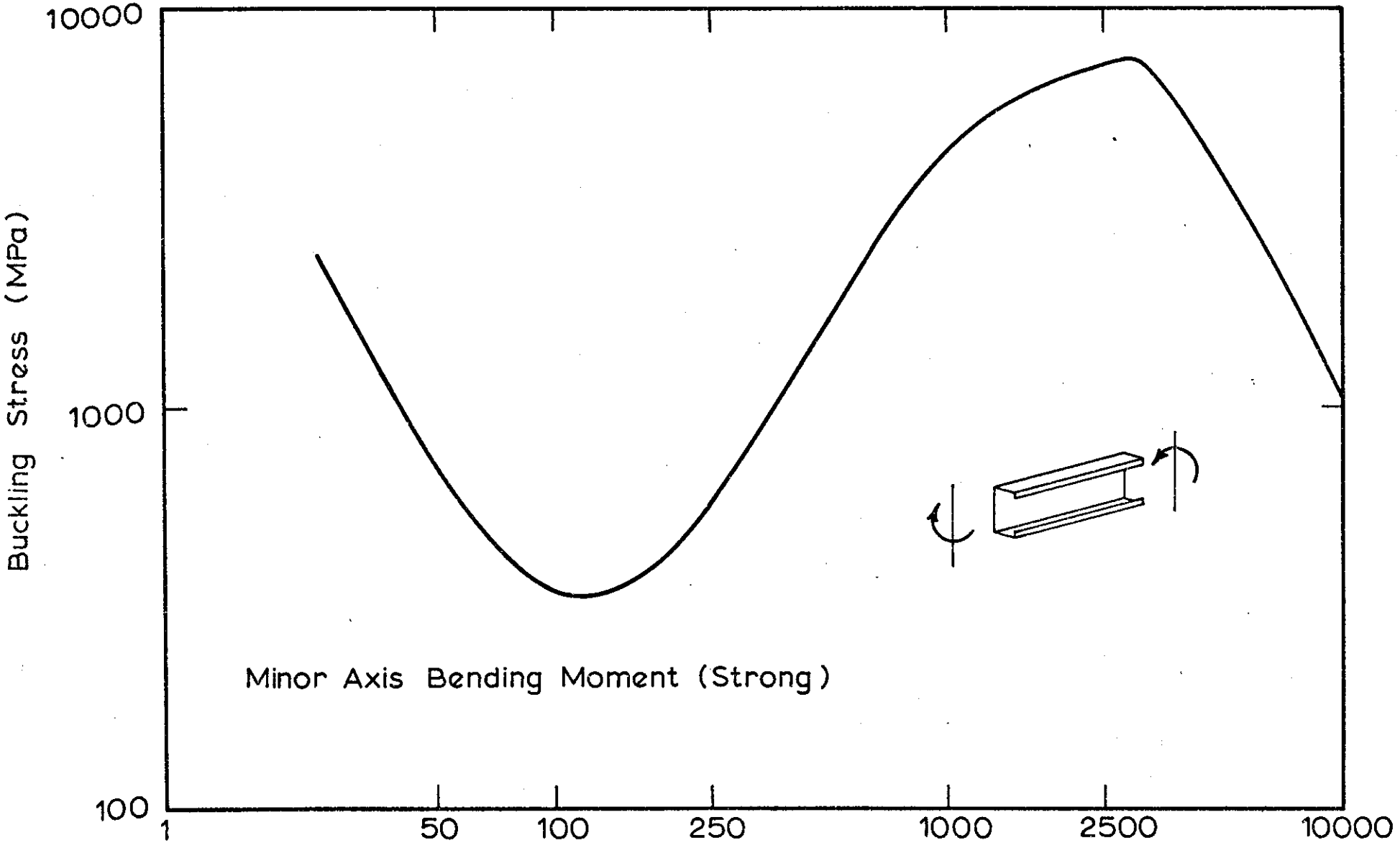

FIG. 7.15 MINOR AXIS BENDING MOMENT BUCKLING CURVE.

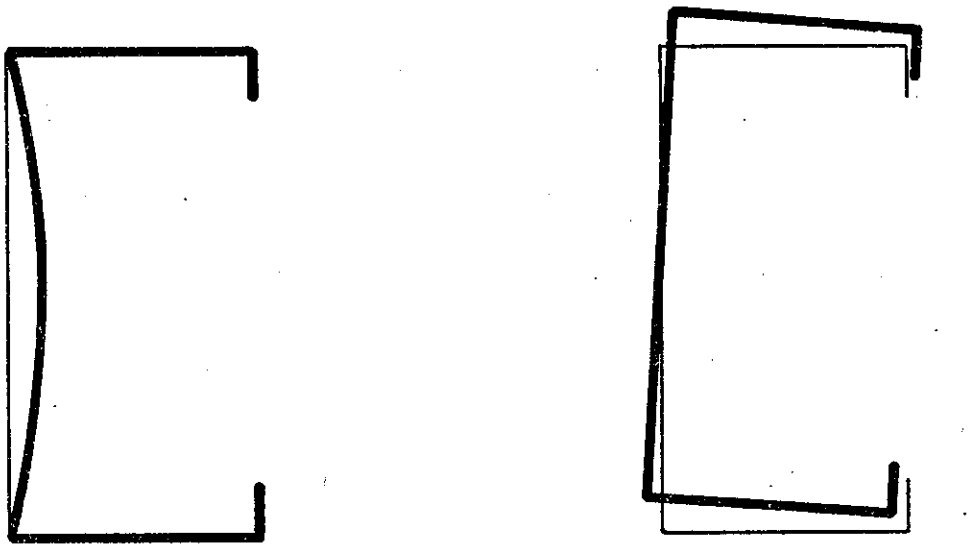

FIG. 7·16 BUCKLING MODES OF CHANNEL UNDER MINOR AXIS BENDING MOMENT - WEB IN COMPRESSION.

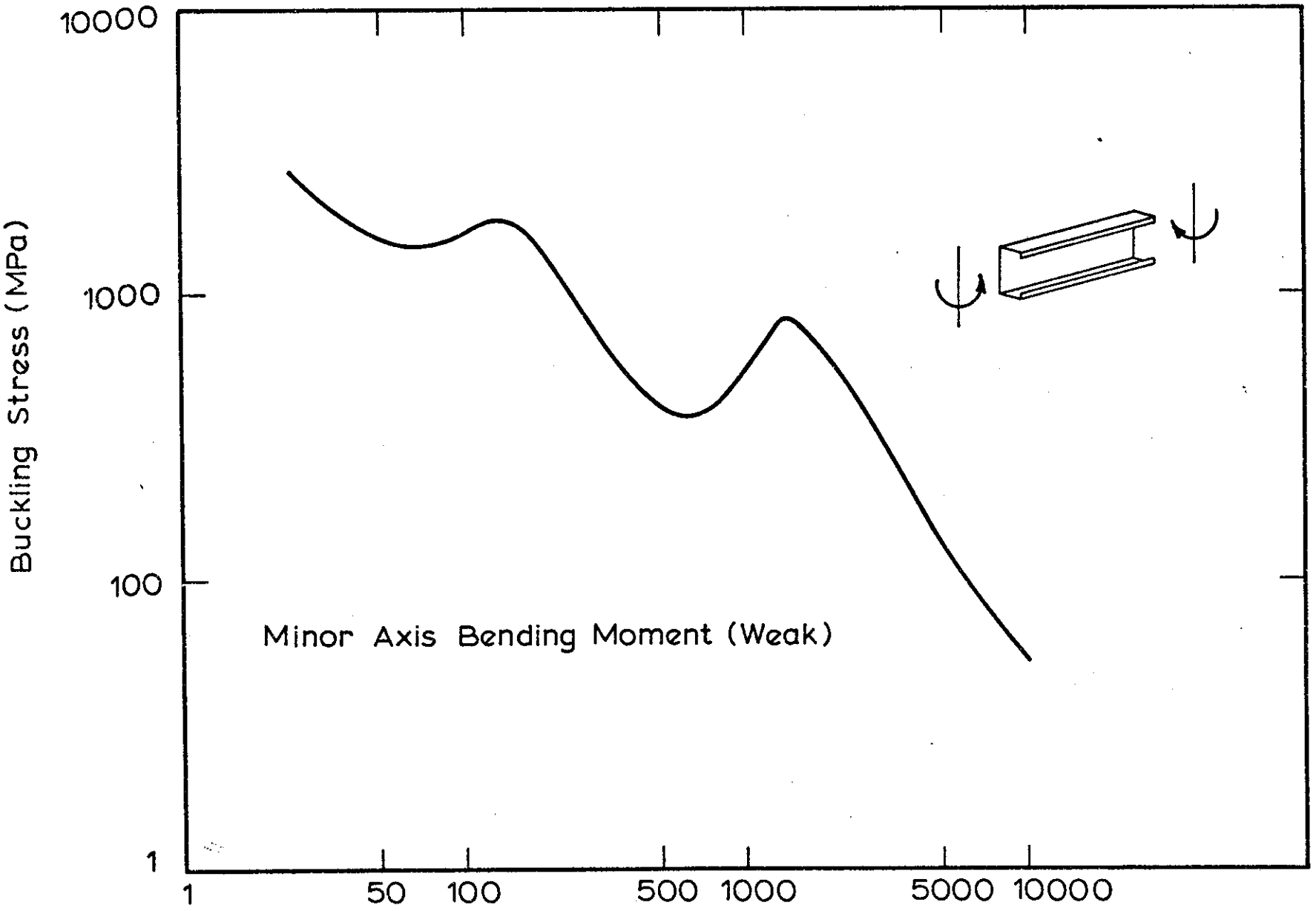
10000
1000
100
1
Buckling Stress (MPa)
Minor Axis Bending Moment (Weak)
1
50
100
500
1000
5000
10000
Buckle Half Wavelength

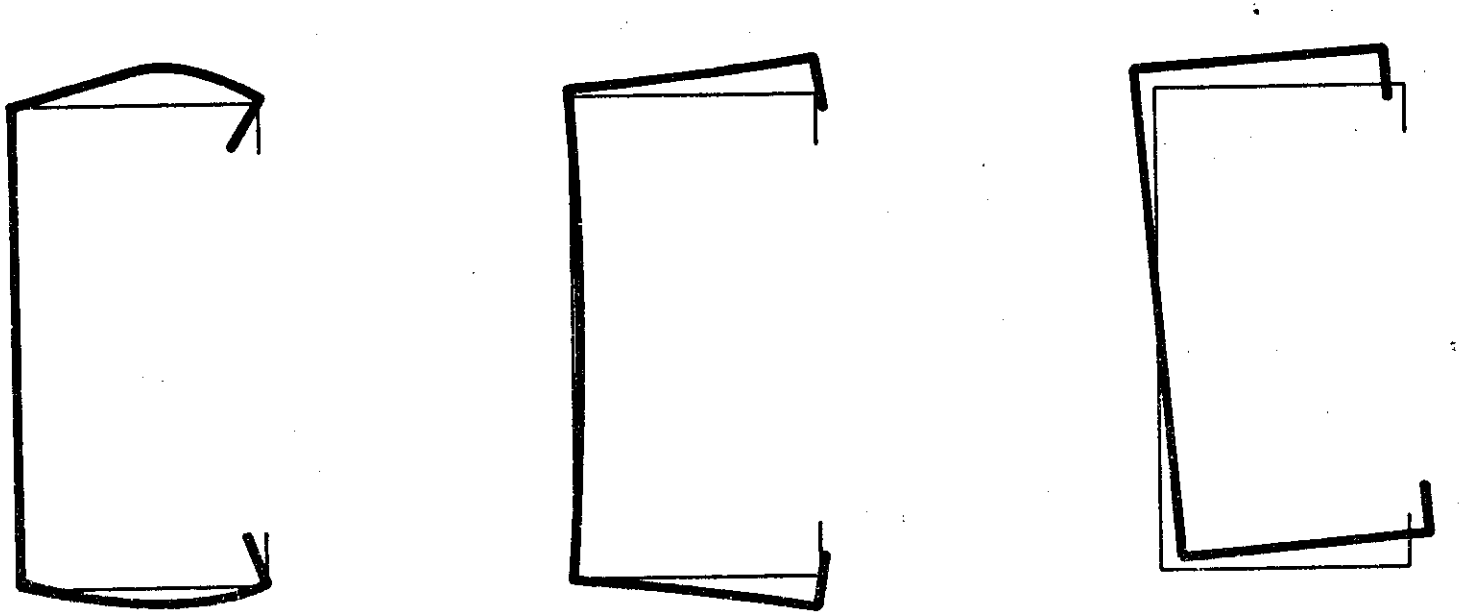

FIG. 7·18 BUCKLING MODES OF CHANNEL UNDER MINOR AXIS BENDING MOMENT - WEB IN TENSION.

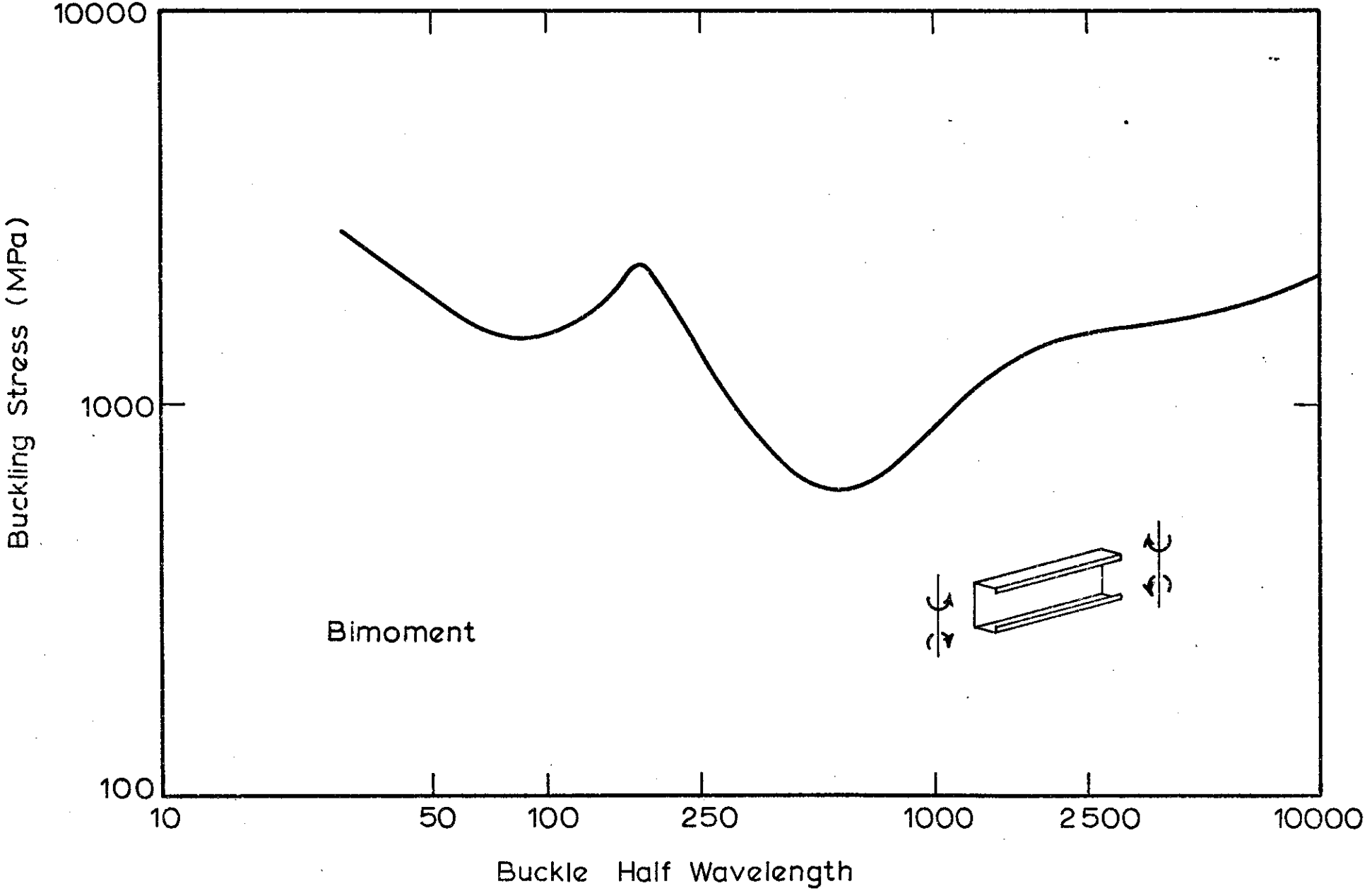

FIG.7-19 BIMOMENT BUCKLING STRESS VERSUS HALF-WAVELENGTH FOR A CHANNEL

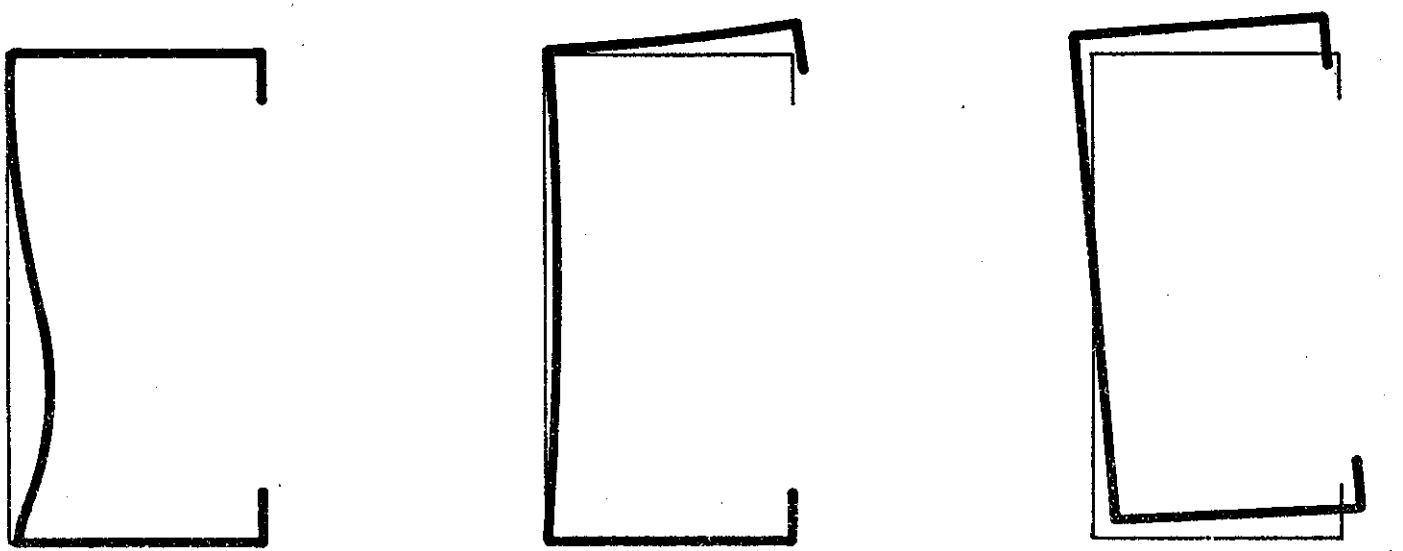

FIG. 7·20 BUCKLING MODES OF CHANNEL UNDER BIMOMENT.

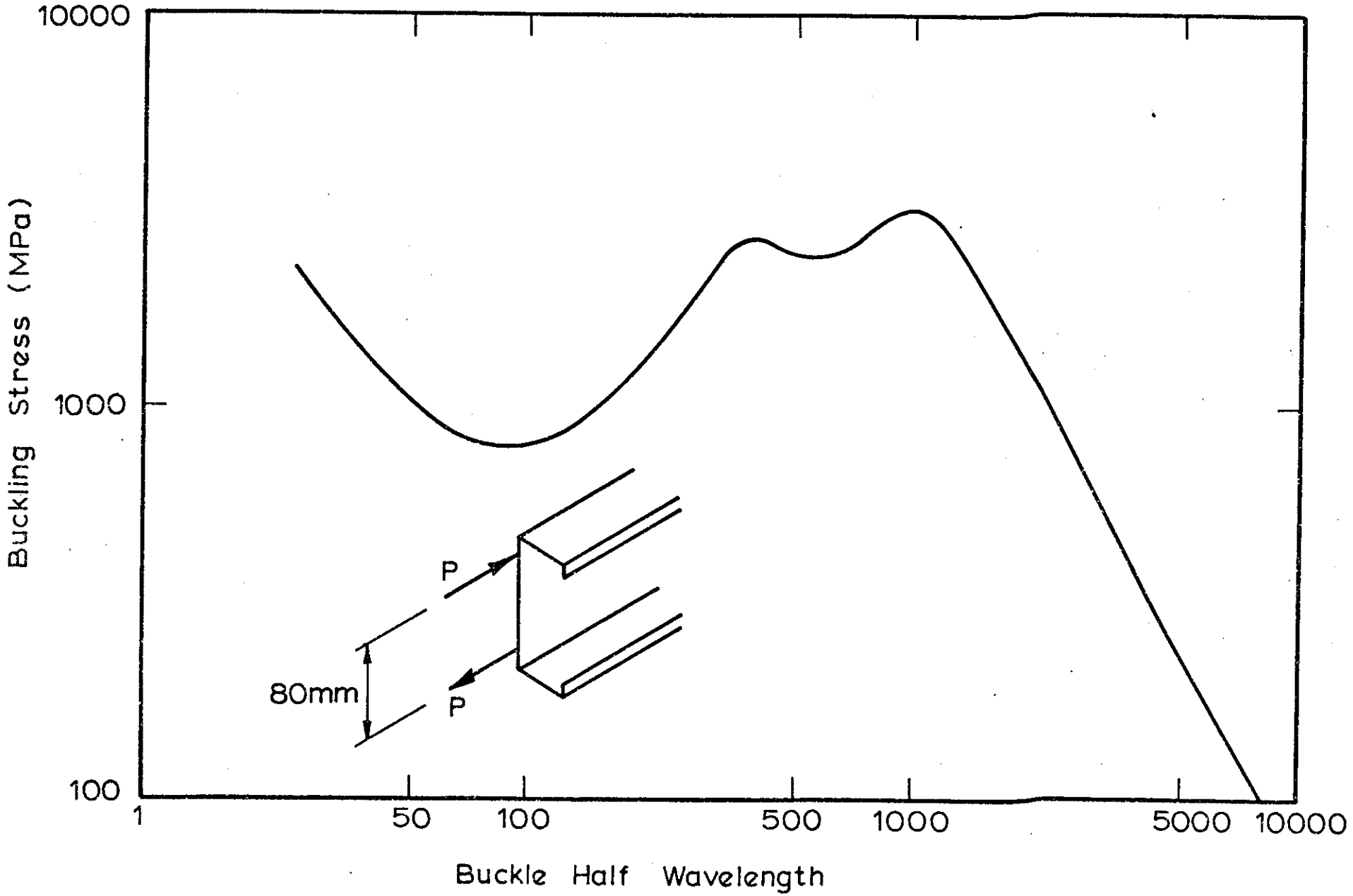

FIG. 7·21 LOAD CASE 1. BUCKLING CURVE.

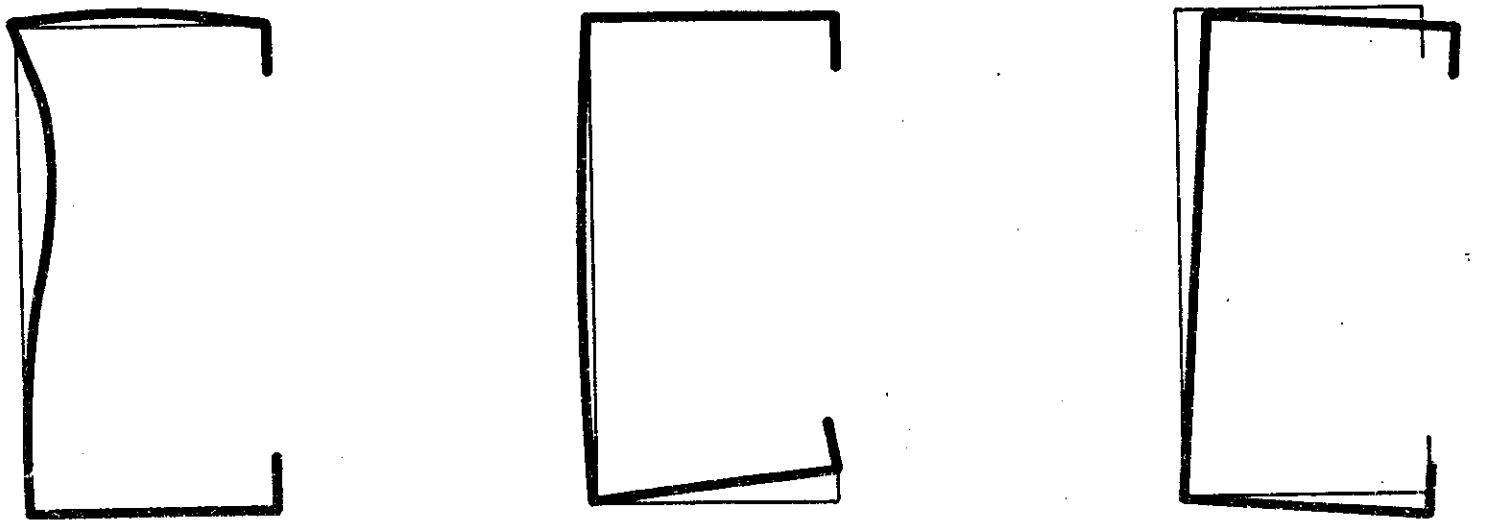

FIG. 7·22 BUCKLING MODES OF CHANNEL FOR LOAD CASE NO. 1.

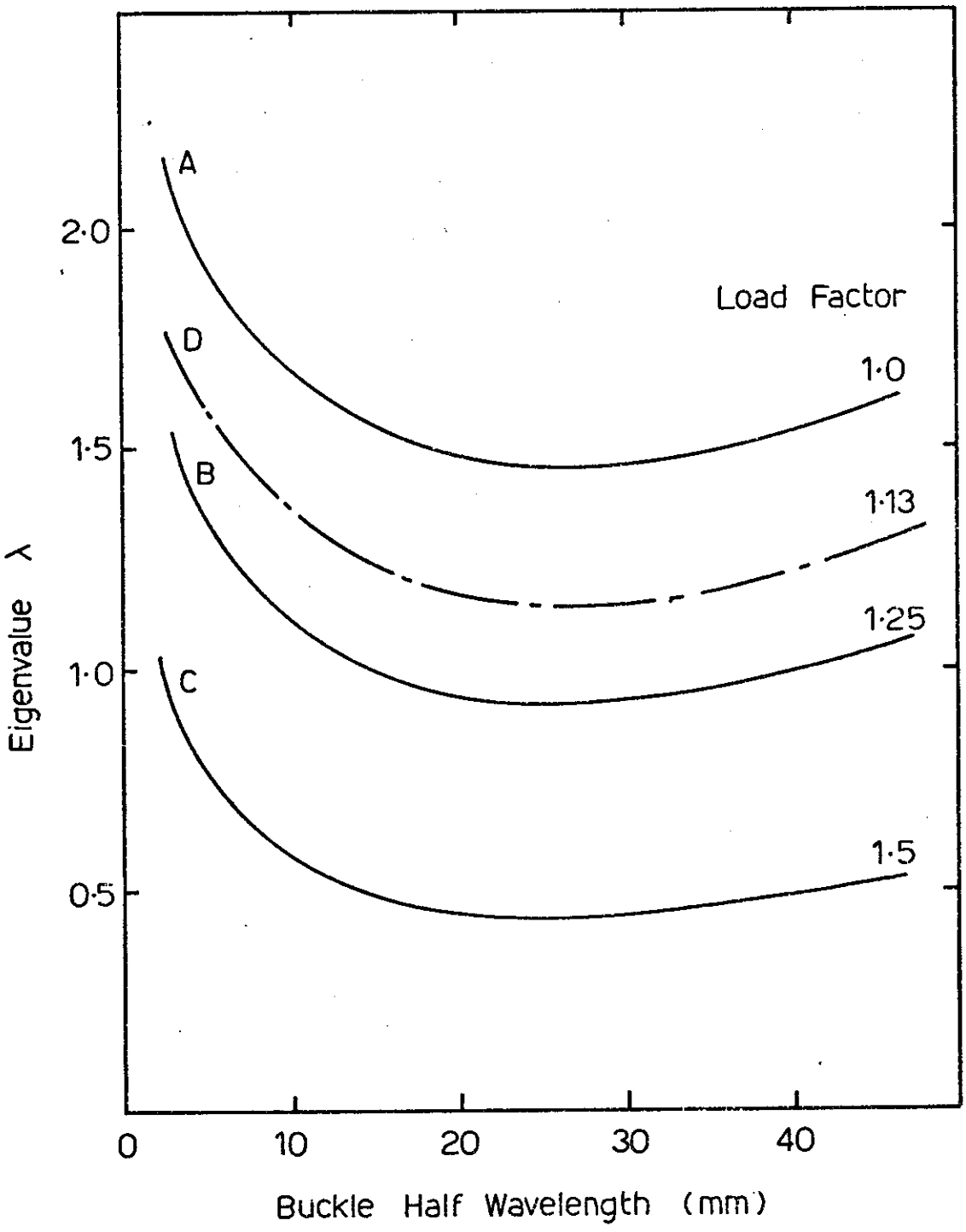

FIG. 7·23 FAMILY OF BUCKLING CURVES

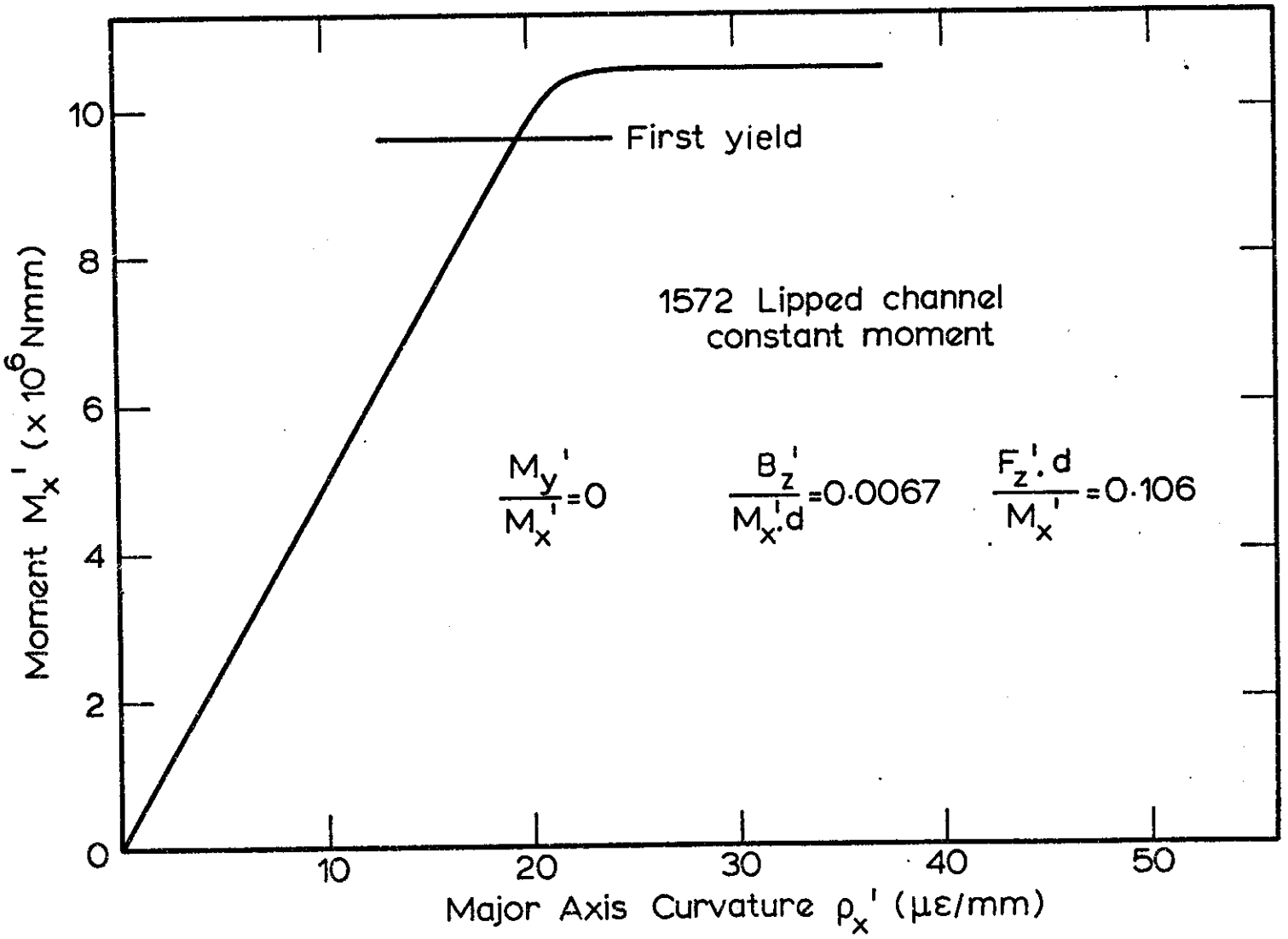

FIG.7·24 THEORETICAL MOMENT - CURVATURE RELATIONSHIP FOR BEAM UNDER CONSTANT MOMENT.

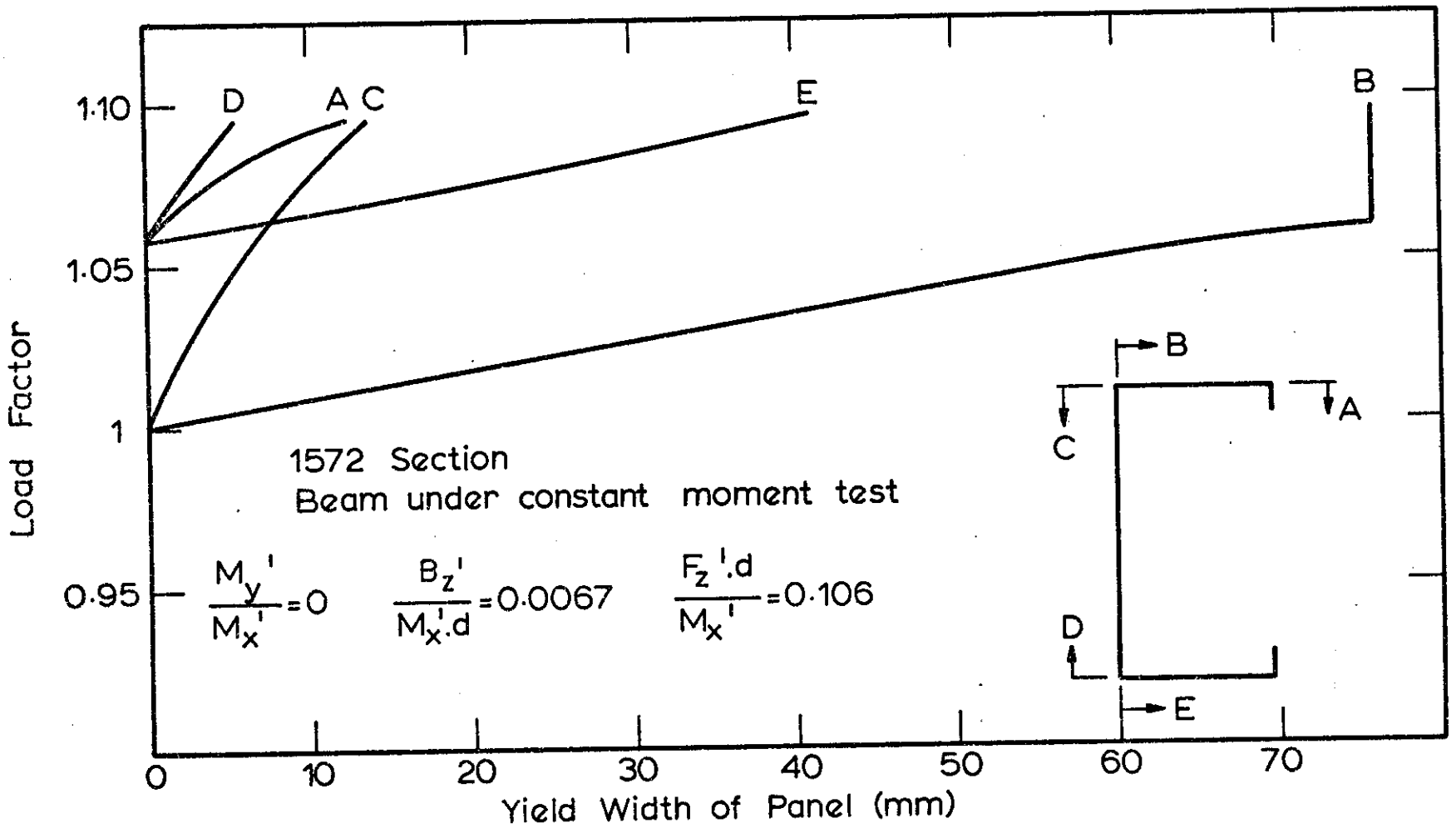

FIG. 7·25 YIELD WIDTH OF PANELS FOR BEAM UNDER CONSTANT MOMENT

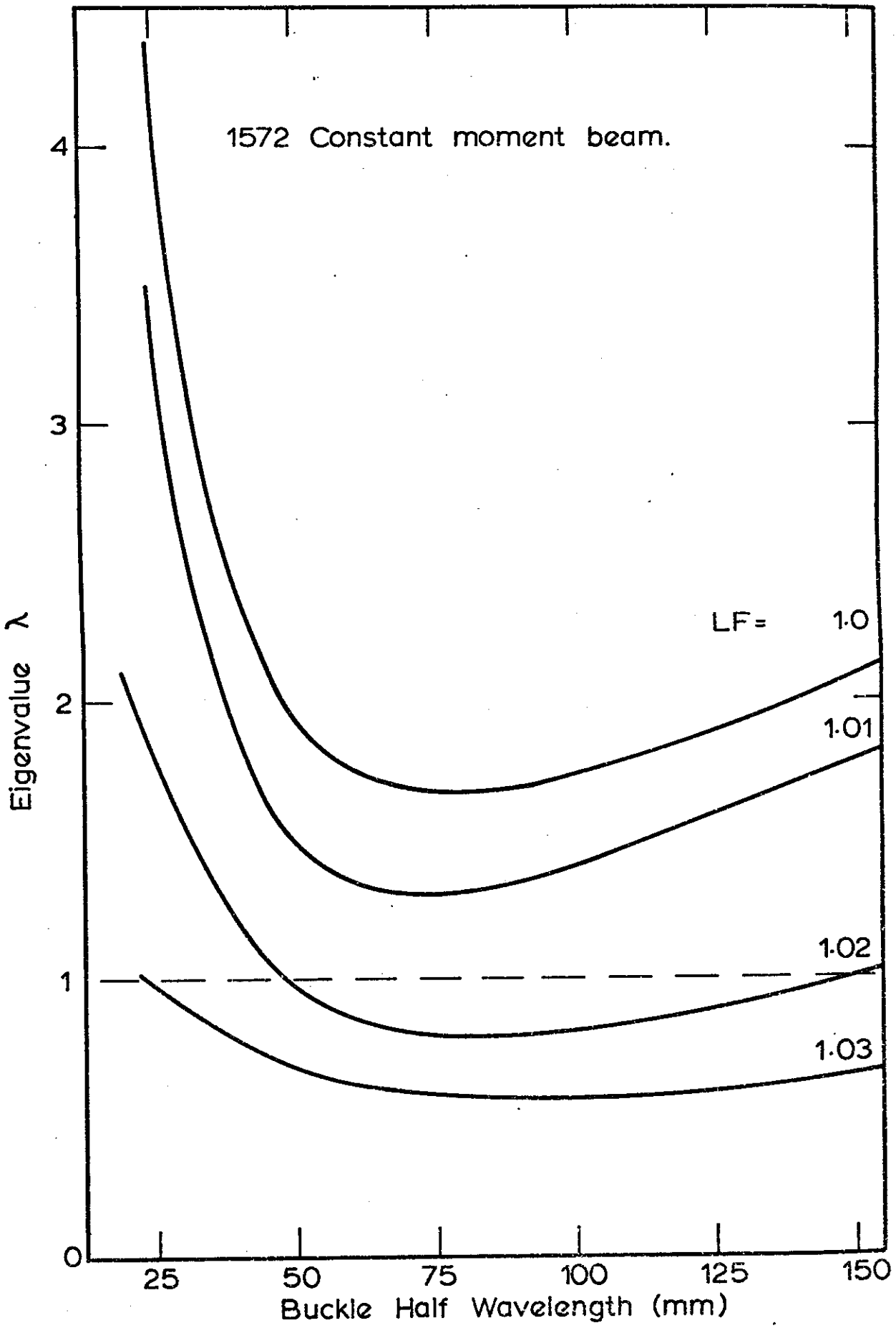

FIG. 7·26 LOCAL BUCKLING CURVES FOR BEAM UNDER CONSTANT BEAM.

CHAPTER 8 - ULTIMATE FRAME BEHAVIOUR

8.1 INTRODUCTION

Stability analysis and design of plane frames has been a subject of extensive investigation for the past decade mainly as a result of the rapid development of high speed computers and the matrix methods of analysis. Investigations in this area have been summarised by Yucel et. al. (1973). From an extensive literature survey their opinion indicates that the elastic and plastic behaviour of braced and unbraced plane frames can be predicted.

As a result of the weakening effects of local buckling, failure can take place at a lower load than the frame would carry in the absence of local buckling. Hence the analysis of the ultimate behaviour of structural systems should contain an interaction of local buckling and overall behaviour. The interaction is important not only for structures composed of thin-walled cold-formed members but also for structures composed of hot rolled and built-up sections where the material used is of high yield strength.

In Section 7.6 a general buckling analysis was presented for a structural element. The analysis can be used to predict the collapse load of single member structures. Recent work by Kalyanaraman (1978), Kavanagh (1978) and Kavanagh and Evans (1978) has also been concerned with the failure of cold-formed steel members by localised

buckling in the elastic and inelastic regions. In predicting the post-local-buckling behaviour of continuous beams and frames, Wang (1974), Wang and Yeh (1974) and Wang and Jsa (1974) have used an effective width approach. Wang and Blandford (1978) have considered the effects of local buckling of the component members on the behaviour of the overall structural system.

In this chapter, a method for estimating a lower bound to the collapse strength of the thin-walled portal frames used in the experimental study and reported in Chapter 4 will be presented. The collapse load for each of the seven frames assuming a local buckling failure mode will be compared with the experimentally determined values.

8.2 INELASTIC BUCKLING OF STRUCTURAL SYSTEMS

In Chapter 7 a method was presented which allowed the collapse strength of a thin-walled structural system to be determined. The method was applicable to systems in which the collapse mechanism was initiated by local buckling which occurred in either the elastic or inelastic range of the material properties. Three analyses were required for locating the failure region and then finding the load factor for collapse. Hence, for a complete analysis the computer programs FEETA, CAFOP and BFINST, which are given in Appendix VIII, were used.

Briefly, the method involved an elastic analysis to determine the ratios of the stress resultants at a particular critical region, such as a region of maximum major-axis bending moment. The ratios of stress resultants were used to perform an inelastic cross-section analysis which enabled the amount of panel yielding at a particular load factor to be calculated. A finite strip buckling analysis assuming deteriorated properties in the yielded regions was performed for various values of load factor until the minimum eigenvalue was equal to the load factor. The load factor for this eigenvalue was then assumed to be a lower bound to the ultimate load of the structural system.

8.3 ULTIMATE LOAD OF TEST FRAMES

The experimental investigation of the seven pitched-roof portal frames described earlier in Chapter 5 included the determination of the ultimate load of each frame. In order to predict this load for each frame the analysis required an estimate of where local instability may develop. Intuitively, the failure zones would be expected to occur in the regions of maximum major-axis bending moment. High compressive axial forces combined with the bending moment would provide an even more favourable location for local instability.

If plastic theory was used for the determination of the collapse mechanism, a total of two plastic hinges would be required for the collapse of pinned-base portal frames. However, a cold-formed section does not have the rotation capacity of a hot-rolled section and hence the formation of plastic hinges is remote. The more likely failure mechanism is a result of local buckling of the section. Since local buckling regions have a falling characteristic with respect to load-carrying capacity, the assumptions used in plastic theory are invalid. However, the experimental investigation indicated that there were two failure regions as suggested by plastic theory and that these regions coincided with the areas of maximum major-axis bending moment. Hence, for a portal frame braced in the manner of the test frames, the determination of likely instability zones was relatively simple.

An elastic thin-walled analysis was performed for each test frame. The most likely zones for local instability for each frame are shown on Table 8.1. The experimental investigation showed that the initiation of one region of local instability caused the second region to buckle almost simultaneously because of the redistribution of major-axis bending moment. Hence, for this reason, two possible regions of local instability for Frames 3, 4, 6 and 7 were investigated as shown in Table 8.1. For all the possible zones, the ratios of the minor-axis bending moment, the axial force and the bimoment

were calculated with respect to the major-axis bending moment. The values of the ratios of the stress resultants are shown in Table 8.1 and the inelastic cross-section analysis was performed for each frame using these ratios. At the onset of yield the elastic and shear moduli were reduced for the reasons set out in Section 7.5.1. The generalised strains produced by the analysis of Frame 1 are plotted against the major-axis bending moment in Fig. 8.1. The major-axis curvature was plotted separately against the major-axis bending moment and is shown in Fig. 8.2. At a moment of 4.40×10^6 Nmm, first yielding of the cross-section occurred at the intersection of the compression flange and the web. The calculated onset of yield is indicated by the first point on the moment-curvature relationship shown in Fig. 8.2. A further five points along the curve for regions of increasing bending moment have been examined. The yielded zones across the panels of the cross-section for each of these six points are shown in Fig. 8.3. Unlike the example given in Section 7.7.2 for the simply supported beam with a constant applied moment, the stanchion for Frame 1 began to yield at the tension flange and web intersection at a relatively small increase in bending moment, as indicated by position 2 in Fig. 8.2.

Of more importance for the inelastic buckling analysis was the determination of the advancement of yielding across the panels of the cross-section for an increasing load factor. The development

of the yielded zone for the top of the stanchion for Frame 1 has been plotted in Fig. 8.4. The figure shows that yielding was initiated at the junction of the web and top flange (positions B and C in Fig. 8.4). For the particular ratios of the stress resultants, yielding progressed along the web at a faster rate than along the top flange. Yielding was initiated next at the junction of the web and bottom flange (positions D and E) when the load factor reached a value of 1.10. Yielding was next initiated at the extremity of the top flange stiffener. Yielding commenced in this position when the load factor was 1.13.

Local buckling curves were produced for each location of local instability for the seven frames. The curves were calculated for a range of load factors and are dependent upon the amount of panel yielding. For a particular load factor the amount of yielding for each panel had already been ascertained from the previous analysis. The local buckling curves for the top of the stanchion for Frames 1 and 2 are shown in Fig. 8.5. The curves for Frames 1 and 2 have been produced for the load factors of 1.0, 1.1 and 1.2. The curves show that the buckle half wavelength for each load factor was of the order of 75 mm to 100 mm. The theoretical half wavelength of the buckle compares with the half wavelength of the buckle produced from the experimental investigation and discussed in Chapter 5. For a load factor of 1.20, the cross-section had undergone sufficient panel

yielding to produce a buckling load factor less than unity. Hence, to determine the value of the factor at failure, the minimum eigenvalue for a particular load factor has been plotted against the load factor. The graph of eigenvalue against load factor for Frames 1 and 2 is shown in Fig. 8.6. The collapse load factor is determined when the values of minimum eigenvalue and load factor are equal and the technique of graphical construction to solve the equation is shown in Fig. 8.6. From these plots, the collapse load factor for local instability of each frame was determined. For the case of Frames 1 and 2, the load factor and minimum eigenvalue were equal when the load factor was 1.17. A buckling analysis was repeated at the calculated collapse load factors in order to verify the minimum value of eigenvalue.

Once the collapse load factor was obtained, the critical major-axis bending moment and hence the collapse load was calculated. The critical major-axis bending moment was simply the product of the collapse load factor and the value of the major-axis bending moment for the initiation of yield. The critical bending moment was converted into a collapse load with the use of the previous elastic analyses. The minimum collapse load for each frame is shown in Table 8.2.

8.4 COMPARISON BETWEEN THEORETICAL AND EXPERIMENTAL ULTIMATE LOADS

The experimental ultimate load, P_E, for each test frame is given in Table 8.2. The ultimate loads can be compared with the theoretical values also shown in Table 8.2. The ratio of experimental ultimate load to the theoretical ultimate load for each frame is also shown in this Table. The ratios show that an approximation which is reasonable for downwards loading but very conservative for uplift loading has been obtained for each frame. For the simulated dead and live loading of Load Case 1, the braced and unbraced frame predictions were remarkably accurate. The reason for the accuracy can be explained by the well predicted elastic behaviour of the frames. The measurement of the major-axis bending moment which was the largest component in the ultimate stress distribution compared well with the theoretical major-axis moment for Frames 2 and 5. Hence, an accurate prediction of the bending moment also enabled an accurate model of the stress distribution to be determined. The accuracy for Frame 5 was further enhanced by the restraining action of the internal bracing. The internal bracing restricted the out-of-plane movement and enabled the stress distribution to be calculated more accurately than for Frame 2. This has been discussed in Section 6.6 The theoretical predictions thus reflected the well behaved nature of the frames.

For the transverse wind loading case applied to Frames 3 and 6, the theoretical collapse loads were more conservative. The predictions for Frames 3 and 6 were 10 and 20 per cent higher respectively than the observed collapse load. The theoretical collapse loads for Frames 4 and 7 were the most conservative. The predictions underestimated the collapse load of the structures by approximately 45 per cent. Both Frames 4 and 7 were subjected to the longitudinal wind loading case in which suction was applied to each element of the structure. The unusual nature of the load case resulted in a tensile force being applied to the stanchions of the frame. The region of maximum major-axis bending moment occurred in the stanchions, however, the presence of the axial force did not allow the formation of local buckling in the peak bending moment regions. Instead, the local instabilities were forced to occur simultaneously in the peak region of bending moment in the rafter.

8.5 ULTIMATE FRAME LOAD DISCREPANCIES

As previously stated, the inelastic buckling analysis produced an ultimate load for each frame which was conservative. The most conservative estimate for the collapse load occurred for Frames 4 and 7. These frames were subjected to suction and it has been mentioned that although the peak major-axis bending moment occurred in the stanchion, the frames did not initially buckle in

For the transverse wind loading case applied to Frames 3 and 6, the theoretical collapse loads were more conservative. The predictions for Frames 3 and 6 were 10 and 20 per cent higher respectively than the observed collapse load. The theoretical collapse loads for Frames 4 and 7 were the most conservative. The predictions underestimated the collapse load of the structures by approximately 45 per cent. Both Frames 4 and 7 were subjected to the longitudinal wind loading case in which suction was applied to each element of the structure. The unusual nature of the load case resulted in a tensile force being applied to the stanchions of the frame. The region of maximum major-axis bending moment occurred in the stanchions, however, the presence of the axial force did not allow the formation of local buckling in the peak bending moment regions. Instead, the local instabilities were forced to occur simultaneously in the peak region of bending moment in the rafter.

8.5 ULTIMATE FRAME LOAD DISCREPANCIES

As previously stated, the inelastic buckling analysis produced an ultimate load for each frame which was conservative. The most conservative estimate for the collapse load occurred for Frames 4 and 7. These frames were subjected to suction and it has been mentioned that although the peak major-axis bending moment occurred in the stanchion, the frames did not initially buckle in

these regions. For a stanchion subjected to an axial compression and a bending moment, the position of the neutral axis of the cross-section is located closer to the extreme fibre stressed in tension. As the load and the moment are increased, the area of the compressive stress region increases more rapidly than that of the tensile stress region. The effect of the increase of the compressive stress region causes local instability to occur at a lower value of bending moment than would normally be the case for a beam subjected to a bending moment alone. However, considering a stanchion subjected to an axial tension and a bending moment, the position of the neutral axis lies closer to the extreme fibre stressed in compression. The position of the neutral axis results in the compressive stress region being considerably smaller than the previous example. As the axial tension and the bending moment increase, the compressive stress region also increases, however, the tensile stress region increases more rapidly. As the local buckling failure of the cross-section is governed by the compressive stress, the cross section can take considerably more load, even though yielding has taken place in the tensile stress region. Hence, this effect explains the larger collapse loads for Frames 4 and 7. However, the larger discrepancies for the two frames are not fully explained, even allowing for the more complex method of failure.

A possible explanation for the discrepancies could be a result of inaccuracies in the modelling of the behaviour of the cross-section in the inelastic range. Inaccuracies may occur in the theoretical analysis because of poor modelling of firstly, the amount of yielding or secondly, the values of the longitudinal stress resulting from incorrect stress resultants. An incorrect choice of stress resultants may be due to either moment gradient or moment redistribution in the complete frame following yielding.

8.5.1 Modelling of Panel Yielding

In all fields associated with inelasticity an accurate model is required for determining the magnitude of the yield stress. The presence of residual stresses in both cold-formed and hot-rolled sections presents difficulties for calculating this quantity. To overcome the variation of yield stress around a cross-section, an average yield stress is used. For cold-formed members the calculation of the average yield stress has been discussed in Chapter 2. Hence, recognising that a source of error is introduced in selecting a material yield stress, the amount of yielding may be calculated for a cross-section which is subjected to a set of forces.

For each of the test frames, the width of yielded material in a panel of the cross-section has been calculated for the inelastic region. An experimental distribution of yield has also been

obtained for Frames 2 to 7. This has been achieved with the aid of electrical resistance strain gauges located to study the strain behaviour at the predicted regions of failure. These strain gauges have been discussed in detail in Chapter 4. A comparison between the experimental and theoretical panel yield widths for Frames 2 to 7 is shown in Figs. 8.7 to 8.12 respectively.

The comparison for Frame 2 is shown on Fig. 8.7. Experimentally, yielding has initially commenced in the compressive region (point C) and has progressed rapidly with increasing load. However, a more interesting feature is displayed by the yielding curves for the tension region (points D and E). For these curves yielding does not progress with an increasing rate for a larger load factor. Instead, the rate of change of yielding with respect to load factor actually decreases. Hence, for a given load factor, the theoretical prediction of panel yielding overestimates the experimentally measured amount of yielding. This results in the prediction of a smaller elastic core for the theoretical analysis. Hence, the collapse load for the theoretical cross-section will be lower than that achieved in the experimental study. For the case of Frame 1, the relative stiffening of the tension region was compensated by a greater amount of yielding in the compression region and hence the collapse load factor for the frame is similar to that measured experimentally. Considering the

errors introduced by the uncertainty of the yield stress alone, the theoretical collapse load of 15.37 kN compares well with the experimental load of 16.40 kN.

The comparison for Frames 3 and 5 shows that the theoretical prediction of the extent of panel yielding is well modelled. In both these cases the steepening characteristic of the curves displayed in Fig. 8.7 is less evident. Hence, the theoretical predictions for the failure loads as shown in Table 8.2 closely model the experimental behaviour. The steepening characteristic is shown in the comparison for Frame 6 in Fig. 8.11. In this case the compression region (points B and C) for the theoretical analysis overestimates the amount of panel yielding which leads to a more conservative collapse load.

The predicted collapse loads for Frames 4 and 7 are much lower than the experimental collapse loads. From a comparison of the panel yield widths in Figs. 8.9 and 8.12 the reason becomes evident. The steepening characteristic displayed to some extent in the previous frames has now become very pronounced. This results in the theoretical elastic core of the yielded cross-section being significantly smaller than that measured in the frames. This is reflected in the reduced collapse load predictions.

Associated with the effects of panel yielding are the loads at which first yielding was observed. The theoretically calculated first yield load and the collapse load factor based upon this load have been compared in Table 8.3 to the similar experimentally observed quantities for each of the seven test frames. As a result of the overestimation of panel yielding in the theoretical analysis, the theoretical collapse load factors indicate a relatively low reserve of strength after first yield. The increases range from 17 per cent for Frames 1, 3 and 6, to 28 per cent for Frame 5. In contrast, the experimental reserve of strength was significantly higher. The increases range from 30 per cent for Frame 3 to 77 per cent for Frame 4. The largest increases are consistent with the frames which displayed the largest amount of steepening in the yielded panel width curves.

Determining the reasons for the decrease in the rate of panel yielding is difficult. Obviously, the variations in the yielding characteristics of the panels around the cross-section contribute to the unexpected behaviour. The steepening of the curves is seen to commence at approximately similar load factors for each frame. This may indicate that strain hardening of the yielded panels is taking place. However, the largest variations have occurred for cases in which the cross-section is subjected to an axial tension. Hence, for a cold-formed section the

axial tension must contribute to the decrease in the rate of panel yielding.

8.5.2 Moment Gradient

A moment gradient condition is used to describe beams subjected to a bending moment diagram that varies along the length of the beam. From elementary statics, the moment gradient with respect to the beam length at any point on the longitudinal axis of the beam is also the shear force at that point. The local buckling of beams under moment gradient has been studied by Lay and Galambos (1967) and Tien and Wang (1979). In a beam under moment gradient, yielding will be concentrated within a restricted region and the possibility of local buckling within this region must be considered. In a beam under uniform moment the critical condition for local buckling is the progression of full yielding across a flange normal to the beam length. However, in the moment gradient case, yielding across the flange will occur in a relatively constant manner. Thus, in the moment gradient case, it is the progression of yielding along the beam length that is critical. The rotation capacity of beams under moment gradient has also been studied by Lukey and Adams (1969).

In the present study of local buckling, it is important to model the distribution of longitudinal stress around a cross-section and

hence the ratios of stress resultants at the critical section must be used. However, if the member is subjected to a moment gradient, the exact position of the critical buckling section is difficult to ascertain. The difficulty in locating the exact cross-section can produce variations in the ratios of the stress resultants. For the experimental frames, local buckling took place in the regions where the moment gradient was very high. Hence, the theoretical ultimate loads which were calculated were very much dependent upon obtaining accurate stress resultant ratios.

8.5.3 Moment Redistribution

For continuous cold-formed structures, additional reserve of strength can be developed through partial plastic moment redistribution, similar to that utilised in the conventional plastic design of compact hot-rolled continuous structures. However, the full development of plastic hinges, on which conventional plastic design is based is generally not attainable in cold-formed sections with their relatively thinner flanges. Therefore, the amount of redistribution which can be attained depends on the amount of rotation or curvature which can develop in the section beyond initial yielding but prior to compression flange failure. Reck et. al. (1975) have shown that even though plastic hinges cannot be achieved with thin-walled members, there exists significant and calculable inelastic moment-

rotation capacity. This capacity enables continuous structures to achieve significant additional reserve strength through inelastic moment redistribution.

The capacity to achieve additional strength through moment redistribution was another contributing factor for the discrepancies in the frame ultimate load predictions. The inelastic buckling analysis presented relies upon the ratios of the stress resultants obtained from an elastic analysis. However, after the initiation of yielding and the redistribution of bending moment, the stress resultant ratios will significantly alter. In order to study the amount of yielding which has taken place, the longitudinal elastic stress distributions at the theoretical ultimate load for each frame are shown in Fig. 8.11 to Fig. 8.18. The stress distributions refer to the local buckle failure zone in the stanchion unless stated otherwise. The cross-hatched areas on the diagrams indicate the amount of panel yielding which has occurred and the dimensions refer to the width of the yielded zone. For a frame which has not undergone a large amount of yielding in the compression region, the results of the theoretical ultimate load prediction are sufficiently accurate. However, where discrepancies occurred such as for Frames 4, 6 and 7, the stress distributions indicated significantly more yielding with subsequent moment redistribution. The stress distributions for the three frames mentioned above also showed that significant

amounts of yielding had occurred in the tensile stress regions when the ultimate load was achieved.

As an interesting comparison to the inelastic local buckling failure loads, the collapse loads were calculated from a full plastic analysis. The mechanisms of failure were the same as those achieved in the experimental study. Using a theoretically calculated full plastic moment for the cross-section, Load Cases 1, 2 and 3 produced ultimate frame loads of 34.47 kN, 33.72 kN and 53.26 kN respectively. When the plastic moment was equated to the failure moment of the Armco 1572 channel beam discussed in Section 4.8.2, the failure loads for Load Cases 1, 2 and 3 were 29.06 kN, 28.43 kN and 44.91 kN respectively. These failure loads can be compared to the experimental failure loads shown in Table 8.2. The comparison shows that whilst a plastic analysis may predict the regions of failure, it is unconservative in determining the safe load carrying capacity of the frames.

8.6 SUMMARY

1. A general analysis has been presented for the prediction of the inelastic buckling load of a structural system.

2. The theoretical ultimate loads for each of the seven test frames were computed with the use of the inelastic buckling analysis.

3. The computed loads were compared with the experimental results. Conservative estimates were produced in all cases.

4. The discrepancies between the predicted and the measured collapse loads were attributed to two major causes. They were inaccuracies in modelling of firstly, the amount of panel yielding and secondly, the longitudinal stress around the cross-section. Theoretical panel yielding when compared with the measured distribution was found to be generally larger and hence significantly contributed to the conservative collapse load predictions. The smaller amounts of panel yielding observed in the experimental study may result from strain hardening of the yielded material. Variations in the longitudinal stress were attributed to moment redistribution and moment gradient.

Frame No	Mode	Position	$\frac{M_{y'}}{M_{x'}}$	$\frac{B_{z'}}{M_{x'}.d}$	$\frac{F_{z'}.d}{M_{x'}}$
1,2	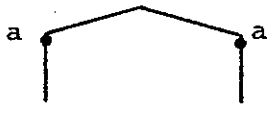	a	0.114	0.222	-0.196
3	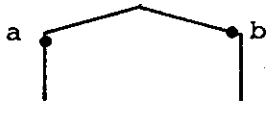	a b	0.139 0.099	0.219 0.233	-0.019 -0.070
4	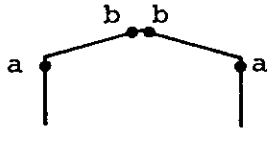	a b	0.108 0.131	0.221 0.198	0.222 0.233
5	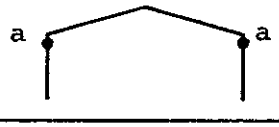	a	-0.009	0.190	-0.206
6	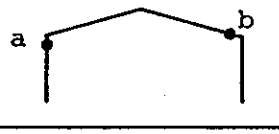	a b	-0.053 -0.058	0.182 0.207	-0.002 -0.070
7	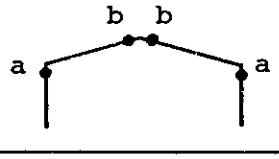	a b	0.001 -0.059	0.194 0.246	0.235 0.241

TABLE 8.1 RATIOS OF STRESS RESULTANTS FOR TEST FRAMES.

Frame No.	Experimental Ultimate Load P_E (kN)	Theoretical Ultimate Load P_c (kN)	P_E/P_c
1	16.40	15.37	1.067
2.	16.40	15.37	1.067
3.	20.44	18.62	1.100
4.	37.81	26.04	1.451
5.	18.40	18.30	1.006
6.	24.44	19.29	1.195
7.	40.15	27.62	1.453

TABLE 8.2 COMPARISON OF THEORETICAL AND EXPERIMENTAL ULTIMATE LOADS FOR THE TEST FRAMES

Frame	THEORETICAL		EXPERIMENTAL	
	First Yield	Collapse Load Factor	First Yield	Collapse Load Factor
1	13.1	1.17	-	-
2	13.1	1.17	11.5	1.42
3	15.0	1.24	15.7	1.30
4	21.5	1.21	21.4	1.77
5	14.3	1.28	13.9	1.32
6	16.5	1.17	15.9	1.54
7	22.6	1.22	22.8	1.76

TABLE 8.3 COMPARISON OF THEORETICAL AND EXPERIMENTAL FIRST YIELD LOADS AND COLLAPSE LOAD FACTORS.

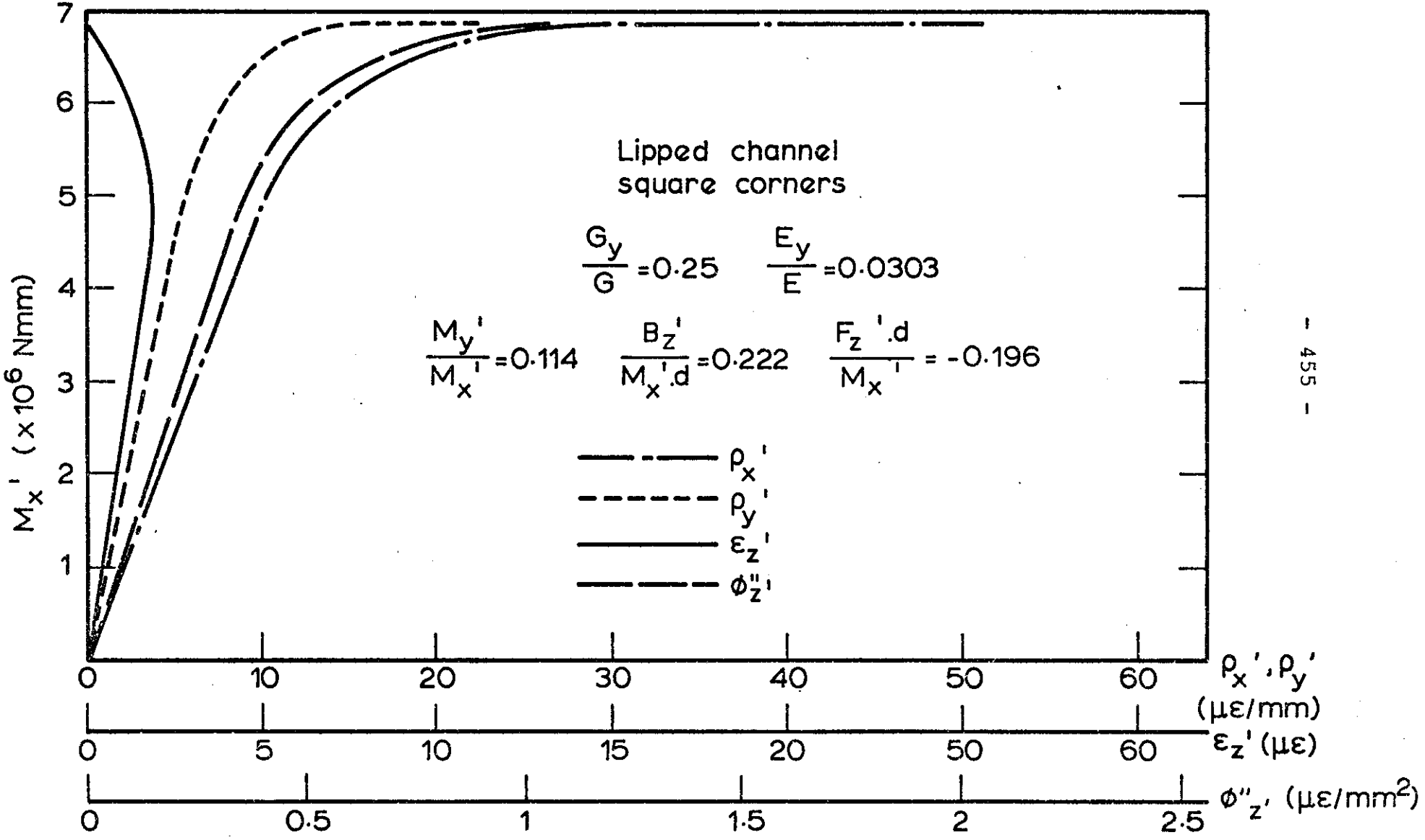

FIG. 8·1 THEORETICAL MOMENT - CURVATURE RELATIONSHIP FOR LOCAL BUCKLE REGION

FRAME 1.

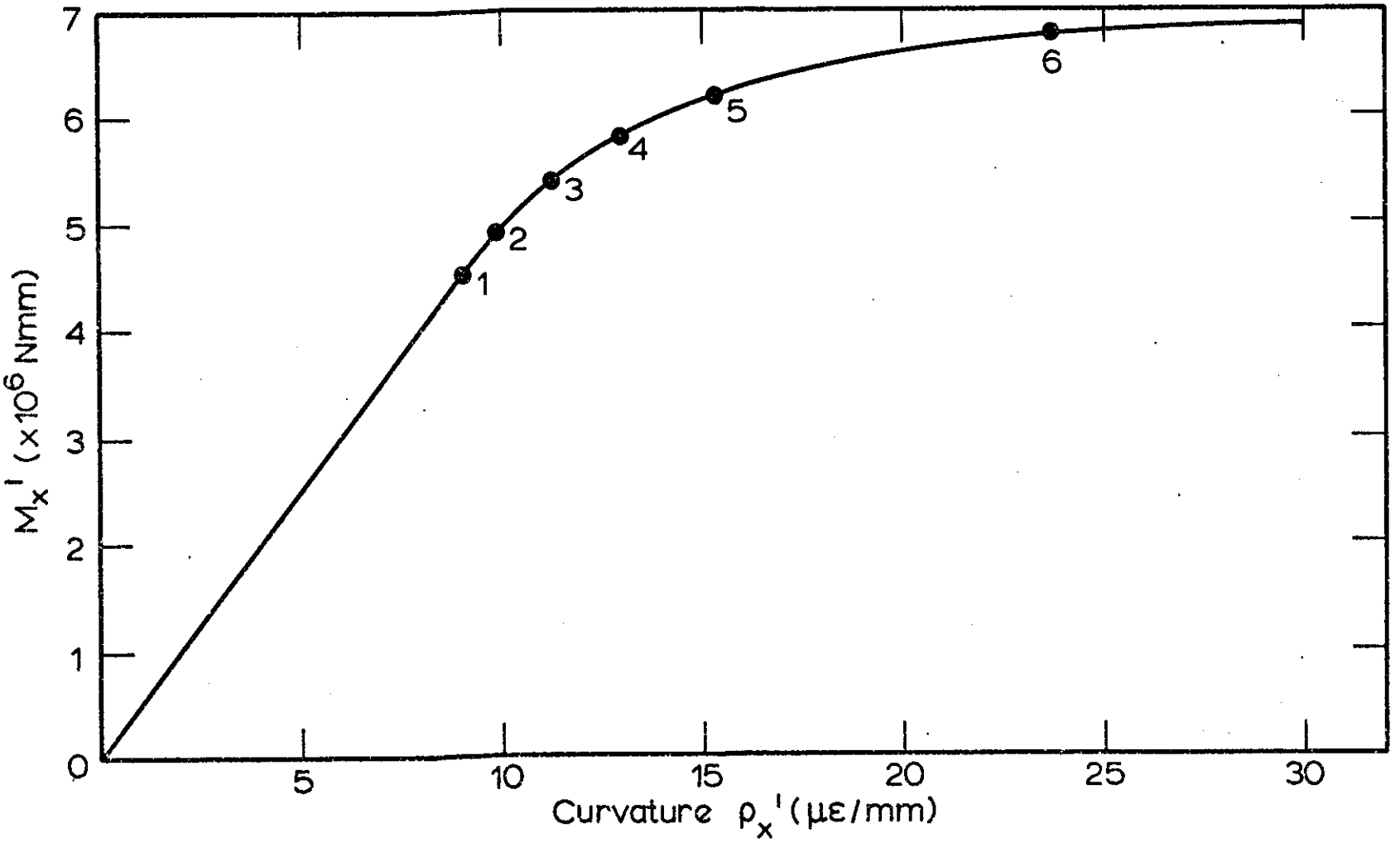

FIG. 8.2 MOMENT - CURVATURE RELATIONSHIP WITH YIELDING PATTERN LOCATIONS.

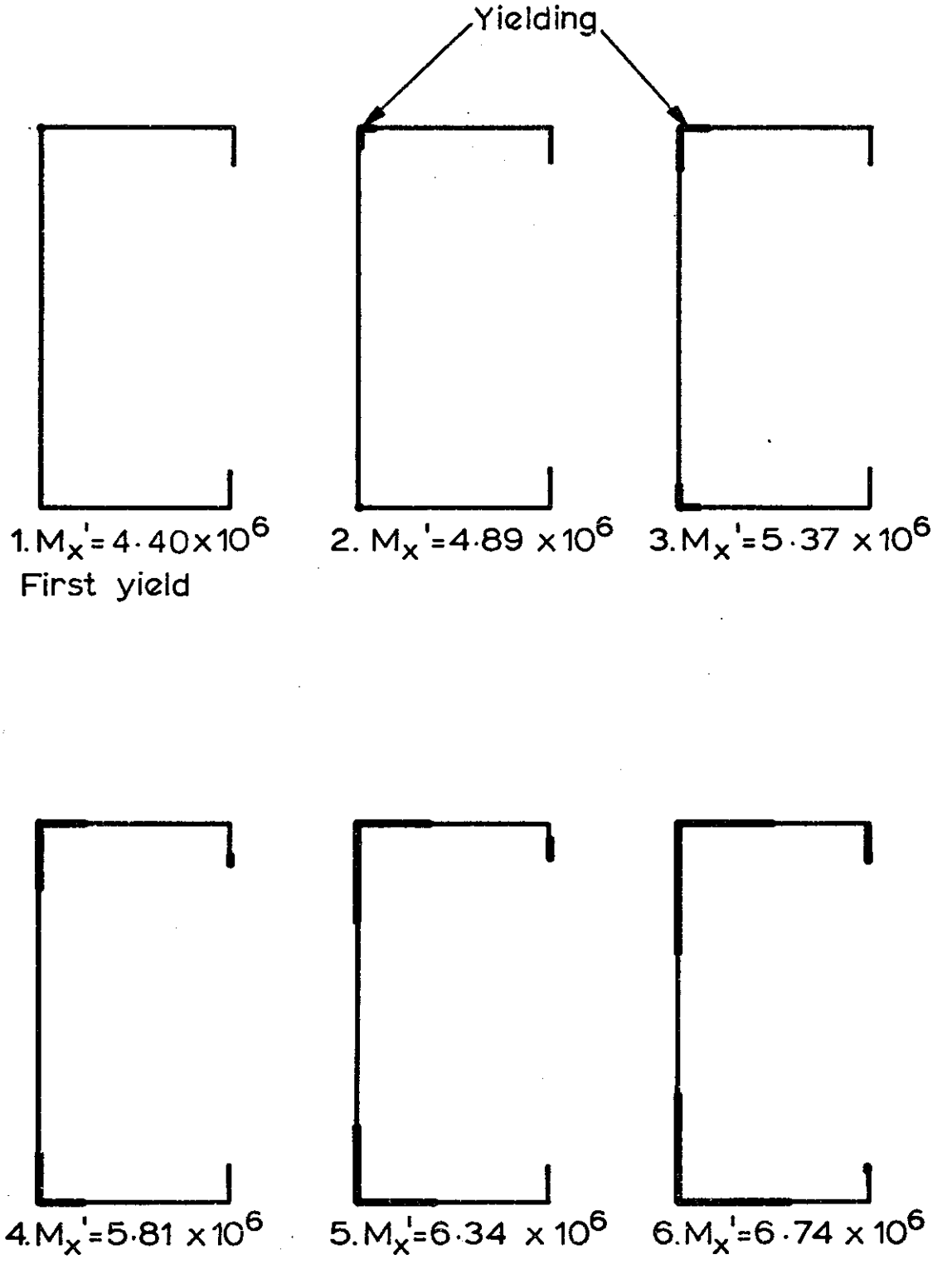

FIG. 8.3 YIELDING LIPPED CHANNEL SECTION.

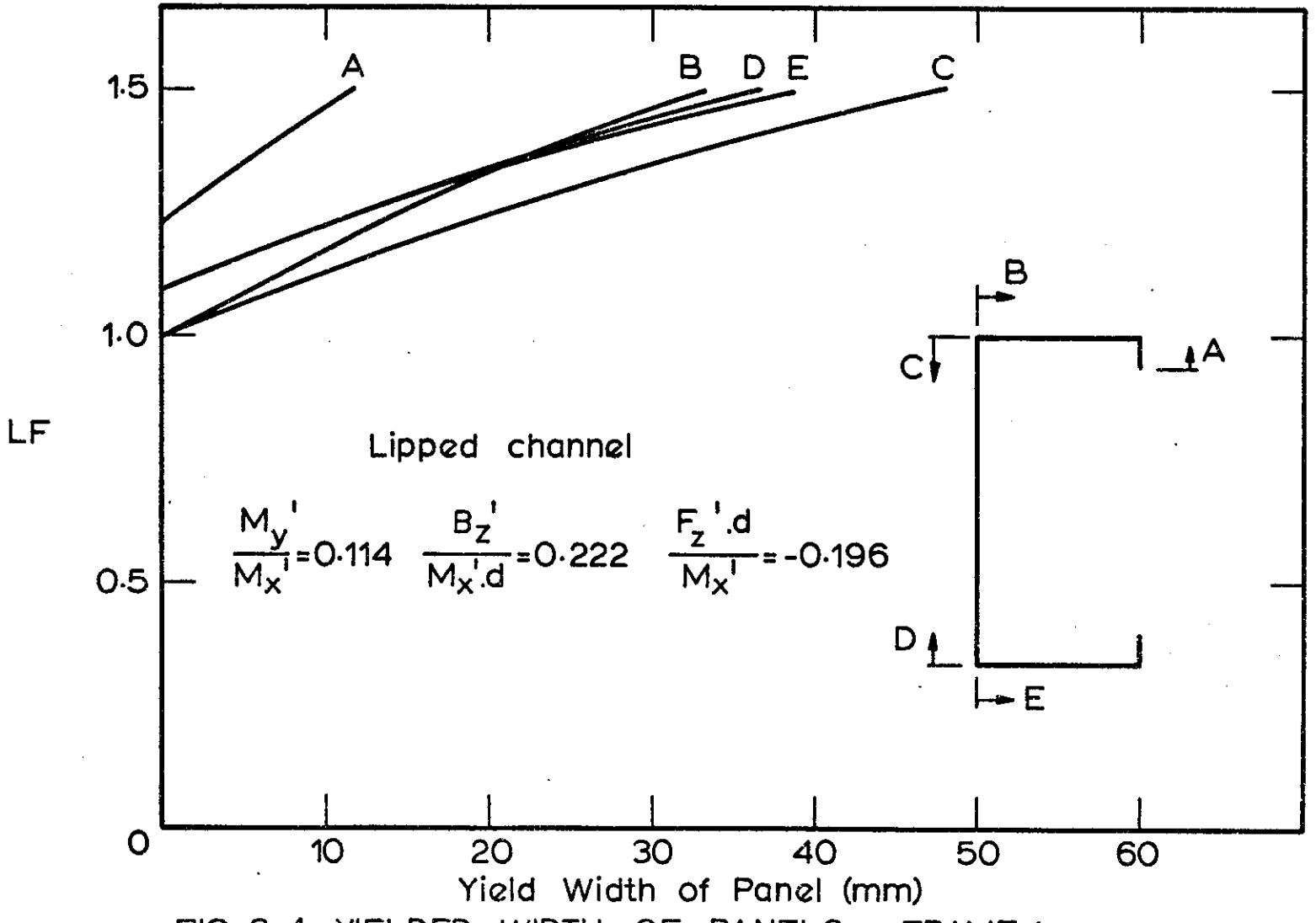

FIG. 8·4 YIELDED WIDTH OF PANELS - FRAME 1.

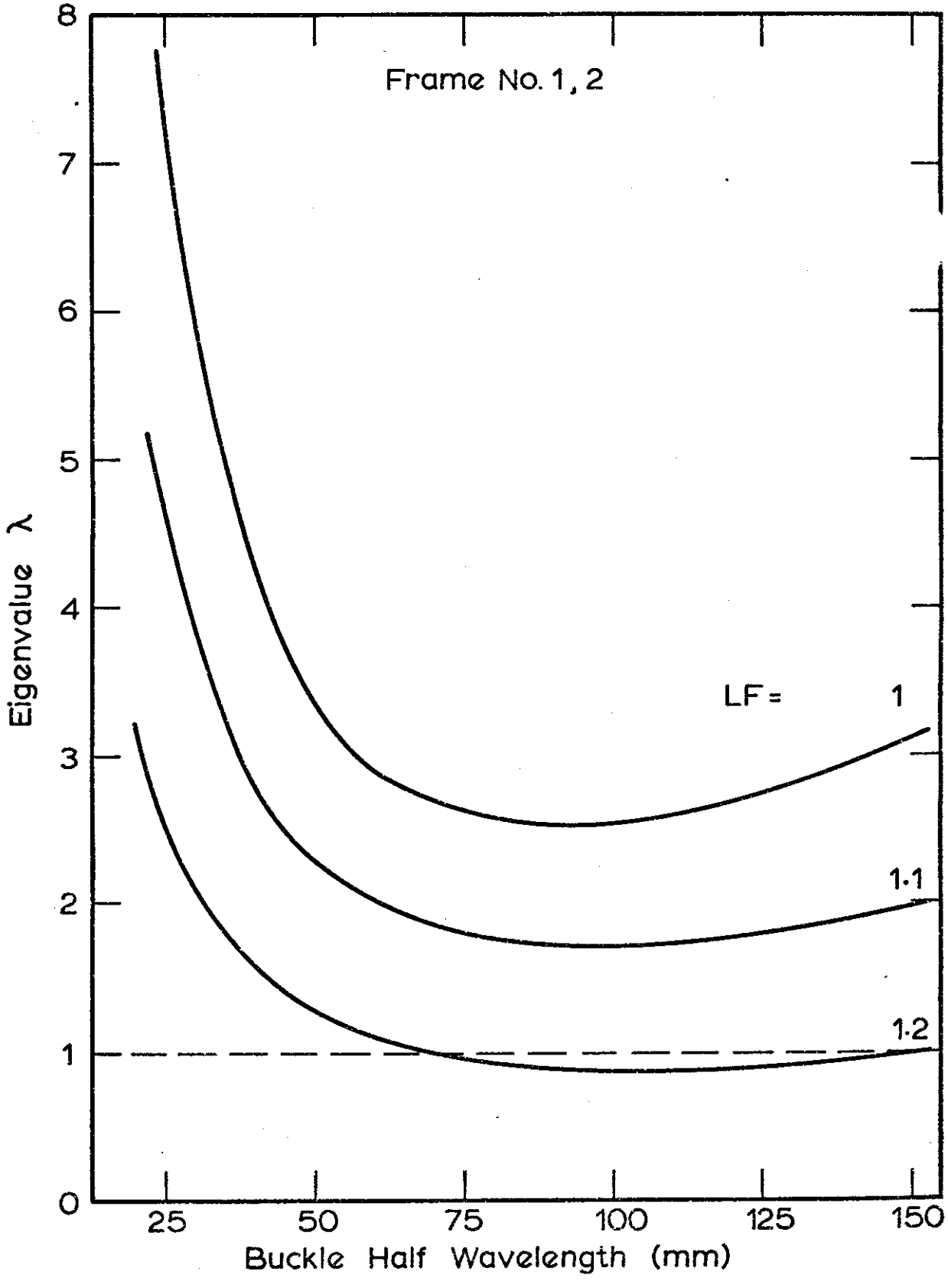

FIG. 8·5 LOCAL BUCKLING CURVES FOR TOP OF STANCHION - FRAME 1,2.

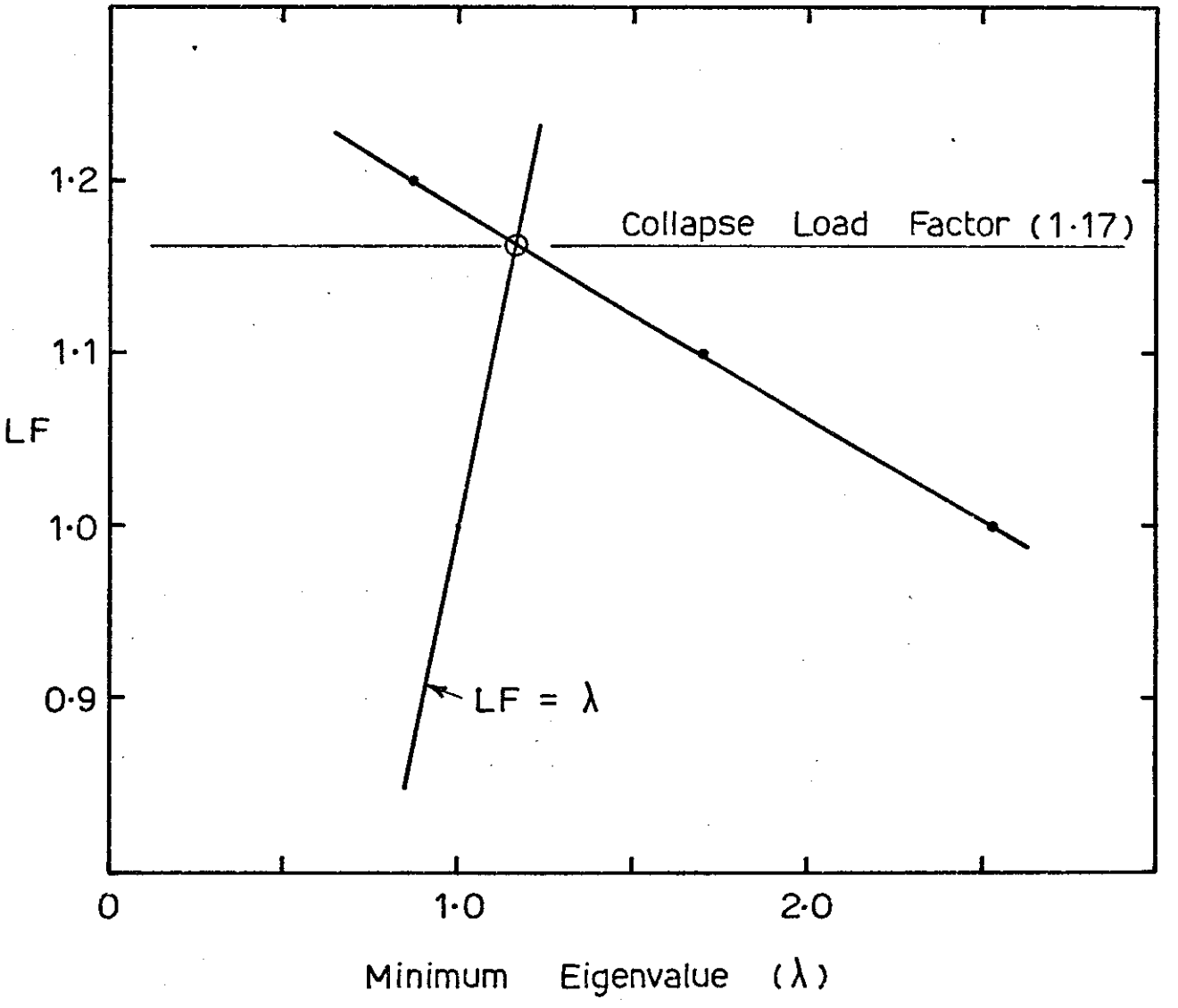

FIG. 8·6 METHOD FOR THE DETERMINATION OF THE COLLAPSE LOAD FACTOR

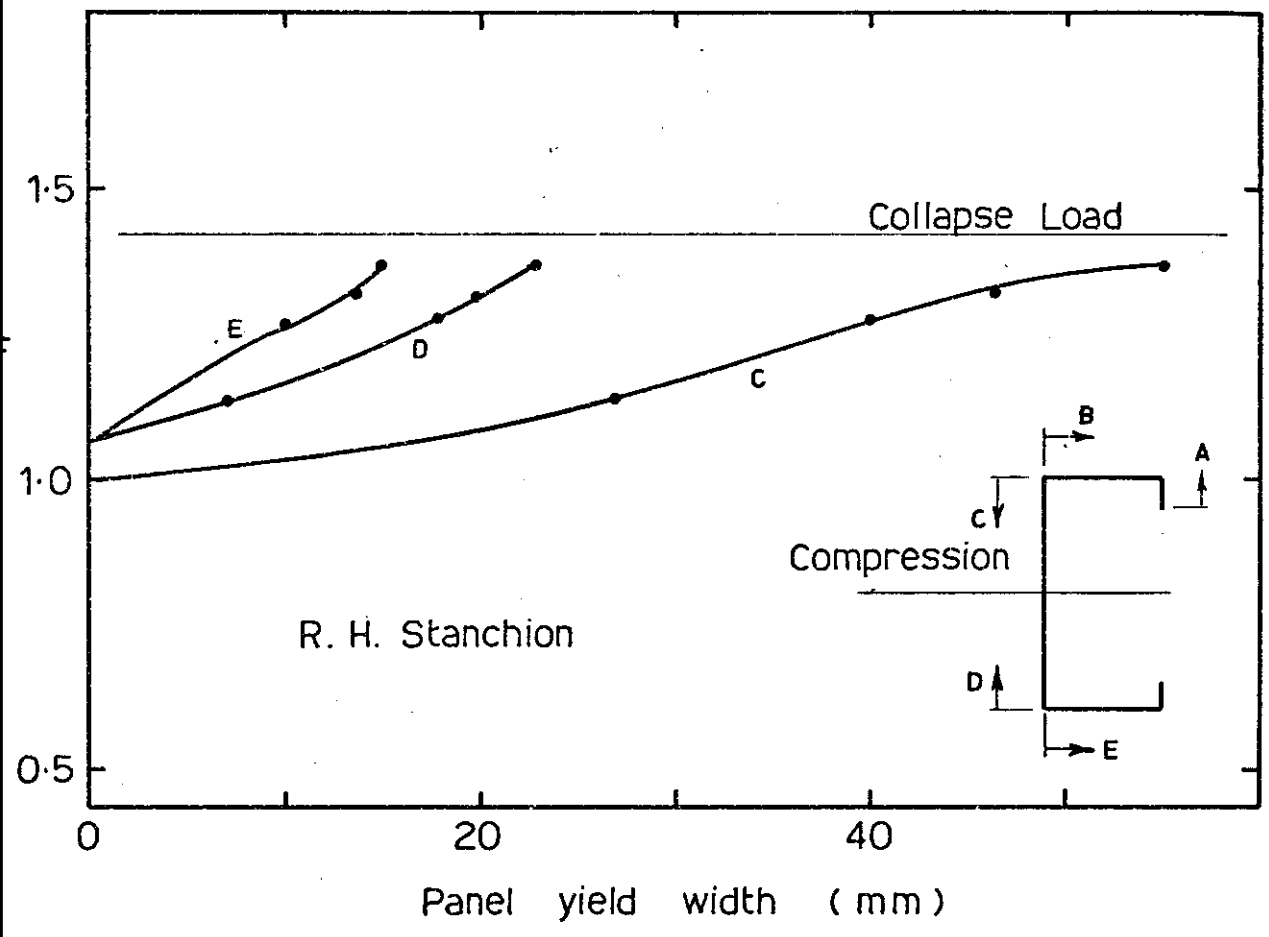

(a) EXPERIMENTAL

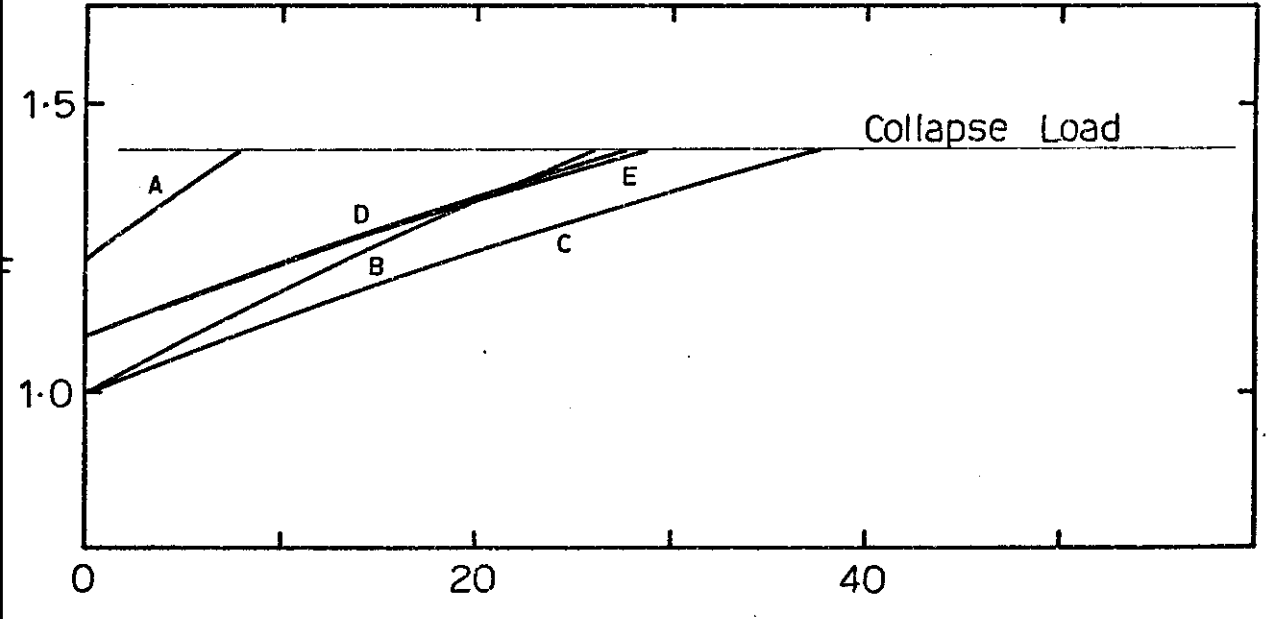

(b) THEORETICAL

FIG. 8·7 COMPARISON OF PANEL YIELDING FOR FRAME 2

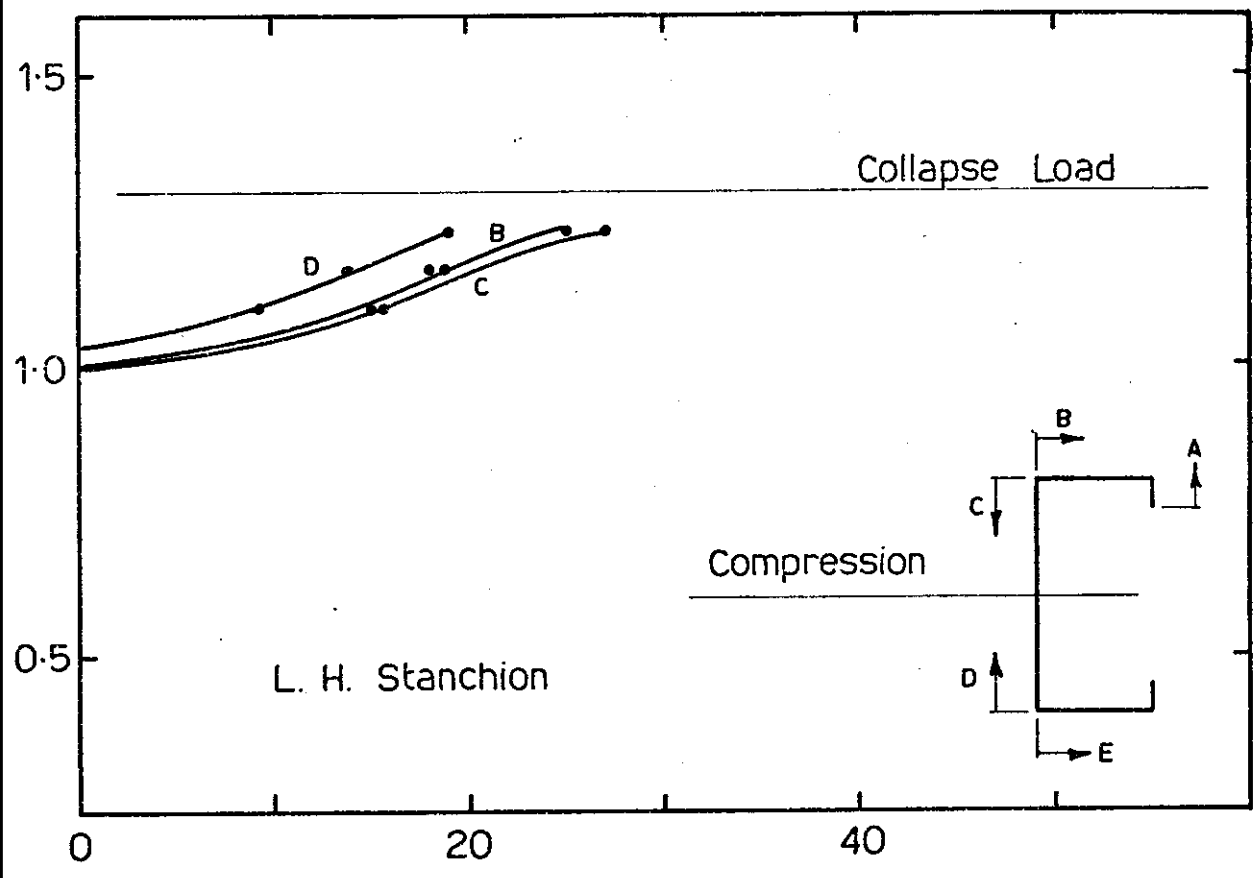

(a) EXPERIMENTAL

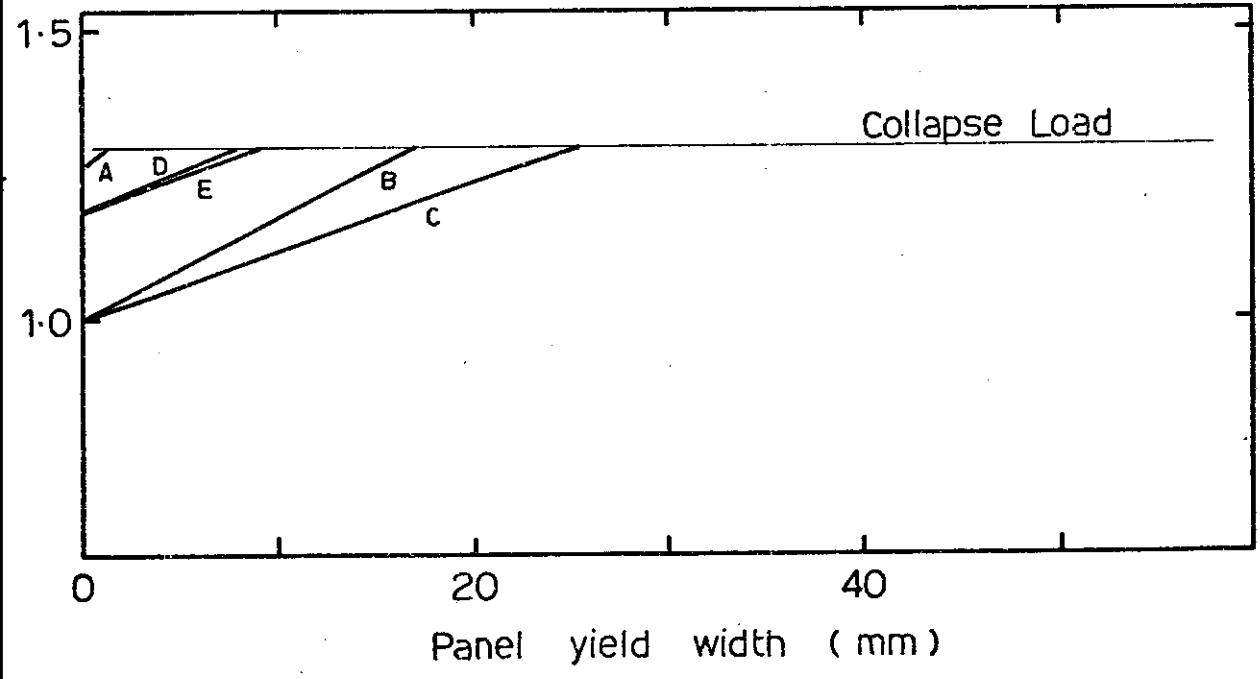

(b) THEORETICAL

FIG. 8-8 COMPARISON OF PANEL YIELDING FOR FRAME 3

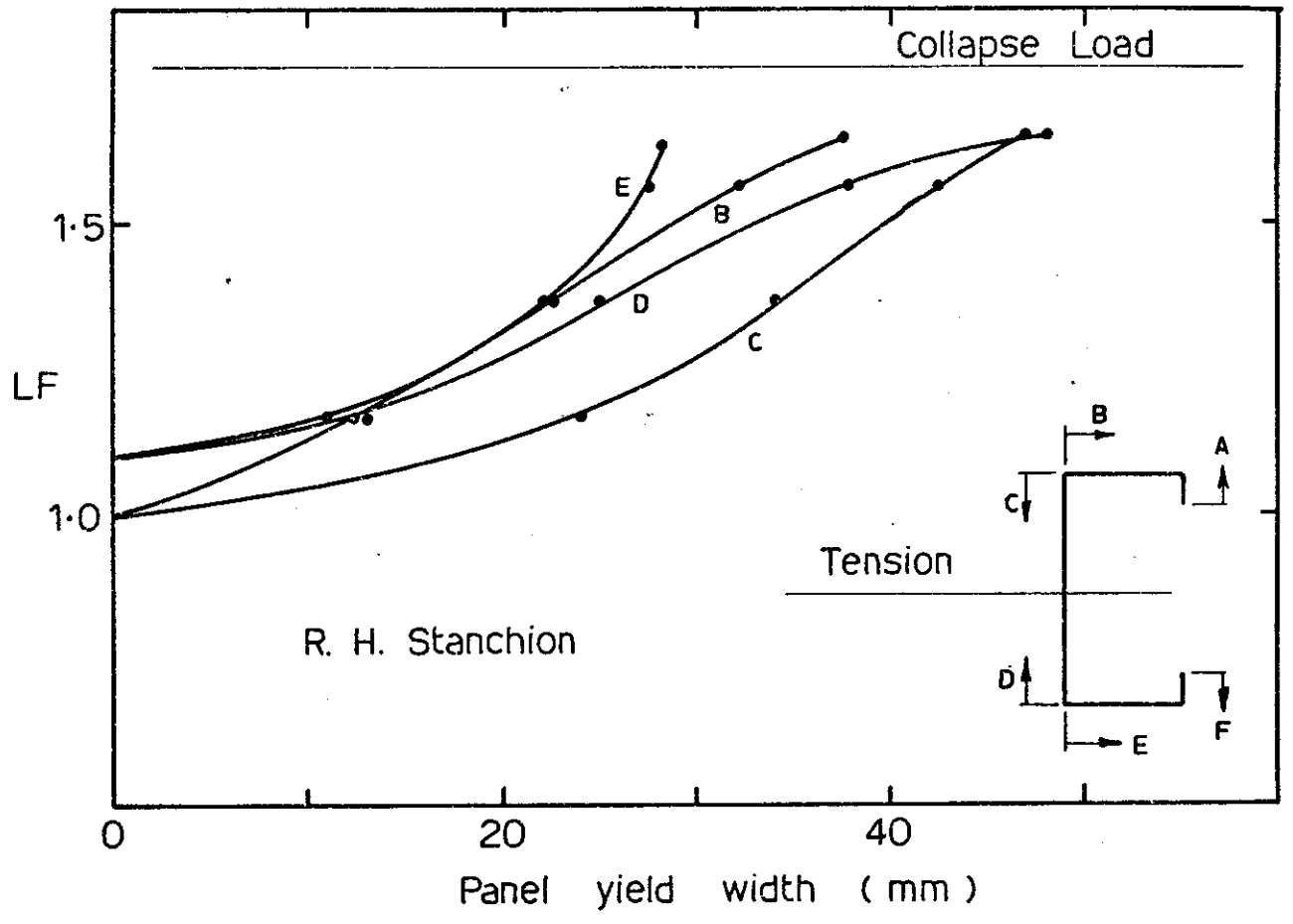

(a) EXPERIMENTAL

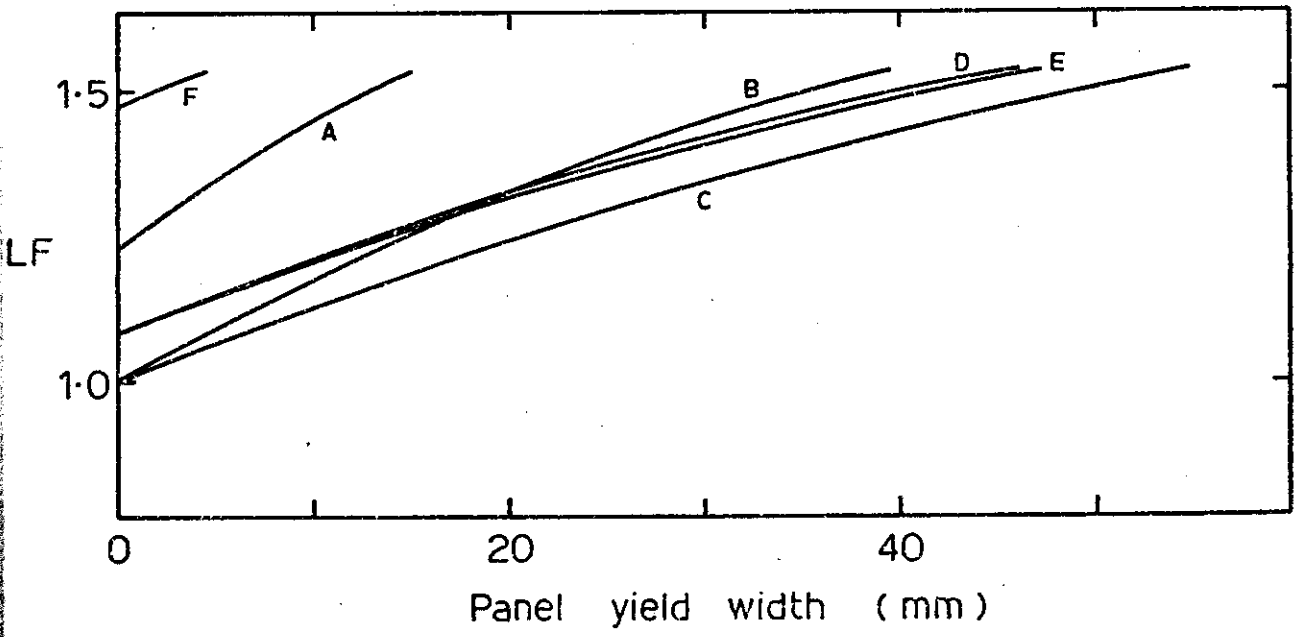

(b) THEORETICAL

FIG. 8·9 COMPARISON OF PANEL YIELDING FOR FRAME 4

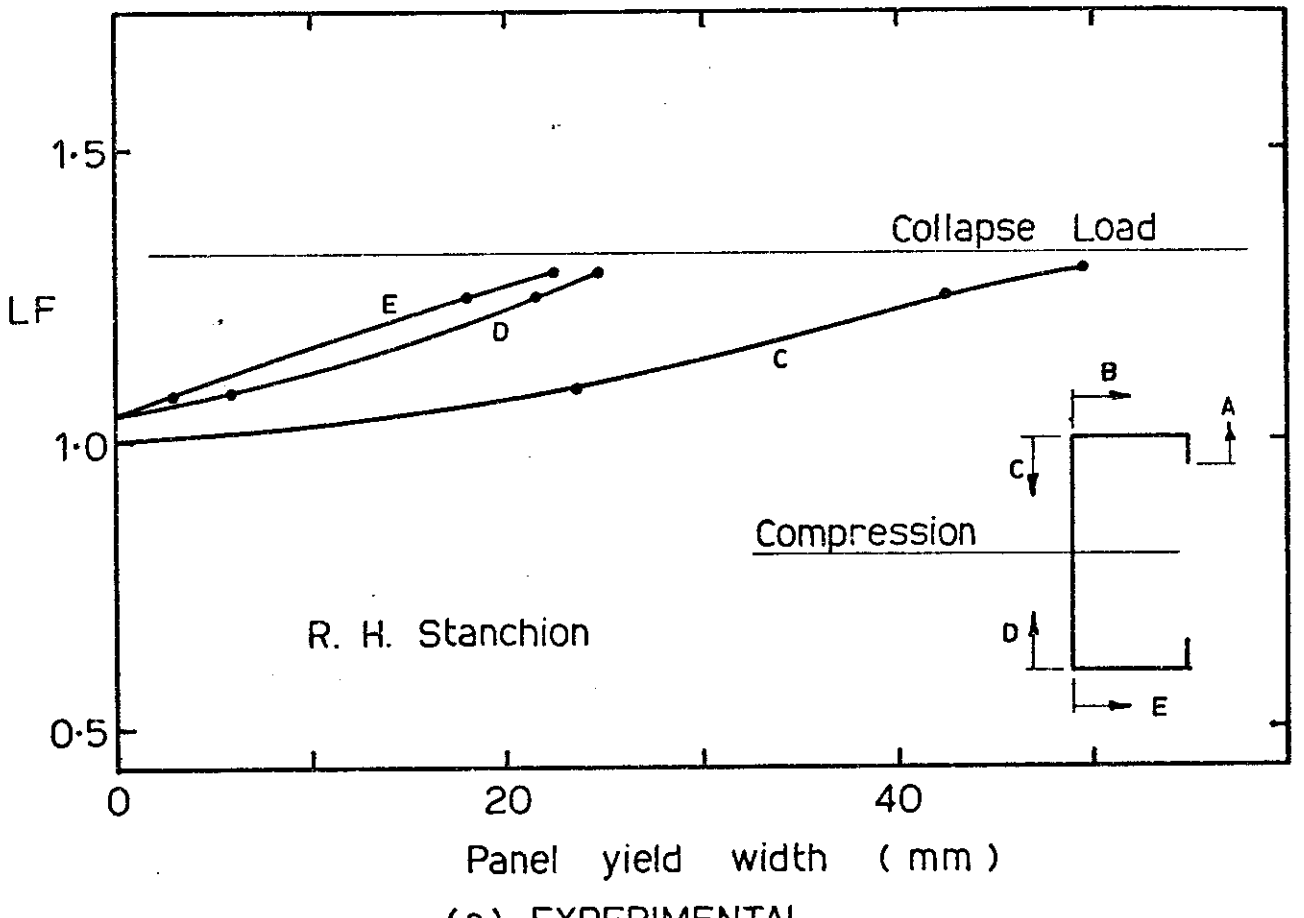

(a) EXPERIMENTAL

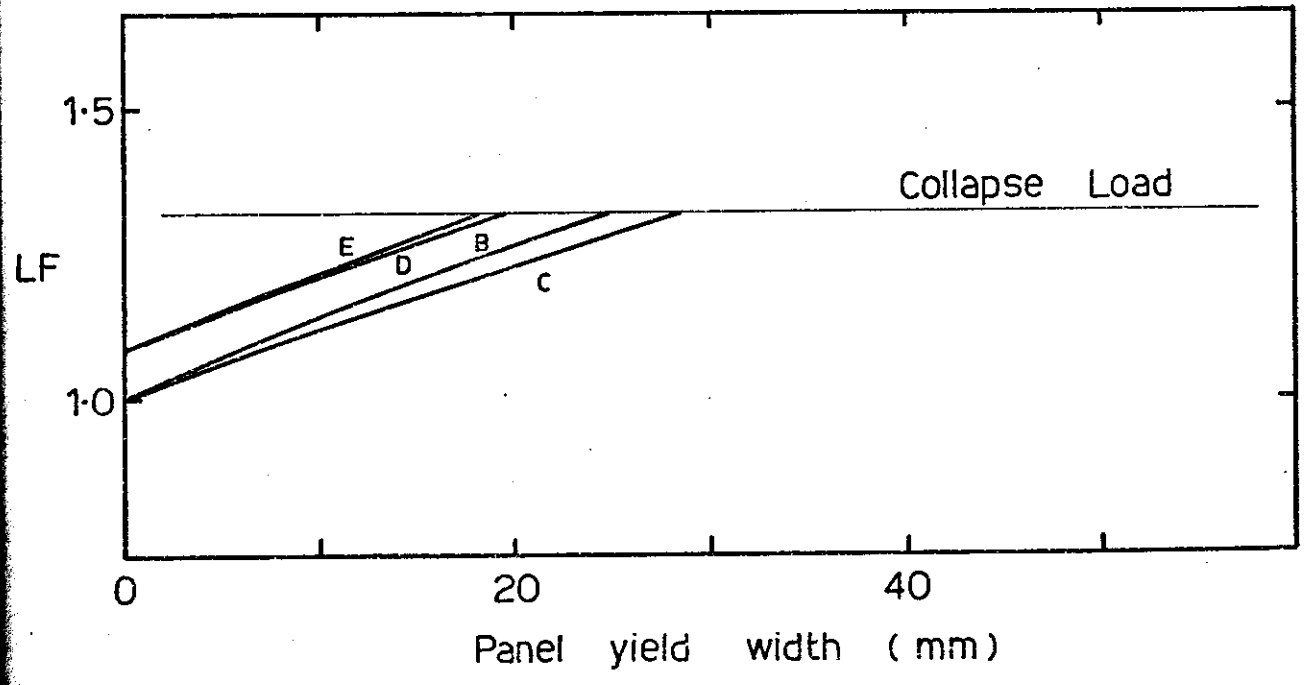

(b) THEORETICAL

FIG. 8·10 COMPARISON OF PANEL YIELDING FOR FRAME 5

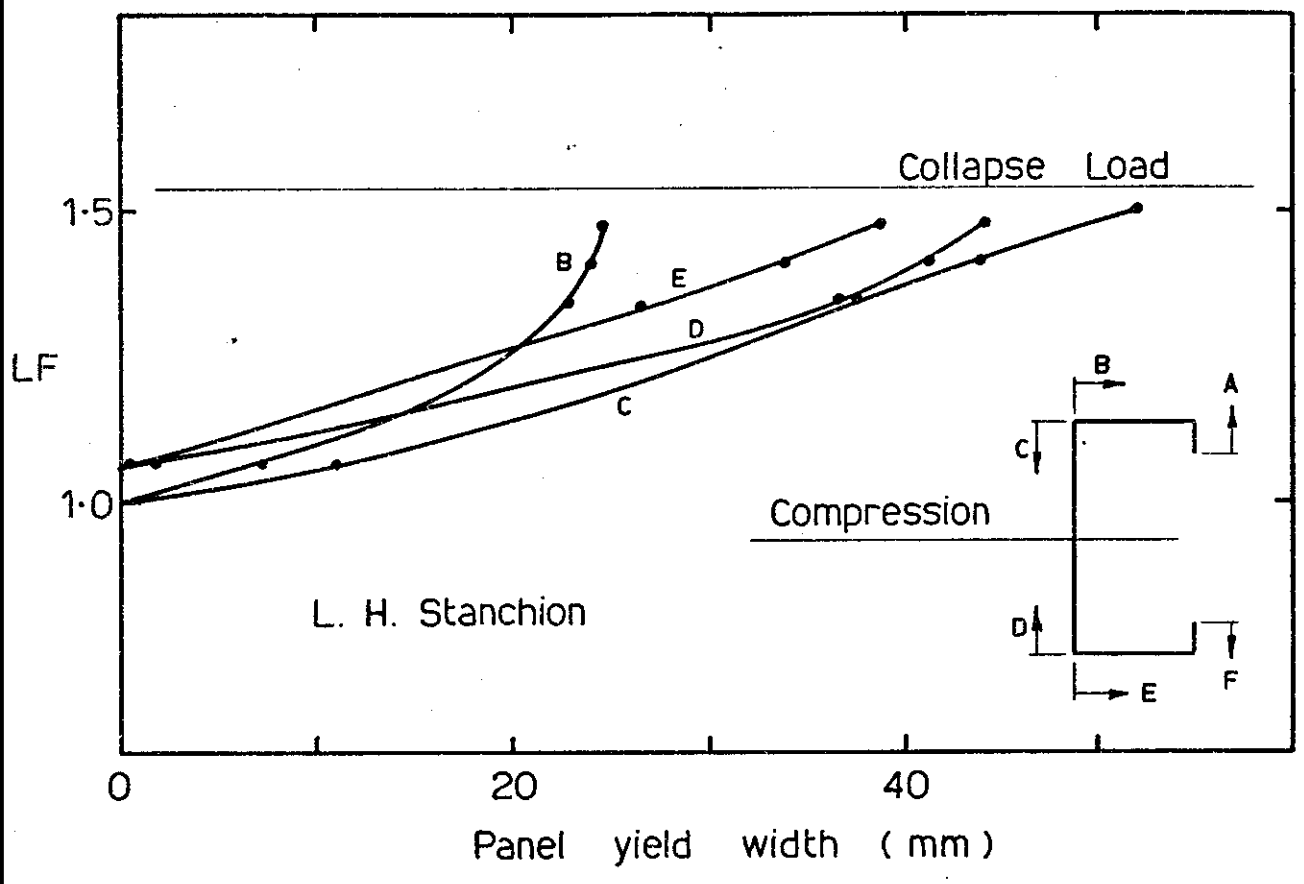

(a) EXPERIMENTAL

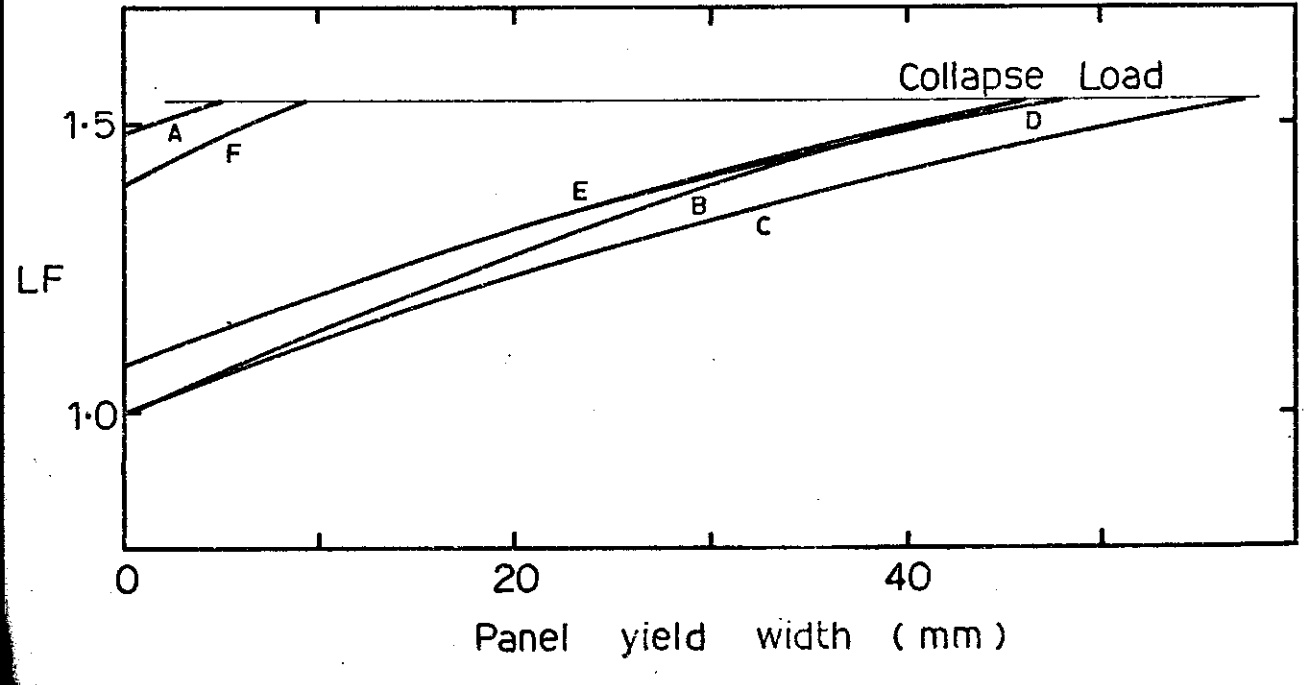

(b) THEORETICAL

FIG. 8·11 COMPARISON OF PANEL YIELDING FOR FRAME 6

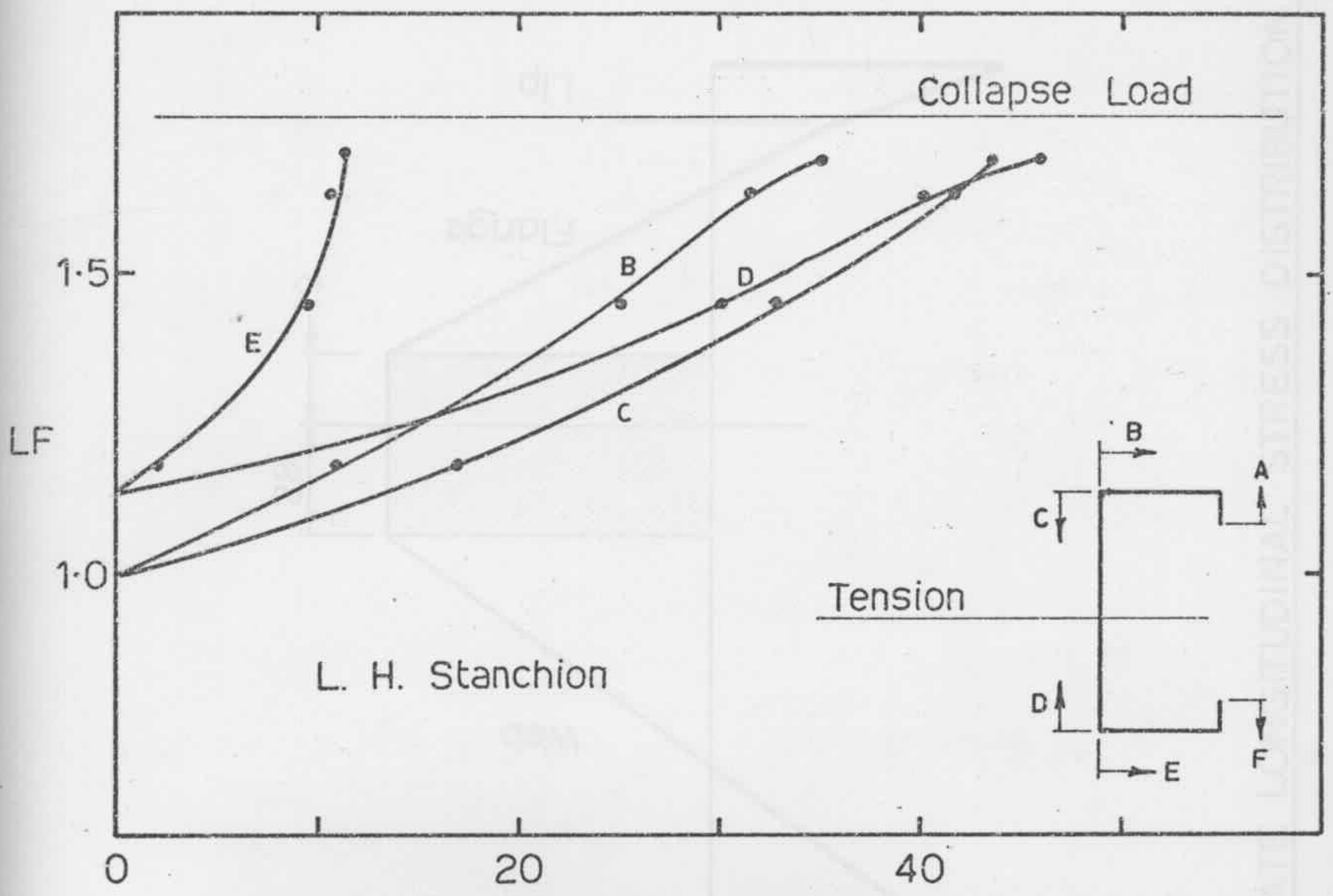

(a) EXPERIMENTAL

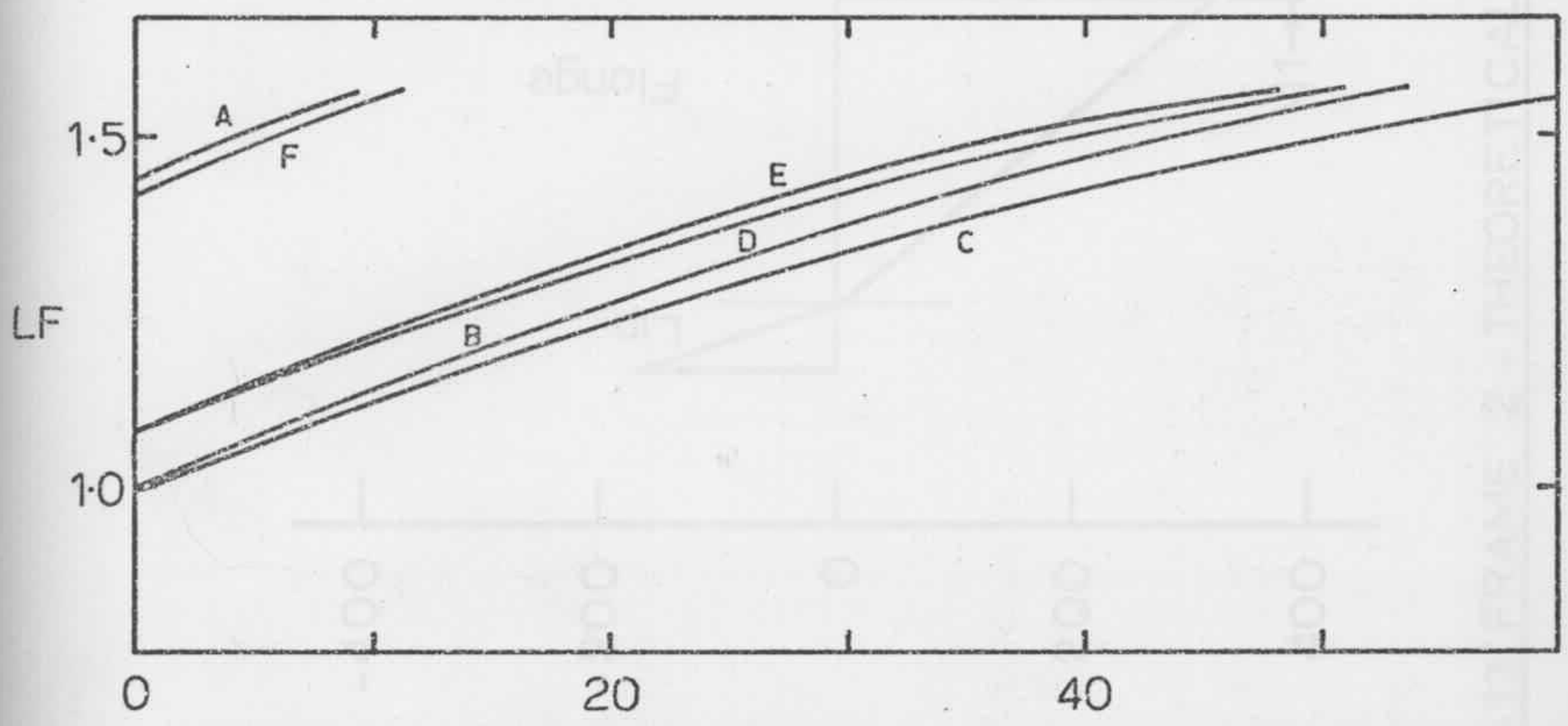

(b) THEORETICAL

FIG. 8·12 COMPARISON OF PANEL YIELDING FOR FRAME 7

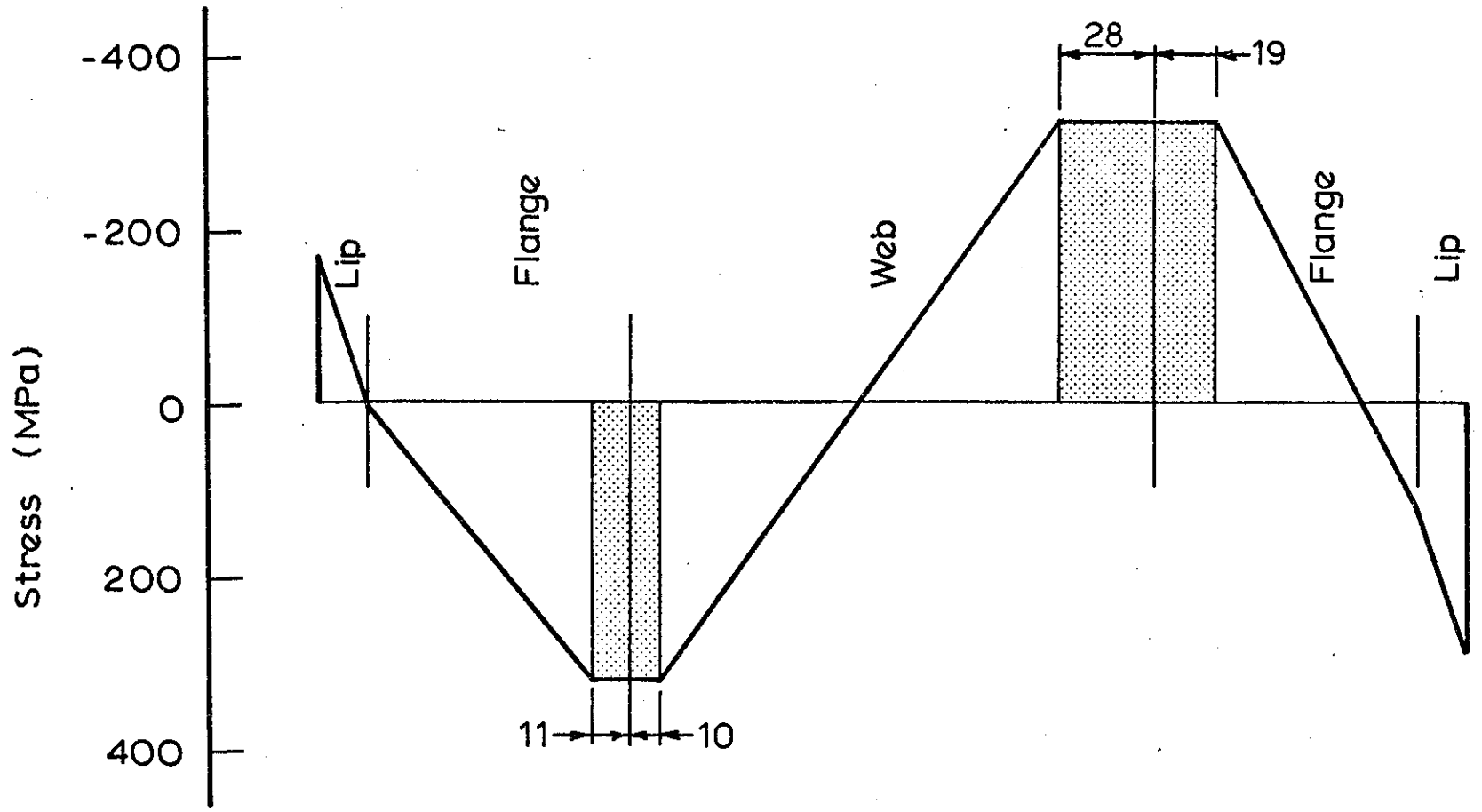

FIG.8.13 FRAME 2 - THEORETICAL ULTIMATE LONGITUDINAL STRESS DISTRIBUTION

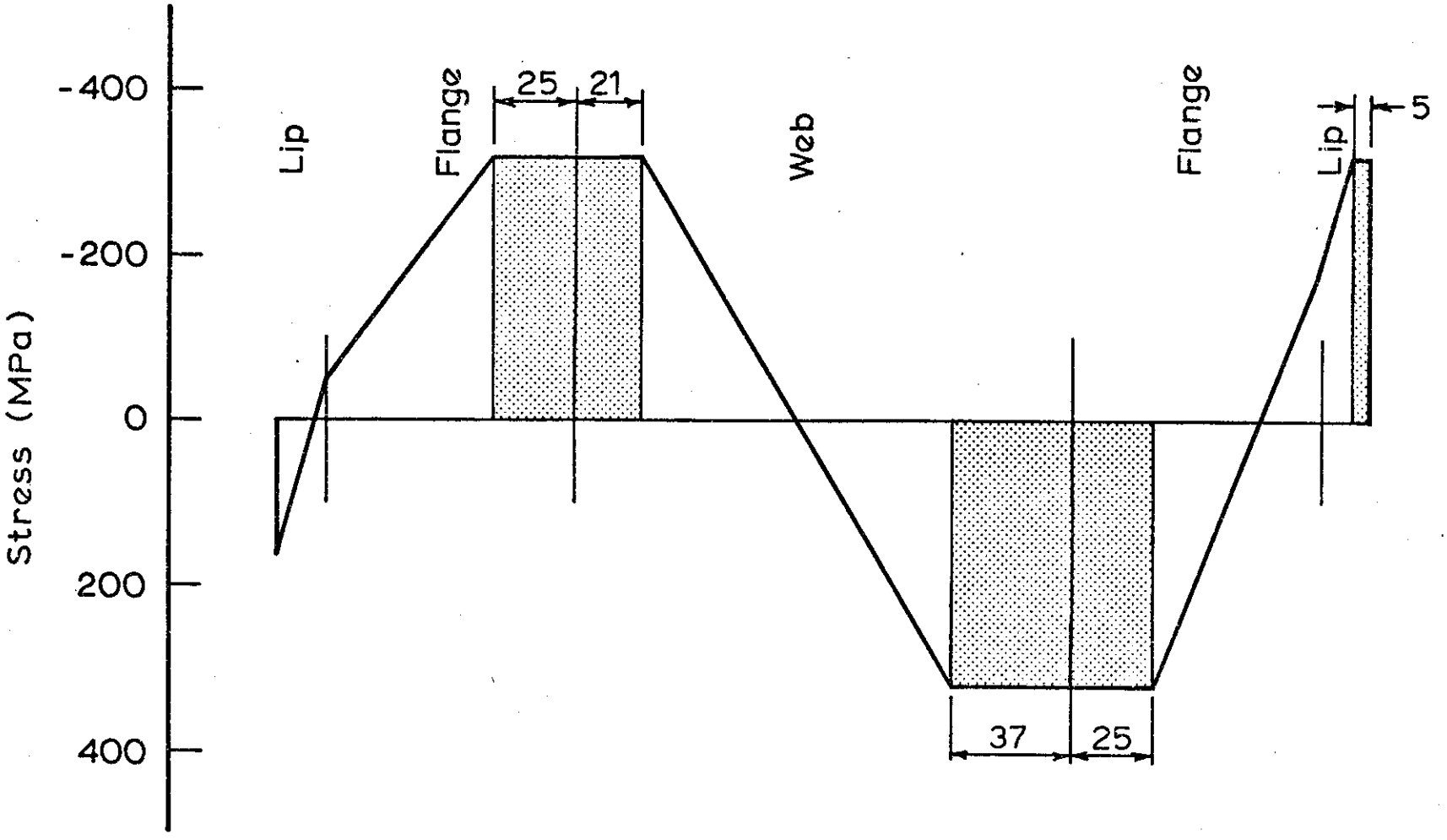

FIG. 8.14 FRAME 3 - THEORETICAL ULTIMATE LONGITUDINAL STRESS DISTRIBUTION - L.H. STANCHION

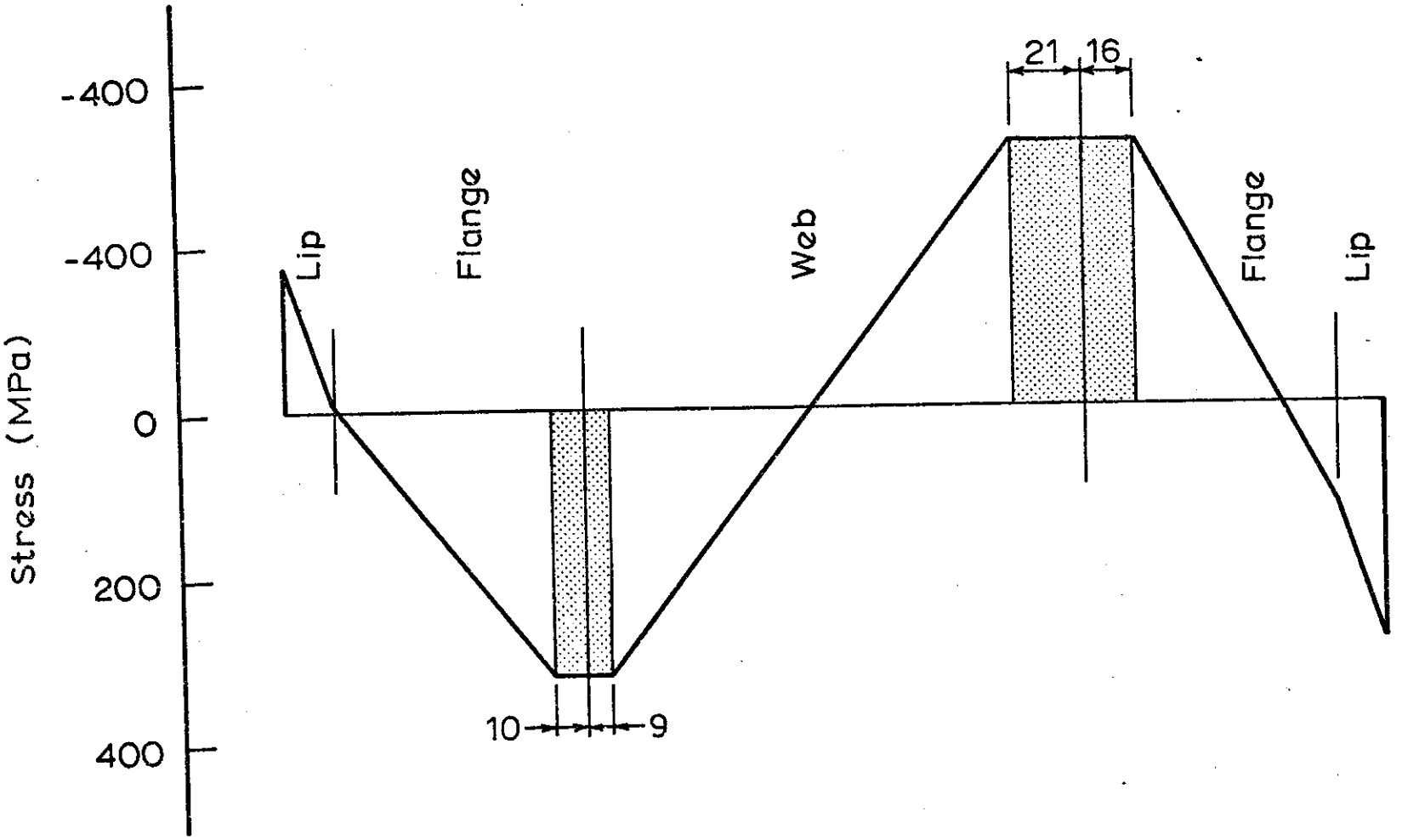

FIG.8.15 FRAME 3 - THEORETICAL ULTIMATE LONGITUDINAL STRESS DISTRIBUTION - R. H. RAFTER

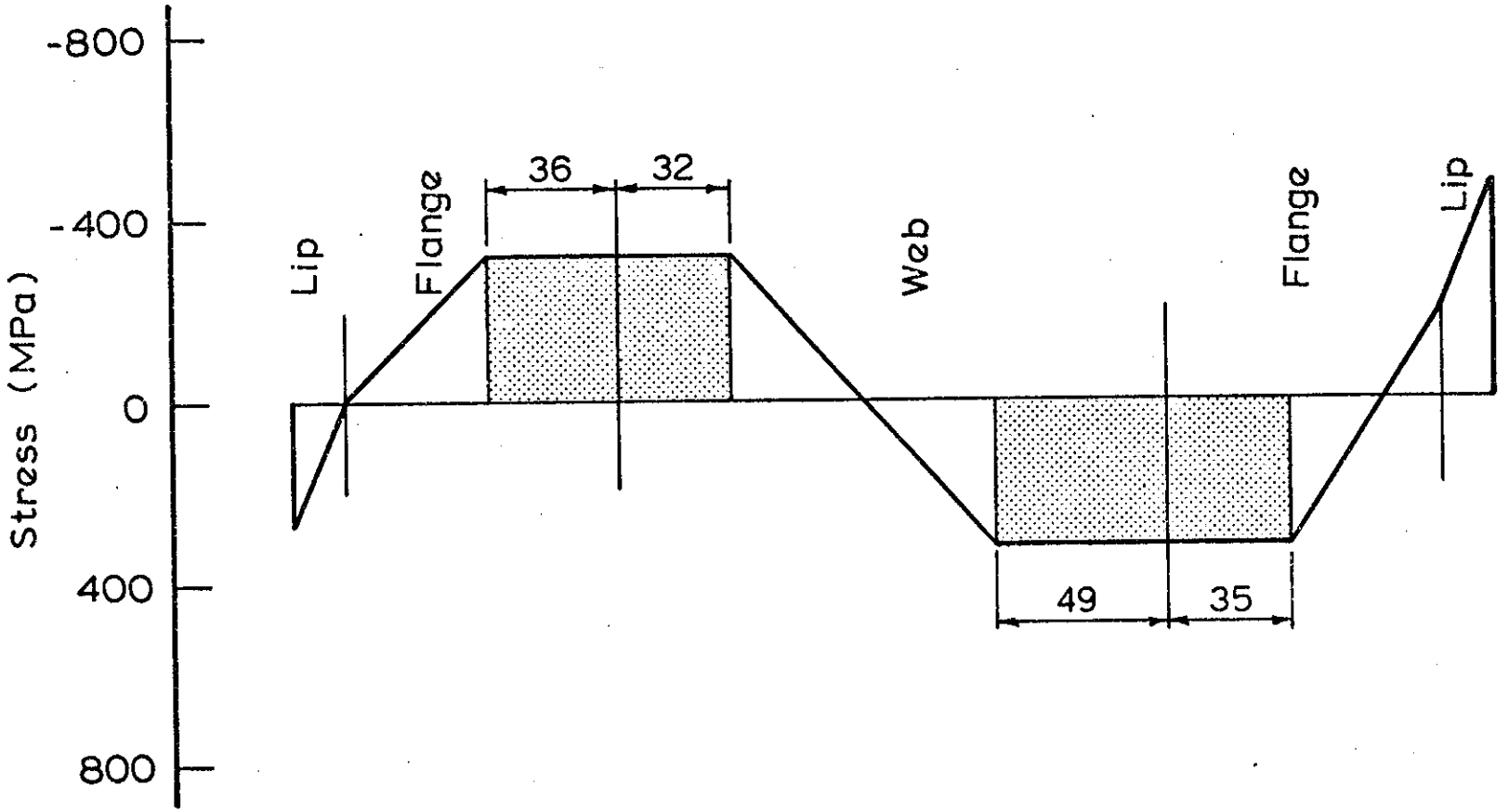

FIG. 8.16 FRAME 4 - THEORETICAL ULTIMATE LONGITUDINAL STRESS DISTRIBUTION

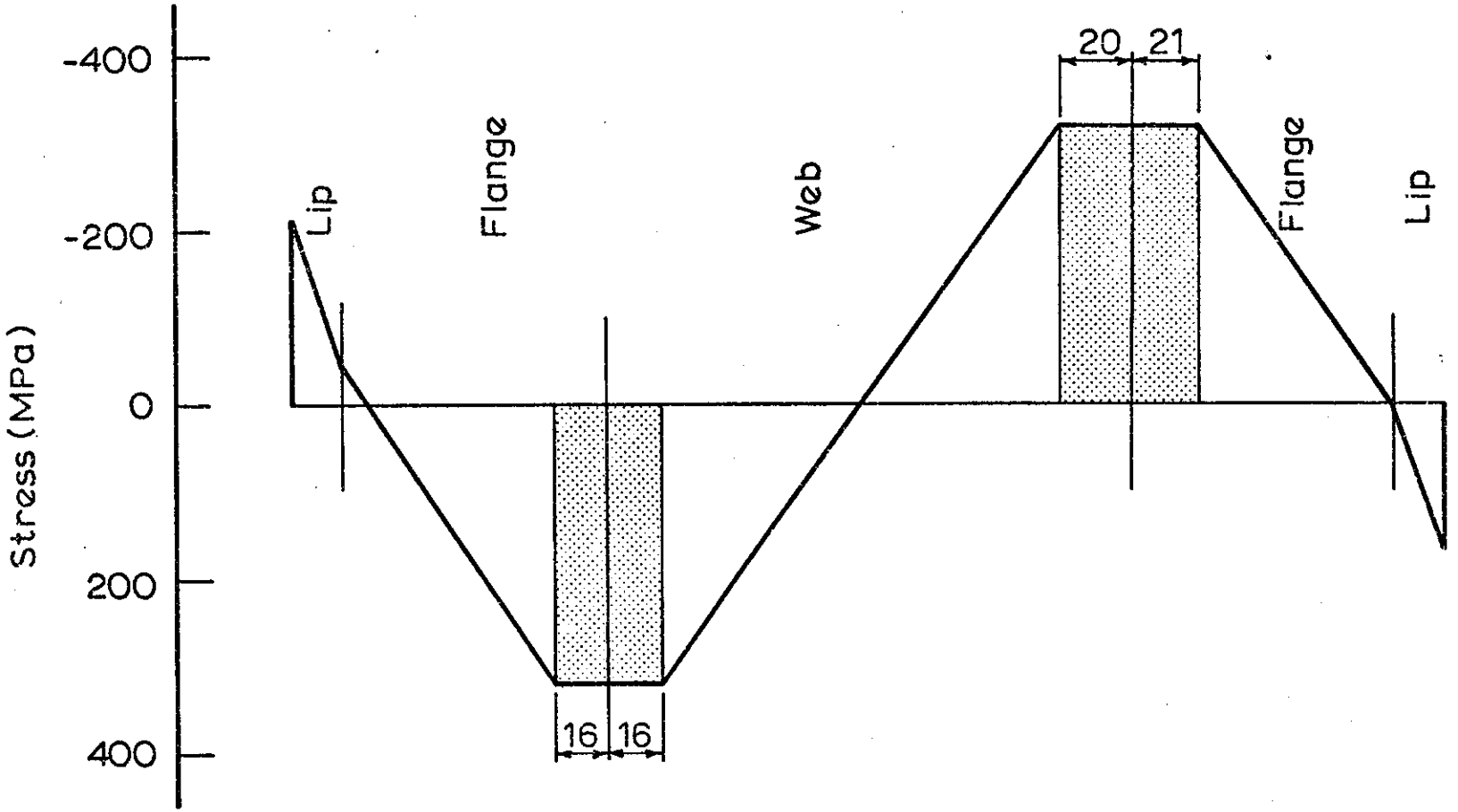

FIG. 8·17 FRAME 5 - THEORETICAL ULTIMATE LONGITUDINAL STRESS DISTRIBUTION

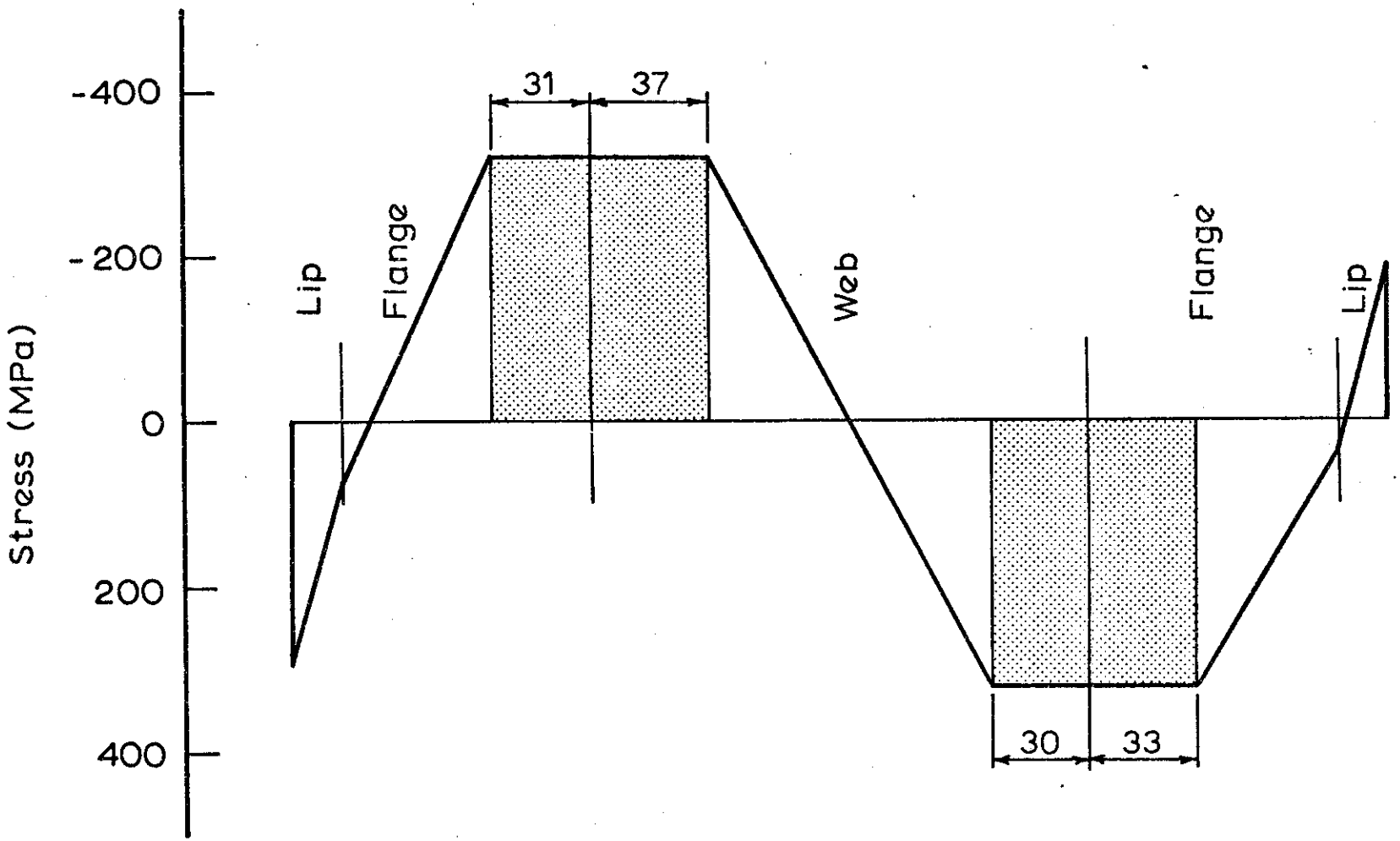

FIG. 8·18 FRAME 6 - THEORETICAL ULTIMATE LONGITUDINAL STRESS DISTRIBUTION - L.H. STANCHION

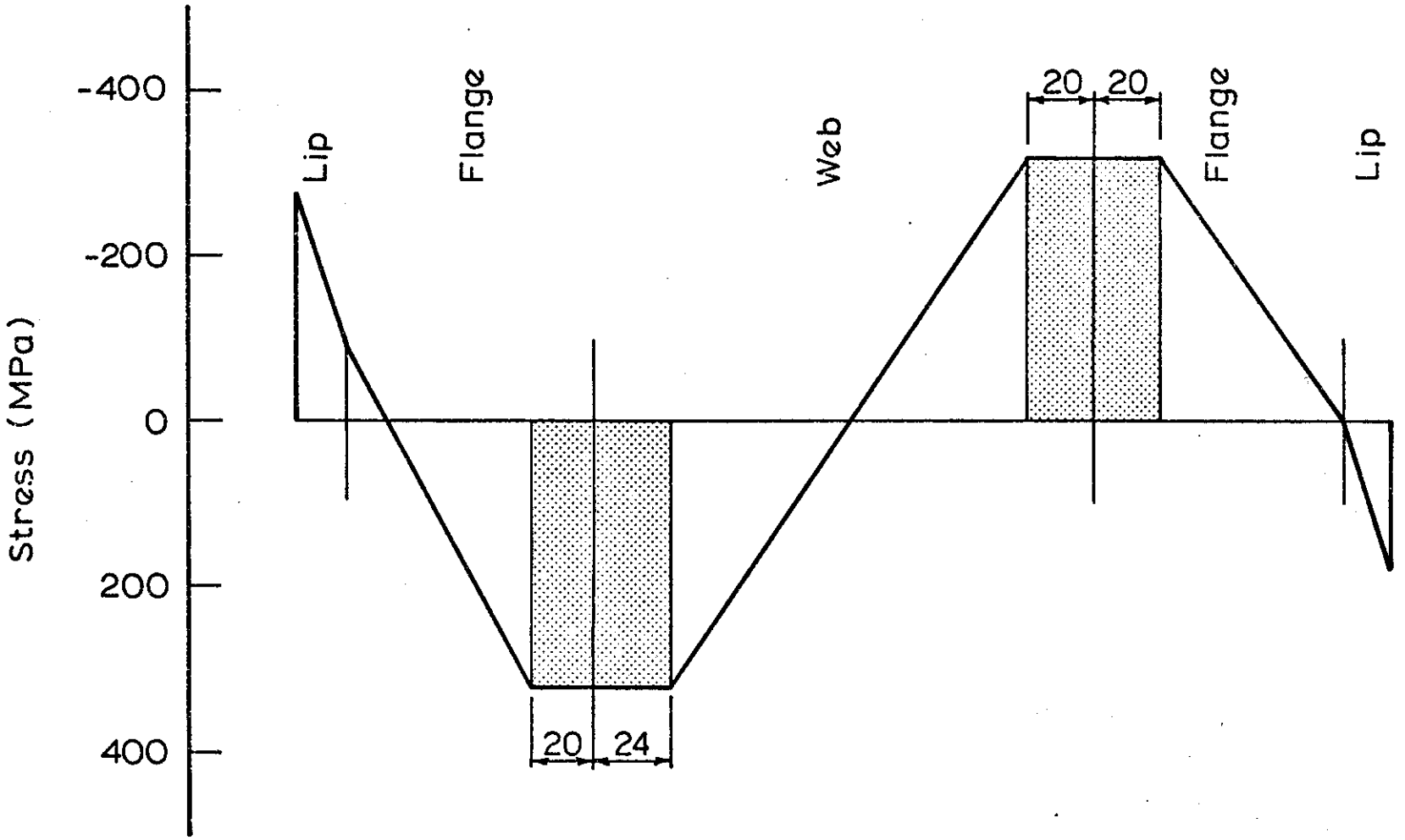

FIG.8.19 FRAME 6 - THEORETICAL ULTIMATE LONGITUDINAL STRESS DISTRIBUTION-R.H.RAFTER

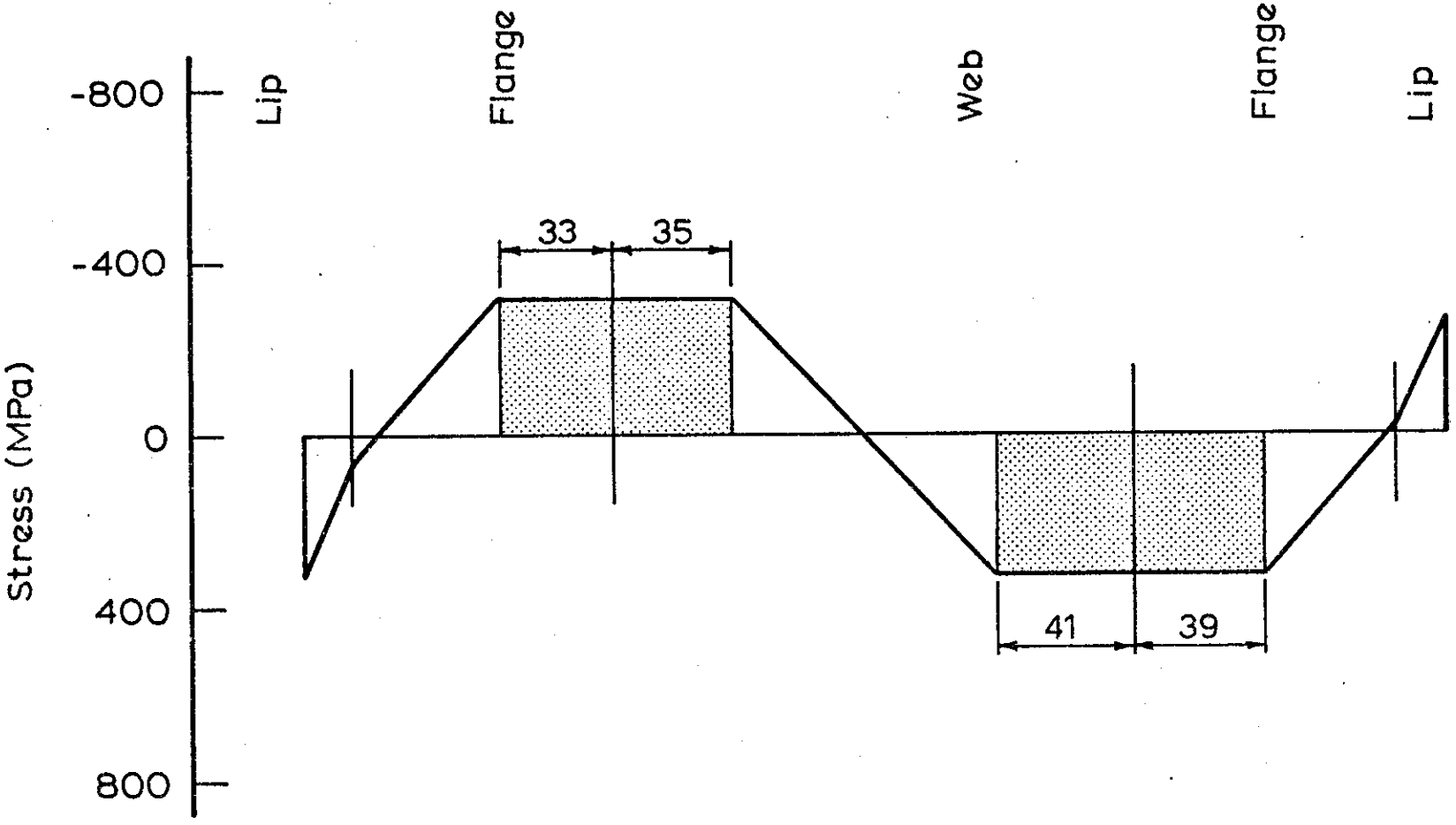

FIG.8·20 FRAME-7 THEORETICAL ULTIMATE LONGITUDINAL STRESS DISTRIBUTION

CHAPTER 9 CONCLUSION

9.1 INTRODUCTION

At the end of each Chapter a summary of the main points covered within that Chapter has been given. For this reason the present conclusions do not summarise completely the work covered in each Chapter. The primary aim here is to summarise the arguments proposed in the thesis and to recapitulate the important results which were based upon these arguments.

Two main themes were interwoven throughout the thesis. The first was based upon analytical models used for solving problems for structural systems composed of thin-walled members. In general, the analytical models were conceptually simpler than classical methods because the computational difficulties were overcome with the immense calculating power of the digital computer. Also the philosophy behind using the analytical methods to model practical structures was presented. The second theme involved the calibration of the theory using carefully designed experimental models. Hence, to observe the behaviour of practical structures, a series of frames composed of thin-walled members was tested. The tests differed from work by previous researchers in that the members of the structural system were composed of cold-formed sections and various loading patterns were used with frames in which the form of lateral and torsional restraint was changed.

9.2 ANALYTICAL MODELS

9.2.1 Elastic Analysis of Complete Structures

The first stage in the analytical development was to produce a method which would perform a linear elastic analysis of a thin-walled structural system. To achieve this objective, a stiffness matrix for a thin-walled element was developed. The stiffness matrix related the displacements of the centroid and shear centre in the direction of the principal axes, to the stress resultants aligned with these axes. Transformation matrices were used to relate the stress resultants and deformations aligned with the principal axes, to the actions and displacements orientated along the frame (or global) axes. The transformation matrices included the bimoments and warping displacements. The stiffness matrix for a complete structural system could then be determined by summation of the elemental stiffness matrices. The stiffness analysis including the effect of warping torsion could therefore be performed. Various conditions of loading and restraint for each member were permitted in the analysis. A member may be supported through the action of either a displacement or torsional restraint. The effect of an eccentricity of a restraint with respect to the centroidal axis of a member was also introduced to permit greater flexibility in the use of the analysis.

A major advantage of the matrix stiffness method is that any set of boundary conditions may be simply incorporated within the analysis. This feature was maintained when thin-walled torsion was incorporated within the method. Care is required in the definition of the warping boundary conditions as they are more difficult to assess than the axial and flexural boundary conditions. Case studies of different joint types showed that inaccuracies in the modelling of joint to member connections resulted in large discrepancies for the in-plane and out-of-plane predicted response. The case of a typical member connection in which the thin-walled members are connected to a prismatic joint was considered. In this case the major-axis moment in the prismatic joint produces both a bimoment and a major-axis moment in the thin-walled members connected to it.

A second advantage of the matrix stiffness method is that it can be fully automated to analyse structural systems of any geometry. This capability was also maintained when thin-walled torsion was included in the analysis. The inclusion of the correct torsional rigidity was important in the analysis of three-dimensional frames since the torsional stiffness contributes significantly to the overall structural stiffness.

9.2.2 Inelastic Analysis of Thin-Walled Cross-Sections

A method has been developed which calculates the elastic-plastic response of the generalised strains for a cross-section subjected to any general load. The method is an extension of the normal moment-curvature analysis of cross-sections in which the usual engineering bending theory assumption that "plane sections remain plane" is not made. Warping displacements and warping strains resulting from restrained torsion are permitted thus allowing yielding as a consequence of restraint to warping in addition to yielding resulting from bending moment and axial force.

Matrix methods were developed for the calculation of section properties. The corresponding equations can be solved for the shear flow distribution and the warping pattern. The section properties derived are for bending about the centroidal axes and twisting about the shear centre axis. For other axes, transformations of the displacements and forces are required to produce a set of stiffnesses about an arbitrary axis system.

As a result of the stresses imposed upon the cross-section, yielding may take place. Once yielding occurs, the total stiffness relationships no longer apply. An alternative approach was clearly required and it involved the use of floating nodes in the panels. The floating nodes

were allowed to move with the yield boundary so that the number of panels in the cross-section remained constant and all panels were either elastic or plastic. The matrix method for calculation of the section properties can be used as before with the modular ratio of the yielded panels being taken as zero. The properties derived using the elastic core can be used as tangent stiffness properties in converging to a non-linear solution, relating the total stress resultants to the generalised cross-section strains. The analysis was useful as it provided information on the amount of yielding that was present in the component plates of the cross-section for a particular value of load. This information was required in the inelastic buckling analysis.

9.2.3 Inelastic Buckling Analysis of Thin-Walled Members

An inelastic buckling analysis was developed which enabled an estimate of the collapse load to be determined, either for a single element or for a light-gauge framework. The method firstly involved obtaining the relevant ratios of the stress resultants at a critical cross-section location for a particular load set. Using the stress resultant ratios, an inelastic cross-section analysis was then performed. The analysis enabled a prediction of the strains in the cross-section which indicated the location and

extent of yielding in the panels as a result of the increasing load.

The results from the analysis were utilised in an inelastic buckling analysis in which the finite strip method was utilised. For the inelastic buckling analysis, the cross-section was described as a number of longitudinal plate elements. If yielding occurred in a panel, the material properties for the panel were altered accordingly. For a particular load set, the minimum buckle half wavelength for the cross-section was obtained. The buckling load factor for this buckle half wavelength was then plotted against the applied loading. Thus the critical load for the cross-section location was given when the minimum buckling load factor had the value of the load factor of the stress resultants applied to the cross-section.

The effect of different stress resultants upon a channel section was studied. The method is useful in that it can produce the buckling load as well as the buckled configuration of the cross-section, enabling the buckle mode to be determined. Hence, a plot of buckling load against the buckle half wavelength may be quickly obtained. However, the method is more useful for the prediction of the ultimate load carrying capacity of a structural system. It is essential that the members within the system are adequately restrained against a lateral-torsional failure. If this is the case, failure will occur through

the formation of a localised buckle enabling the analysis to provide an estimate of the collapse load.

9.3 EXPERIMENTAL RESULTS

The aim of the experimental study was to investigate the elastic response and collapse behaviour of thin-walled plane frames. The frames were modelled on the typical geometry of a low-rise industrial framed building. A restraint system was employed which modelled the restraining action of the purlins and girts. Each restraint was designed kinematically to prevent lateral movement but to allow all other deformations to occur. Restraint from rotation about the longitudinal axis could be achieved at various locations. Three different loading patterns were chosen. In turn, each loading pattern was applied firstly to a frame with lateral displacement restraints only and secondly to a frame with both lateral and torsional restraints. The loading was applied to the members of the frame at the positions of the lateral restraints. This was equivalent to the loading from the cladding of the frame being transmitted to the frame by way of the purlins and girts.

The tests were successful in achieving their aims. Firstly, relevant deformations were obtained both in the elastic and inelastic regions for the response of the frame. The deformations

were classed as either in-plane or out-of-plane responses. The effect of the loading pattern upon the deformations was successfully determined from the first series of tests. The second series, in which lateral and torsional restraints were attached to the frame, provided a comparison between the deformations not only for different loading patterns but also for a different level of restraint. The deformations for each series showed correlation to the applied pattern of loading. The effect of torsional restraint had a marked effect in both the out-of-plane as well as in-plane responses. The stiffness of the second series of frames was enhanced through the presence of the torsional restraints.

Secondly, the experimental investigation enabled the in-plane bending moment distribution to be examined. Because the cross-sectional dimensions of cold-formed members are too thin to develop plastic hinge action, little rotation occurred in the members before collapse. However, the response was not strictly linear as a small amount of moment redistribution was observed. The minor-axis bending moment, axial force and bimoment distributions were also determined from the experimental study. The response of the minor-axis bending moment and axial force at a particular location were not always linear. However, the discrepancy may be explained because of the much smaller magnitude of these strains.

The experimental analysis also enabled a closer examination of the transmission of the moments and forces from one member to another through a joint. The joint chosen for the study did not allow full continuity of the members. The web of each member was rigidly attached to the joint plate and the flanges were free to warp relative to the web. However, the study revealed that even though the joint could not restrain warping, continuity of the moments and forces was achieved across the joint. The experimental investigation also showed that the system used for the joining of the members could have a large influence on the in-plane and out-of-plane deformations. The joint system chosen permitted a more flexible response than a system in which full continuity of members was achieved.

The joint system was also important because of its influence on the collapse behaviour of the frame. The system chosen for the experimental study produced higher stresses near the joints than if full continuity of members was used. The higher stresses were responsible for localised failure in the component plates of the cross-section. The localised failures, in turn, had an effect upon the ultimate load of the overall structural system. Also, the nature of the connection of the member at the joint allowed the torsional response to influence the stress distribution in the member. Hence, it is possible to predict the effect of the joint detail on the collapse load of the structure with

confidence. It may be concluded that a joint in which full continuity of each member is achieved will result in the attainment of a higher collapse load than for the type of joint used in the experimental study. For a joint in which the flanges of each member are partially prevented from warping but are not connected to the joint, the collapse load would lie between the experimental model and the fully continuous case. This is because the torsional stresses are reduced allowing the major-axis bending moment to become the dominant failure inducing stress resultant.

Lastly, the experimental study permitted the collapse modes and ultimate loads for the frames to be studied. The effect of the lateral and torsional restraints upon ultimate characteristics was also displayed. Each frame failed because of a localised instability effect and not because of an overall member failure. The localised failure zones were situated adjacent to the joints in the regions of highest in-plane bending moment and highlighted the importance of the jointing system upon the ultimate load carrying capacity. The first series of tests showed that failure occurred when the compressive load carrying capacity of the cross-section was exceeded. The deformations of the compression flange were a significant contribution to the failure mechanism. The second series of tests restricted the capacity of the cross-section, particularly the compression flange, to rotate. The restraint of the flange

resulted in an increase of the ultimate load for corresponding loading patterns. The tests also revealed that very little plastic deformation occurred in the members of each frame. Apart from the regions of localised failure in each member, there was no evidence of plastic deformation in any other region.

9.4 QUANTITATIVE COMPARISON OF ANALYTICAL MODELS AND EXPERIMENTAL RESULTS

The simulation of the test frame behaviour using the analytical models was generally quite successful. Two separate and distinct responses were modelled. Firstly, the linear elastic deformational response is important because it is used by designers as a guide to the performance of the structural system under working loads. Secondly, the ultimate load carrying capacity of the thin-walled structural system was predicted. The ultimate load carrying capacity is also of importance to the designer as it permits the stresses to be determined and enables the members in the system to be proportioned according to the stresses.

The data from the experimental tests was compared with predictions produced using a linear elastic matrix displacement analysis. The analysis included the thin-walled torsion theory derived by Vlasov and cross-section monosymmetry. The analytical predictions were quite accurate for the in-plane response. The

effect of torsional deformations on the in-plane deflections was accurately modelled. The importance of the precise modelling of joints in thin-walled structural systems was emphasised. It was only through an understanding of the bimoments in members adjacent to a joint that the in-plane response was able to be precisely determined. However, the nature of the problem presented difficulties for the accurate prediction of the out-of-plane response. It was discovered that an analysis assuming rigid body deformation of the members was insufficient to predict the elastic response of the structure at the load points. This situation arose because of the distortional rotation which was taking place within the cross-section. It was found necessary to superimpose the distortional deformations, derived from a finite strip analysis, on the rigid body rotations. The distortional analysis clearly showed that significant deformations can arise through cross-sectional distortion occurring at points of concentrated load. However, the distortional analysis appeared to be inadequate for the determination of the longitudinal rotation of the rafter in Frame 3. It was also observed that this particular member in Frame 3 displayed other pecularities. The major-axis bending moment distribution was a pertinent example. Associated with this was the behaviour of the rafter stress distribution which was plotted for the load at which first yield was observed. In both these cases the correlation between theory and experiment was particularly poor. Hence, for

all the frames, with the exception of the rafter members in Frame 3, the comparison between the theoretical and experimental in-plane and out-of-plane elastic responses was sufficiently accurate for engineering purposes.

All three analytical models were used for the determination of the ultimate load of each frame. The ultimate load of a thin-walled structural system which is adequately restrained was found to be limited to the local buckling resistance of the cross-section. Local buckling took place in the regions of peak major-axis bending moment. The analytical model showed that the local buckling load was dependent upon the ratios of the stress resultants acting at a particular cross-section location. This occurred because the ratios of the stress resultants affect the position and rate of yielding which occurs in the cross-section. In some cases the analytically determined buckling loads were reasonably accurate. However, the predictions were all conservative. The conservatism was attributable to inaccuracies in the modelling of the behaviour of the cross-section in the inelastic range. Inaccuracies may result from a number of causes. The most obvious is the distribution of material yield stress around the cross-section which is dependent upon the residual stresses caused by cold-forming. The position of the yield boundaries at a particular load factor is also very important. The experimental measurements of strain showed that the simulation

of panel yielding was not accurately modelled for some panels of the cross-section. Moveover, it was observed that for these panels the rate of yielding decreased with increasing load, probably as a result of strain hardening. Hence for a particular load factor, the theoretical elastic core of the cross-section was smaller than the experimental cross-section resulting in a lower collapse load for the frames. The collapse load predictions for Frames 4 and 7 were the most conservative and it was for these two frames that the decreasing rate of yielding was most evident. As collapse occurred adjacent to the eave joints in the stanchions of these frames it appears that the decrease in the rate of panel yielding was influenced by the presence of axial tension in these members.

Further inaccuracies may result from an incorrect choice of stress resultants which may be caused by two main effects. Firstly, the method for predicting the collapse loads required that the buckling location be accurately chosen. The choice of position influences the ratios of the stress resultants through the presence of moment gradients. Secondly, the stress resultant ratios will change by the process of moment redistribution a the ultimate load is approached. In this thesis the problem of moment redistribution was not attempted. This was firstly because of the complex nature of the problem and secondly because of the thinness of the sections used in the experimental study in

which it was envisaged that local buckling failure would occur at loads not too far above first yield.

9.5 SUMMARY AND RECOMMENDATIONS

The work presented in this thesis has dealt exclusively with thin-walled structures. Their analysis and behaviour has been of particular interest. Analytical methods have been developed and compared with the results of a comprehensive experimental investigation. Theory and experiment have correlated quite well.

In conclusion, this thesis goes further than the consideration of thin-walled members alone and includes the behaviour of complete structures. It includes their linear elastic response as well as the ultimate behaviour of representative structural systems. Such studies are currently justified to help designers understand the complex behaviour of thin-walled structural systems.

The work in this thesis has inevitably opened new fields which need to be studied in greater detail. Firstly, the experimental investigation could be further refined and extended by considering new jointing systems as well as different forms of lateral restraint and variations in the cross-section of the members of the structure. Structures of differing geometry would also make an interesting study. Secondly, the analytical models could be further refined. The most obvious development would be in the prediction of the ultimate behaviour. The separate analyses presented in this thesis could be combined and the prediction of lateral-

torsional failures could be investigated. It would then be possible to finally predict the full load-deformation response of the structural system under prescribed static loading.

REFERENCES

Abeld-Sayed, G. (1969), "Effective Width of Thin Plates in Compression", ASCE, Journal of the Struct. Divn., Vol. 95, ST10, pp. 2183-2203.

Akay, H.V., Johnson, C.P. and Will, K.M. (1977), "Local and Lateral Buckling of Beams and Frames", ASCE, Journal of the Struct. Divn., Vol. 103, No. ST9, September, pp. 1821-1832.

American Iron and Steel Institute, (1968), "Specification for the Design of Cold-Formed Steel Structural Members."

Ammar, A.R. and Nilson, A.H. (1973), "Analysis of Light Gauge Steel Shear Diaphragms, Parts I and II", Research Reports Nos. 350 and 351, Department of Civil Engineering, Cornell University, Ithaca.

Argyris, J.H. (1960), "Energy Theorems and Structural Analysis", Butterworths, Originally published in Aircraft Engineering Oct., Nov., 1954: Feb., March, April, May, 1955.

Argyris, J.H. and Dunne, P.C. (1952), "Structural Principles and Data, Handbook of Aeronautics, No. 1," (Part II, Structural Anaysis, Fourth Ed.) Pitman Publishing Corp., New York.

Argyris, J.H. and Radaj, D. (1971), "Steifigkeitsmatrizen dunnwandiger Stabe und Stabsysteme", Ingenieur - Archiv., Vol. 40, pp. 198-210.

Bartels, D. and Bos, C. A. M. (1973), "Investigation of the Effect of the Boundary Conditions on the Lateral Buckling Phenomenon, taking account of Cross-Sectional Deformation", Heron, Vol. 19, No. 1.

Bazant, Z. P. and El Nimeiri, M. (1973), "Large-Deflection Spatial Buckling of Thin-Walled Beams and Frames", ASCE, Journal of the Engineering Mechanics Divn., Vol. 99, No. EM6, December, pp. 1259-1281.

Beck, V.R. (1974), "Behaviour and Design of Cold Formed Members", Steel Construction, Vol. 8, No. 3.

Becker, H. (1957), "Handbook of Structural Stability. Part II - Buckling of Composite Elements", NACA TN 3782, July.

Bernoulli, J. (1744), "Veritable hypothese de la resistance des Solides, avec la demonstration de la Courbure des Corps qui font ressort", Varia Posthuma, Vol. II, pp. 976-989.

Bijlaard, P.P. and Fisher, G.P. (1953) "Column Strength of H-Sections and Square Tubes in Post-Buckling Range of Component Plates", NACA TN2994.

Bishop, R.E.D., Gladwell, G.M.L. and Michaelson, S. (1965), The Matrix Analysis of Vibration, Cambridge University Press.

Black, M. M. (1967), "The Analysis and Design of Thin-Walled Open Section Beams", Proceedings, Symposium on Thin-Walled Steel Structures, University College, Swansea.

Black, M. M. and Semple, H. M. (1969), "Torsion-Bending Analysis of Continuous Thin-Walled Beams", Int. J. Mech. Sci., Vol. II, No. 10, October, pp. 791-810.

Bleich, F. (1924), "Theorie und Berechnung der eisernen Brucken", Julius Springer, Berlin.

Bleich, F. (1952), Buckling Strength of Metal Structures, McGraw-Hill Book Co. Inc., New York.

British Standards Institution (1974), "Specification for the Use of Cold Formed Steel Sections in Buildings", PD 4064, Addendum No.1 to BS449: 1969.

Brunel, I. K. (1851), Discussion, An Investigation of the Strains upon the Diagonals of Lattice Beams, with the Resulting Formulae, W. T. Boyne and W. B. Blood., Minut. Proc. Instn. Civ. Engrs., Vol. 11, p. 14.

Bryan, E. R. (1972), The Stressed Skin Design of Steel Buildings, Crosby Lockwood Staples, London.

Bryan, E. R. and Deakin, W. H. (1979), "Design and Testing of a Light Gauge Steel Storage Platform", International Conference on Thin-Walled Structures, University of Strathclyde.

Bryan, G. H. (1890), "On the Stability of a Plane Plate Under Thrusts in its own Plane", Proc. London Math. Soc., Vol. 22, Dec., pp. 54-67.

Budiansky, B., Daw, N. F., Peters, R. W. and Shepherd, R. P. (1952), "Experimental Studies of Polyaxial Stress-Strain Laws of Plasticity", Proc. of First National Congress on Applied Mechanics.

Bulson, P. S. (1967), "Local Instability and Strength of Structural Sections", Thin-Walled Structures, Edited by A. H. Chilver, Chatto and Windus, London, pp. 153-207.

Bulson, P. S. (1970), The Stability of Flat Plates, Chatto and Windus, London.

Campbell, J. D. (1978), Program FOFEA, C. A. Hawkins Computing Laboratory, Dept. of Civil Engineering, Sydney University.

Chajes, A., Britvec, S. J. and Winter, G. (1963), "Effects of Cold Straining on Structural Sheet Steels", ASCE, Journal of the Struct. Divn., Vol. 89, No. ST2, April, pp. 1-32.

Chajes, A., Fang, P. J. and Winter, G. (1966), "Torsional Flexural Buckling, Elastic and Inelastic of Cold Formed Thin Walled Columns", Cornell Engineering Research Bulletin, 66-1, Cornell University.

Cheung, Y. K. (1969), "Folded Plate Structures by Finite Strip Method", ASCE, Journal of the Struct. Divn., Vol. 95, No. ST12, December, pp. 2963-2979.

Cheung, V. K. (1976), Finite Strip Method in Structural Analysis, Pergamon Press, Oxford.

Chilver, A. H. (1953A), "The Stability and Strength of Thin-Walled Steel Struts", The Engineer, pp. 180-183.

Chilver, A. H. (1953B), "A Generalised Approach to the Local Instability of Certain Thin-Walled Struts", Aeronautical Quarterly, Vol.4, August, pp. 245-260.

Chwalla, E. (1940), Erlauterungen zur Begrundung des Normblattentwurfes, Knick-und Beulvorschriften fur Stahlbau. (DIN E 4114).

Clark, E. (1850), "Britannia and Conway Tubular Bridges", Longmans, London.

Clough, R. W. (1956), "Structural Analysis by Means of a Matrix Algebra Program", ASCE, 1st Conference on Electronic Computation.

Coan, J. M. (1951), "Large Deflection Theory for Plates with Small Initial Curvature Loaded in Edge Compression", ASME, Journal of Applied Mechanics, Vol. 18, June, pp. 143-151.

Coker, E. G., Chakko, K. C., and Ahmed, M. S. (1921), "Contact Pressures and Stresses", Proceedings, Institution of Mech. Engineers, May, pp. 365-467.

Column Research Committee of Japan (1971), Handbook of Structural Stability, Corona Publishing Company.

Column Research Council (1976), Guide to Design Criteria for Metal Compression Members, 3rd Edition, Ed. Johnston, B. G., John Wiley, New York.

Cox, H. L. (1933), "Buckling of Thin Plates in Compression", Technical Report and Memorandum No. 1554, Aeronautical Research Council, London.

Davies, J. M. (1976), "Calculation of Steel Diaphragm Behaviour", ASCE, Journal of the Struct. Divn., Vol. 102, No. ST7, July, pp. 1411-1430.

Davies, J. M. (1977), "Simplified Diaphragm Analysis", ASCE, Journal of the Struct. Divn., Vol. 103, No. ST11, Nov., pp. 2093-2109.

Davies, J. M. and Bryan, E. R. (1979), "Design Tables for Light Gauge Steel Diaphragms", International Conference on Thin-Walled Structures, University of Strathclyde.

Dawson, R. G. and Walker, A. C. (1972A), "A Proposed Method for the Design of Thin-Walled Beams which Buckle Locally", The Structural Engineer, Vol. 50, No. 2, February, pp.95-105.

Dawson, R. G. and Walker, A. C. (1972B), "Post-Buckling of Geometrically Imperfect Plates", Proc. of the ASCE, Journal of the Struct. Divn., Vol. 98, ST1, January, pp. 75-94.

Desmond, T. P. (1977), "The Behaviour and Strength of Thin-Walled Compression Elements with Longitudinal Stiffeners", Dept. of Structural Eng. Report No. 369, Cornell University, Ithaca, N. Y., April.

Desmond, T. P., Pekoz, T. and Winter, G. (1978), "Edge Stiffeners for Cold-Formed Steel Members", Fourth International Speciality Conference on Cold-Formed Steel Structures, University of Missouri - Rolla, June.

De Wolf, J. T., Pekoz, T. and Winter, G. (1974), "Local and Overall Buckling of Cold-Formed Members", Proc. of the ASCE, Journal of the Struct. Divn., Vol. 100, ST10, October pp. 2017-2038.

Dhalla, A. K. and Winter, G. (1971), "Ductility Criteria and Performance of Low Ductility Steels for Cold Formed Members", Proc. of First Speciality Conference on Cold Formed Steel Structures, Dept. of Civil Engineering, University of Missouri - Rolla, August.

Divakaran, S. (1966), "Local Instability of Thin-Walled Channel Columns with Formed Longitudinal Stiffeners of Circular Cross-Section", Ph. D. Thesis, University of Toronto.

Dooley, J.R. (1967), "On the Torsional Buckling of Columns of I-Section Restrained at Finite Intervals", International Journal of Mechanical Sciences, Vol. 9, No.1, Jan., pp. 1-9.

El Darwish, I. A. and Johnston, B. G. (1965), "Torsion of Structural Shapes", ASCE, Journal of the Struct. Divn., Vol. 91, No. ST1, February, pp. 203-227.

Falkenheimer, H. (1953), "Systematic Analysis of Redundant Elastic Structures by Means of Matrix Calculus", Journal Aeronautical Sciences, Vol. 20, No. 4, pp. 293.

Feigen, M. (1954), "Inelastic Behaviour Under Combined Tension and Torsion", Proc. of the Second National Congress on Applied Mechanics.

Fischer, M. (1967), "Dass Kipp - Problem querbelasteter exzentrisch durch Normalkraft beanspruchter I-Trager bei Verzicht auf Voraussetzung der Querschnittstreue", Der Stahlbau, No. 3, March, pp. 77-86.

Galambos, T. V. (1968), Structural Members and Frames, Prentice-Hall, Englewood Cliffs, New Jersey.

Ghobarah, A. A. and Tso, W. K. (1969), "Overall and Local Buckling of Channel Columns", ASCE, Journal of the Eng. Mech. Divn., Vol. 95, No. EM2, April, pp. 447-462.

Gibson, E. B. (1974), "Modern Use of Cold-Formed Steel Products", Design in Cold-Formed Steel, University of Waterloo, Waterloo, Ontario, pp. 1-36.

Goldberg, J. E., Bogdanoff, J. L. and Glauz, W. D. (1964), "Lateral and Torsional Buckling of Thin-Walled Beams", Publ. IABSE, Vol. 24, pp. 92-100.

Goodier, J. N. and Barton, M. V. (1944), "The Effects of Web Deformation on the Torsion of I-Beams", ASME, Transactions, Vol. 66, pp. A35-A40.

Gozum, A. T. and Huber, A. W. (1958), "Material Properties, Residual Stresses and Column Strength", Fritz Lab. Report 220A.33, Lehigh University, November.

Graves-Smith, T.R. (1968), "The Post-Buckled Strength of Thin-Walled Columns", Final Report of the Eighth Congress, International Association for Bridge and Structural Engineering, New York, pp. 311-320.

Graves-Smith, T.R. (1969), Proceedings of the International Conference on Structures, Solid Mechanics and Engineering Design, J. Wiley.

Guyon, Y. (1951), "Constraintes dans les pieces prismatiques soumises a des forces appliquees sur leurs bases au voisinage de ces bases", "IABSE, Publications Vol. 11, pp. 165-226.

Haaijer, G. (1957), "Plate Buckling in the Strain-Hardening Range", ASCE, Journal of the Eng. Mech. Divn., Vol. 83, No. EM2, April, pp. 1212-1 to 1212-47.

Hancock, G. J. (1975), The Behaviour of Structures Composed of Thin-Walled Members, Ph.D. Thesis, School of Civil Engineering, University of Sydney.

Hancock, G. J. (1977A), "Elastic-Plastic Analysis of Thin-Walled Cross-Sections", Sixth Australasian Conference on the Mechanics of Structures and Materials, University of Canterbury, Christchurch, New Zealand, August.

Hancock, G. J. (1977B), "Local, Distortional and Lateral Buckling of I-Beams", University of Sydney, School of Civil Engineering, Research Report R312, December.

Hancock, G. J. (1978), "Local, Distortional and Lateral Buckling of I-Beams", ASCE, Journal of the Struct. Divn., Vol. 104, No. ST11, November, pp. 1787-1798.

Hancock, G. J. and Harrison, H. B. (1972), "A General Method of Analysis of Stresses in Thin-Walled Sections with Open and Closed Parts, Civil Eng. Trans., Inst. Eng. Aust., Vol. CE14, No. 2, October, pp. 181-188.

Harrison, H. B. (1973), Computer Methods in Structural Analysis, Prentice-Hall Inc., New Jersey.

Harvey, J. M. (1953), "Structural Strength of Thin-Walled Channel Sections", Engineering, Vol. 75, pp. 291-293.

Hasegawa, A. and Maeno, H. (1979), "Design of Edge Stiffened Elements", International Conference on Thin-Walled Structures, University of Strathclyde.

Hemans, G. W. (1844), "Description of a Wrought-Iron Lattice Bridge Lately Erected on the Line of the Dublin and Drogheda Railway, Minut. Proc. Instn. Civ. Engrs., Vol. 3, pp. 63-65.

Horne, M. R. (1963), "Elastic Plastic Failure Loads of Plane Frames", Proceedings of the Royal Society, London, England, Series A, Vol. 274, pp. 342-364.

Horne, M. R. and Ajmani, J. L. (1971), "Design of Columns Restrained by Side-Rails", The Structural Engineer, Vol. 50, No. 8, August, pp. 339-345.

Horne, M. R. and Narayanan, R. (1976), "Strength of Axially Loaded Stiffened Panels", IABSE 36-I, pp. 125-157.

Hu, P. C., Lundquist, E. E. and Batdorf, S. B., (1946), "Effect of Small Deviations from Flatness on Effective Width and Buckling of Plates in Compression", NACA TN 1124, Sept.

Hu, P. C. and McCulloch, J. C. (1947), "The Local Buckling Strength of Lipped Z-Columns with Small Lip Width", NACA TN 1335, June.

Hutchings, R. H. (1973), "The Elastic-Plastic Behaviour of Columns under Biaxial Loading", Ph.D. Thesis, University of Manchester.

Ilyushin, A. A. (1947), "The Elasto-plastic Stability of Plates", (translation from Russian), NACA TM 1188.

Jennings, A. and Majid, K. I. (1965), "Elastic-Plastic Analysis by Computer", Structural Engineer, Vol. 43, December, pp. 407-412.

Johnson, A. L. and Winter, G. (1966), "Behaviour of Stainless Steel Columns and Beams", ASCE, Journal of the Struct. Divn., Vol. 92, No. ST5, October, pp. 97-118.

Johnson, C. P. and Will, K. M. (1974), "Beam Buckling by Finite Element Procedure", ASCE, Journal of the Struct. Divn., Vol. 100, No. ST3, March, pp. 669-685.

Johnson, J. H. and Noel, R. G. (1953), "Critical Bending Stress for Flat Rectangular Plates Supported along all Edges and Elastically Restrained Against Rotation along the Unloaded Compression Edge", Journal of Aeronautical Services, Aug.

Jombock, J. R. and Clark, J. W. (1961), "Postbuckling Behaviour of Flat Plates", ASCE, Journal of the Struct. Divn., Vol. 87, ST5, pp. 17-31.

Kalyanaraman, V. (1978), "Local Buckling of Cold-Formed Steel Members", Fourth International Speciality Conference on Cold-Formed Steel Structures, University of Missouri - Rolla, June.

Kalyanaraman, V. and Pekoz, T. (1978), "Analytical Study of Unstiffened Elements", ASCE, Journal of the Struct. Divn., Vol. 104, No. ST9, September, pp. 1507-1524.

Kalyanaraman, V., Pekoz, T. and Winter, G. (1977), "Unstiffened Compression Elements", ASCE, Journal of the Struct. Divn., Vol. 103, No. ST9, September, pp. 1833-1848.

Kavanagh, K. T. (1978), "Flange-Web Buckling Modes in Cold Formed Steel Purlins", University of Western Australia, Civil Engineering Research Report No. CE-78-003, June.

Kavanagh, K. T. and Evans, E. P. (1978), "Failure of Cold-Formed Steel Zed and Channel Sections by Localised Buckling of the Web and Flange", Institution of Engineers Australia, Metal Structures Conference, Perth, November.

Karren, K. W. (1965), "Effects of Cold-Forming on Light-Gage Steel Members", Ph.D. Thesis, Cornell University, Ithaca.

Karren, K. W. (1967), "Corner Properties of Cold-Formed Steel Shapes", ASCE, Journal of the Struct. Divn., Vol. 93, No. ST1, February, pp. 401-432.

Karren, K. W. and Winter, G. (1967), "Effects of Cold-Forming on Light-Gage Steel Members", ASCE, Journal of the Struct. Divn., Vol. 93, No. ST1, February, pp. 433-469.

Kenedi, R. M. and Harvey, J. M. (1950), "Use of Equal Strength Sections in Structural Design", Transactions Institution of Engineers and Shipbuilders in Scotland, Vol. 94, pp. 89-109.

Kitipornchai, S. and Richter, N. J. (1978), "Elastic Lateral Buckling of I-Beams with Discrete Intermediate Restraints", Civil Engineering Transactions, Instn. Eng. Aust., Vol. CE20, No. 2, pp. 105-111.

Kloppel, K. and Schubert, J. (1971), "Die Berechnung der Traglast mittig und assermittig gedruckter, dunnwandiger Stuteen mit kastenformigem Querschnitt in uberkritischen Bereich", Heft 13, Veroffentlichung des Institutes furer Statik und Stahlbau der Technischen Hochschule Darmstadt, Darmstadt, West Germany.

Kollbrunner, C. F. and Hajdin, N. (1968), "Displacement-Method in the Theory of Thin-Walled Members and a New Calculation-Model for the Thin-Walled Bars with Deformable Contours", Publ. IABSE, Vol. 28-II, pp. 87-100.

Korn, A. and Galambos, T. V. (1968), "Behaviour of Elastic-Plastic Frames", ASCE, Journal of the Struct. Divn., Vol. 94, No. ST5, May, pp. 1119-1142.

Krahula, J. L. (1967), "Analysis of Bent and Twisted Bars Using the Finite Element Method", Journal AIAA, Vol. 5, No. 6, pp.1194-1197.

Krajcinovic, D. (1969), "A Consistent Discrete Elements Technique for Thin-Walled Assemblages", International Journal of Solids and Structures, Vol. 5, pp. 639-662.

Krajcinovic, D. (1970), "Matrix Force Analysis of Thin-Walled Structures", ASCE, Journal of the Struct. Divn., Vol. 96, No. ST1, January, pp. 107-121.

Kroll, W. D. (1943), "Tables of Stiffnesses and Carry-over Factors for Flat Rectangular Plates Under Compression", NACA ARR 3K27, Nov.

Kroll, W. D., Fisher, G. P. and Heimerl, G. P. (1943), "Charts for Calculations of Critical Stress for Local Instability of Columns with I, Z, Channel and Rectangular Tube Sections", (NACA Wartime Report L-429), NACA ARR 3K04, Nov.

Lansing, W. (1949), "Stresses in Thin-Walled Open Section Beams due to Combined Torsion and Flexure", Ph.D. Thesis, Cornell University.

Lay, M. G. (1964), "The Static Load-Deflection Behaviour of Planar Steel Structures", Ph.D. Thesis, Lehigh University.

Lay, M. G. (1965), "Flange Local Buckling in Wide-Flange Shapes", ASCE, Journal of the Struct. Divn., Vol. 91, No. ST6, December, pp. 95-116.

Lay, M. G. and Galambos, T. V. (1967), "Inelastic Beams under Moment Gradient", ASCE, Journal of the Struct. Divn., Vol. 93, No. ST1, February, pp. 381-399.

Litton, E. (1973), Automatic Computational Techniques in Civil and Structural Engineering, Crosby Lockwood, London.

Livesley, R.K. (1953), "Analysis of Rigid Frames by Electronic Digital Computer", Engineering, Vol. 76, August, pp. 230-3, 277-8.

Livesley, R. K. (1975), Matrix Methods of Structural Analysis, 2nd Ed., Pergamon Press, Oxford.

Low, M. W. (1959), "Some Model Tests on Multi-Storey Rigid Steel Frames", Proceedings, Institution of Civil Engineers, Vol 13, July, pp. 287-298.

Lu, L. W. (1965), "Inelastic Buckling of Steel Frames", ASCE, Journal of the Struct. Divn., Vol. 91, No. ST6, December, pp. 185-214.

Lukey, A. F. and Adams, P. F. (1969), "Rotation Capacity of Beams under Moment Gradient", ASCE, Journal of the Struct. Divn., Vol. 95, No. ST6, June, pp. 1173-1188.

Lundquist, E. E. and Stowell, E. Z. (1942), "Critical Compressive Stress for Outstanding Flanges", Report 734, National Advisory Council for Aeronautics.

Macadam, J. M. (1967), Discussion on the paper "Effects of Cold-forming on Light Gauge Steel Members" by Karren and Winter, ASCE, Journal of the Struct. Divn., Vol. 93, No. ST5, October, pp. 654-660.

MacNamee, B. M. and Lu, L. W. (1972), "Inelastic Multistorey Frame Buckling", ASCE, Journal of the Struct. Divn., Vol. 98, No. ST7, July, pp. 1613-1631.

Marguerre, K. (1937), "The Apparent Width of Plate in Compression", NACA TN 833.

Massey, P. C. (1963), "The Torsional Rigidity of Steel I-Beams Already Yielded Under Uniform Bending Moment", Civil Engineering and Public Work Review, Vol. 58, No. 680, March, p. 367, and No. 681, April, p. 488.

McCalley, Jr., R. B. (1952), "Contributions to the Theory of Combined Flexure and Torsion", Ph.D. Thesis, Cornell University.

Melosh, R. J. (1961), "A Stiffness Matrix for the Analysis of Thin Plates in Bending", Journal of the Aeronautical Sciences, Vol. 28, No. 1, January, pp. 34-42.

Merchant, W. (1954), "The Failure Load of Rigid Jointed Frameworks as Influenced by Stability", The Structural Engineer, Vol. 32, July, pp. 185-190.

Milner, H. R. (1977), "The Design of Simple Supported Beams Braced Against Twisting on the Tension Flange", Civil Engineering Transactions, Instn. Eng. Aust., Vol. CE19, No. 1, pp. 84-91.

Morrell, P. J. B. (1979), "The Influence of Joint Detail on the Torsional Behaviour of Thin-Walled Structures having an Axial Discontinuity", International Conference on Thin-Walled Structures, University of Strathclyde.

Morrison, J. C. M. and Shepherd, W. M. (1950), "An Experimental Investigation of Plastic Stress-Strain Relations", Proceedings, Institution of Mechanical Engineers, Vol. 163, pp. 1-18.

Moses, F. (1964), "Inelastic Frame Buckling", ASCE, Journal of the Struct. Divn., Vol. 90, No. ST6, December, pp. 105-122.

Navier, M. (1826), Resume des Lecons donees a l'ecole des ponts et chaussees sur l'application de la Mecanique a l'establissement des constructions et des machines, Premiere Partie.

Neal, B. G. (1950), "The Lateral Instability of Yielded Mild Steel Beams of Rectangular Cross-Section", Philosophical Transactions, Royal Society of London, Vol. 242 (A), January, p. 197.

Nethercot, D. A. and Rockey, K.C. (1972), "The Lateral Buckling of Beams Having Discrete Intermediate Restraints", the Structural Engineer, Vol. 50, No. 10, Oct., pp. 391-403.

Nishino, F., Tall, L. and Okumura, T. (1968), "Residual Stresses and Torsional Buckling Strength of H and Cruciform Columns", Transactions, Japan Society of Civil Engineers, No. 100, December, p. 75.

Patterson, O. (1952), "Combined Bending and Torsion of I-Beams of Monosymmetrical Cross-Section", Bull. No. 10, Div. Building Statics and Struct. Eng., Royal Inst. of Tech., Stockholm, Sweden.

Pekoz, T. (1979), "Design of Cold-Formed Steel Storage Racks", International Conference on Thin-Walled Structures, University of Strathclyde.

Peters, R. W., Dow, F. and Batdorf, S. B. (1950), "Preliminary Experiments for Testing Basic Assumptions of Plasticity Theories", Proc. of the Society of Experimental Stress Analysis, Vol. 7, pp. 127-140.

Plank, R. J. and Wittick, W. H. (1974), "Buckling Under Combined Loading of Thin, Flat-Walled Structures by a Complex Finite Strip Method", International Journal for Numerical Methods in Engineering, Vol. 8, No. 2, pp. 323-339.

Popov, E.P. and Medwadowski, S. J. (1979), 'Stability of Reinforced Concrete Shells State-of-the-Art Overview", Draft Report, July.

Przemieniecki, J. S. (1968), Theory of Matrix Structural Analysis, McGraw-Hill Book Company, New York.

Przemieniecki, J. S. (1973), "Finite Element Structural Analysis of Local Instability", AIAA Journal, Vol. 11, pp 33-39.

Rajasekaran, S. and Murray, D. W. (1973), "Coupled Local Buckling in Wide-Flange Beam Columns", ASCE, Journal of the Struct. Divn., Vol. 99, No. ST6, June, pp. 1003-1023.

Rao, N. R. N., Lohrmann, M. and Tall, L. (1966), "The Effect of Strain Rate on the Yield Stress of Structural Steels", ASTMJ Materials, Vol.1, No. 1, pp. 241-262.

Reck, H. P., Pekoz, T. and Winter, G. (1975), "Inelastic Strength of Cold-Formed Steel Beams", ASCE, Journal of the Struct. Divn., Vol. 101, ST11, November, pp. 2193-2203.

Reis, A. J. and Branco, F. A. (1979), "Lateral and Local Stability of Thin-Walled Sections under Eccentric Loading", International Conference on Thin-Walled Structures, University of Strathclyde.

Renton, J. D. (1962), "Stability of Space Frames by Computer Analysis", ASCE, Journal of the Struct. Divn., Vol. 88, No. ST4, August, pp. 81-103.

Renton, J. D. (1967), "Buckling of Frames Composed of Thin-Walled Members", Thin Walled Structures, edited by A. H. Chilver, Chatto and Windus, London.

Renton, J. D. (1974), "On the Transmission of Non-Uniform Torsion through Joints", Report No. 1086/74, Department of Engineering Science, Oxford University, January.

Rhodes, J. and Harvey, J. M. (1971A), "The Local Buckling and Post Local Buckling of Thin-Walled Beams", Aeronautical Quarterly, Vol. 22, November, pp. 363-388.

Rhodes, J. and Harvey, J. M. (1971B), "Plates in Uniaxial Compression with Various Support Conditions at the Unloaded Boundaries", Int. J. Mech. Sci., Vol. 13, pp. 787-802.

Robinson, H. (1974), Ultimate Strength Design of Composite Beams with Cellular Metal Floor", Design in Cold-Formed Steel, University of Waterloo, Waterloo, Ontario, pp. 199-214.

Ros, M. and Eichinger, A. (1932), Final Report, 1st Congress, International Assoc. Bridge and Structural Eng., Paris, P. 144.

Saint Venant (1855), Memoires Acad. Sci. Savants Etrangers, Vol. 14, pp. 233-560.

Saint Venant (1883), Discussion in "Theorie de l'elasticitie des Corps Solides", by Clebsch, final note to Sec. 73, p. 689.

Sangdahl, G. S., Aul, E. L. and Sachs, G. (1948), "An Investigation of the Stress and Strain States Occurring in Rectangular Bars", Proceedings, Soc. for Experimental Stress Analysis, Cambridge, Mass., Vol. 6, No.1, pp. 1-18.

Santathadaporn, S. and Chen, W. F. (1972), "Tangent Stiffness Method for Biaxial Bending", ASCE, Journal of the Struct. Divn., Vol. 98, No. ST1, January, pp. 153-163.

Schmied, R. (1967), "Die Gesamtstabilitat von zweiachsig aussermittig gedruckten dunnwandigen I-Staben unter Berucksichtigung der Querschnittsuerformung nach der nichtlinearen Plattentheorie", Der Stahlbau, No. 1., January, pp. 1-12, No. 2, February, pp. 50-60.

Schuette, E. H. and McCulloch, J. C. (1947), "Charts for Minimum Weight Design of Multiweb Wings in Bending", NACA TN 1323, June.

Schuster, R. M. (1974), "Composite Steel-Deck Reinforced Concrete Floor Systems", Design in Cold-Formed Steel, University of Waterloo, Waterloo, Ontario, pp. 87-114.

Scidenfaden, J. (1954), "Interaction in the Post-Buckled Range for the Channel Section", Zietschrift fuer Flugwissenschaften, Vol. 2, No. 7, pp. 169-179.

Shanley, F. R. (1947), "Inelastic Column Theory", Journal Aero. Sciences, Vol. 14, No. 5, May, p. 261.

Skaloud, M. and Zornerva, M. (1970), "Experimental Investigation into the Interaction of Buckling of Compressed Thin-Walled Columns with Buckling of Their Plate Elements", Acta Technica, CSAV, Vol. 15, No. 4, pp. 389-424.

Som, P. K. and Ghosh, K. (1964), "Anchor Zone Stresses in Prestressed Concrete Beams", ASCE, Journal of the Struct. Divn., Vol. 90, No. ST4, August, pp. 49-62.

Standards Association of Australia, AS 1170, Part 2 - 1973, SAA Loading Code, Part 2 - Wind Forces, Sydney.

Standards Association of Australia, AS 1511 - 1973, "SAA High-Strength Structural Bolting Code", Sydney.

Standards Association of Australia, AS 1391 - 1974, "SAA Method for Tensile Testing of Metals", Sydney.

Standards Association of Australia, AS 1538 - 1974, "SAA Cold-Formed Steel Structures Code", Sydney.

Stowell, E. A. (1948), "A Unified Theory of Plastic Buckling of Columns and Plates", NACA TN 1556.

Suzuki, Y. and Okumura, T. (1968), "Influence of Cross-Sectional Distortion on Flexural-Torsional Buckling", Final Report, Eighth Congress, IABSE, pp. 321-331.

Swartz, S.E. and Rosebraugh,V. H. (1974), "Buckling of Reinforced Concrete Plates", ASCE, Journal of the Struct. Divn., Vol. 100, No. ST1, January, pp. 195-208.

Tarlton, D. L. (1974), "Diaphragm Action", Design in Cold-Formed Steel, edited by R. M. Schuster, University of Waterloo, Waterloo, Ontario, pp. 161-181.

Tesar, V. (1932), "Experimental Determination of the Stresses at the Ends of Prismatic Members with Imperfect Joint", IABSE, Publications, Vol. 1, pp. 497-506.

Tien, Y. L. and Wang, S. T. (1978), "Strength of Buckled Rectangular Plates", Fourth International Specialty Conference on Cold-Formed Steel Structures, University of Missouri-Rolla, June.

Tien, Y. L. and Wang, S. T. (1979), "Local Buckling of Beams under Stress Gradients", ASCE, Journal of the Struct. Divn., Vol. 105, No. ST8, August, pp. 1571-1588.

Timoshenko, S. P. (1905), "On the Stability in Plane Bending of a T-Beam", Bull. Pol. Inst. St. Petersburg, Nos. 4-5.

Timoshenko, S. P. (1945), "Theory of Bending, Torsion and Buckling of Thin-Walled Members of Open Cross-Section", Journal of the Franklin Institute, March/April/May.

Timoshenko, S. P.and Gere, J. M. (1961), Theory of Elastic Stability, 2nd Edition, McGraw-Hill, New York.

Timoshenko, S. P. and Goodier (1970), Theory of Elasticity, 3rd Edition, McGraw-Hill Book Company, New York.

Timoshenko, S. P. and Woinowsky-Krieger, S., (1959), Theory of Plates and Shells, McGraw-Hill, New York.

Trahair, N. S. (1977), The Behaviour and Design of Steel Structures, Chapman and Hall Ltd., London.

Tranberg, W. Swannell, P. and Meek, J. L. (1976), "Frame Collapse Using Tangent Stiffness", ASCE, Journal of the Struct. Divn., Vol. 102, No. ST3, March, pp. 659-675.

Turner, M. J., Clough, R. W., Martin, H. C. and Topp, L. J. (1956), "Stiffness and Deflection Analysis of Complex Structures", Journal of the Aeronautical Sciences, Vol. 23, No. 9, September, pp. 805-823.

Uribe, J. (1969), "Aspects of the Effects of Cold-Forming on the Properties and Performance of Light-Gage Structural Members", Report No. 333, Dept. of Struct. Eng., Cornell University, Ithaca, N. Y., May.

Uribe, J. and Winter, G. (1970), "Cold-Forming Effects in Thin-Walled Steel Members", Cornell Engineering Research Bulletin, 70-1, Cornell University, pp. 147-196.

Vacharajittiphan, P. and Trahair, N. S. (1973A), "Elastic Lateral Buckling of Portal Frames", ASCE, Journal of the Struct. Divn., Vol. 99, No. ST5, May, pp. 821-835.

Vacharajittiphan, P. and Trahair, N. S. (1973B), Warping and Distortion at I-Section Joints, University of Sydney, School of Civil Engineering, Research Report R211, May.

Vacharajittiphan, P. and Trahair, N. S. (1974), "Direct Stiffness Analysis of Lateral Buckling", University of Sydney, School of Civil Engineering, Research Report R 233, January.

Van Der Maas, C. (1954), "Charts for the Calculation of Critical Compressive Stress for Local Instability of Columns with Hat Sections", Journal of Aeronautical Science, Vol. 21, No. 6, June, pp. 399-403.

Venkataramaiah, K. R. and Roorda, J. (1978), "Local Buckling of Thin Walled Channels", Fourth International Specialty Conference on Cold-Formed Steel Structures, University of Missouri- Rolla, June.

Vlasov, V. Z. (1959), Thin-Walled Elastic Beams, Moscow. (English Translation, Isael Program for Scientific Translations, Jerusalem, 1961).

Von Karman, T. (1910), "Encyklopadie der Mathematischen Wissenschaften", Vol. 4, p. 349.

Von Karman, T. (1932), "The Strength of Thin Plates in Compression", Calif. Inst. of Tech., Pasadena, Publication No. 13.

Walker, A. C. (1966), "Local Instability in Plates and Channel Struts", ASCE, Journal of the Eng. Mech. Divn., Vol. 92, No. ST3, June, pp. 39-55.

Walker, A. C. (1969), "The Post-Buckling Behaviour of Simply-Supported Square Plates", The Aeronautical Quarterly, Vol. XX, pp. 203-222.

Walker, A. C. (1975), Design and Analysis of Cold-Formed Sections, International Textbook Company Limited, London.

Wallis, M. A. (1971), "A Survey of Sheet Metal Cold Roll Forming", British Steel Corporation, Corporate Laboratories, Rep. MW/36/71.

Wang, C. K. (1973), Computer Methods in Advanced Structural Analysis, Intext Educational Publishers, New York.

Wang, S. T. (1974), "Nonlinear Analysis of Locally Buckled Thin-Walled Structures", Proceedings, First International Conference on Computational Methods in Nonlinear Mechanics, Austin, Texas, September.

Wang, S. T. and Blandford, G. E. (1978), "Stability Analysis of Locally Buckled Frames", Proceedings of the Fourth International Speciality Conference on Cold-Formed Steel Structures, University of Missouri - Rolla, June.

Wang, S. T. and Jsa S. T., (1974), "Post-Local-Buckling Behaviour of Multistorey Frames", Proceedings, Symposium on Planning Design and Construction of Tall Buildings, Nashville, Tennessee, November.

Wang, S. T. and Tien, Y. L. (1973), "Post-Local-Buckling Behaviour of Thin Walled Columns", Proceedings of the Second Speciality Conference on Cold-Formed Steel Structures, University of Missouri - Rolla, October.

Wang, S. T.and Yeh, S. S. (1974), "Post-Local-Buckling Behaviour of Continuous Beams", ASCE, Journal of the Struct. Divn., Vo. 100, No. ST6, June, pp. 1169-1187.

Wang, S. T., Yost, M. I. and Tien, Y. L. (1977), "Lateral Buckling of Locally Buckled Beams Using Finite Element Techniques", Journal of Computer and Structures, Vol. 7, pp. 469-475.

Wilkinson, J. H. (1958), "The Calculation of Eigenvectors of Codiagonal Matrices", Computer Journal, Vol. 1, pp. 90-96.

Wilkinson, J. H. (1960), "Householder's Method for the Solution of the Algebraic Eigenproblem", Computer Journal, Vol. 3, pp. 23-27.

Williams, F. W. and Wittrick, W. M. (1971), "A General Algorithm for Computing Natural Frequencies of Elastic Structures", Quarterly Journal of Mechanics and Applied Mathematics, Vol. 24, Part 3, August, pp. 263-284.

Winter, G. (1947), "Strength of Thin Steel Compression Flanges", Transactions, ASCE, Vol. 112, pp. 527-554.

Winter, G. (1968), "Thin-walled Structures-Theorectical Solutions and Test Results", Preliminary Publication of the Eighth Congresss, Internation Association for Bridge and Structural Engineering, pp. 101-112.

Winter, G., Lansing, W. and McCalley, Jr. R. B., (1950), "Performance of Laterally Loaded Channel Beams", Cornell University Eng. Exp. Station Reprint No.33, November.

Wittrick, W. H. (1968A), "A Unified Approach to the Inital Buckling of Stiffened Panels in Compression", Aeronautical Quarterly, Vol.19, pp. 265-283.

Wittrick, W. H. (1968B), "General Sinusoidal Stiffness Matrices for Buckling and Vibration Analyses of Thin Flat-Walled Strucures", International Journal Mech. Sciences, Vol. 10, pp. 949-966.

Wood, R. H. (1958), "The Stability of Tall Buildings", Proc. of the Institution of Civil Engineers, Vol. 11, September, pp. 69-102.

Yucel, O., Sendil, U. and Tall, L. (1973), "Bibliography on Tall Buildings", Report No. 8C, ASCE-IABSE Joint Committee on Planning and Design of Tall Buildings, Fritz Engineering Laboratory, Lehigh University, Bethleham.

Zbirohowski-Koscia, K. (1967), Thin-Walled Beams, Crosby Lockwood, London.

Zienkiewicz, O. C. (1977), The Finite Element Method, Third Edition, McGraw-Hill, London.

APPENDICES

APPENDIX I

Matrix Displacement Method

APPENDIX II

Test Frame and Test Rig Specifcation Drawings

APPENDIX III

Calculation of Deformations of Test Frame

APPENDIX IV

Tension Coupon Results

APPENDIX V

Calculation of Generalised Strains and Strss Resultants

APPENDIX VI

Channel Cross - Section Dimensions

APPENDIX VII

Inelastic Cross - Section Analysis

APPENDIX VIII

Program Listings and Sample Data

1. Program FEETA
2. Program CAFOP
3. Program BFINST

APPENDIX I

MATRIX DISPLACEMENT METHOD

I.1 MEMBER STIFFNESS MATRICES

a) Axial Stiffness Matrix

$$\begin{bmatrix} F_{zA} \\ F_{zB} \end{bmatrix} = \frac{EA}{L} \begin{bmatrix} 1 & -1 \\ -1 & 1 \end{bmatrix} \cdot \begin{bmatrix} \delta_{zA} \\ \delta_{zB} \end{bmatrix}$$

b) Flexural Stiffness Matrices

$$\begin{bmatrix} F_{yA} \\ M_{xA} \\ F_{yB} \\ M_{xB} \end{bmatrix} = \frac{EI_x}{L^3} \begin{bmatrix} 12 & 6L & -12 & 6L \\ 6L & 4L^2 & -6L & 2L^2 \\ -12 & -6L & 12 & -6L \\ 6L & 2L^2 & -6L & 4L^2 \end{bmatrix} \begin{bmatrix} \delta_{yA} \\ \theta_{xA} \\ \delta_{yB} \\ \theta_{xB} \end{bmatrix}$$

$$\begin{bmatrix} F_{xA} \\ M_{yA} \\ F_{xB} \\ M_{yB} \end{bmatrix} = \frac{EI_y}{L^3} \begin{bmatrix} 12 & 6L & -12 & 6L \\ 6L & 4L^2 & -6L & 2L^2 \\ -12 & -6L & 12 & -6L \\ 6L & 2L^2 & -6L & 4L^2 \end{bmatrix} \cdot \begin{bmatrix} \delta_{xA} \\ \theta_{yA} \\ \delta_{xB} \\ \theta_{yB} \end{bmatrix}$$

c) Torsional Stiffness Matrix

$$\begin{bmatrix} M_{zA} \\ B_{zA} \\ M_{zB} \\ B_{zB} \end{bmatrix} = -\frac{EI_w \lambda}{g} \begin{bmatrix} \lambda^2 \ell & -\lambda m & -\lambda^2 \ell & -\lambda m \\ -\lambda m & n & \lambda m & -p \\ -\lambda^2 \ell & \lambda m & \lambda^2 \ell & \lambda m \\ -\lambda m & -p & \lambda m & -n \end{bmatrix} \begin{bmatrix} \theta_{zA} \\ -\theta'_{zA} \\ \theta_{zB} \\ -\theta'_{zB} \end{bmatrix}$$

$$\lambda = \sqrt{\frac{GJ}{EI_w}} \quad , \quad \ell = \sinh\lambda L$$

$$g = 2(\cosh\lambda L - 1) - \lambda L \sinh\lambda L$$

$$n = \lambda L \cosh\lambda L - \sinh\lambda L$$

$$p = \lambda L - \sinh\lambda L$$

$$m = \cosh\lambda L - 1$$

$$\begin{bmatrix} F_X \\ F_Y \\ F_Z \end{bmatrix} = \begin{bmatrix} 1 & 0 & 0 \\ 0 & \cos\alpha_X' & \sin\alpha_X' \\ 0 & -\sin\alpha_X' & \cos\alpha_X' \end{bmatrix} \cdot \begin{bmatrix} \cos\alpha_Y' & 0 & \sin\alpha_Y' \\ 0 & 1 & 0 \\ -\sin\alpha_Y' & 0 & \cos\alpha_Y' \end{bmatrix} \cdot \begin{bmatrix} \cos\alpha_Z' & -\sin\alpha_Z' & 0 \\ \sin\alpha_Z' & \cos\alpha_Z' & 0 \\ 0 & 0 & 1 \end{bmatrix} \cdot \begin{bmatrix} F_X' \\ F_Y' \\ F_Z' \end{bmatrix}$$

$$\begin{bmatrix} F_X \\ \hline F_Y \\ \hline F_Z \end{bmatrix} = \left[\begin{array}{l|l|l} \cos\alpha_Y'.\cos\alpha_Z' & -\cos\alpha_Y'.\sin\alpha_Z' & \sin\alpha_Y' \\ \hline -\sin\alpha_X'.\sin\alpha_Y'.\cos\alpha_Z' + \cos\alpha_X'.\sin\alpha_Z' & \sin\alpha_X'.\sin\alpha_Y'.\sin\alpha_Z' + \cos\alpha_X'.\cos\alpha_Z' & \sin\alpha_X'.\cos\alpha_Y' \\ \hline -\cos\alpha_X'.\sin\alpha_Y'.\cos\alpha_Z' - \sin\alpha_X'.\sin\alpha_Z' & \cos\alpha_X'.\sin\alpha_Y'.\sin\alpha_Z' - \sin\alpha_X'.\cos\alpha_Z' & \cos\alpha_X'.\cos\alpha_Y' \end{array}\right] \cdot \begin{bmatrix} F_X' \\ \hline F_Y' \\ \hline F_Z' \end{bmatrix}$$

c) ROTATION MATRIX [M]

i) FORCE TRANSFORMATION [RM]

$$\begin{bmatrix} F_X \\ F_Y \\ F_Z \end{bmatrix} = \begin{bmatrix} 1 & 0 & 0 \\ 0 & \cos\alpha_X' & \sin\alpha_X' \\ 0 & -\sin\alpha_X' & \cos\alpha_X' \end{bmatrix} \cdot \begin{bmatrix} \cos\alpha_Y' & 0 & \sin\alpha_Y' \\ 0 & 1 & 0 \\ -\sin\alpha_Y' & 0 & \cos\alpha_Y' \end{bmatrix} \cdot \begin{bmatrix} \cos\alpha_Z' & -\sin\alpha_Z' & 0 \\ \sin\alpha_Z' & \cos\alpha_Z' & 0 \\ 0 & 0 & 1 \end{bmatrix} \cdot \begin{bmatrix} F_X' \\ F_Y' \\ F_Z' \end{bmatrix}$$

$$\left[\begin{array}{c} F_X \\ \hline F_Y \\ \hline F_Z \end{array}\right] = \left[\begin{array}{c|c|c} \cos\alpha_Y'.\cos\alpha_Z' & -\cos\alpha_Y'.\sin\alpha_Z' & \sin\alpha_Y' \\ \hline -\sin\alpha_X'.\sin\alpha_Y'.\cos\alpha_Z' + \cos\alpha_X'.\sin\alpha_Z' & \sin\alpha_X'.\sin\alpha_Y'.\sin\alpha_Z' + \cos\alpha_X'.\cos\alpha_Z' & \sin\alpha_X'.\cos\alpha_Y' \\ \hline -\cos\alpha_X'.\sin\alpha_Y'.\cos\alpha_Z' - \sin\alpha_X'.\sin\alpha_Z' & \cos\alpha_X'.\sin\alpha_Y'.\sin\alpha_Z' - \sin\alpha_X'.\cos\alpha_Z' & \cos\alpha_X'.\cos\alpha_Y' \end{array}\right] \cdot \left[\begin{array}{c} F_X' \\ \hline F_Y' \\ \hline F_Z' \end{array}\right]$$

c) ROTATION MATRIX [M]

i) FORCE TRANSFORMATION [RM]

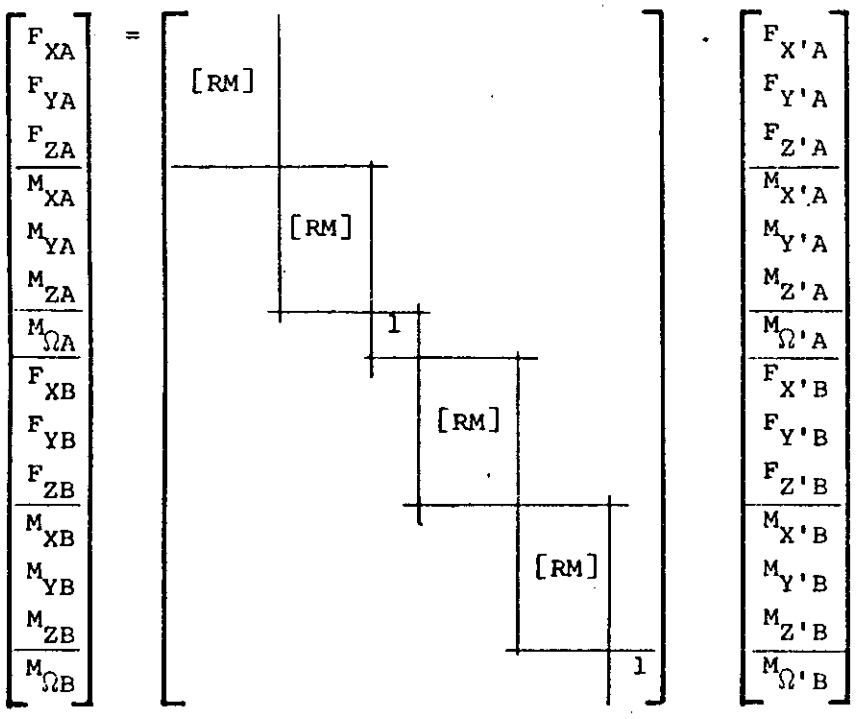

ii) COMPLETE ROTATION MATRIX [M]

I.2 STATICS MATRIX [A]

The statics matrix can be assembled from three independent matrices as given by Eq. (I.1),

$$[A] = [N] \cdot [G] \cdot [M] \qquad \text{(I.1)}$$

where $[N]$ = Member Equilibrium Matrix
$[G]$ = Cross-Section Transformation Matrix
$[M]$ = Rotation Matrix

The three matrices are as follows:

$$\begin{bmatrix} F_{xA} \\ F_{xA} \\ F_{zA} \\ M_{xA} \\ M_{yA} \\ M_{zA} \\ M_{\omega A} \\ F_{xB} \\ F_{yB} \\ F_{zB} \\ M_{xB} \\ M_{yB} \\ M_{zB} \\ M_{\omega B} \end{bmatrix} = \begin{bmatrix} & & & 1/L & 1/L & & & \\ & -1/L & -1/L & & & & & \\ -1 & & & & & & & \\ & 1 & & & & & & \\ & & & 1 & & & & \\ & & & & & -1 & & \\ & & & & & & 1 & \\ & & & -1/L & -1/L & & & \\ & 1/L & 1/L & & & & & \\ 1 & & & & & & & \\ & & 1 & & & & & \\ & & & & 1 & & & \\ & & & & & 1 & & \\ & & & & & & & 1 \end{bmatrix} \cdot \begin{bmatrix} P \\ M_{xAB} \\ M_{xBA} \\ M_{yAB} \\ M_{yBA} \\ M_z \\ M_{\omega AB} \\ M_{\omega BA} \end{bmatrix}$$

a) MEMBER EQUILIBRIUM MATRIX [N]

F_X'	=	cosα	-sinα						·	F_x
F_Y'		sinα	cosα							F_y
F_Z'				1						F_z
M_X'				b_Y'	cosα	-sinα				M_x
M_Y'				$-b_X'$	sinα	cosα				M_y
M_Z'		$-a_y$	a_x				1			M_z
M_Ω'					a_x	a_y		1		M_ω

b) CROSS-SECTION TRANSFORMATION MATRIX [G]

APPENDIX II -

TEST FRAME AND TEST RIG SPECIFICATION DRAWINGS

PFT - 1	Test Rig Layout
PFT - 2	Frame Geometry
PFT - 3	Pinned Base Joint Details
PFT - 5	Stanchion Loading and Restraint Assembly
PFT - 6	Eave Joint Details
PFT - 8	Rafter Loading and Restraint Assembly
PFT - 9	Apex Joint Details
PFT - 11	Member Details
PFT - 12	Lateral Restraint Details
PFT - 13	Fly Bracing Restraint Details
PFT - 18	Vertical Loading Details 1
PFT - 19	Vertical Loading Details 2
PFT - 20	Uplift Pulley Bracket
PFT - 21	Loading Frame Beam Details
PFT - 22	Loading Frame Stanchion Details
PFT - 23	Pulley Bracket
PFT - 24	Loading Frame Details 1
PFT - 25	Horizontal Pulley Bracket
PFT - 26	Loading Frame Details 2

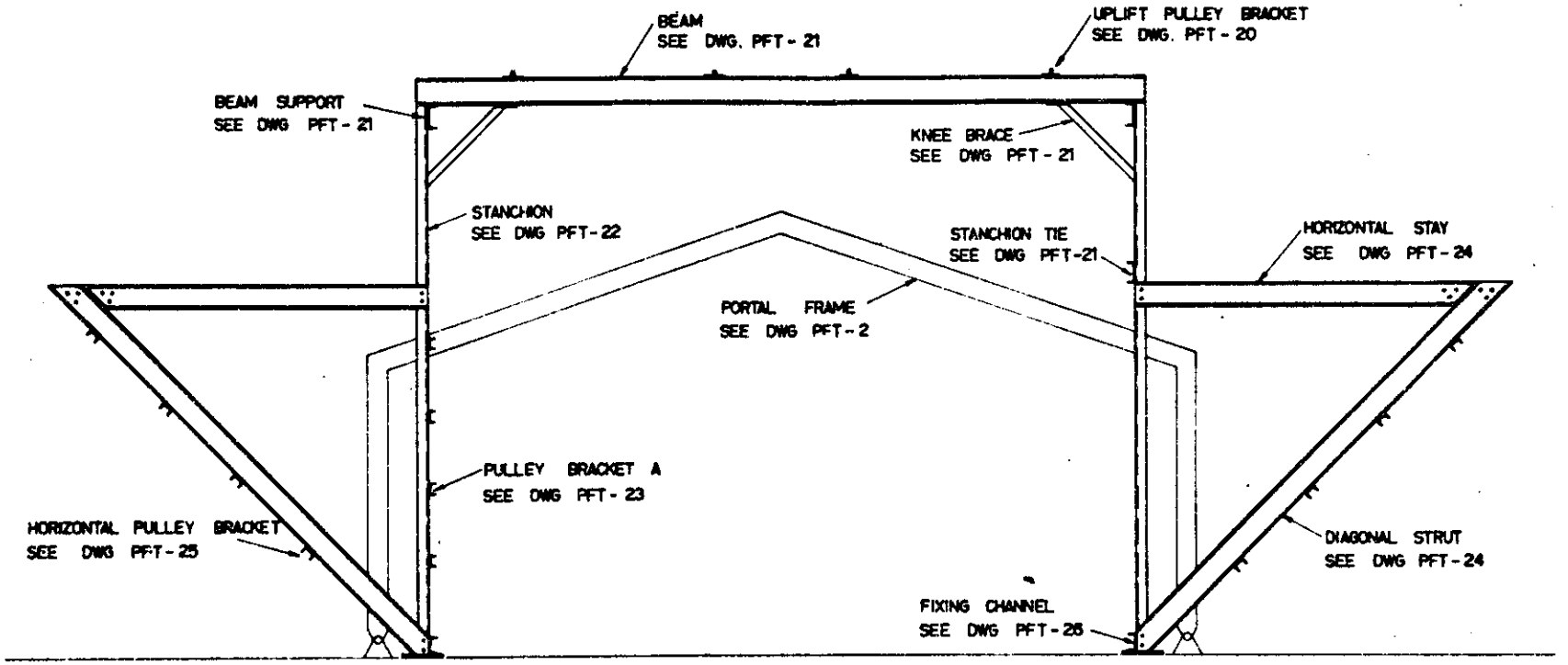

ELEVATION

DO NOT SCALE DRAWING	REFERENCE DRAWINGS		ITEM	DESCRIPTION	QTY.	MATL OR REF. No.	REMARKS
EXCEPT WHERE OTHERWISE INDICATED	DRAWN	A. K. B.	UNIVERSITY OF SYDNEY	DEPT. CIVIL ENG		SCALE	1 : 25
REMOVE BURRS & SHARP EDGES	TRACED		TITLE			ISSUE No.	A
FRACTIONAL DIMENSIONS ±	CHECKED		TESTING RIG LAYOUT			DRAWING No.	
DECIMAL DIMENSIONS ±	APPROVED		PORTAL FRAME TESTS				PFT - 1

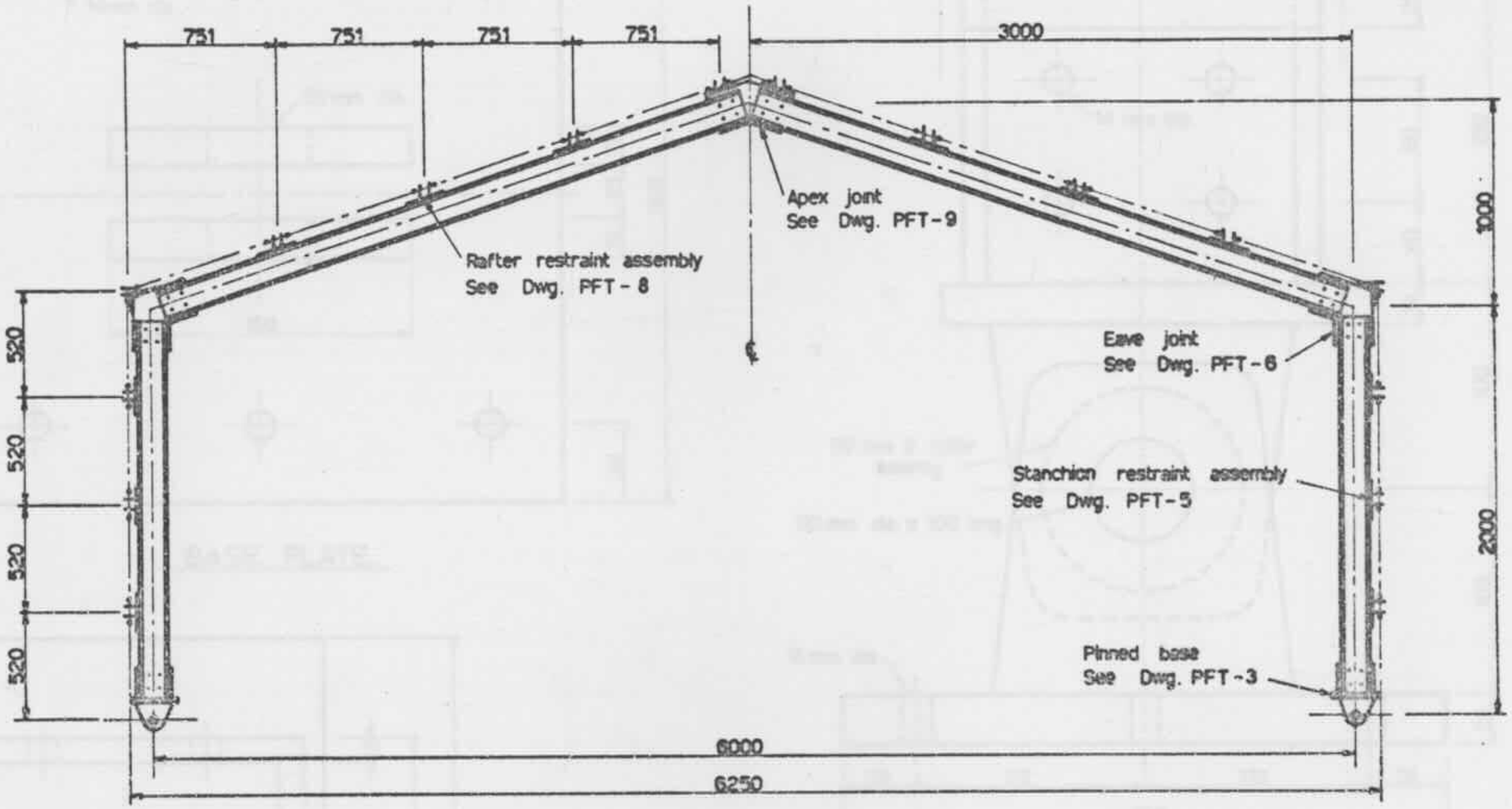

PORTAL FRAME

NOTE: ALL DIMENSIONS IN MM.

DO NOT SCALE DRAWING	REFERENCE DRAWINGS			ITEM	DESCRIPTION	QTY.	MAT'L OR REF. No.	REMARKS
EXCEPT WHERE OTHERWISE INDICATED REMOVE BURRS & SHARP EDGES FRACTIONAL DIMENSIONS ± DECIMAL DIMENSIONS ±	DRAWN	A.H.B.		UNIVERSITY OF SYDNEY	DEPT. CIVIL ENG.		SCALE: 1:20	
	TRACED			TITLE FRAME GEOMETRY PORTAL FRAME TESTS			ISSUE No. A	
	CHECKED						DRAWING No. PFT-2	
	APPROVED							

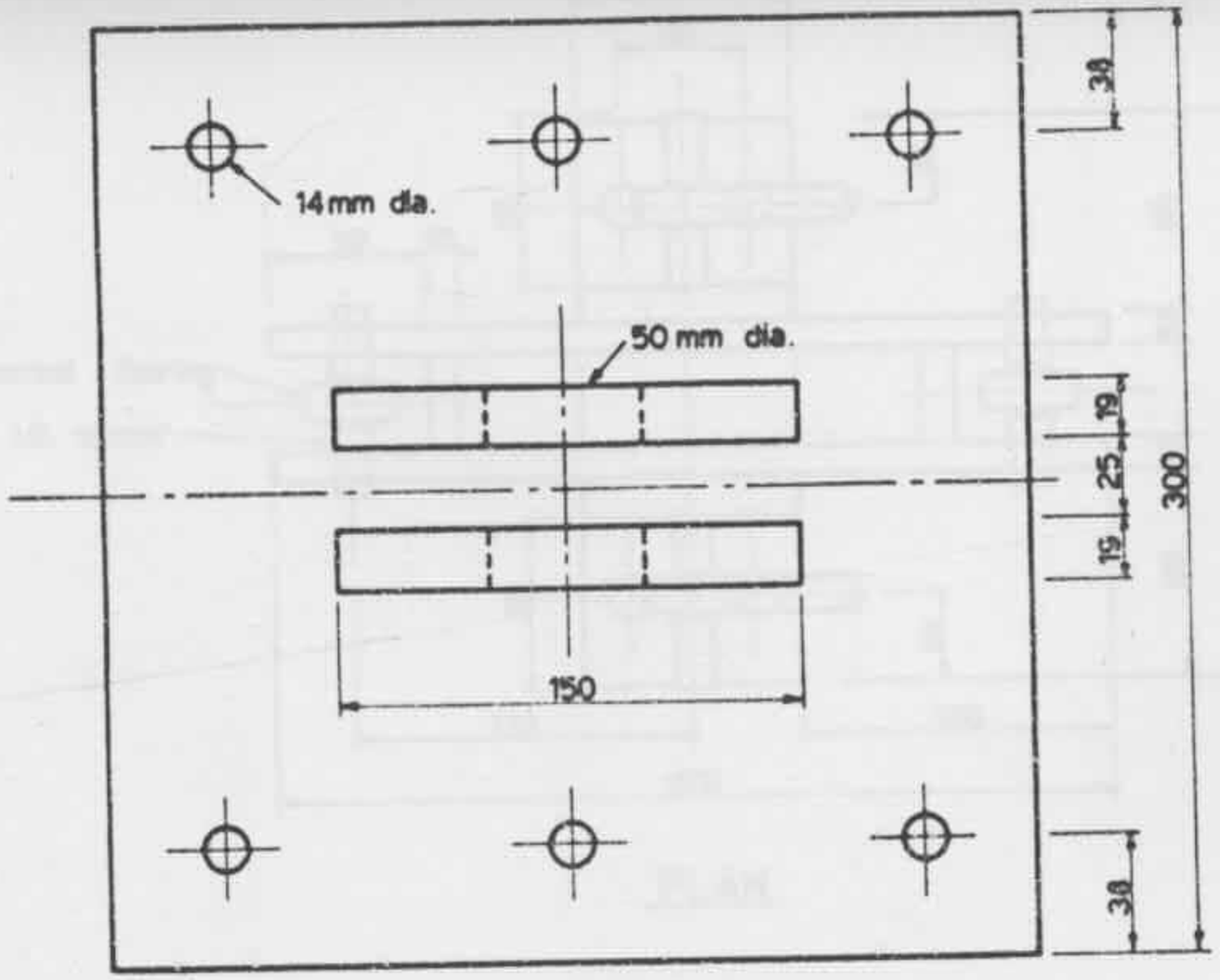

BASE PLATE

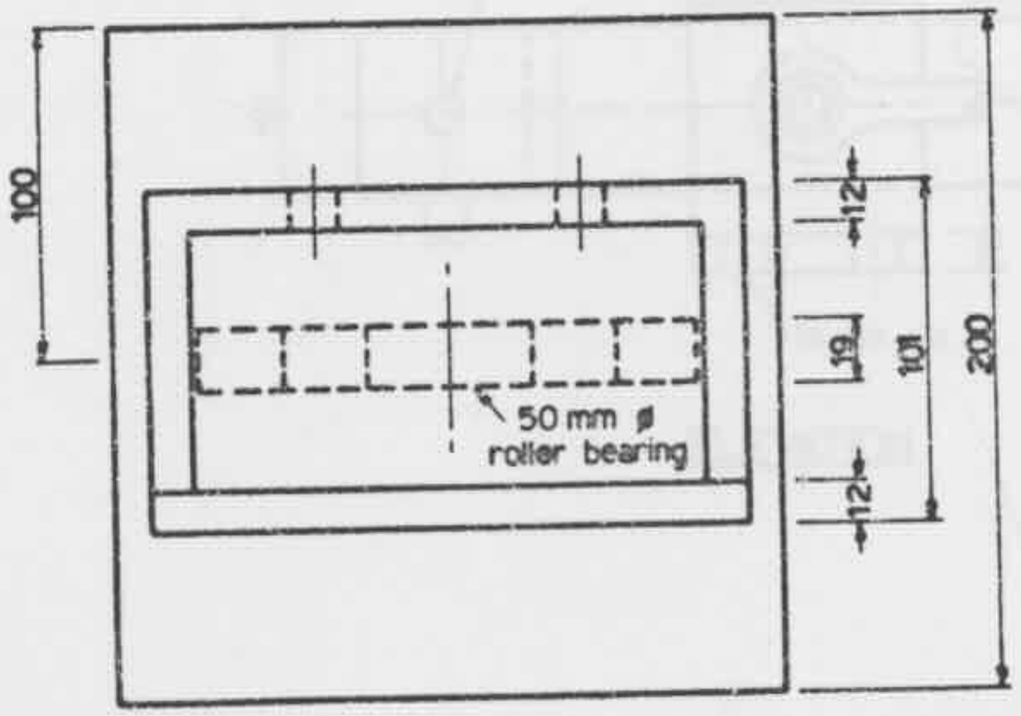

STANCHION BASE PLATE

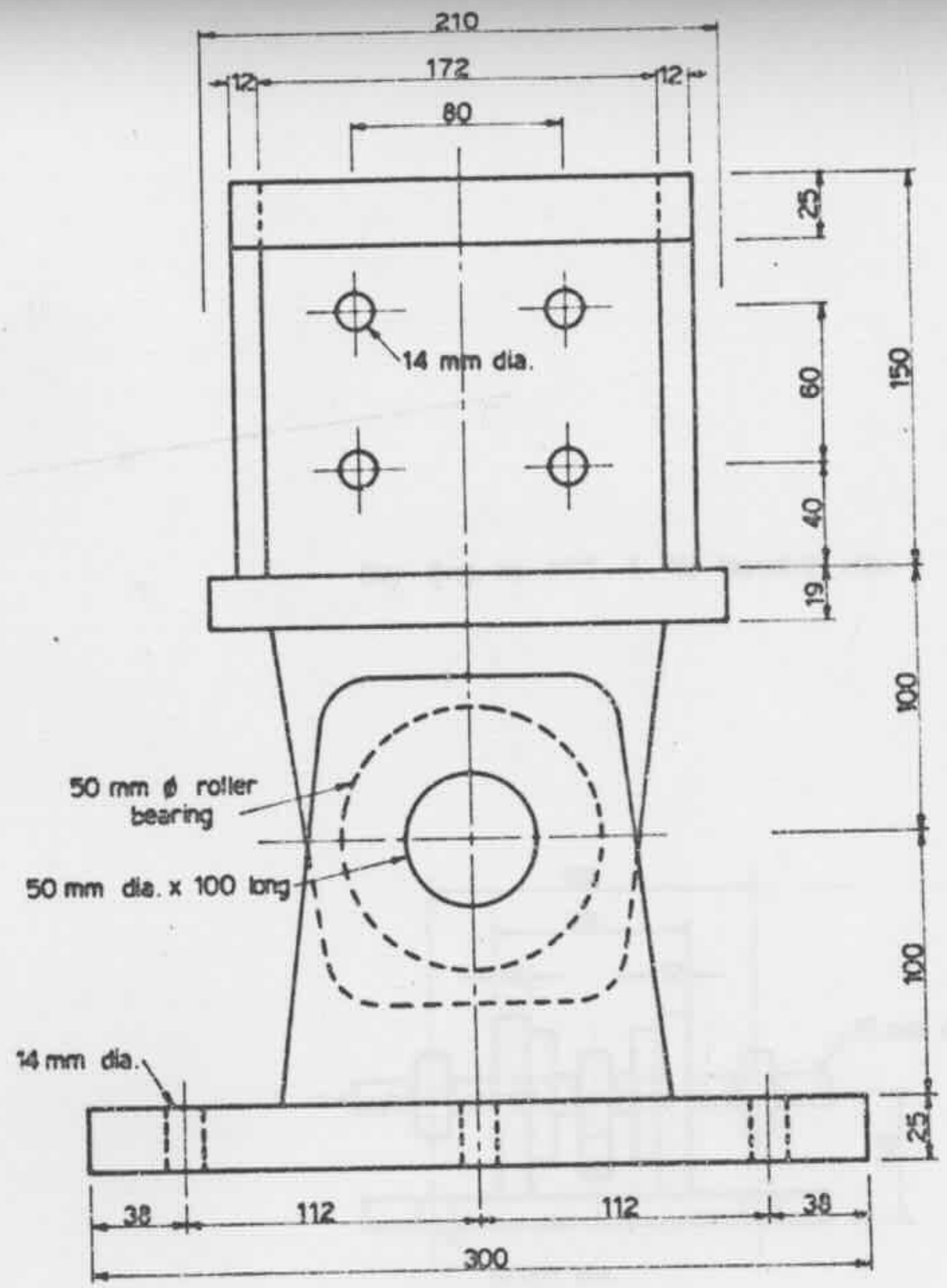

ELEVATION

See Dwg. No. PFT-4 for isometric view.

NOTE: ALL DIMENSIONS IN MM.

ITEM	DESCRIPTION	QTY.	MAT'L OR REF. No.	REMARKS
	PINNED BASE JOINT	2		

DO NOT SCALE DRAWING
EXCEPT WHERE OTHERWISE INDICATED
REMOVE BURRS & SHARP EDGES
FRACTIONAL DIMENSIONS ±
DECIMAL DIMENSIONS ±

REFERENCE DRAWINGS

DRAWN	A.H.B.		
TRACED			
CHECKED			
APPROVED			

UNIVERSITY OF SYDNEY — DEPT. CIVIL ENG

TITLE
PINNED BASE JOINT DETAILS
PORTAL FRAME TESTS

SCALE 1 : 2

ISSUE No. A

DRAWING No.
PFT - 3

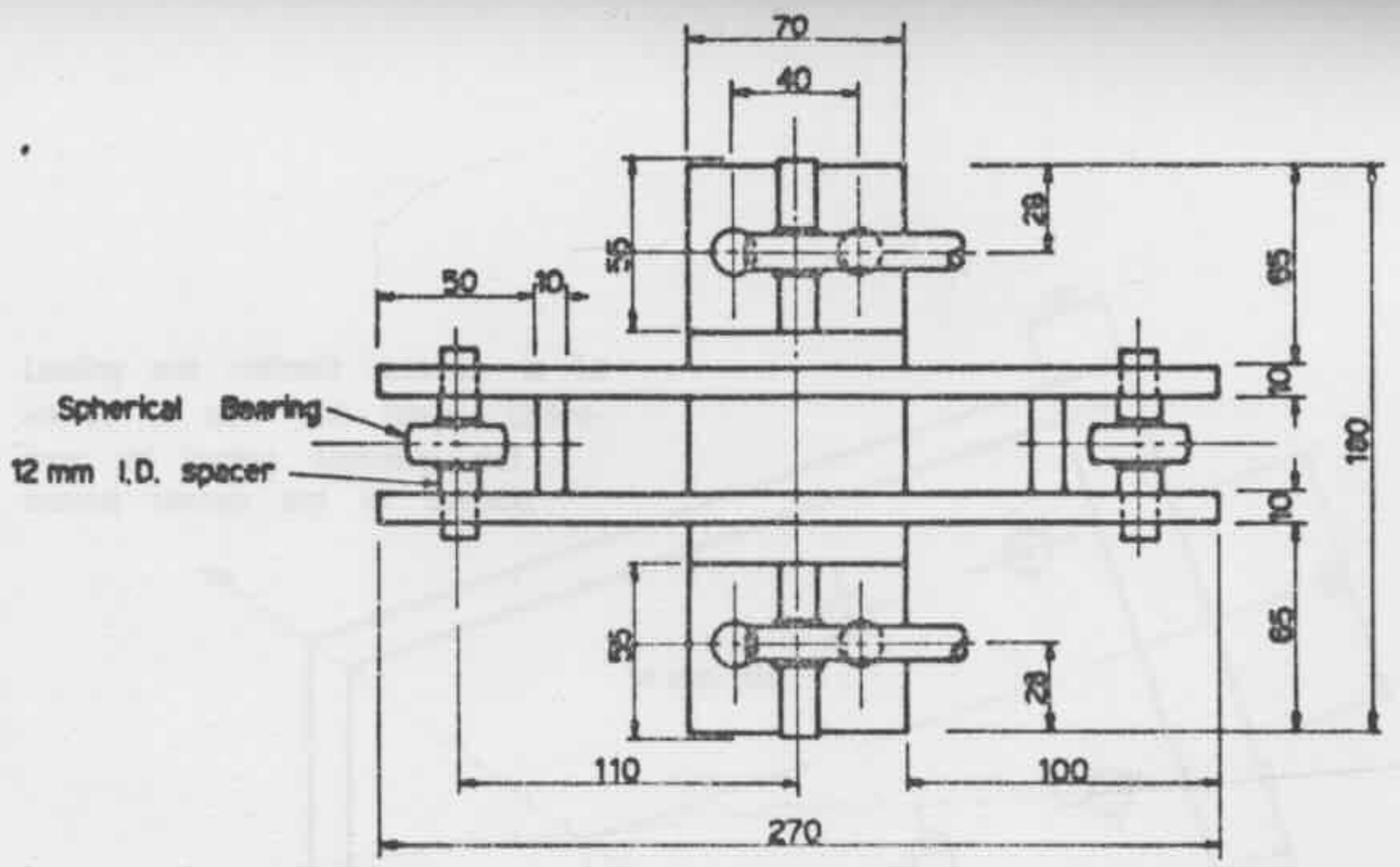

PLAN

See Dwg. No. PFT-4 for isometric view.

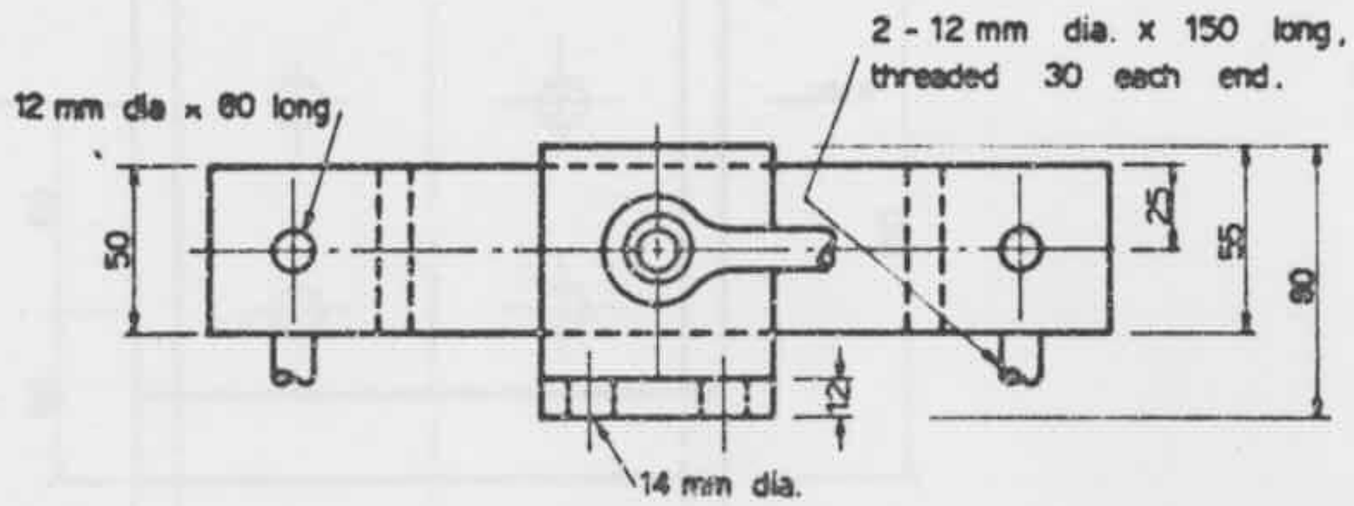

ELEVATION

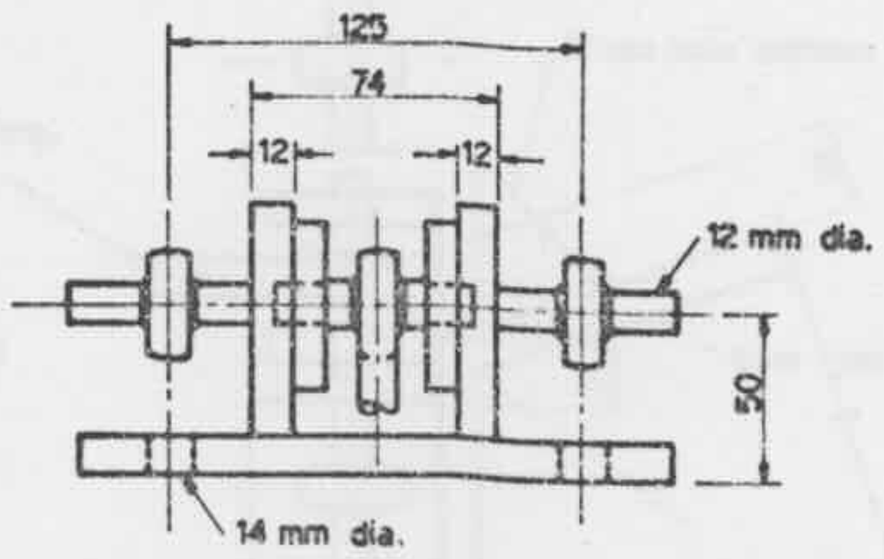

END ELEVATION

NOTE: ALL DIMENSIONS IN MM.

				STANCHION ASSEMBLY	6			
DO NOT SCALE DRAWING	REFERENCE DRAWINGS			ITEM DESCRIPTION	QTY.	MATL. OR REF. No.		REMARKS
EXCEPT WHERE OTHERWISE INDICATED REMOVE BURRS & SHARP EDGES FRACTIONAL DIMENSIONS ± DECIMAL DIMENSIONS ±	DRAWN	A.H.B.		UNIVERSITY OF SYDNEY	DEPT. CIVIL ENG.		SCALE 1:2	
	TRACED			TITLE STANCHION LOADING & RESTRAINT ASSEMBLY PORTAL FRAME TESTS			ISSUE No. B	
	CHECKED						DRAWING No. PFT-5	
	APPROVED							

Loading and restraint assembly to be welded to eave joint flange. Centre-lines of loading assembly and channel section are to coincide.

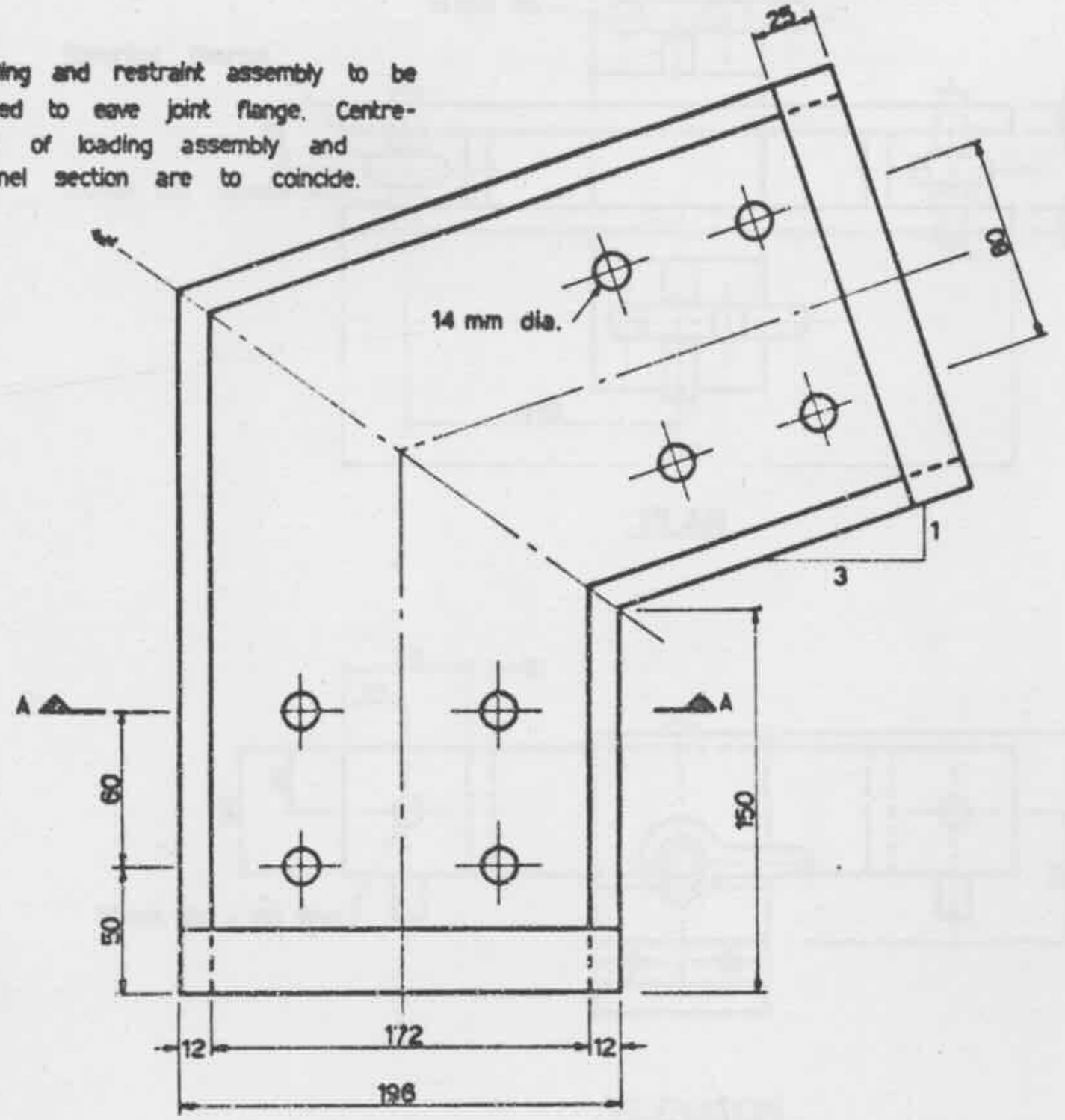

ELEVATION

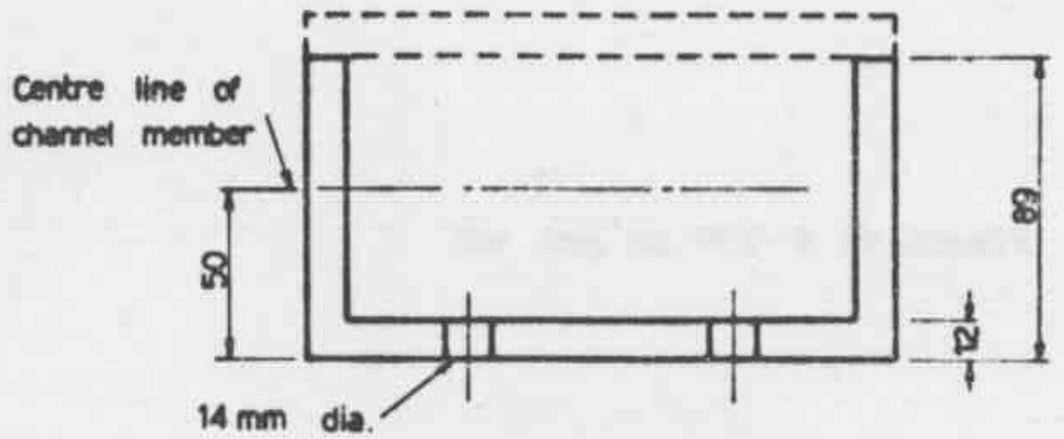

SECTION A-A

2 - 12 mm dia. x 150 long, threaded 30 each end.

For details of loading and restraint assembly see Dwg. PFT-5.

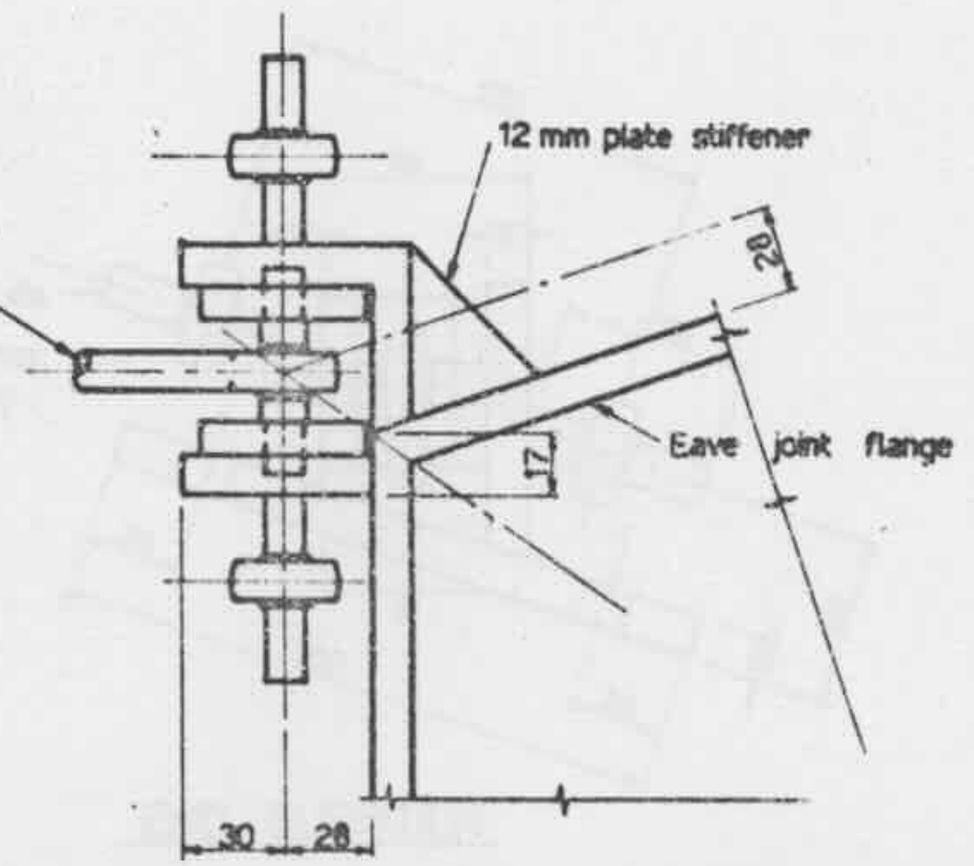

LOADING & RESTRAINT ASSEMBLY

NOTE: ALL DIMENSIONS IN MM.

See Dwg. No. PFT-7 for isometric view.

				LOADING ASSEMBLY	2		
				EAVE JOINT	2		
DO NOT SCALE DRAWING	REFERENCE DRAWINGS		ITEM	DESCRIPTION	QTY.	MAT'L OR REF. No.	REMARKS
EXCEPT WHERE OTHERWISE INDICATED REMOVE BURRS & SHARP EDGES FRACTIONAL DIMENSIONS ± DECIMAL DIMENSIONS ±	DRAWN	A. H. B.	UNIVERSITY OF SYDNEY	DEPT. CIVIL ENG	SCALE 1 : 2		
	TRACED		TITLE EAVE JOINT DETAILS PORTAL FRAME TESTS		ISSUE No. 8		
	CHECKED				DRAWING No. PFT-6		
	APPROVED						

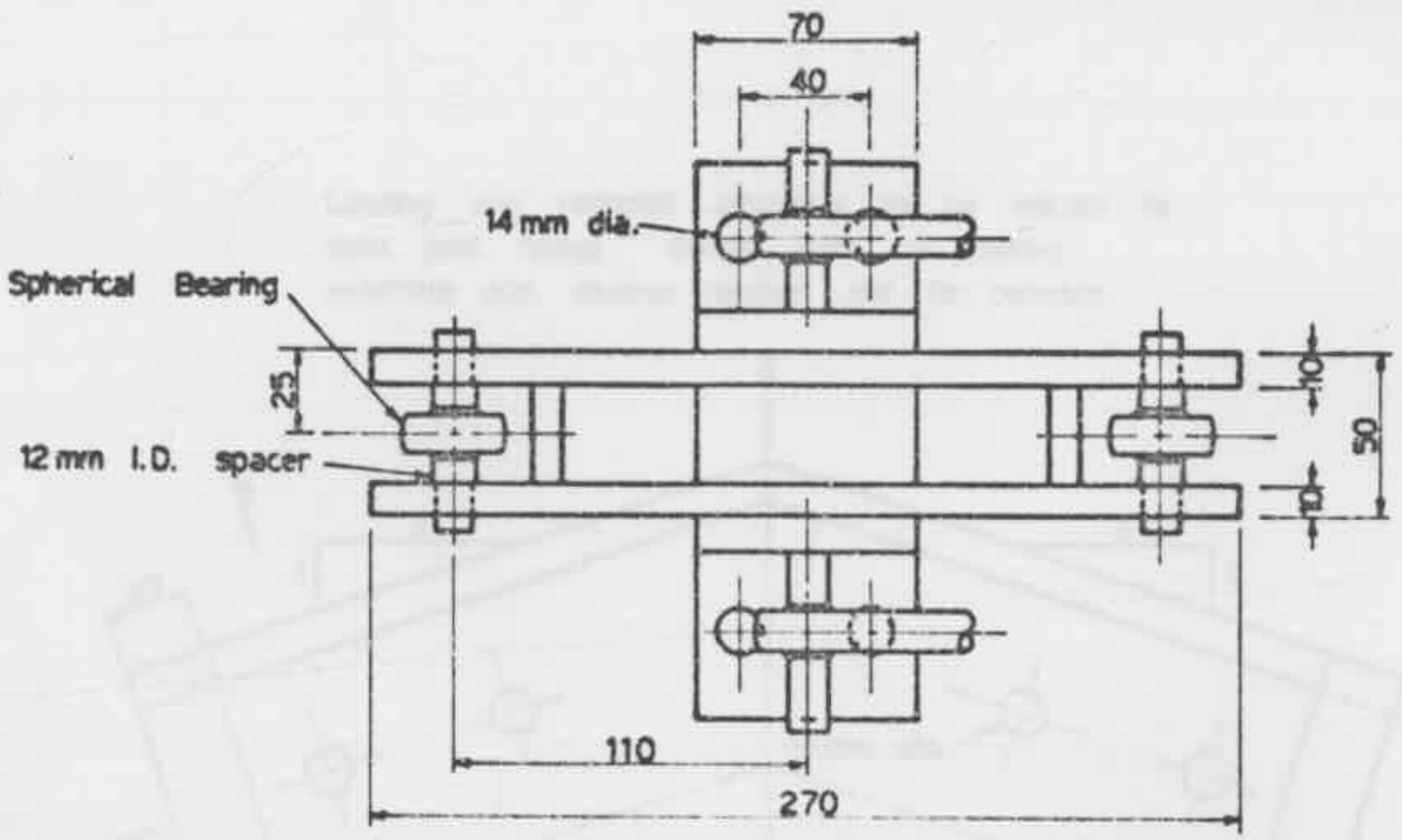

PLAN

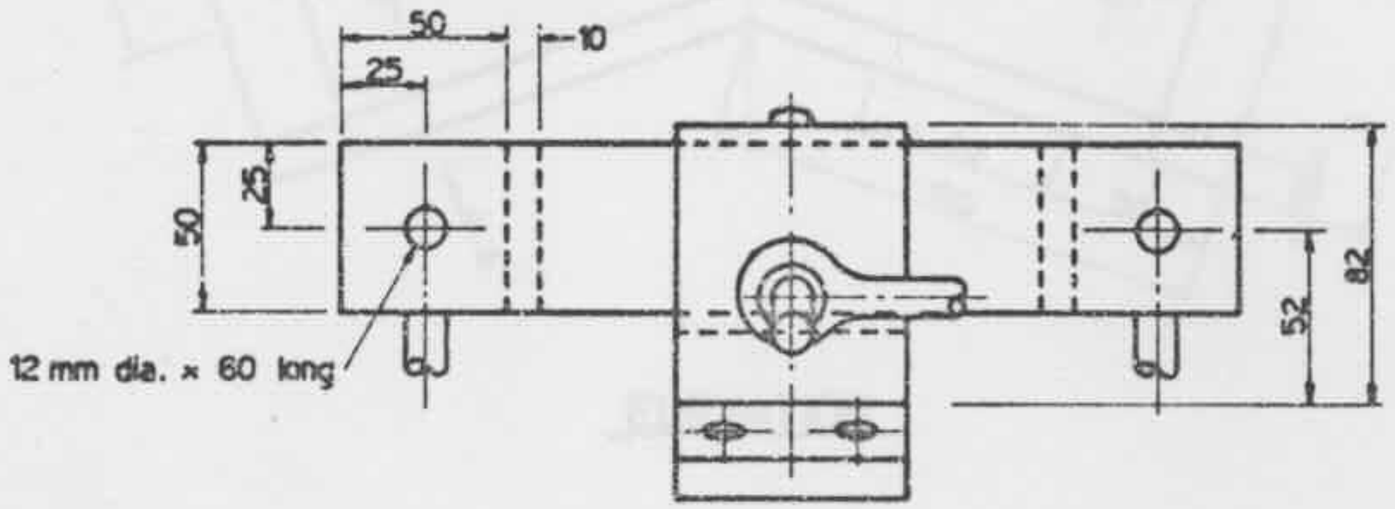

ELEVATION

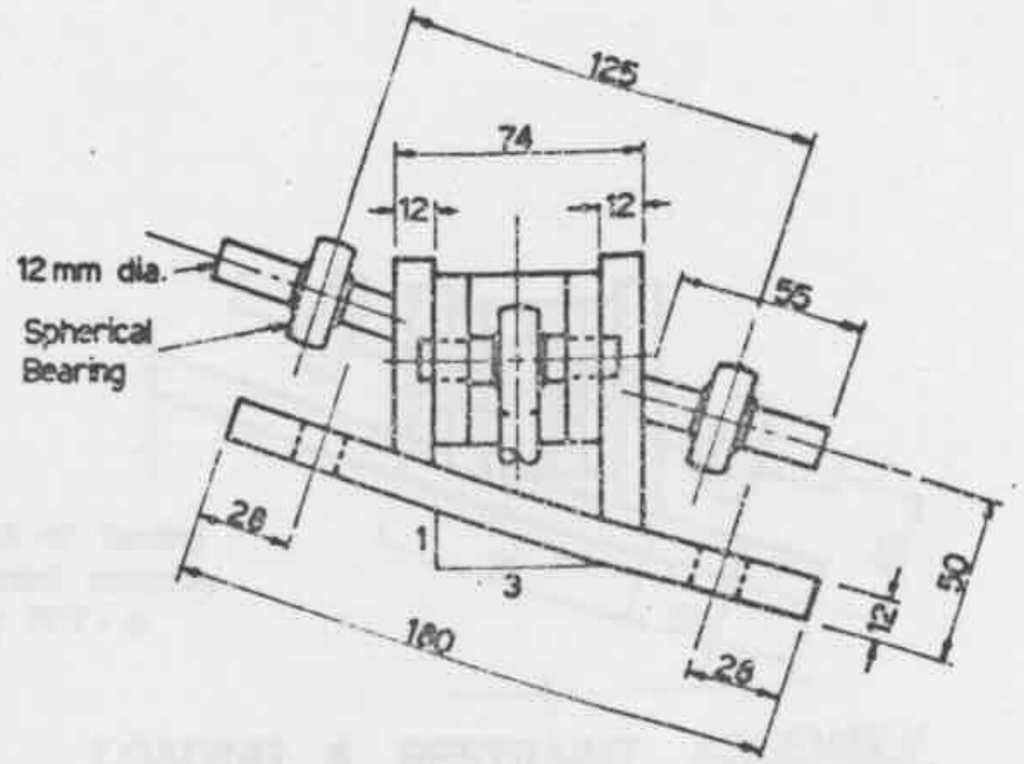

END ELEVATION

See Dwg. No. PFT-4 for isometric view.

NOTE: ALL DIMENSIONS IN MM.

				RAFTER ASSEMBLY		6			
DO NOT SCALE DRAWING	REFERENCE DRAWINGS			ITEM	DESCRIPTION	QTY.	MAT'L OR REF. No.	REMARKS	
EXCEPT WHERE OTHERWISE INDICATED:	DRAWN	A.H.B.		UNIVERSITY OF SYDNEY		DEPT. CIVIL ENG.		SCALE 1:2	
REMOVE BURRS & SHARP EDGES	TRACED			TITLE				ISSUE No. A	
FRACTIONAL DIMENSIONS ±	CHECKED			RAFTER LOADING & RESTRANT ASSEMBLY					
DECIMAL DIMENSIONS ±	APPROVED			PORTAL FRAME TESTS				DRAWING No. PFT-8	

- 527 -

Loading and restraint assembly to be welded to apex joint flange. Centre lines of loading assembly and channel section are to coincide.

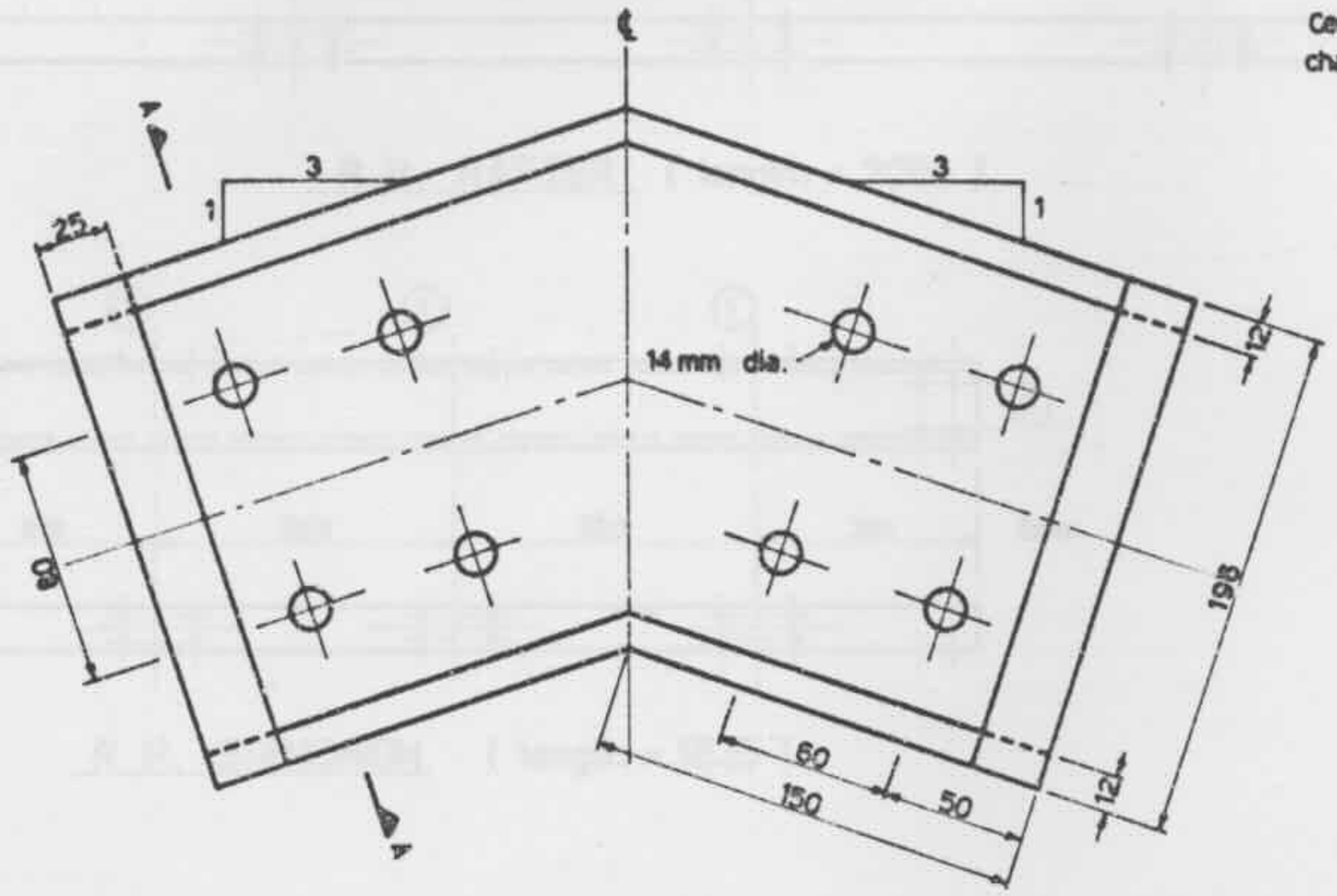

ELEVATION

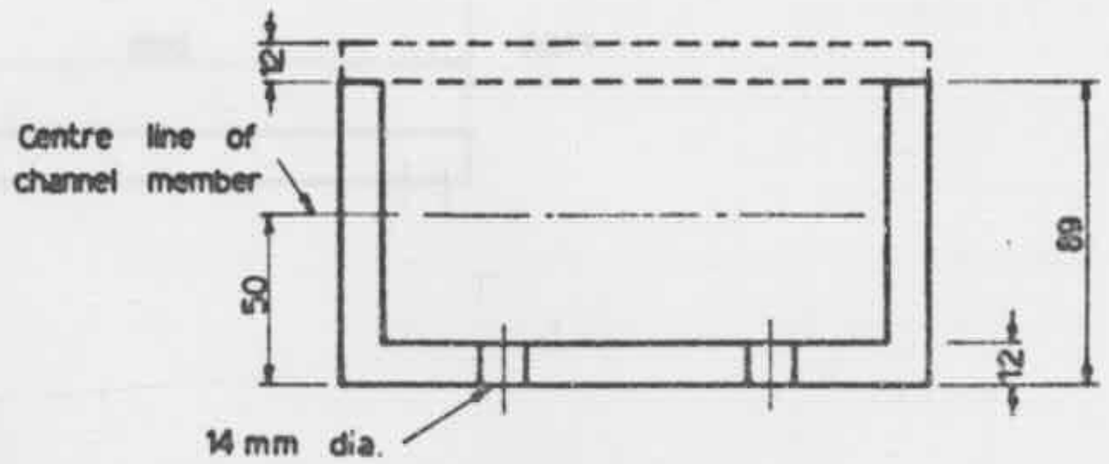

SECTION A-A

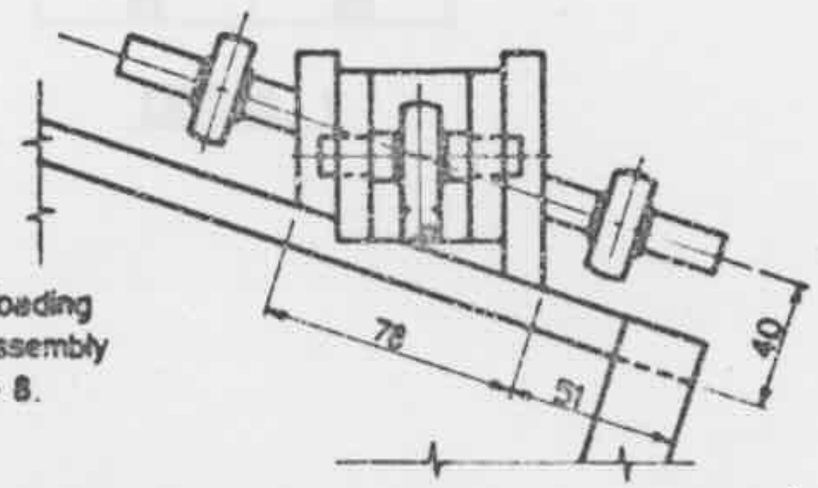

For details of loading and restraint assembly see Dwg PFT-8.

LOADING & RESTRAINT ASSEMBLY

See Dwg. No. PFT-10 for isometric view.

NOTE: ALL DIMENSIONS IN MM.

ITEM	DESCRIPTION	QTY.	MAT'L OR REF. No.	REMARKS
	LOADING ASSEMBLY	2		
	APEX JOINT	1		

DO NOT SCALE DRAWING — REFERENCE DRAWINGS

EXCEPT WHERE OTHERWISE INDICATED:
REMOVE BURRS & SHARP EDGES
FRACTIONAL DIMENSIONS ±
DECIMAL DIMENSIONS ±

DRAWN	A.H.B.		
TRACED			
CHECKED			
APPROVED			

UNIVERSITY OF SYDNEY — DEPT. CIVIL ENG.

TITLE
APEX JOINT DETAILS
PORTAL FRAME TESTS

SCALE 1:2
ISSUE No. A
DRAWING No. PFT-9

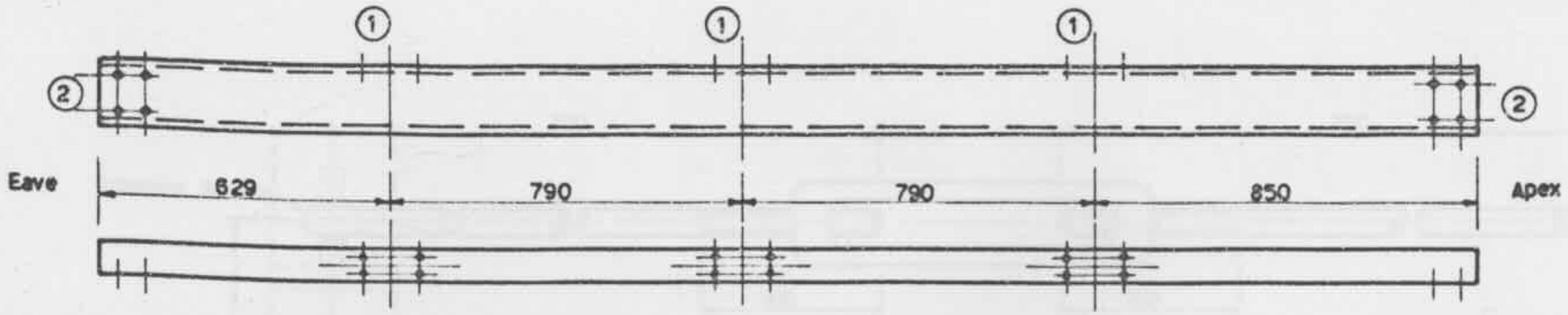

R.H. RAFTER (length = 3059)

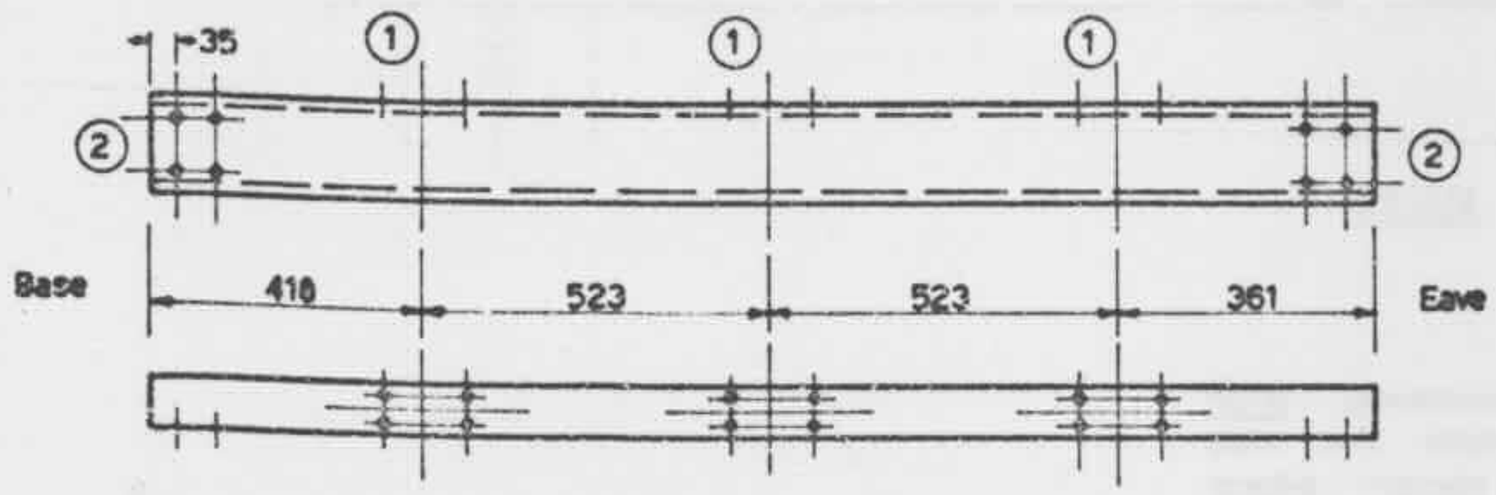

R.H. STANCHION (length = 1825)

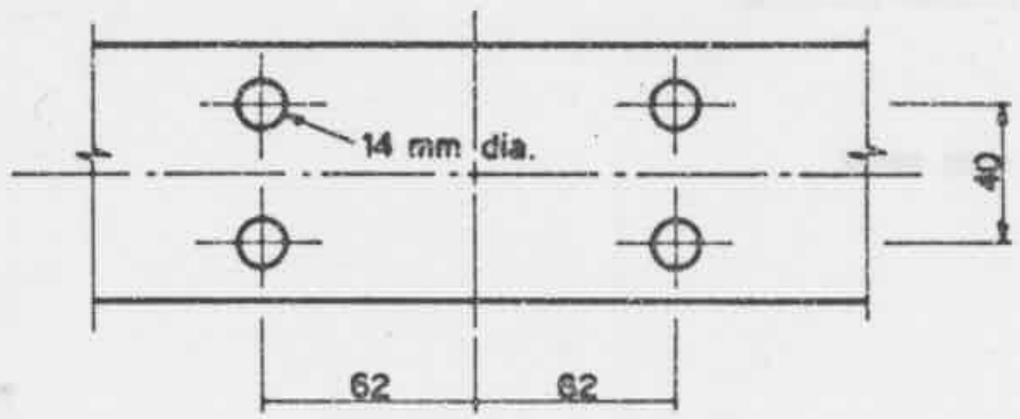

DETAIL 1

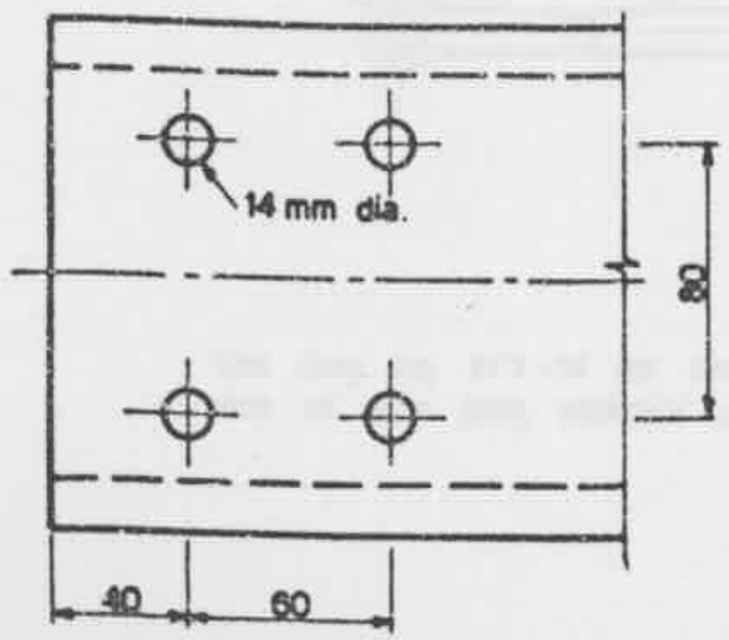

DETAIL 2

NOTE: ALL DIMENSIONS IN MM.

DO NOT SCALE DRAWING	REFERENCE DRAWINGS	ITEM	DESCRIPTION	QTY.	SUPPL. OR REF. No.	REMARKS
EXCEPT WHERE OTHERWISE INDICATED	DRAWN A.H.B.		UNIVERSITY OF SYDNEY	DEPT. CIVIL ENG.	SCALE 1:2 , 1:10	
REMOVE BURRS & SHARP EDGES	TRACED		TITLE MEMBER DETAILS		ISSUE No. B	
FRACTIONAL DIMENSIONS ±	CHECKED		PORTAL FRAME TESTS		DRAWING No. PFT - 11	
DECIMAL DIMENSIONS ±	APPROVED					

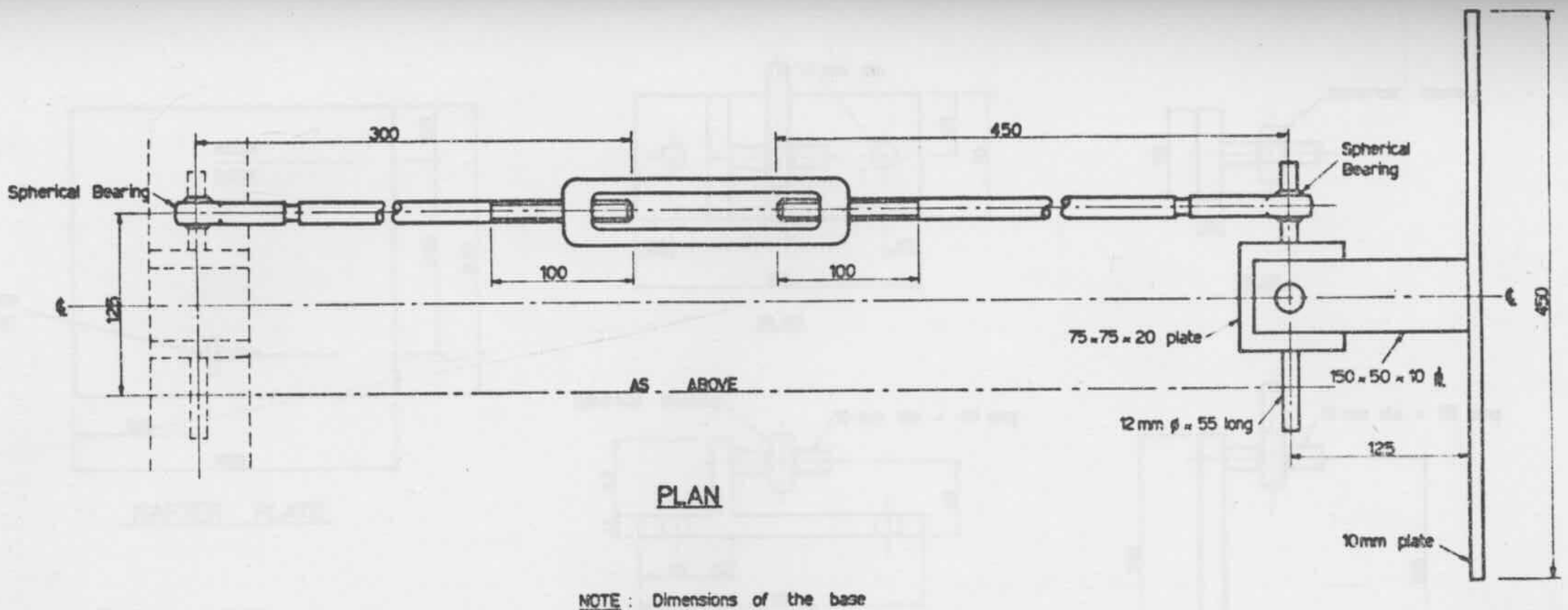

PLAN

NOTE : Dimensions of the base plate vary where the fly bracing restraint is used. See Dwg. PFT-13 for details.

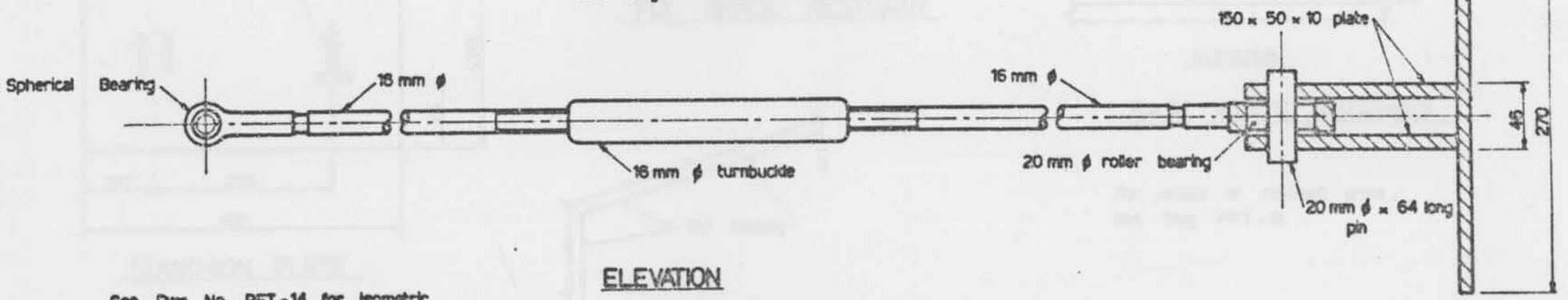

ELEVATION

See Dwg. No. PFT-14 for isometric view of apex joint restraint plate.

NOTE: ALL DIMENSIONS IN MM.

ITEM	DESCRIPTION	QTY.	MAT'L OR REF. No.	REMARKS
	LATERAL RESTRAINT	18		

DO NOT SCALE DRAWING	REFERENCE DRAWINGS	UNIVERSITY OF SYDNEY	DEPT. CIVIL ENG.
EXCEPT WHERE OTHERWISE INDICATED: REMOVE BURRS & SHARP EDGES; FRACTIONAL DIMENSIONS ±; DECIMAL DIMENSIONS ±	DRAWN A.H.B.	TITLE LATERAL RESTRAINT DETAILS PORTAL FRAME TESTS	SCALE 1 : 2·5
	TRACED		ISSUE No A
	CHECKED		DRAWING No. PFT - 12
	APPROVED		

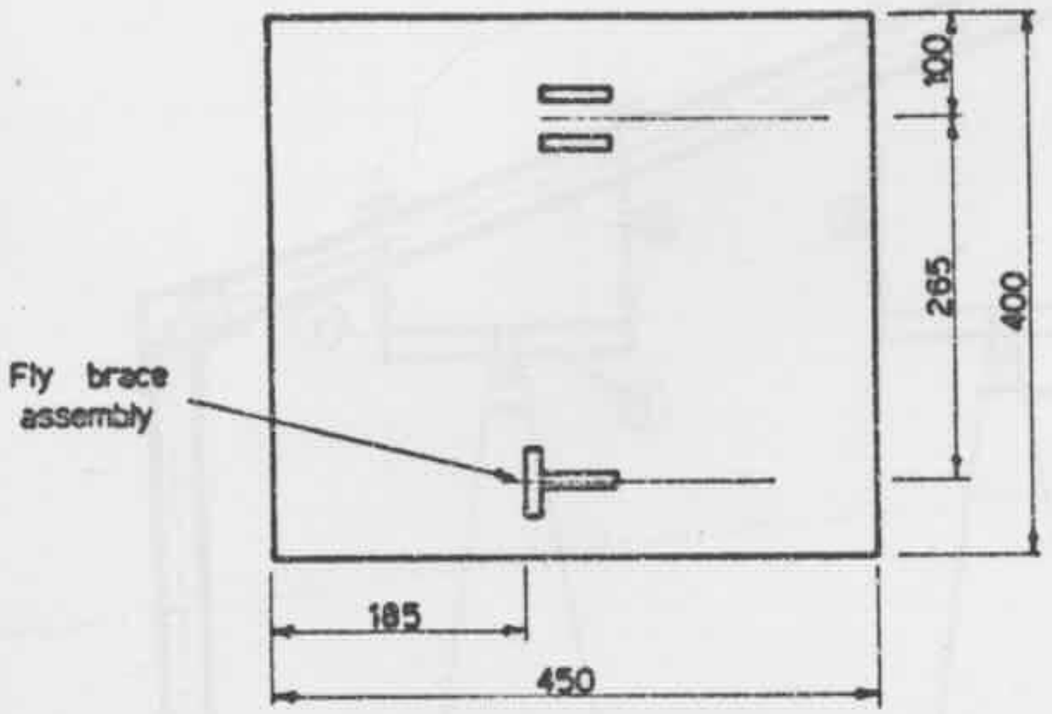

RAFTER PLATE

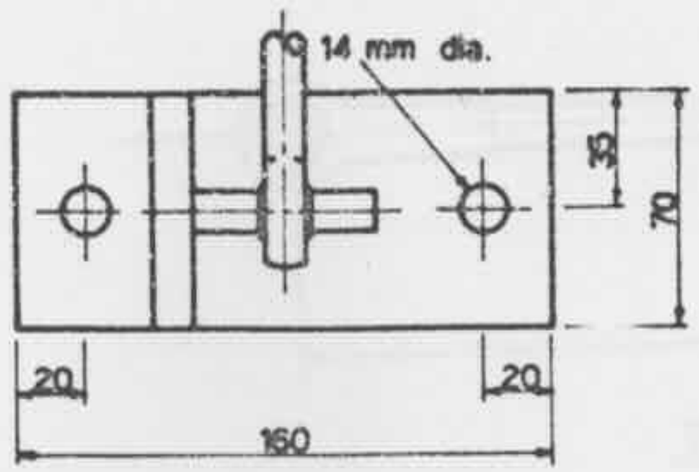

PLAN

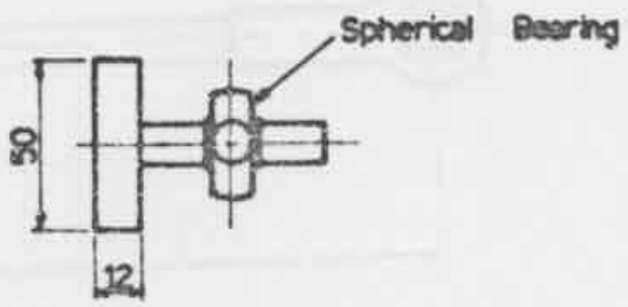

PLAN

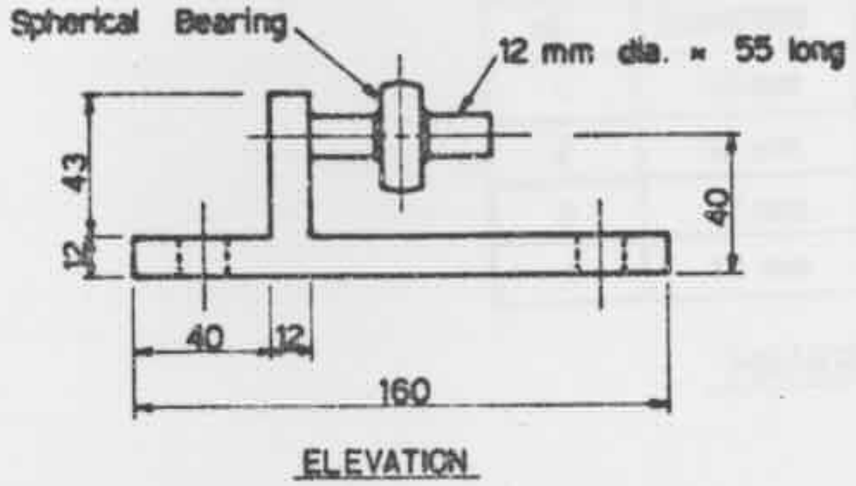

ELEVATION

FLY BRACE RESTRAINT

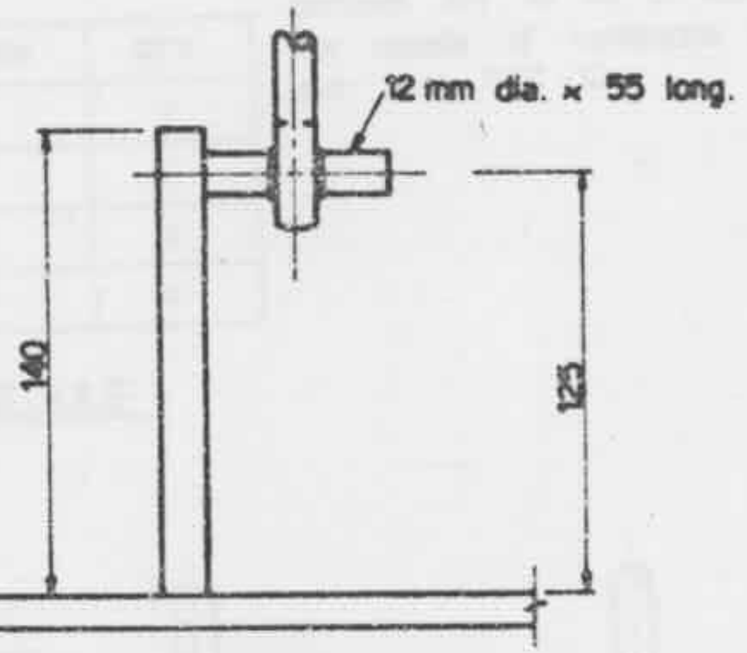

ELEVATION

BASE PLATE ASSEMBLY

For details of restraint arms, see Dwg. PFT-12

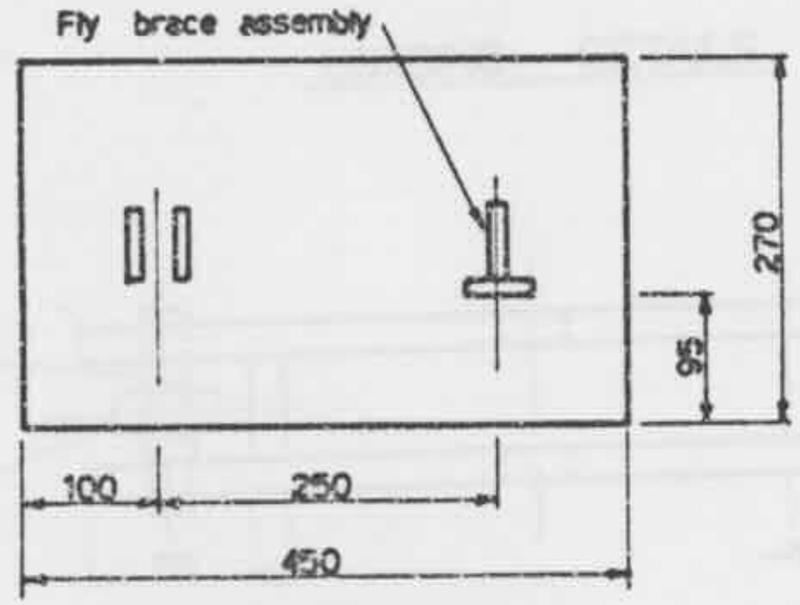

STANCHION PLATE

See Dwg. PFT-13 for isometric view.

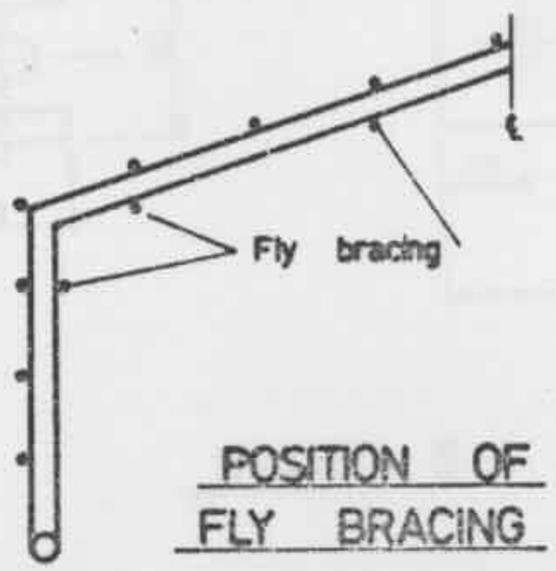

POSITION OF FLY BRACING

NOTE: ALL DIMENSIONS IN MM.

ITEM	DESCRIPTION	QTY.	MAT'L OR REF. No.	REMARKS
	RESTRAINT ARM	6		
	FLY BRACE RESTRAINT	6		
	STANCHION PLATE	2		
	RAFTER PLATE	4		

DO NOT SCALE DRAWING (EXCEPT WHERE OTHERWISE INDICATED)
REMOVE BURRS & SHARP EDGES
FRACTIONAL DIMENSIONS ±
DECIMAL DIMENSIONS ±

REFERENCE DRAWINGS

DRAWN A.H.B.
TRACED
CHECKED
APPROVED

UNIVERSITY OF SYDNEY — DEPT. CIVIL ENG

TITLE
FLY BRACING RESTRAINT DETAILS
PORTAL FRAME TESTS

SCALE 1:2 , 1:5
ISSUE No. A
DRAWING No. PFT-13

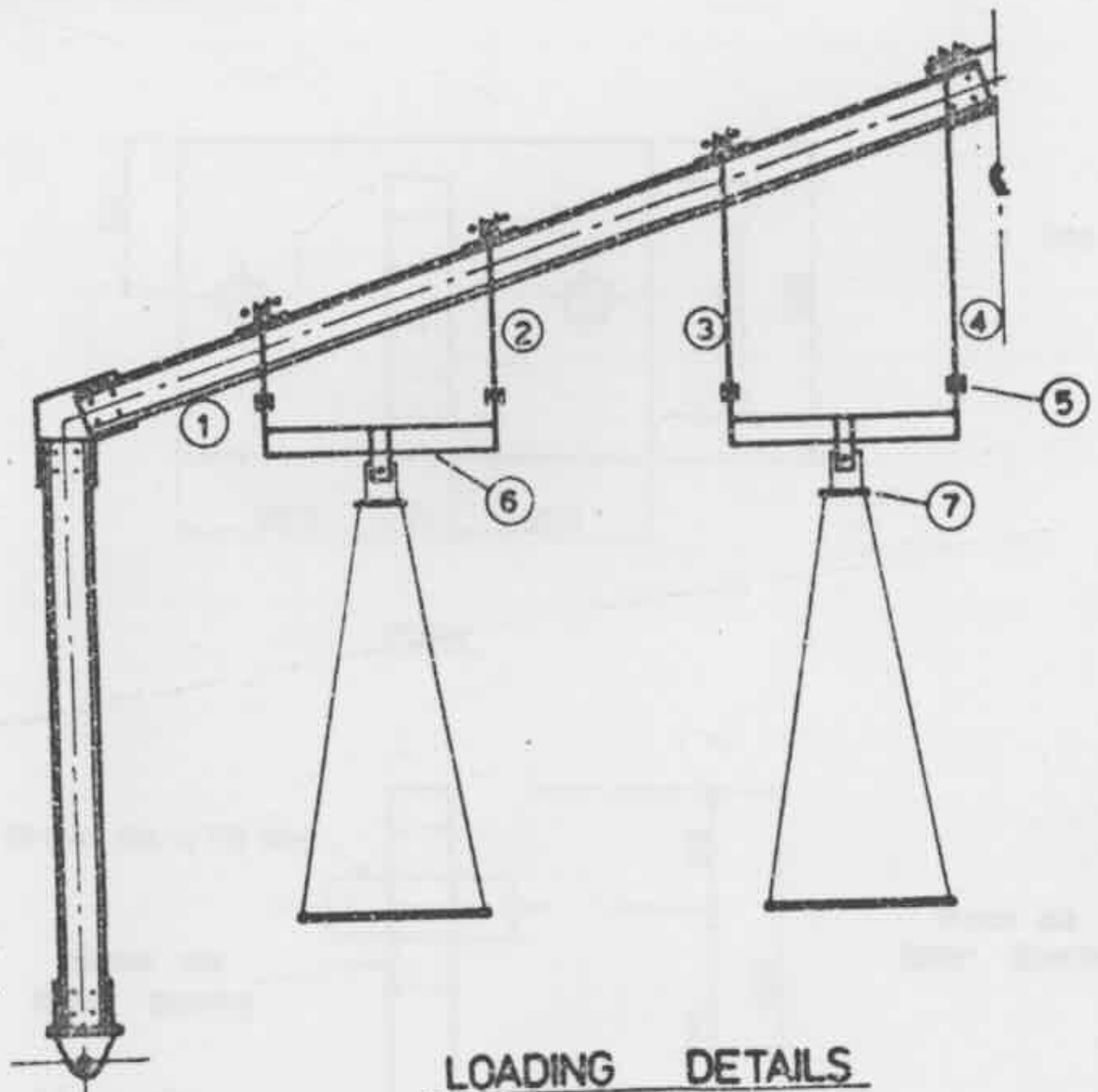

LOADING DETAILS

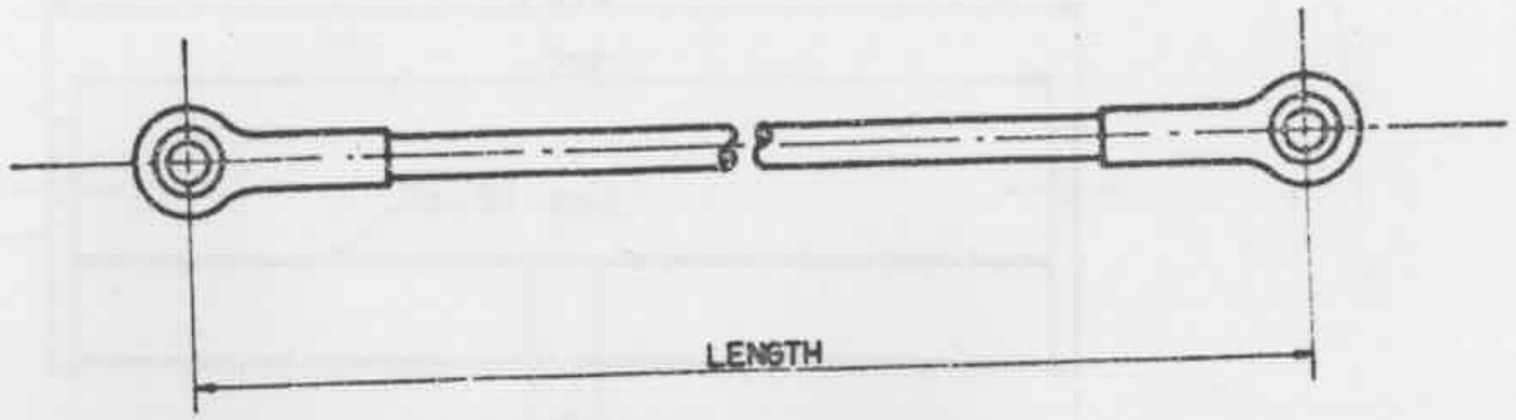

TYPICAL HANGER

Note :
Turnbuckle to be situated at centre position of hanger and hanger portions are to be of equal length.
For details of turnbuckle arrangement see Dwg PFT-12.

№	DIAMETER	LENGTH	QTY.
1	12 mm	300	4
2	12 mm	550	4
3	12 mm	800	4
4	12 mm	1050	4

HANGER SCHEDULE

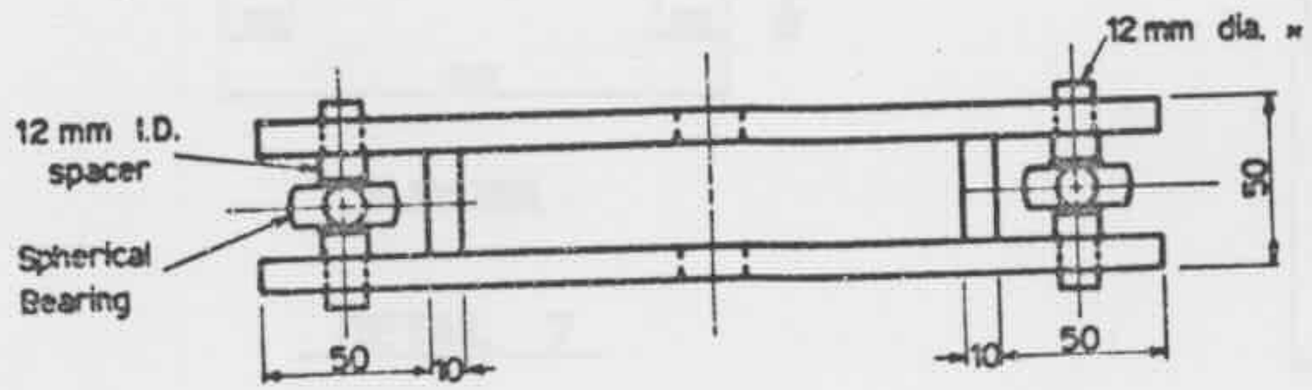

PLAN

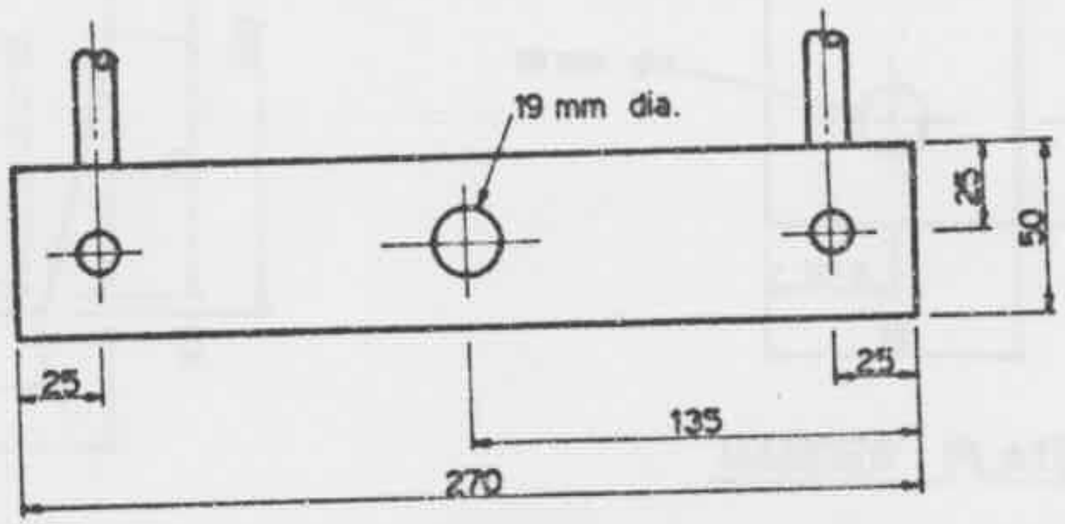

ELEVATION

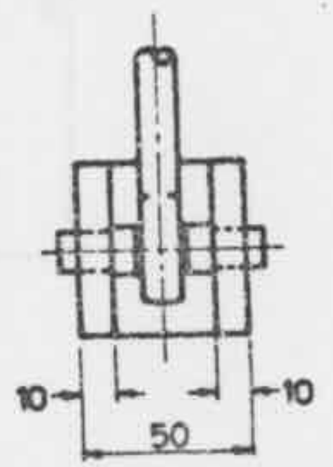

END ELEVATION

DETAIL 5

NOTE: ALL DIMENSIONS IN MM.

ITEM	DESCRIPTION	QTY.	MAT'L OR REF. No.	REMARKS
5	HANGER CONNECTOR	8		
	HANGERS	16		AS SCHEDULE

DO NOT SCALE DRAWING
EXCEPT WHERE OTHERWISE INDICATED
REMOVE BURRS & SHARP EDGES
FUNCTIONAL DIMENSIONS ±
DECIMAL DIMENSIONS ±

REFERENCE DRAWINGS

DRAWN	A.H.B.	
TRACED		
CHECKED		
APPROVED		

UNIVERSITY OF SYDNEY — DEPT. CIVIL ENG

TITLE
VERTICAL LOADING DETAILS 1
PORTAL FRAME TESTS

SCALE 1:2 , 1:20
ISSUE No. A
DRAWING No. PFT-18

I 532 I

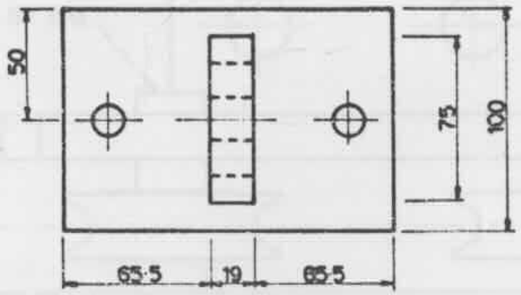

PLAN

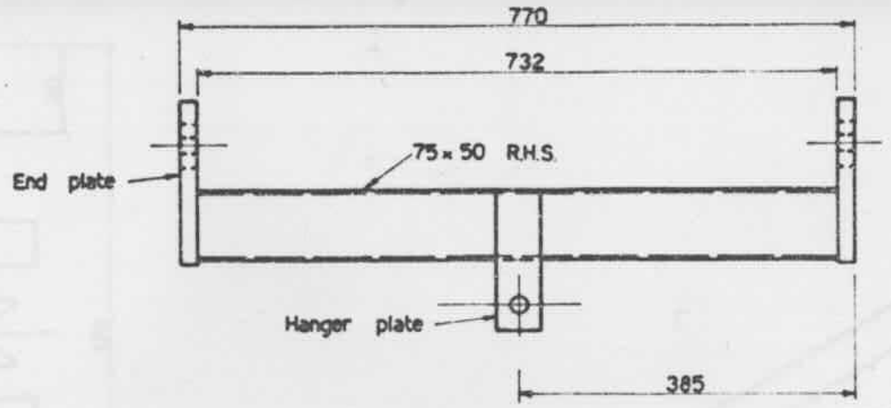

DETAIL 6

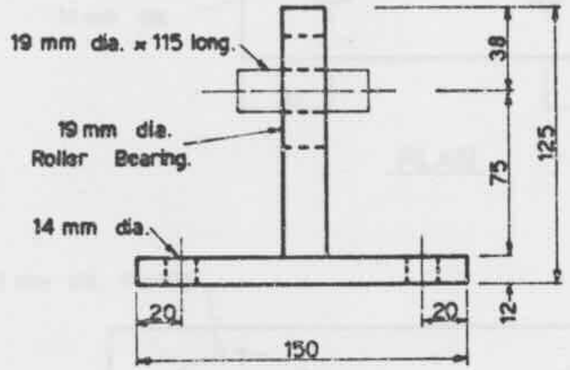

ELEVATION

DETAIL 7

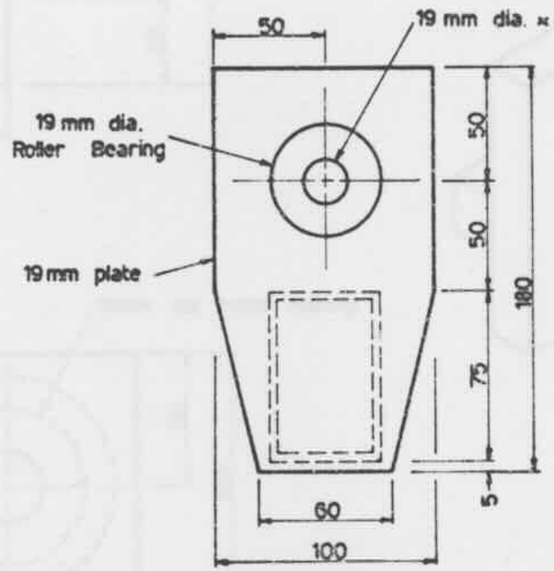

END PLATE

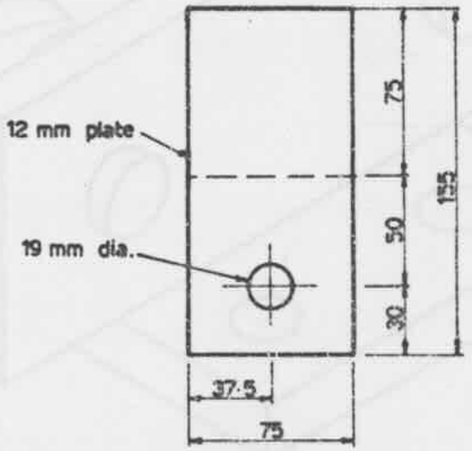

HANGER PLATE

NOTE: ALL DIMENSIONS IN MM.

	LOAD CARRIER	4			
	HANGER PLATE	8			
	END PLATE	8			
	75 x 50 R.H.S	4			
ITEM	DESCRIPTION	QTY.	PART OR REF. No.	REMARKS	

DO NOT SCALE DRAWING

REFERENCE DRAWINGS

EXCEPT WHERE OTHERWISE INDICATED
REMOVE BURRS & SHARP EDGES
FRACTIONAL DIMENSIONS ±
DECIMAL DIMENSIONS ±

DRAWN	A.H.B.		
TRACED			
CHECKED			
APPROVED			

UNIVERSITY OF SYDNEY — DEPT. CIVIL ENG.

TITLE
VERTICAL LOADING DETAILS 2
PORTAL FRAME TESTS

SCALE 1:2 , 1:5

ISSUE No. A

DRAWING No.
PFT-19

I 5333 I

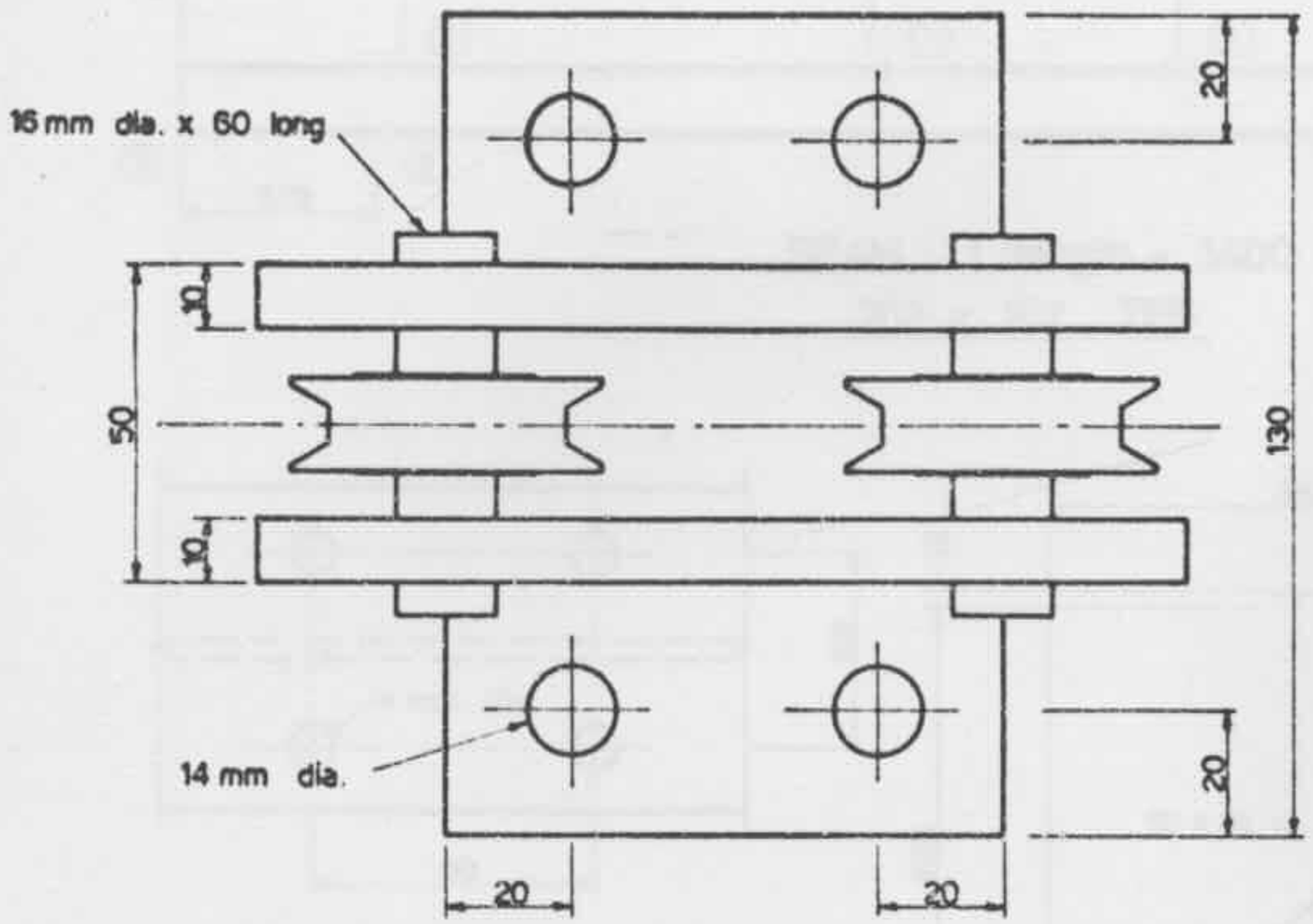

PLAN

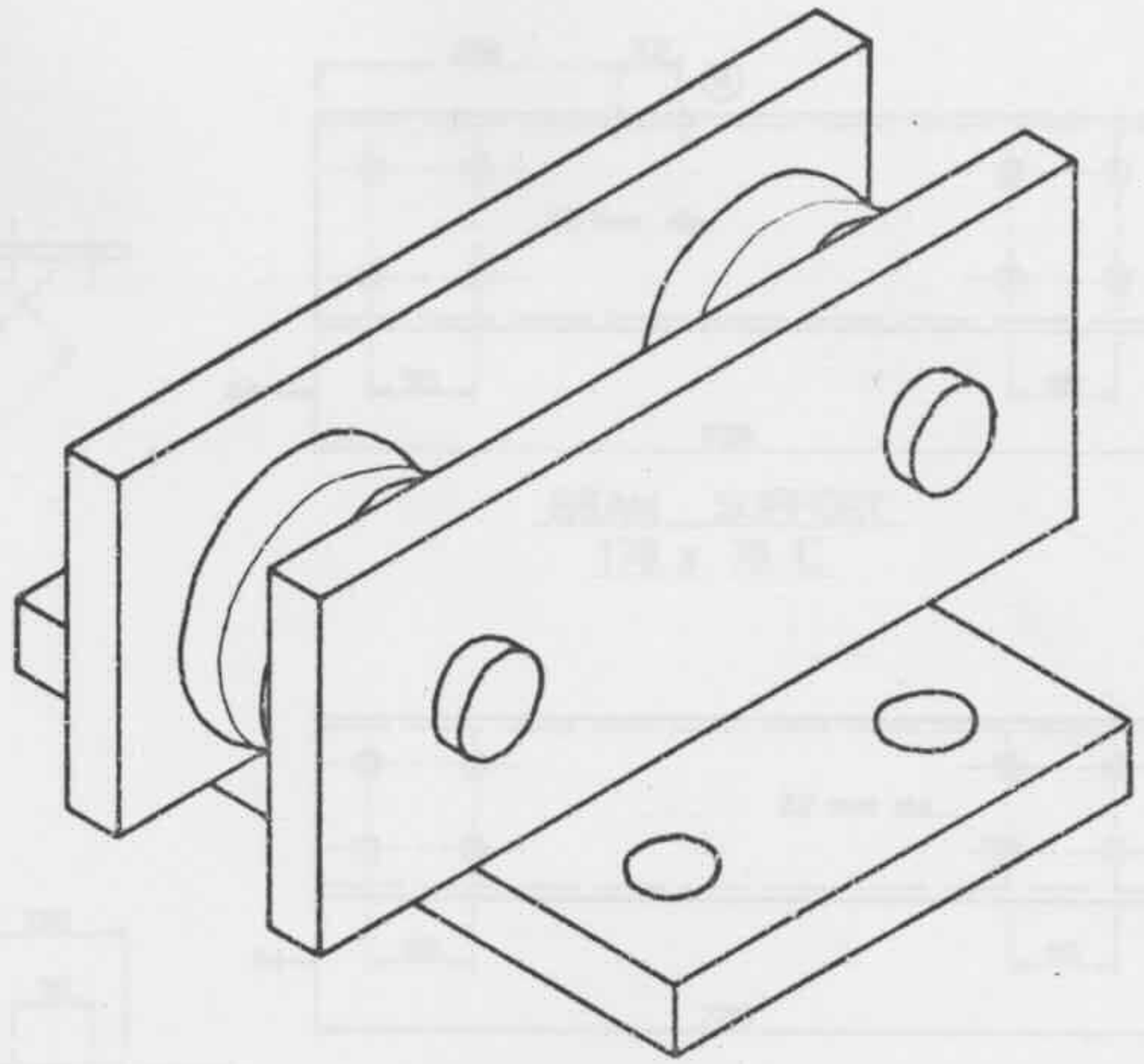

ISOMETRIC VIEW

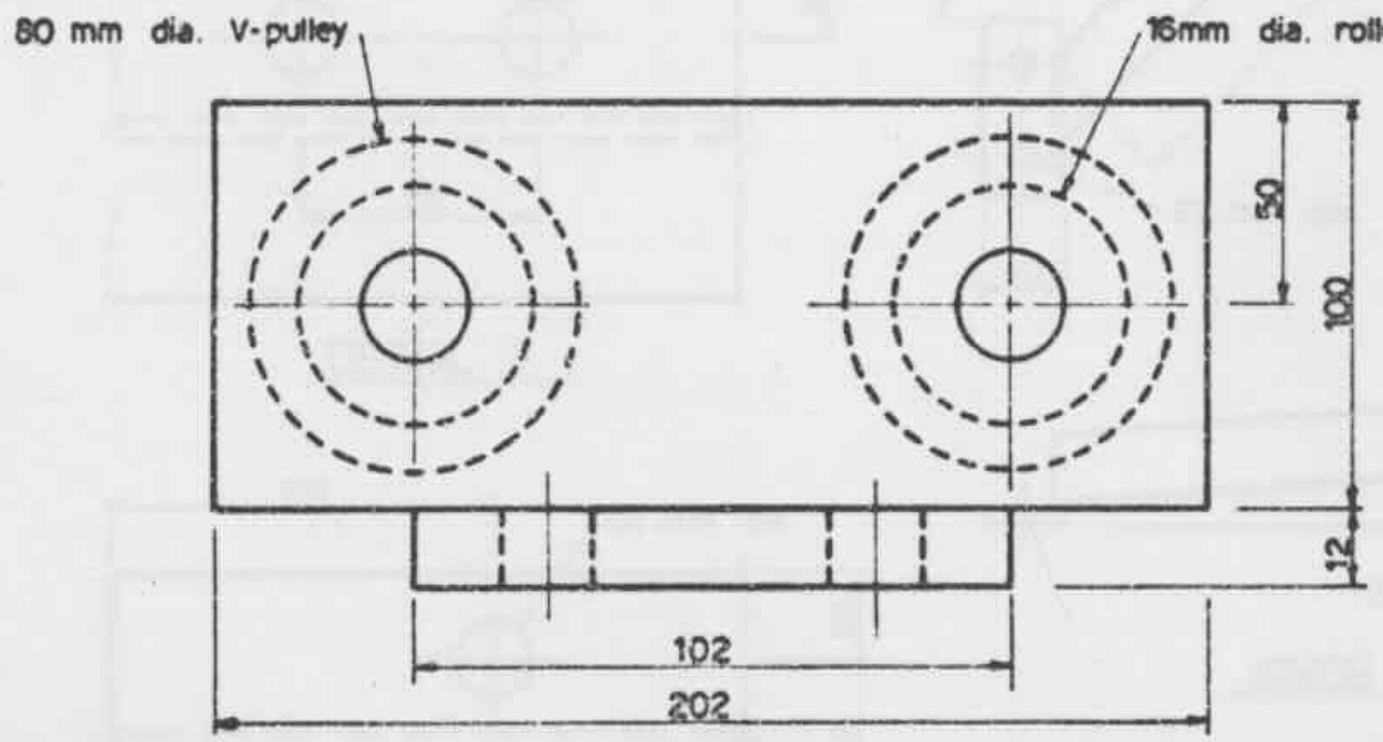

ELEVATION

NOTE: ALL DIMENSIONS IN MM.

ITEM	DESCRIPTION	QTY.	MAT'L OR REF. No.	REMARKS
	PULLEY BRACKET	4		

DO NOT SCALE DRAWING	REFERENCE DRAWINGS		
EXCEPT WHERE OTHERWISE INDICATED REMOVE BURRS & SHARP EDGES FRACTIONAL DIMENSIONS ± DECIMAL DIMENSIONS ±	DRAWN A. H. B.	UNIVERSITY OF SYDNEY	DEPT. CIVIL ENG
	TRACED	TITLE UPLIFT PULLEY BRACKET PORTAL FRAME TESTS	SCALE 1 : 1
	CHECKED		ISSUE No. 8
	APPROVED		DRAWING No. PFT-20

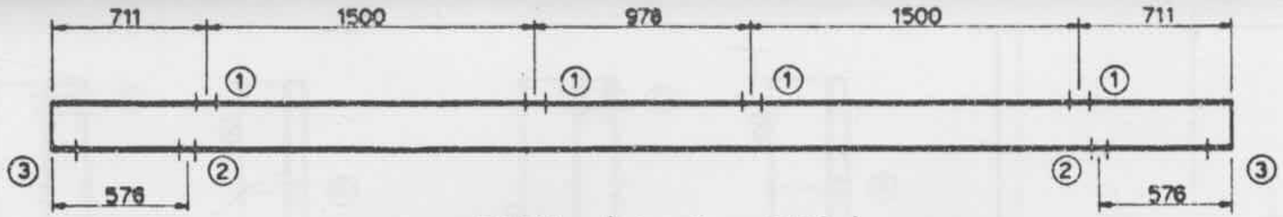

BEAM (length = 5400)
203 x 102 TFB

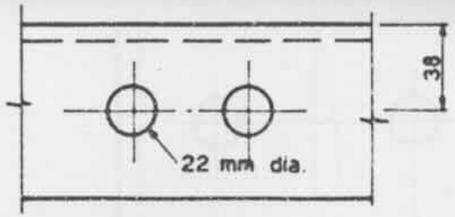

DETAIL 4

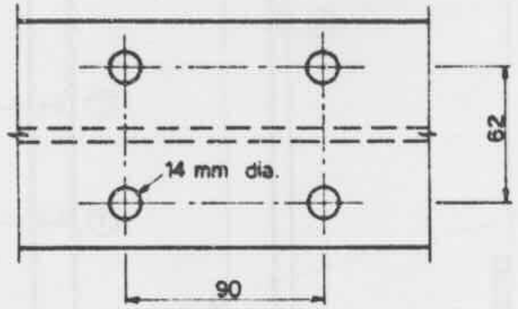

DETAIL 1

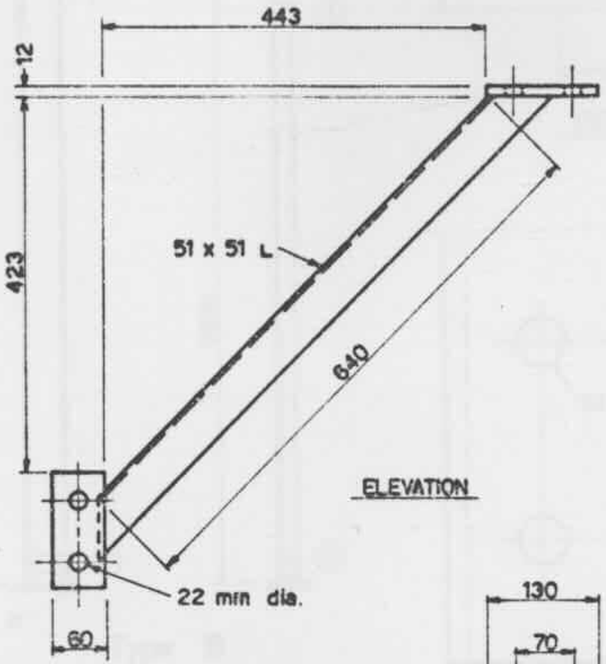

ELEVATION

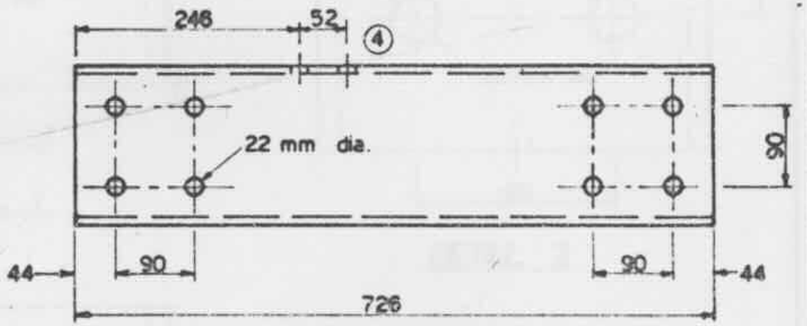

BEAM SUPPORT
178 x 76 C

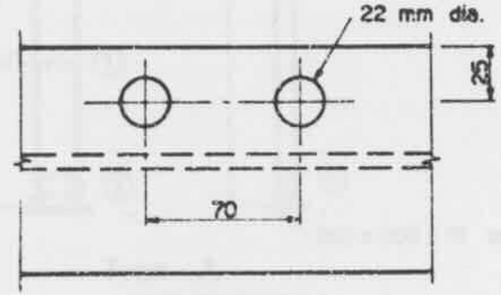

DETAIL 2

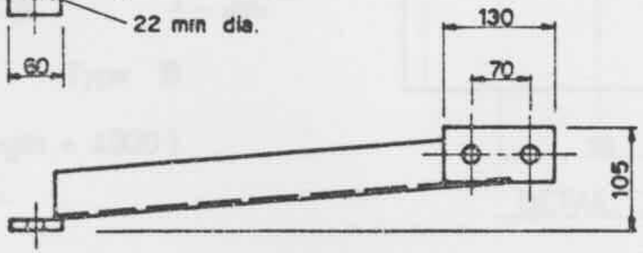

PLAN

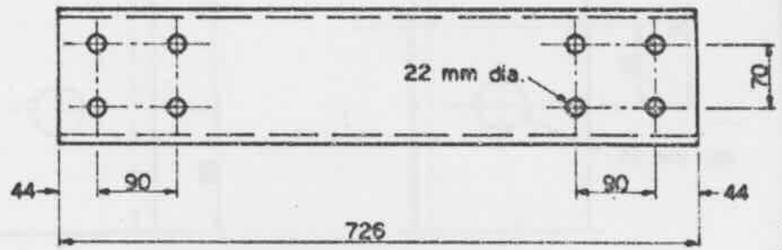

STANCHION TIE
152 x 76 C

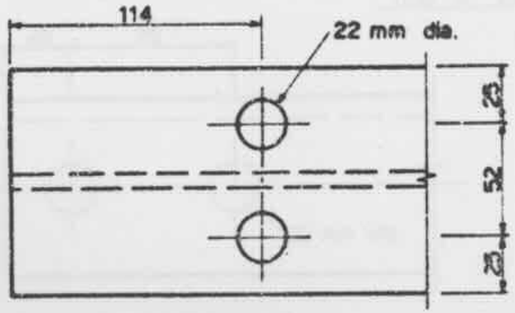

DETAIL 3

KNEE BRACE (L.H.)

NOTE: ALL DIMENSIONS IN MM.

	R.H. KNEE BRACE	1		
	L.H. KNEE BRACE	1		
	STANCHION TIE	1		
	R.H. BEAM SUPPORT	1		
	L.H. BEAM SUPPORT	1		
	203 x 102 T.F. BEAM	1		
ITEM	DESCRIPTION	QTY.	MAT'L OR REF. No.	REMARKS

DO NOT SCALE DRAWING
EXCEPT WHERE OTHERWISE INDICATED
REMOVE BURRS & SHARP EDGES
FUNCTIONAL DIMENSIONS ±
DECIMAL DIMENSIONS ±

REFERENCE DRAWINGS

DRAWN A.H.B.
TRACED
CHECKED
APPROVED

UNIVERSITY OF SYDNEY — DEPT. CIVIL ENG

TITLE
LOADING FRAME BEAM DETAILS
PORTAL FRAME TESTS

SCALE 1:2 , 1:5 , 1:20
ISSUE No. B
DRAWING No. PFT-21

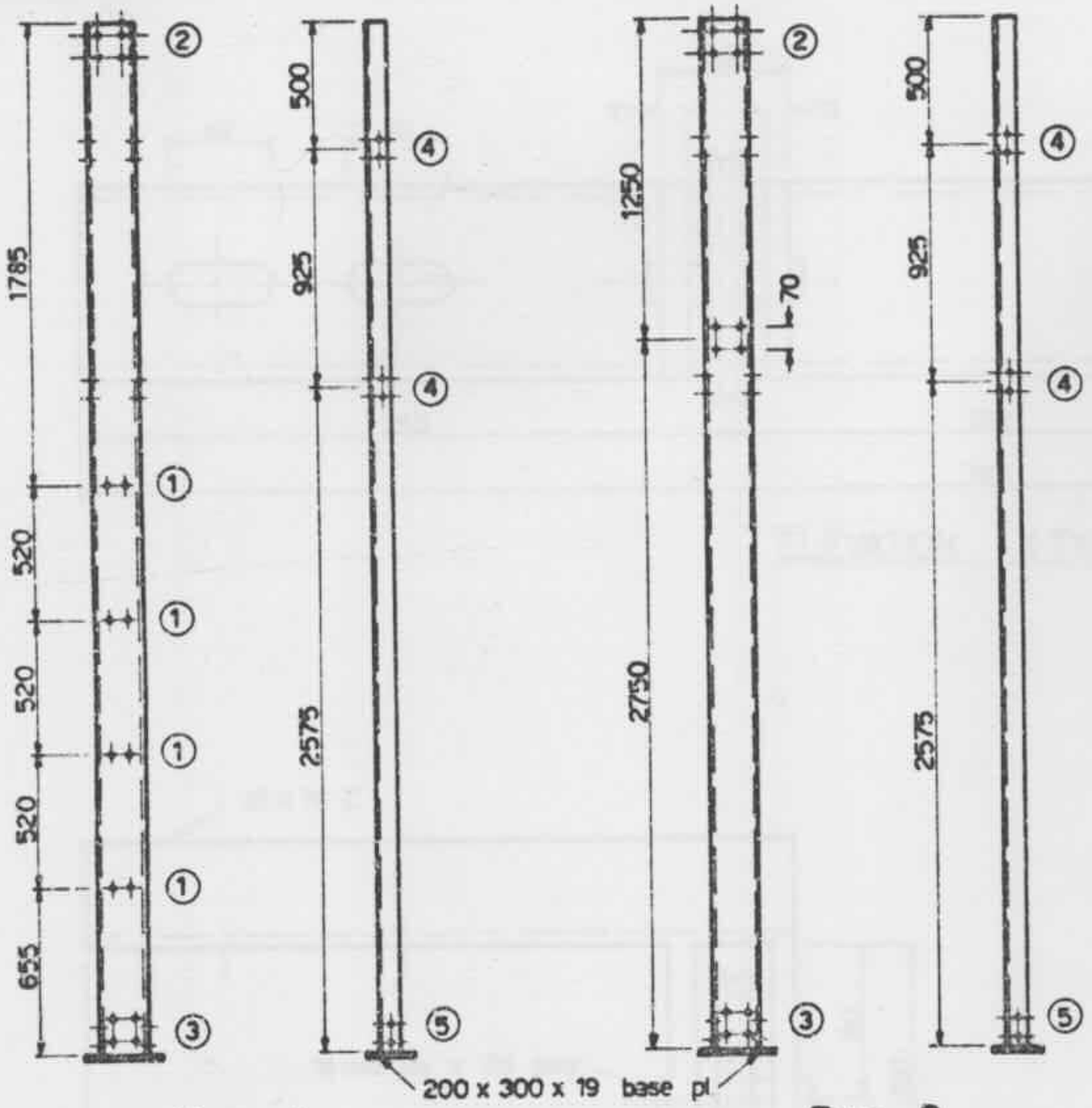

Type A

Type B

STANCHIONS (length = 4000)

178 x 76 C

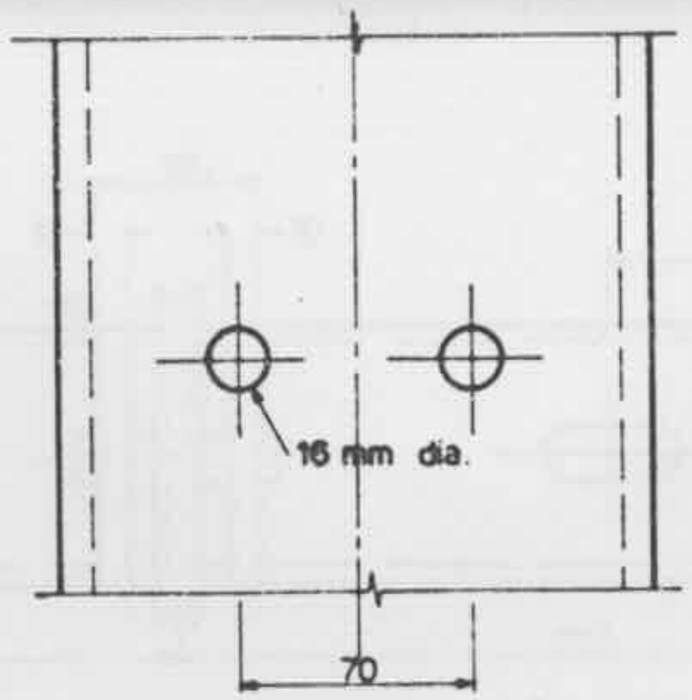

DETAIL 1

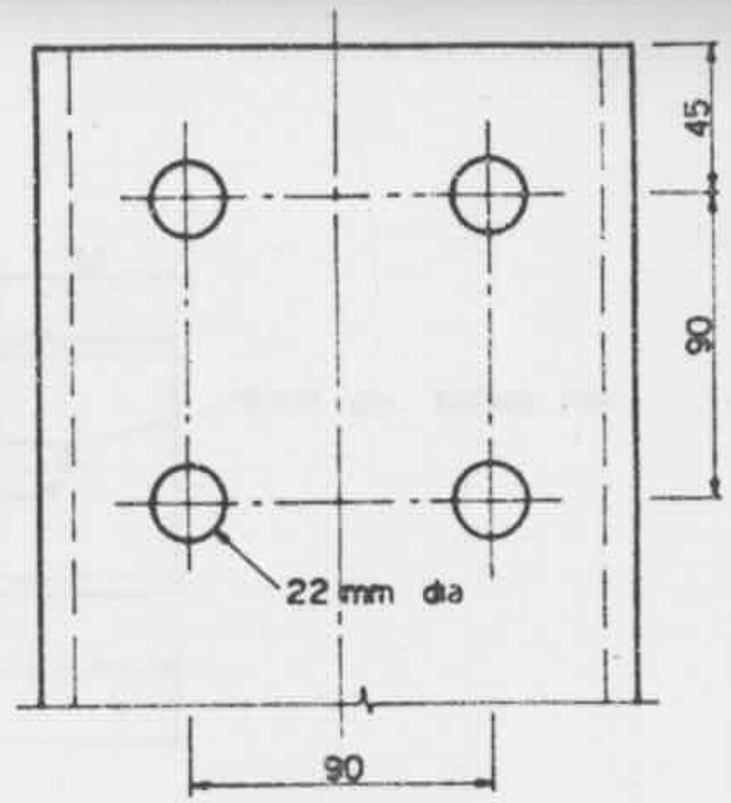

DETAIL 2

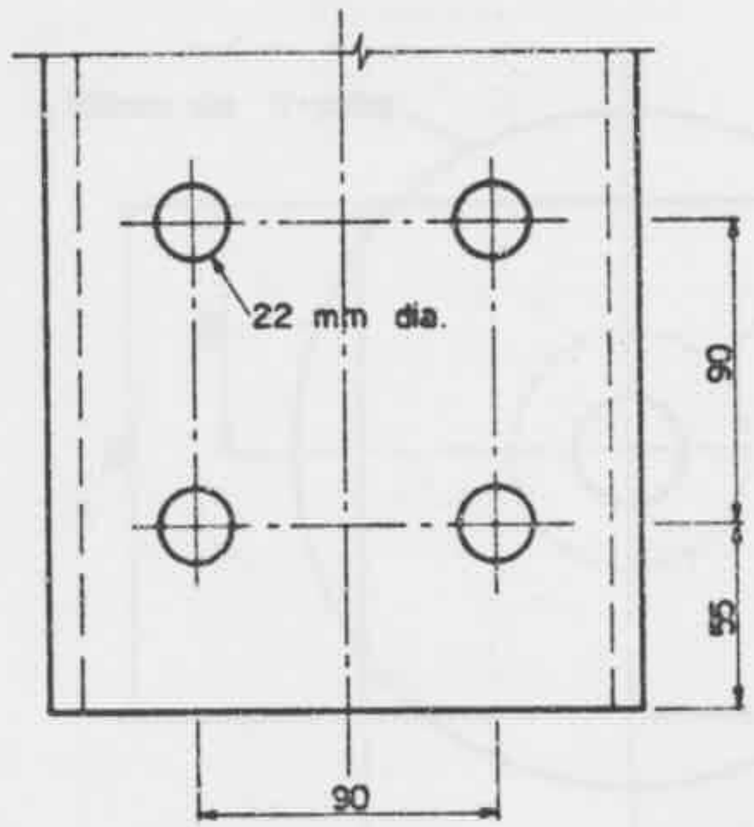

DETAIL 3

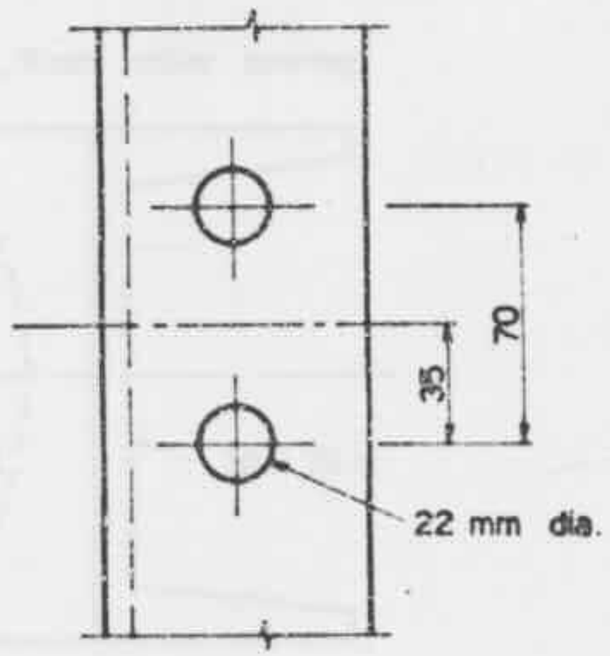

DETAIL 4

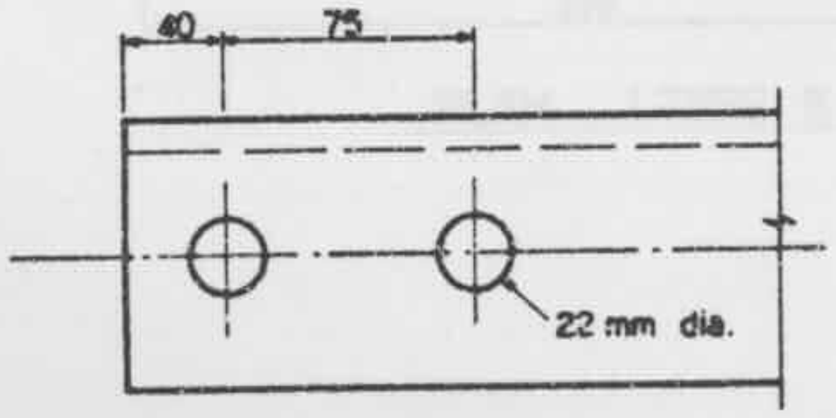

DETAIL 5

NOTE: ALL DIMENSIONS IN MM

ITEM	DESCRIPTION	QTY.	MAT'L OR REF. No.	REMARKS
	BASE PLATES	4		
	TYPE B STANCHION	2		
	TYPE A STANCHION	2		

DO NOT SCALE DRAWING

EXCEPT WHERE OTHERWISE INDICATED:
REMOVE BURRS & SHARP EDGES
FRACTIONAL DIMENSIONS ±
DECIMAL DIMENSIONS ±

REFERENCE DRAWINGS

DRAWN	A.H.B.	
TRACED		
CHECKED		
APPROVED		

UNIVERSITY OF SYDNEY DEPT. CIVIL ENG

TITLE
LOADING FRAME STANCHION DETAILS
PORTAL FRAME TESTS

SCALE 1 : 2 . 1 : 20

ISSUE No. A

DRAWING No.
PFT-22

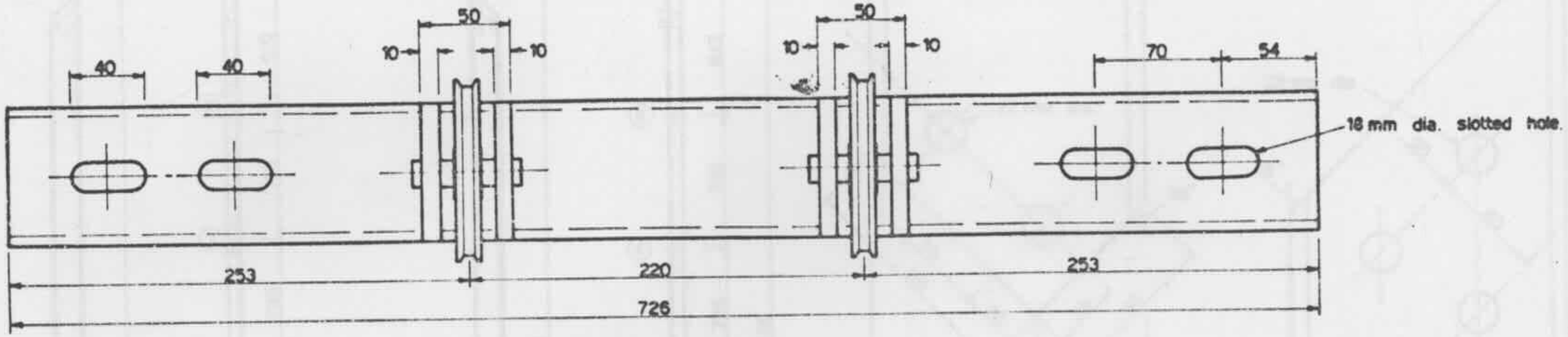

ELEVATION (TYPE A)

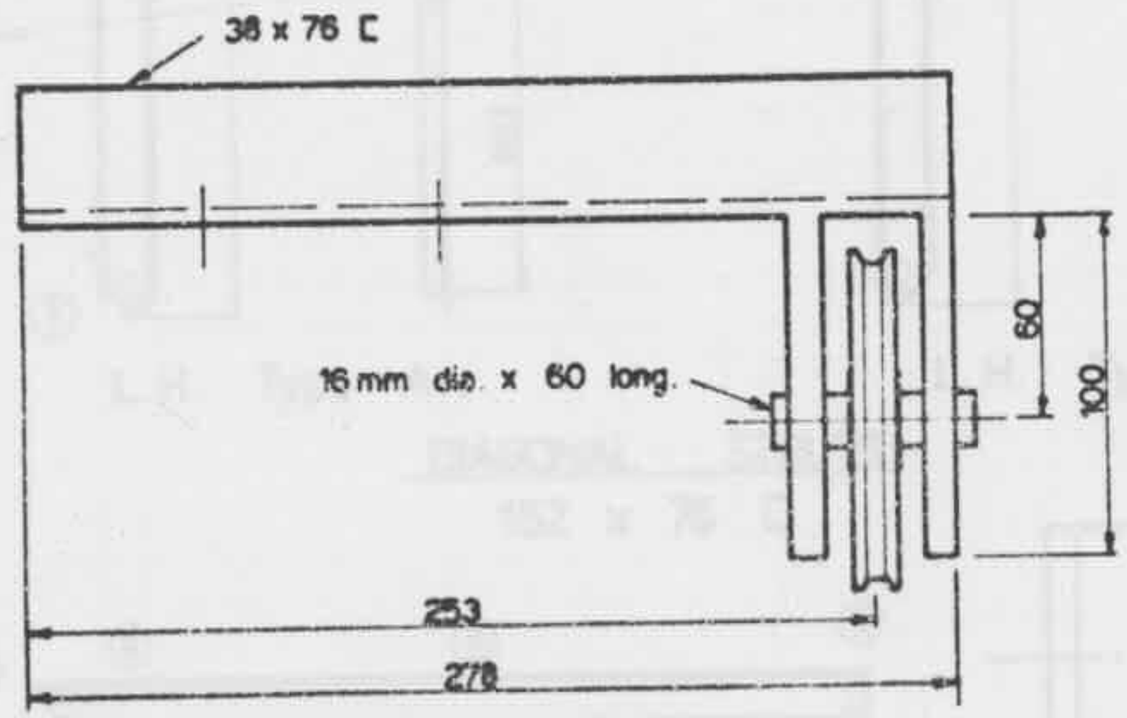

PLAN (TYPE B)

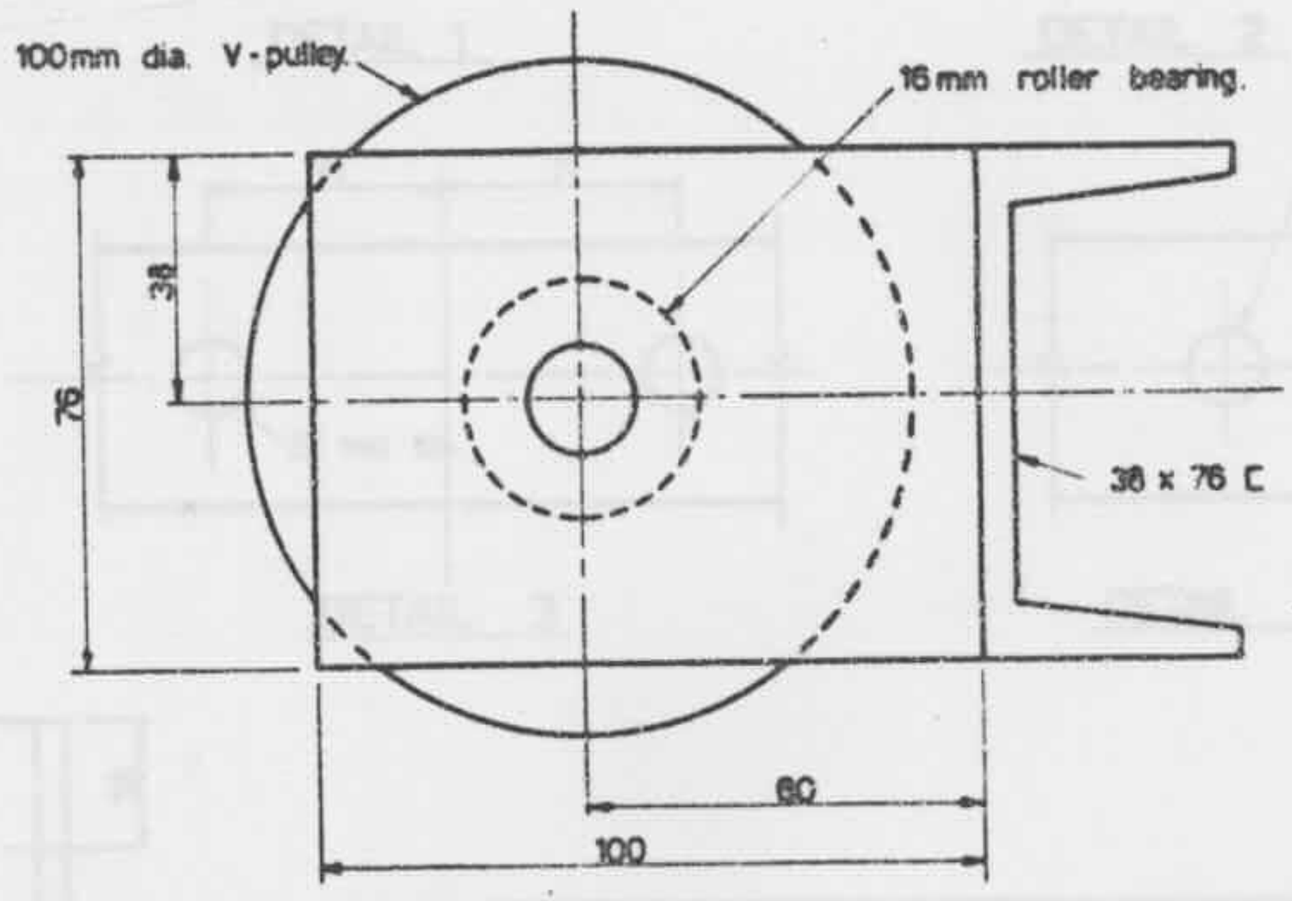

END ELEVATION

NOTE: ALL DIMENSIONS IN MM.

ITEM	DESCRIPTION	QTY.	MATL OR REF. No.	REMARKS
	TYPE B BRACKET	2		
	TYPE A BRACKET	3		

DO NOT SCALE DRAWING
EXCEPT WHERE OTHERWISE INDICATED
REMOVE BURRS & SHARP EDGES
FRACTIONAL DIMENSIONS ±
DECIMAL DIMENSIONS ±

REFERENCE DRAWINGS

DRAWN	A.H.B.	
TRACED		
CHECKED		
APPROVED		

UNIVERSITY OF SYDNEY — DEPT. CIVIL ENG

TITLE
PULLEY BRACKET
PORTAL FRAME TESTS

SCALE 1:1 . 1:2
ISSUE No. B
DRAWING No. PFT-23

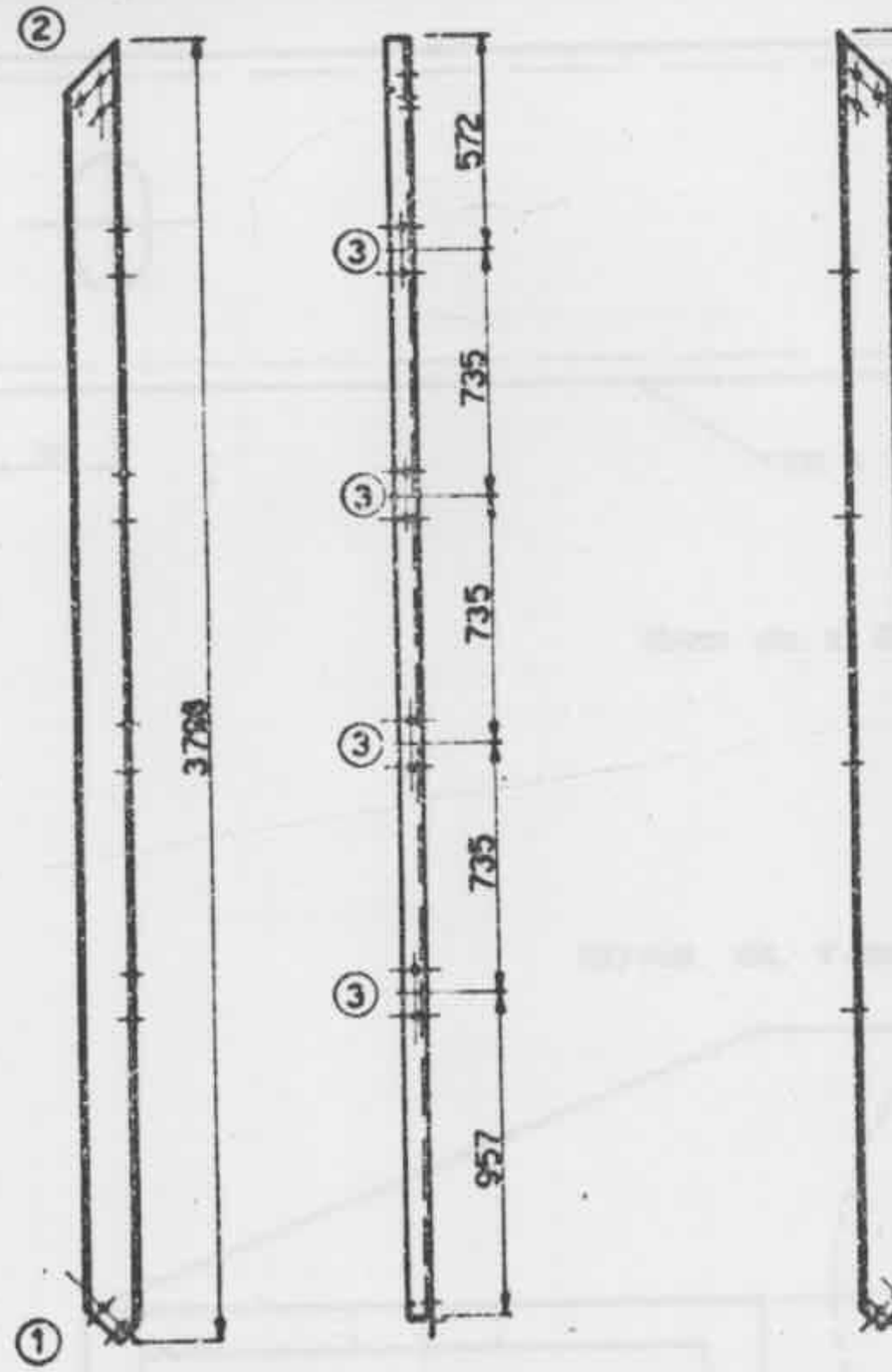

L.H. Type A

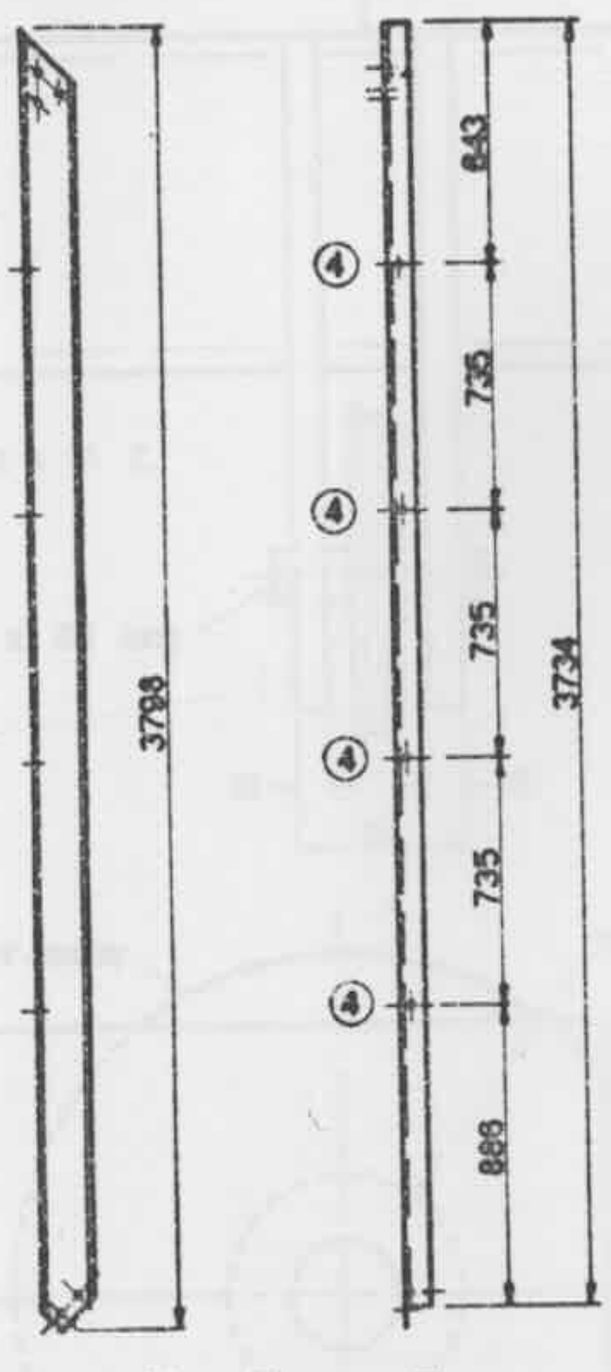

L.H. Type B

DIAGONAL STRUTS
152 x 76 C

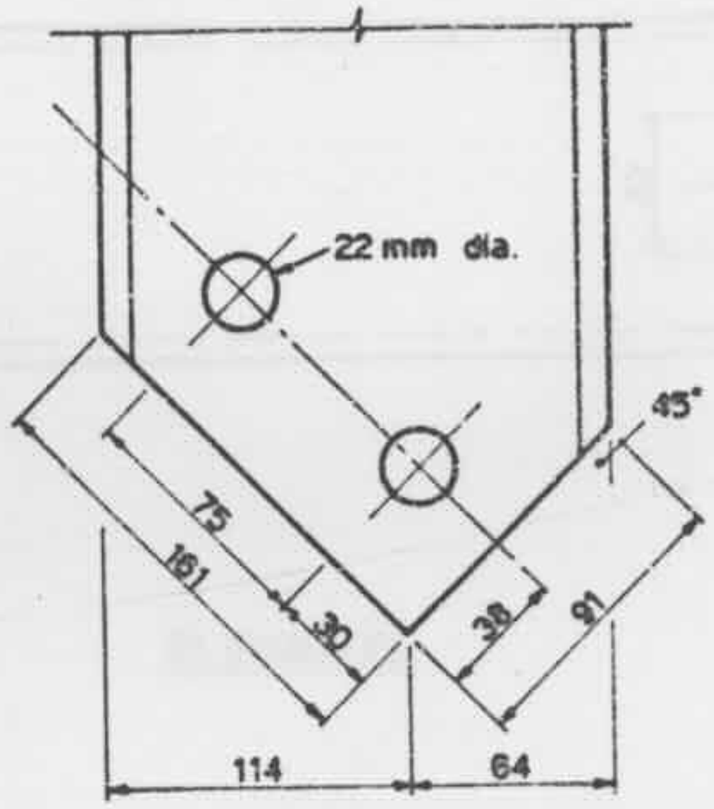

DETAIL 1

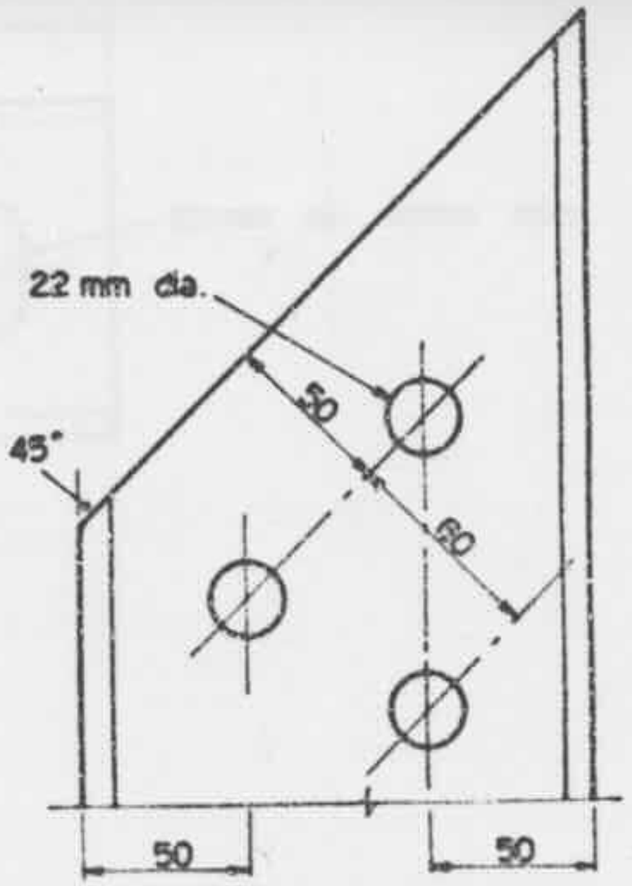

DETAIL 2

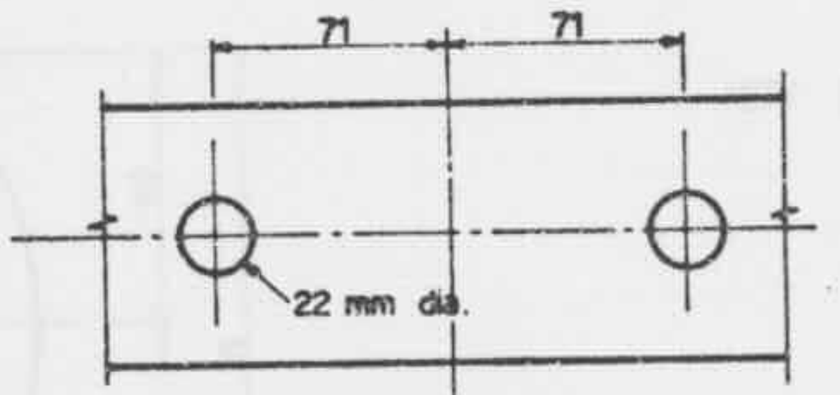

DETAIL 3

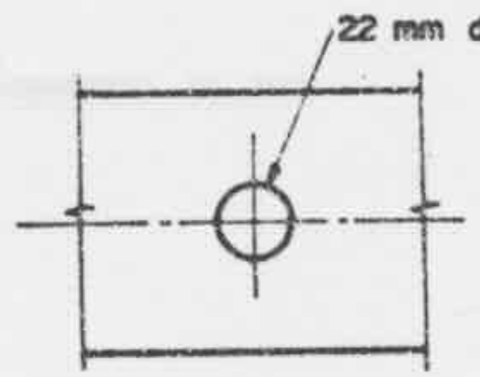

DETAIL 4

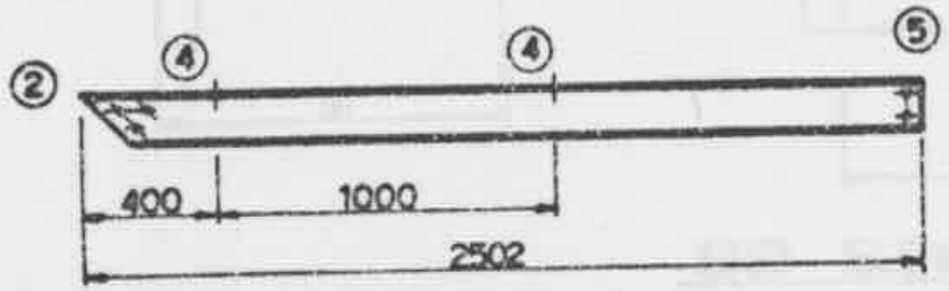

L.H. HORIZONTAL STAY
152 x 76 C

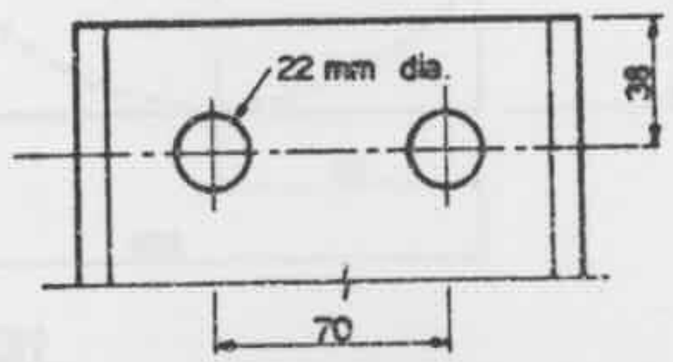

DETAIL 5

ITEM	DESCRIPTION	QTY.	MAT'L OR REF. No.	REMARKS
	R.H. STAY	2		
	L.H. STAY	2		
	R.H. TYPE B STRUT	1		
	L.H. TYPE B STRUT	1		
	R.H. TYPE A STRUT	1		
	L.H. TYPE A STRUT	1		

DO NOT SCALE DRAWING
EXCEPT WHERE OTHERWISE INDICATED
REMOVE BURRS & SHARP EDGES
FRACTIONAL DIMENSIONS ±
DECIMAL DIMENSIONS ±

REFERENCE DRAWINGS

DRAWN A.H.B
TRACED
CHECKED
APPROVED

UNIVERSITY OF SYDNEY — DEPT. CIVIL ENG

SCALE 1 : 2 . 1 : 20

TITLE
LOADING FRAME DETAILS 1
PORTAL FRAME TESTS

ISSUE No.

DRAWING No.
PFT - 24

NOTE : ALL DIMENSIONS IN MM.

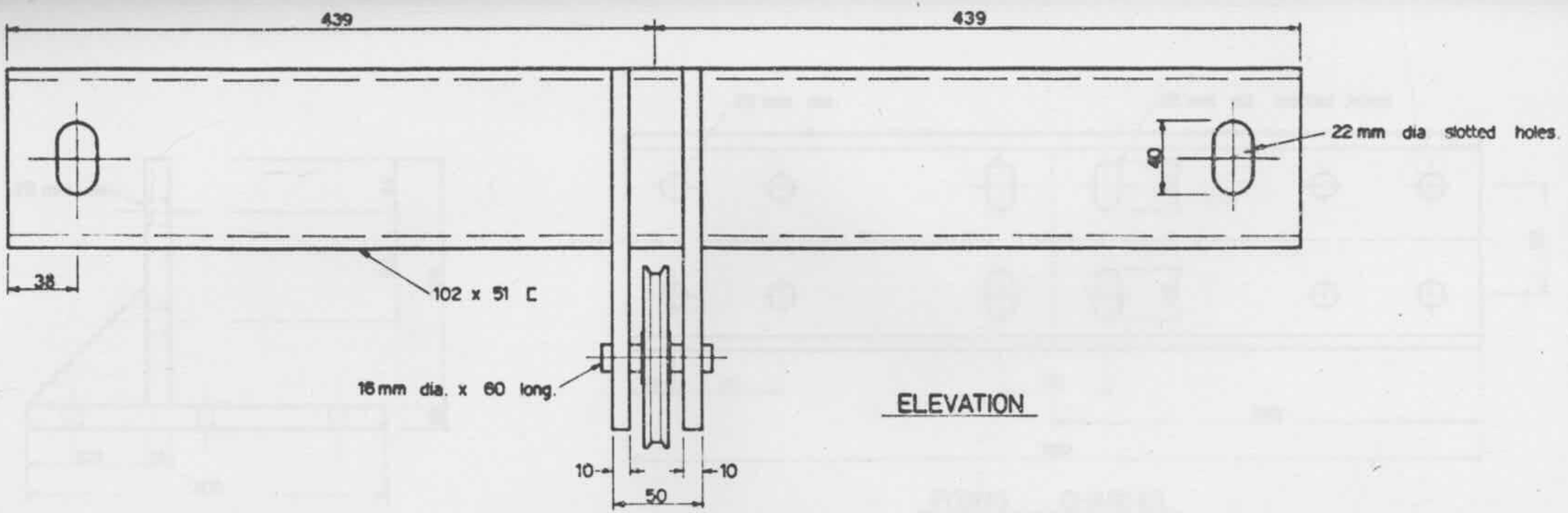

ELEVATION

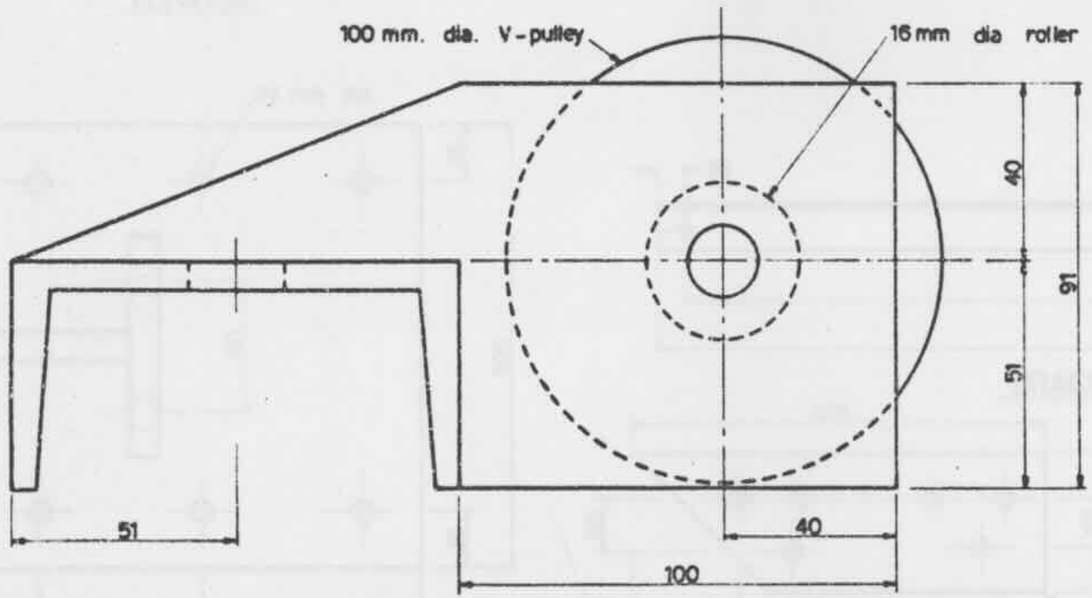

END ELEVATION

NOTE: ALL DIMENSIONS IN MM.

				PULLEY BRACKET	8		
DO NOT SCALE DRAWING	REFERENCE DRAWINGS		ITEM	DESCRIPTION	QTY.	MAT'L OR REF. No.	REMARKS
EXCEPT WHERE OTHERWISE INDICATED REMOVE BURRS & BREAK EDGES FRACTIONAL DIMENSIONS ± DECIMAL DIMENSIONS ±	DRAWN	A.N.B.	UNIVERSITY OF SYDNEY	DEPT. CIVIL ENG		SCALE 1:1 . 1:2	
	TRACED		TITLE HORIZONTAL PULLEY BRACKET PORTAL FRAME TESTS			ISSUE No. B	
	CHECKED					DRAWING No. PFT-25	
	APPROVED						

- 539 -

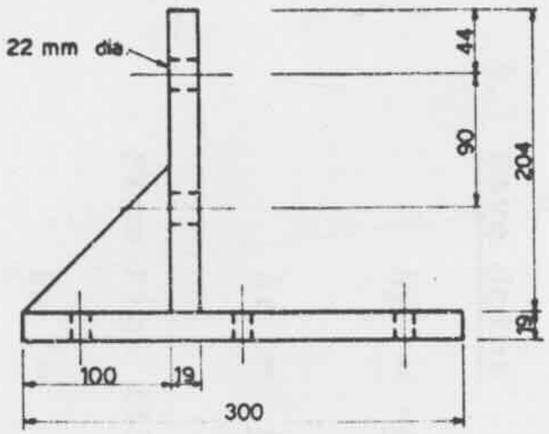

ELEVATION

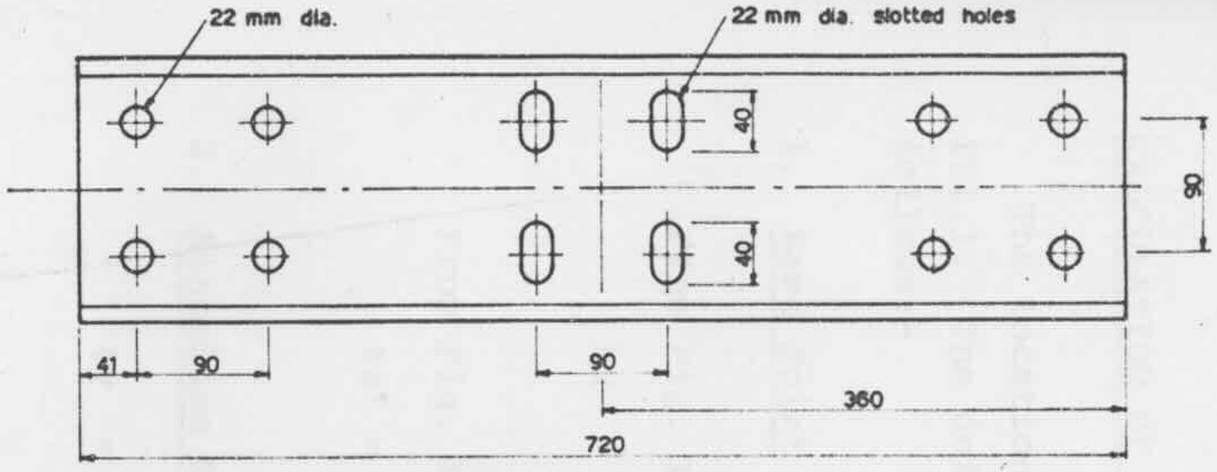

FIXING CHANNEL
178 x 76 C

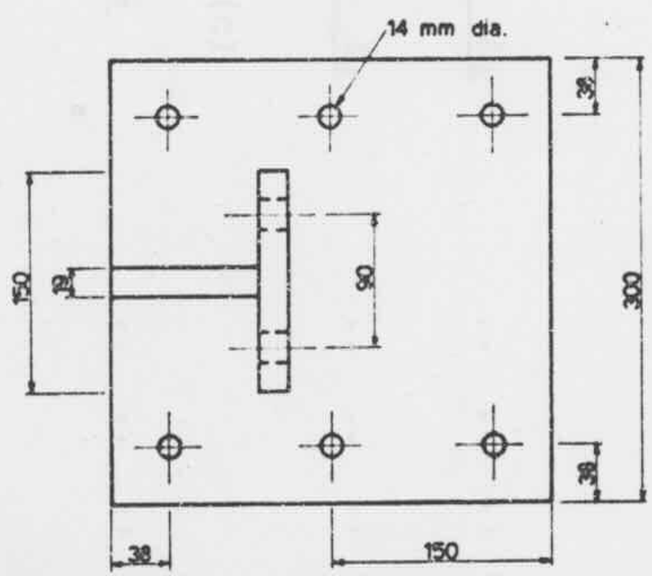

PLAN

FIXING PLATE

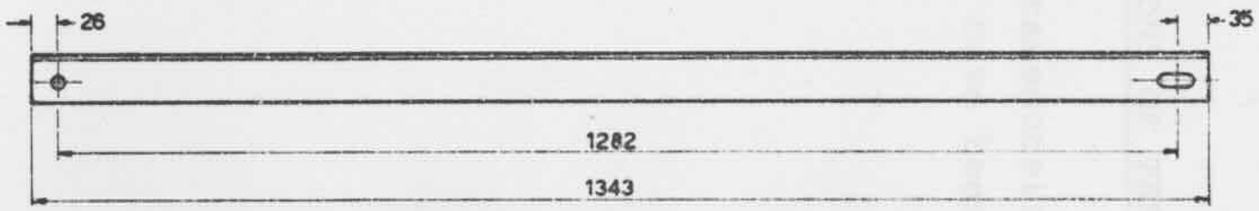

BRACING ANGLE 51 x 51 L

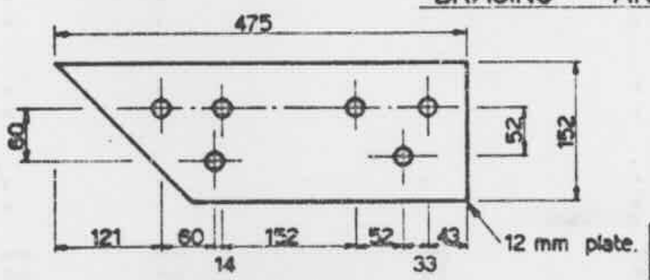

WEB PLATE

NOTE : ALL DIMENSIONS IN MM.

ITEM	DESCRIPTION	QTY.	MATL OR REF. No.	REMARKS
	WEB PLATE	4		
	BRACING ANGLE	4		
	FIXING CHANNEL	2		
	FIXING PLATE	2		

DO NOT SCALE DRAWING
EXCEPT WHERE OTHERWISE INDICATED
REMOVE BURRS & SHARP EDGES
FRACT./DIMENSIONS ±
DECIMAL DIMENSIONS ±

REFERENCE DRAWINGS

DRAWN A.H.B
TRACED
CHECKED
APPROVED

UNIVERSITY OF SYDNEY DEPT. CIVIL ENG.

SCALE 1:3 . 1:5

TITLE
LOADING FRAME DETAILS 2
PORTAL FRAME TESTS

ISSUE No. A

DRAWING No.
PFT-26

APPENDIX III -

CALCULATION OF DEFORMATIONS OF TEST FRAME

The location of the transducers is shown in Fig. III.1. The deformations have been calculated as follows:-

1. Base Joint

From Fig. III.2 (a)

$$\theta x = \frac{\Delta_1 + \Delta_2}{2b} \quad .. \quad .. \quad .. \quad (III.1)$$

From Fig. III.2 (b)

$$\theta z = \frac{-\Delta_1 + \Delta_2}{2a} \quad .. \quad .. \quad .. \quad (III.2)$$

2. Stanchion Mid-Point

$$\theta y = \frac{-\Delta_3 - \Delta_4}{2} \quad .. \quad .. \quad .. \quad (III.3)$$

$$\theta z = \frac{-\Delta_3 + \Delta_4}{a} \quad .. \quad .. \quad .. \quad (III.4)$$

3. Eave Joint

$$\Delta y = \frac{-\Delta_5 - \Delta_6}{2} \quad .. \quad .. \quad .. \quad (III.5)$$

$$\Delta z = \frac{\Delta_7 + \Delta_8}{2} \quad .. \quad .. \quad .. \quad (III.6)$$

From Fig. III.2 (c)

$$\theta x = \frac{2\Delta'_9}{d} \quad .. \quad .. \quad .. \quad (III.7)$$

where $\Delta'_9 = \Delta_9 - \Delta y$

$= \Delta_9 - \frac{\Delta_5}{2} + \frac{\Delta_6}{2}$

$$\theta y = - \frac{\Delta_7 + \Delta_8}{a} \quad .. \quad .. \quad .. \quad \text{(III.8)}$$

$$\theta z = - \frac{\Delta_5 + \Delta_6}{a} \quad .. \quad .. \quad .. \quad \text{(III.9)}$$

4. Rafter Mid-Point

$$\Delta y = - \Delta_{12} \quad .. \quad .. \quad .. \quad \text{(III.10)}$$

$$\Delta z = \frac{\Delta_{10} + \Delta_{11}}{2} \quad .. \quad .. \quad .. \quad \text{(III.11)}$$

$$\theta y = - \frac{\Delta_{10} + \Delta_{11}}{a} \quad .. \quad .. \quad .. \quad \text{(III.12)}$$

5. Apex Joint

$$\Delta y = - \Delta_{15} \quad .. \quad .. \quad .. \quad \text{(III.13)}$$

$$\Delta z = \frac{\Delta_{13} + \Delta_{14}}{2} \quad .. \quad .. \quad .. \quad \text{(III.14)}$$

$$\theta y = - \frac{\Delta_{13} + \Delta_{14}}{a} \quad .. \quad .. \quad .. \quad \text{(III.15)}$$

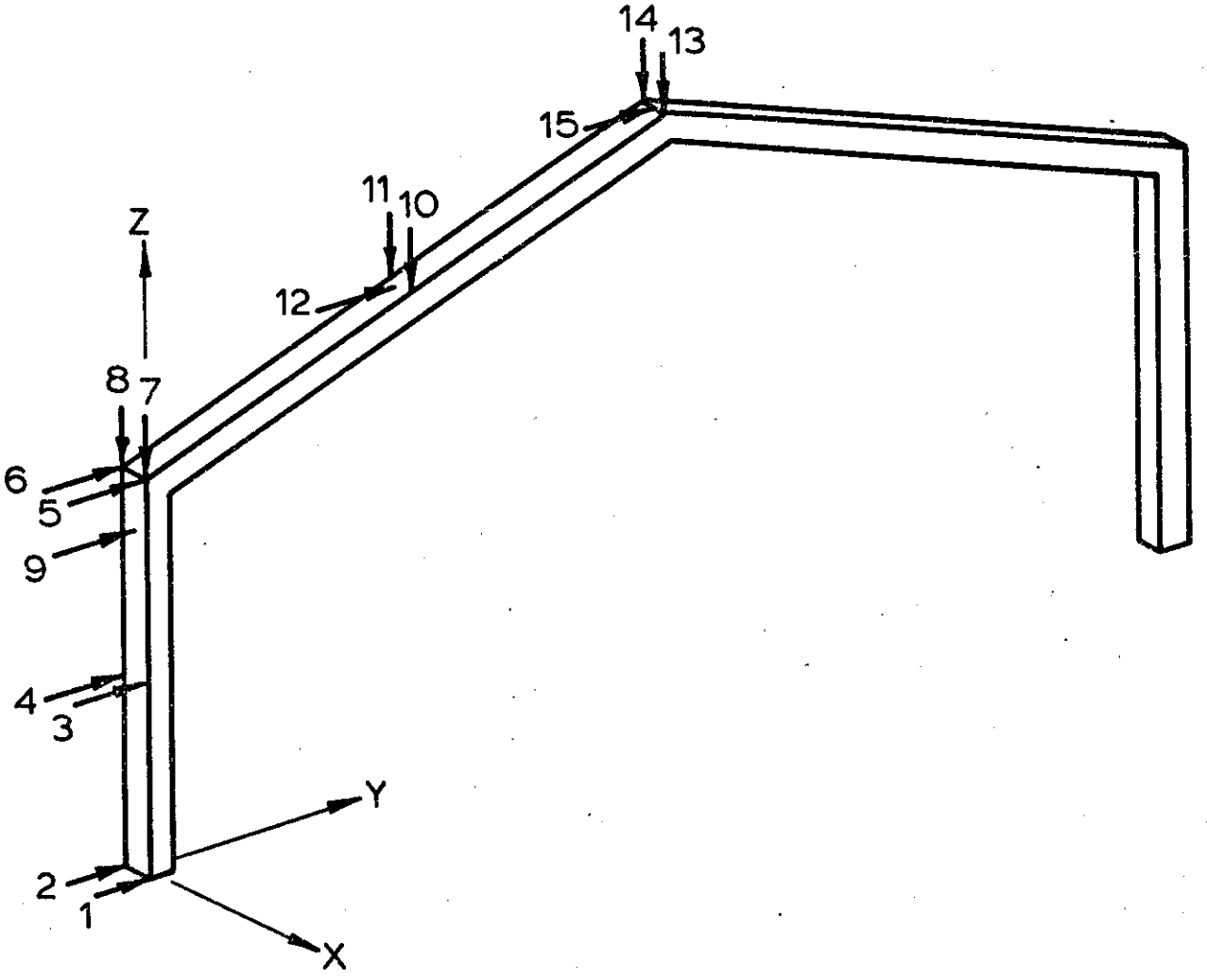

FIG. III.1 TRANSDUCER LOCATIONS

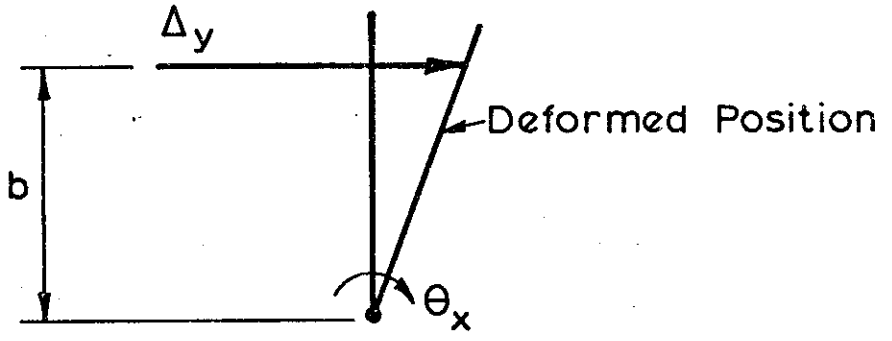

(a) Base Joint

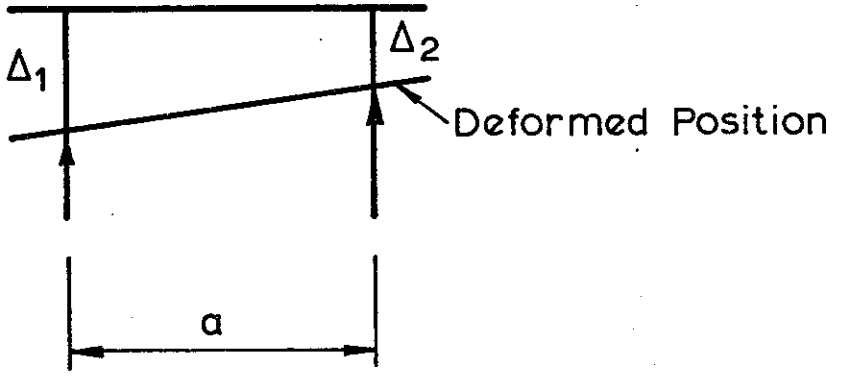

(b) Simple Translation

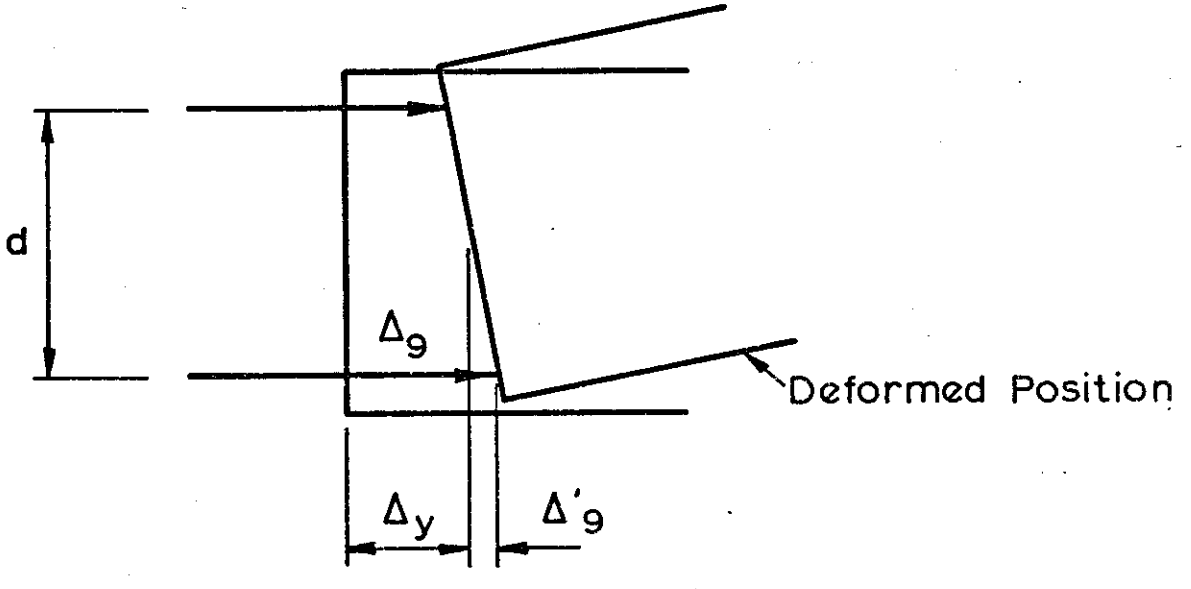

(c) Eave Joint

FIG. III.2 FRAME TRANSLATIONS

APPENDIX IV -

TENSION COUPON RESULTS

1. Tension Coupons - Lower and Static Yield Prints.

Specimen		FRAME					
		2		3		4	
		Lower Yield Point	Static Yield Point	Lower Yield Point	Static Yield Point	Lower Yield Point	Static Yield Point
1	1	332.8	318.6	339.5	335.1	343.9	336.4
	2	314.2	306.9	326.5	317.3	351.5	344.4
	3	320.1	312.2	324.5	318.8	341.6	333.5
	4	318.1	311.6	327.3	320.7	331.6	322.7
	5	329.5	321.6	320.5	316.6	334.3	327.1
	6	338.9	332.3	333.4	328.1	342.2	332.9
	7	336.8	330.2	341.8	336.0	349.1	342.4
2	1	319.3	313.9	340.7	335.4	328.2	319.7
	2	327.7	324.1	342.0	338.4	338.5	331.0
	3	330.4	328.2	341.6	335.0	333.7	327.0
	4	319.9	313.3	340.6	334.9	326.8	321.1
	5	322.9	316.1	324.2	317.2	333.8	325.4
	6	336.3	333.2	338.8	328.0	345.6	339.3
	7	333.0	326.2	324.1	314.8	346.9	341.2

TABLE 1 (a) TENSION COUPONS - LOWER AND STATIC YIELD POINTS

Specimen		FRAME 5		FRAME 6		FRAME 7	
		Lower Yield Point	Static Yield Point	Lower Yield Point	Static Yield Point	Lower Yield Point	Static Yield Point
1	1	329.0	322.1	326.4	318.5	344.3	337.2
	2	333.6	327.2	338.1	331.4	342.1	334.6
	3	326.7	320.3	326.4	319.0	332.7	323.6
	4	321.1	313.8	320.9	311.9	317.7	312.4
	5	328.8	322.4	330.9	323.5	322.9	315.9
	6	334.8	327.5	347.2	341.4	340.1	335.5
	7	341.2	334.0	340.0	333.8	330.4	320.0
2	1	340.3	331.9	323.4	317.6	336.6	331.2
	2	342.3	336.5	339.1	332.0	340.2	331.9
	3	335.9	330.2	320.9	312.7	325.2	319.4
	4	335.7	329.5	319.0	312.4	319.1	310.8
	5	330.2	323.5	326.2	319.6	317.8	310.4
	6	346.9	338.9	341.4	336.4	334.6	328.8
	7	329.0	322.3	339.4	334.5	322.8	318.6

TABLE 1 (b) TENSION COUPONS - LOWER AND STATIC YIELD POINTS

2. Tension Coupons - Young's Modulus.

Specimen		FRAME					
		2	3	4	5	6	7
		$x10^5$ MPa	$x10^5$ MPa	$x10^5$ MPa	$x10^5$ MPA	$x10^5$ MPa	$x10^5$ MPa
1	1	2.0678	2.0318	1.8934	1.8353	2.3103	1.8876
	2	2.1678	1.7865	2.4720	-	2.0817	2.2190
	3	2.0725	2.0699	2.1723	2.3754	2.3103	2.5892
	4	2.0447	2.2027	2.1009	-	2.0885	2.1688
	5	2.1670	2.2610	2.0259	2.0835	2.2925	2.4259
	6	2.2094	1.7734	1.9577	2.2594	2.1753	2.4278
	7	2.2637	2.2676	1.9630	1.9863	2.5852	2.2921
2	1	2.3469	2.1318	1.9887	2.0091	-	2.1204
	2	1.8625	2.1066	1.9265	2.2648	2.2600	1.9806
	3	2.3213	2.2204	1.9434	2.5257	2.1099	1.9701
	4	1.7292	2.1892	1.9281	1.9306	2.2721	2.1250
	5	2.1590	1.7713	1.9590	2.1163	2.2323	2.1809
	6	2.2533	1.9596	1.9818	2.4772	1.8412	2.1960
	7	1.9734	1.8048	2.2155	2.0208	2.0698	2.0958

TABLE 2 TENSION COUPONS - YOUNG'S MODULUS

APPENDIX V -

CALCULATION OF GENERALISED STRAINS AND STRESS RESULTANTS.

There are four stress resultants, which, when applied to a thin-walled section, produce longitudinal stresses. They are the moments about the x and y axes (M_x, M_y), the axial tension (P) and the bimoment (M_ω). The corresponding generalised strains are the x and y curvatures (ρ_x, ρ_y), the axial strain (ε_z) and the negative rate of change of twist ($-\phi''_z$). They can be related to the stress resultant by using Eq. (V.1)

$$\left.\begin{aligned} P &= EA.\ \varepsilon_z \\ M_x &= EIx.\ \rho_x \\ M_y &= EIy.\ \rho_y \\ M\omega &= EI\omega.\ (-\phi''_z) \end{aligned}\right\} \quad .. \quad .. \quad .. \quad (V.1)$$

From the position of the strain gauges shown in Fig. 4.7, the relative strain due to the four stress resultants can be calculated. Hence, for a particular strain gauge, the components of the generalised strain may be separated. This is represented in matrix format by:-

$$\begin{bmatrix} \varepsilon_1 \\ \varepsilon_2 \\ \varepsilon_3 \\ \varepsilon_4 \end{bmatrix} = \begin{bmatrix} -75.95 & 44.67 & 1.0 & -0.2105 \times 10^4 \\ -75.95 & -15.53 & 1.0 & 0.1772 \times 10^4 \\ 75.95 & -15.53 & 1.0 & -0.1772 \times 10^4 \\ 75.95 & 44.67 & 1.0 & 0.2105 \times 10^4 \end{bmatrix} \begin{bmatrix} \rho_x \\ \rho_y \\ \varepsilon_z \\ -\phi''_z \end{bmatrix}$$

Inverting the matrix enables the generalised strains to be calculated. Hence, the stress resultants can be calculated from Eq. (V.1).

$$\begin{Bmatrix} \rho_x \\ \rho_y \\ \varepsilon_z \\ -\phi_z'' \end{Bmatrix} = \begin{bmatrix} -0.003009 & -0.003575 & 0.003575 & 0.003009 \\ 0.008333 & -0.008333 & -0.008333 & 0.008333 \\ 0.129440 & 0.370560 & 0.370560 & 0.129440 \\ -0.000129 & 0.000129 & -0.000129 & 0.000129 \end{bmatrix} \begin{Bmatrix} \varepsilon_1 \\ \varepsilon_2 \\ \varepsilon_3 \\ \varepsilon_4 \end{Bmatrix}$$

APPENDIX VI -

CHANNEL CROSS-SECTION DIMENSIONS

The dimensions of the cross-section were measured at three locations along each member. Hence, the cross-section numbers shown in the tables below, refer to the three measured positions along the left hand stanchion and rafter and the right hand rafter and stanchion respectively.

Number	d (mm)	b_1 (mm)	b_2 (mm)	t (mm)
1	152.72	80.78	80.84	1.88
2	153.34	80.78	80.81	1.89
3	153.30	80.96	80.12	1.90
4	154.32	80.48	79.64	1.89
5	155.34	80.76	79.30	1.87
6	154.78	80.60	80.66	1.87
7	154.70	79.12	80.76	1.89
8	154.64	79.35	80.51	1.89
9	152.22	79.36	80.62	1.90
10	153.28	80.44	80.66	1.87
11	152.98	80.18	80.34	1.88
12	153.30	80.50	80.27	1.87

TABLE VI.1 FRAME 1

Number	d (mm)	b_1 (mm)	b_2 (mm)	t
1	153.46	78.18	80.58	1.88
2	152.40	78.34	80.72	1.88
3	153.46	78.64	80.16	1.84
4	153.36	80.50	79.58	1.88
5	154.60	80.70	78.90	1.89
6	153.34	80.74	78.24	1.88
7	153.82	78.68	80.68	1.87
8	154.12	78.34	80.76	1.85
9	153.82	78.46	80.60	1.84
10	154.06	78.92	80.40	1.86
11	152.44	78.46	80.80	1.88
12	152.70	78.32	80.68	1.87

TABLE VI.2 FRAME 2

Number	d (mm)	b_1 (mm)	b_2 (mm)	t (mm)
1	152.94	78.26	80.56	1.88
2	152.10	78.36	80.62	1.85
3	153.52	79.18	80.58	1.85
4	152.78	80.52	78.42	1.84
5	154.12	80.60	79.12	1.83
6	153.52	80.36	78.14	1.84
7	152.60	78.62	80.58	1.88
8	154.22	78.80	80.94	1.86
9	153.82	78.16	80.50	1.89
10	153.92	78.68	80.80	1.85
11	152.94	78.46	80.20	1.84
12	152.40	78.20	80.38	1.84

TABLE VI.3 FRAME 3

Number	d (mm)	b_1 (mm)	b_2 (mm)	t (mm)
1	152.58	81.58	78.76	1.85
2	152.60	80.38	78.54	1.85
3	153.18	80.70	78.84	1.85
4	154.80	80.88	79.80	1.85
5	154.52	80.44	78.46	1.85
6	153.48	80.40	78.56	1.85
7	153.12	78.92	81.02	1.84
8	154.54	78.30	80.42	1.86
9	155.20	78.42	81.00	1.90
10	154.40	78.62	80.22	1.84
11	152.88	78.24	80.82	1.83
12	152.56	78.66	81.48	1.83

TABLE VI.4 FRAME 4

Number	d (mm)	b_1 (mm)	b_2 (mm)	t (mm)
1	153.32	80.50	78.26	1.86
2	152.70	80.44	78.86	1.85
3	152.74	80.34	78.66	1.86
4	154.32	78.06	80.40	1.91
5	152.66	78.32	80.46	1.90
6	152.34	80.24	78.32	1.91
7	152.46	80.60	78.18	1.85
8	153.04	80.38	78.40	1.85
9	154.52	80.32	78.28	1.85
10	153.56	79.70	78.34	1.91
11	152.54	80.48	78.76	1.90
12	152.90	80.30	78.12	1.89

TABLE VI.5 FRAME 5

Number	d (mm)	b_1 (mm)	b_2 (mm)	t (mm)
1	153.21	78.69	81.00	1.87
2	152.96	78.90	80.63	1.87
3	152.87	78.96	80.59	1.86
4	153.01	80.41	79.76	1.86
5	153.62	80.47	79.23	1.86
6	152.98	80.69	79.30	1.88
7	152.20	80.91	79.30	1.88
8	152.36	80.72	79.25	1.86
9	152.89	80.48	79.42	1.86
10	153.02	80.06	79.10	1.85
11	153.61	79.99	79.23	1.86
12	153.42	80.41	79.16	1.86

TABLE VI.6 FRAME 6

Number	d (mm)	b_1 (mm)	b_2 (mm)	t (mm)
1	152.28	79.06	80.29	1.84
2	152.71	78.82	80.31	1.84
3	153.08	78.87	80.15	1.85
4	153.66	78.08	80.40	1.86
5	153.39	78.25	80.13	1.86
6	153.38	78.27	80.17	1.86
7	152.16	80.41	79.61	1.87
8	152.31	80.29	76.63	1.86
9	152.69	80.32	79.50	1.86
10	152.71	80.11	79.33	1.85
11	152.54	80.09	79.45	1.86
12	152.58	80.43	79.60	1.86

TABLE VI.7 FRAME 7

APPENDIX VII

INELASTIC CROSS-SECTION ANALYSIS

VII.1 Rigidity Matrix

The rigidity matrix [k] relates the stress resultants to the generalised strains. The relationship is given by Eq. (7.12). The rigidity matrix [k] is shown in Fig. VII.1.

VII.2 Force Transformation Matrix

The stress resultants acting upon a cross-section are generally described relative to the principal axis system x,y. When yielding of the cross-section takes place a new set of principal axes ξ, η are produced for the elastic core. The stress resultants acting relative to the original principal axis are defined as the major-axis moment (M_x), minor-axis moment (M_y), axial force (F_z) and bimoment (B_z). It is possible to transform the stress resultants acting relative to the new principal axes ξ, η to stress resultants acting relative to the original principal axes. The transformation for the axial force and moments are derived from a consideration of Fig. VII.2 and are given in Eq. (VII.1).

$$
\begin{aligned}
F_\zeta &= F_z \\
M_\xi &= -F_z \cdot b^*_\eta + M_x \cos \alpha^* + M_y \sin \alpha^* \qquad \text{(VII.1)} \\
M_\eta &= F_z \cdot b^*_\xi - M_x \sin \alpha^* + M_y \cos \alpha^*
\end{aligned}
$$

The transformation for the bioment is more complex. From Fig. VII.3, the unit warping distribution of the cross-section is given by Eq. (VII.2).

$$\alpha_{n_2} = \alpha_{n_1} + \int_1^2 \rho_o \, . \, ds \quad .. \quad .. \quad \text{(VII.2)}$$

The warping distribution is a function of $\rho_o.ds$ for the instantaneous shear centre position S. However, for the original shear centre position, S_o, the warping pattern is a function of $r_o ds$. Hence, the transformation of the warping pattern from S to S_o is given by Eq. (VII.3).

$$\alpha_{ns} = \alpha_{ns_o} + \int_1^2 (r_o - \rho_o) \, . \, ds \quad .. \quad \text{(VII.3)}$$

By replacing r_o, ρ_o and ds with expressions derived from the ξ, η axis system the resulting warping pattern is given by Eq. (VII.4).

$$\alpha_{ns} = \alpha_{ns_o} + a^*_\xi \, . \, \xi - a^*_\eta \, . \, \eta + C_o \quad .. \quad \text{(VII.4)}$$

After normalisation of both warping patterns, C_o is equal to zero.

The bimoment with respect to the principal axes x,y is obtained from Eq. (VII.5).

$$B_z = \int_A f. \, \alpha_{ns} \, ds \quad .. \quad .. \quad \text{(VII.5)}$$

where f is defined in Eq. (3.16) and α_{ns} in Eq. (VII.4). Substituting these eqations into Eq. (VII.5) produces Eq. (VII.6).

$$B_z = a^*_\xi . M_\xi + a^*_\eta . M_\eta + B_\zeta \quad .. \quad .. \quad (VII.6)$$

Substituting into this equation the expression for the new principal axis moments and force given in Eq. (VII.1)produces Eq. (VII.7).

$$B_z = -F_z.C + a^*_x . M_x + a^*_y . M_y + B_\xi \quad .. \quad (VII.7)$$

where $C = - a^*_\xi . b^*_\eta + a^*_\eta . b^*_\xi$

Rearranging Eq. (VII.7) gives Eq. (VII.8).

$$B_\zeta = F_z.C - a^*_x.M_x - a^*_y.M_y + B_z \quad .. \quad (VII.8)$$

Eq. (VII.1) and Eq. (VII.7) can be used to describe the new principal axis stress resultants in terms of the original principal axis stress resultants. The relationship in matrix notation is given in Eq. (VII.9).

$$\{W_{\xi,\eta}\} = [H] . \{W_{x,y}\} \quad .. \quad .. \quad (VII.9)$$

where [H] is given in Fig. VII.4
comparing this equation with Eq. (7.13) gives Eq. (VII.10).

$$[G^*] = [H]^{-1} \quad .. \quad .. \quad (VII.10)$$

The force transformation matrix $[G^*]$is shown in Fig. VII.5.

VII.3 Displacement Transformation Matrix

The displacement transformation matrix is simply the transpose of the force transformation matrix and is shown in Fig. VII.6.

$$\begin{bmatrix} F_\zeta \\ M_\xi \\ M_\eta \\ B_\zeta \end{bmatrix} = \begin{bmatrix} EA^* & 0 & 0 & 0 \\ 0 & EI_\xi^* & 0 & 0 \\ 0 & 0 & EI_\eta^* & 0 \\ 0 & 0 & 0 & EI_\omega^* \end{bmatrix} \cdot \begin{bmatrix} \varepsilon_\zeta \\ \rho_\xi \\ \rho_\eta \\ -\phi''_\zeta \end{bmatrix}$$

FIG. VII.1 RIGIDITY MATRIX [k]

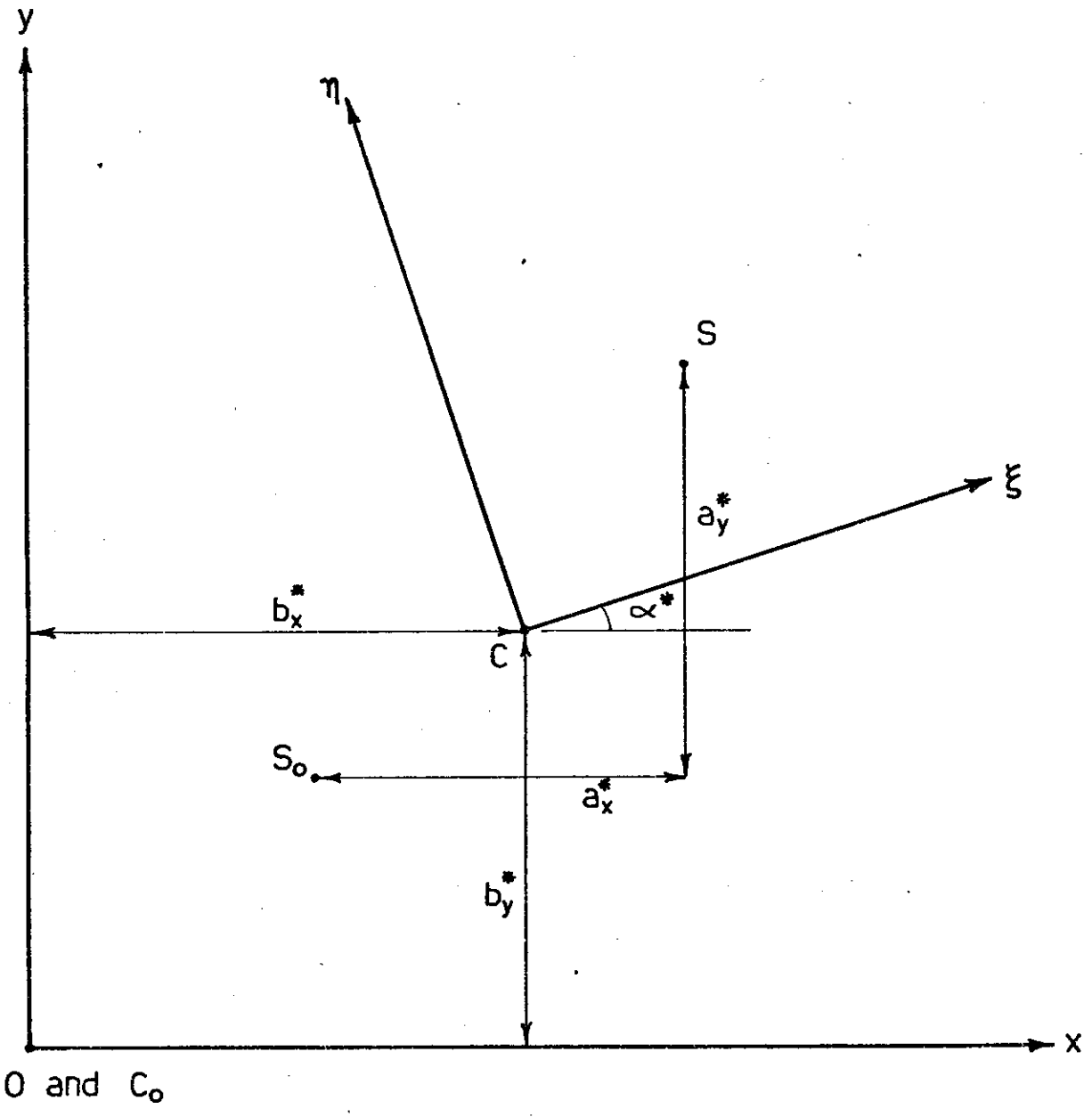

C_o , S_o = Original positions

C , S = Position after yield

FIG. VII·2 AXIS TRANSFORMATION

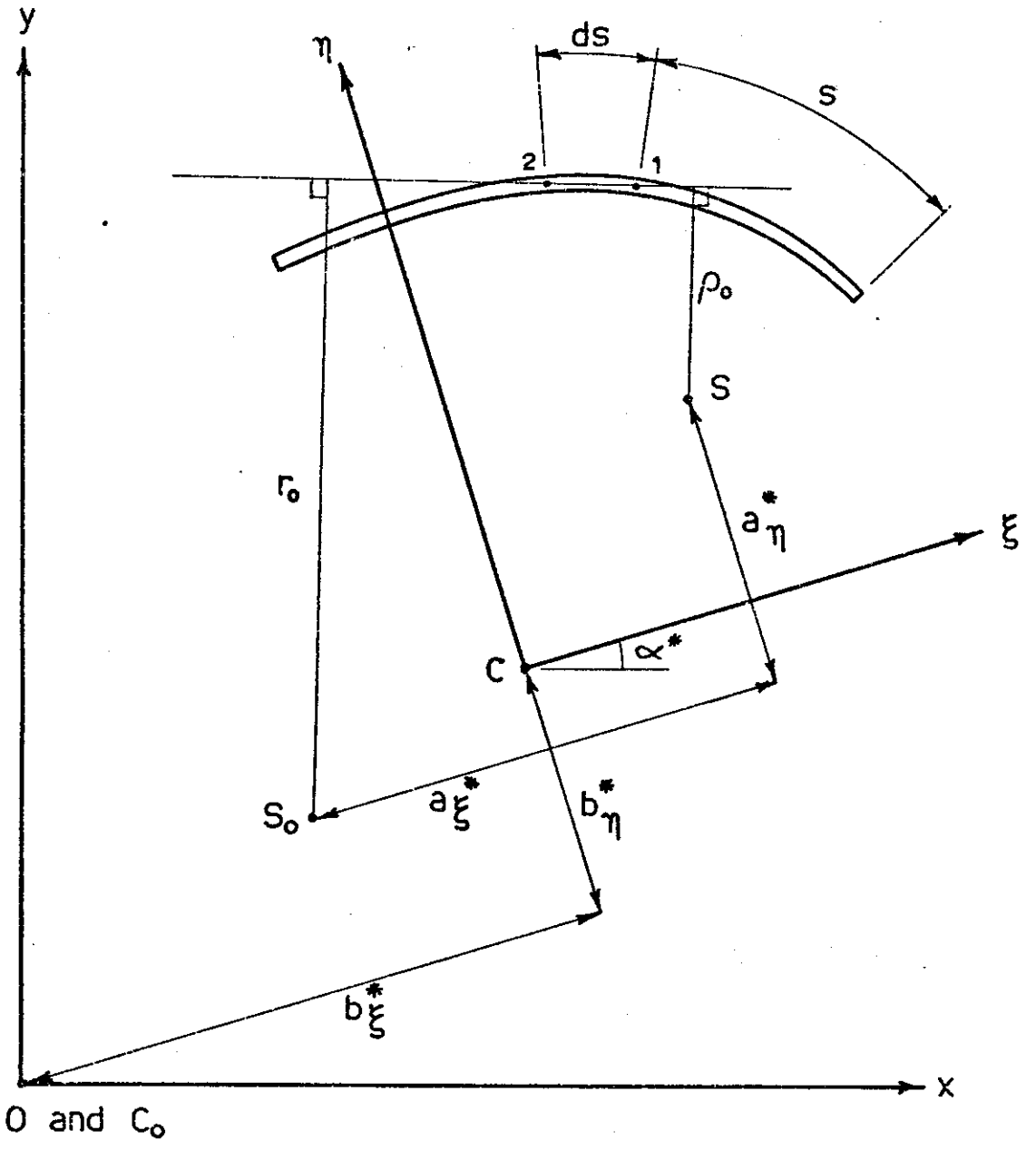

FIG. VII·3 TRANSFORMATION OF THE WARPING PATTERN

1	0	0	0
$-b_\eta^*$	$\cos\alpha^*$	$\sin\alpha^*$	0
b_ξ^*	$-\sin\alpha^*$	$\cos\alpha^*$	0
c	$-a_x^*$	$-a_y^*$	1

FIG. VII.4 MATRIX [H]

1	0	0	0
b_y^*	$\cos\alpha^*$	$-\sin\alpha^*$	0
$-b_x^*$	$\sin\alpha^*$	$\cos\alpha^*$	0
0	a_ξ^*	a_η^*	1

FIG. VII.5 FORCE TRANSFORMATION MATRIX [G*]

$$\begin{bmatrix} 1 & b_y^* & -b_x^* & 0 \\ 0 & \cos\alpha^* & \sin\alpha^* & a_\xi^* \\ 0 & -\sin\alpha^* & \cos\alpha^* & a_\eta^* \\ 0 & 0 & 0 & 1 \end{bmatrix}$$

FIG. VII.6 DISPLACEMENT TRANSFORMATION MATRIX $[G^*]^T$

APPENDIX VIII

PROGRAM LISTINGS AND SAMPLE DATA

a) Program FEETA
(Thin-walled matrix displacement analysis)

PROGRAM FEETA

THIS PROGRAM ENABLES AN ELASTIC ANALYSIS OF A GENERAL THREE-DIMENSIONAL STRUCTURAL SYSTEM. PRISMATIC OR THIN-WALLED CROSS-SECTIONS ARE PERMITTED. THE STRUCTURE MAY BE LOADED OR RESTRAINED ECCENTRICALLY WITH RESPECT TO THE FRAME AXIS SYSTEM.

DATA SPECIFICATION

1. FRAME NUMBER.

2. NUMBER OF ELEMENTS

3. JOINT COORDINATES (X,Y AND Z) AND THE CONSTRAINTS WHICH MAY BE APPLIED TO THE JOINT. THE CONSTRAINTS CONSIST OF DISPLACEMENT AND ROTATION RESTRAINTS ABOUT THE X,Y AND Z AXES AS WELL AS A WARPING RESTRAINT.

4. ELEMENT PROPERTIES. THE PROPERTIES REQUIRED IN THE ANALYSIS ARE :-

   YOUNG'S MODULUS
   SHEAR MODULUS
   CROSS-SECTIONAL AREA
   MAJOR-AXIS MOMENT OF INERTIA
   MINOR-AXIS MOMENT OF INERTIA
   TORSION CONSTANT
   WARPING CONSTANT
   ANGLE OF ROTATION OF THE ELEMENT ABOUT ITS LONGITUDINAL AXIS

   THE PROPERTIES ABOVE AND THOSE IN 5. AND 6. ARE REQUIRED FOR EACH ELEMENT IN THE STRUCTURE.

5. ECCENTRICITIES OF THE CENTROID AND SHEAR CENTRE WITH RESPECT TO THE MEMBER ORIGIN AXIS SYSTEM AND THE ANGLE OF ROTATION OF THE PRINCIPAL AXES WITH RESPECT TO THE MEMBER ORIGIN AXIS SYSTEM.

6. MEMBER PINS LOCATED AT EACH END OF THE ELEMENT. THE PINS CONSIST OF FLEXURAL PINS ABOUT THE MAJOR- AND MINOR-AXES AND A WARPING PIN.

7. NUMBER OF INCLINED RESTRAINTS. IF THE NUMBER IS SET TO ZERO , 8. IS NOT APPLICABLE.

8. INCLINED RESTRAINT JOINT NUMBER , RESTRAINT FIXITY

DIRECTIONS AND THE COSINE AND SINE OF THE RESTRAINT ANGLE.

9. NUMBER OF JOINTS ECCENTRICALLY RESTRAINED. IF THE NUMBER IS SET TO ZERO 10. IS NOT APPLICABLE.

10. JOINT NUMBER AND THE ECCENTRICITY FROM THE JOINT IN THE X,Y AND Z DIRECTIONS.

11. NUMBER OF LOADED JOINTS.

12. JOINT NUMBER AND SEVEN LOADINGS PERMISSIBLE AT THE JOINT. THE LOADINGS ARE THE FORCES ALIGNED WITH THE X,Y AND Z AXES , THE MOMENTS ABOUT THESE AXES AND A BIMOMENT. 13. MUST FOLLOW THE JOINT AND LOADING DATA FOR EACH JOINT.

13. JOINT NUMBER AND THE LOADING ECCENTRICITY FROM THE JOINT WITH RESPECT TO THE X,Y AND Z AXES. IF THE JOINT IS ECCENTRICALLY RESTRAINED THE LOADING ECCENTRICITY IS DEFINED WITH RESPECT TO THE POINT OF RESTRAINT.

14. PROGRAM EXIT (-1).

SAMPLE DATA

THE DATA FOR THE PORTAL FRAME SHOWN IN FIG. 3.16 IS GIVEN BELOW

```
1
5
0.0 0.0 0.0 0 0 0 1 1 0 1
0.0 0.0 3000.0 0 1 1 1 1 1 1
0.0 3000.0 3000.0 0 1 1 1 1 1 1
0.0 6000.0 3000.0 0 1 1 1 1 1 1
0.0 6000.0 0.0 0 0 0 1 1 0 1
2.05E5 8.2E4 7.0E2 3.0E6 6.0E5 1.0E3 3.0E9 0.0
0.0 0.0 -30.0 0.0 0.0
0 0 0 0 0 0
2.05E5 8.2E4 7.0E2 3.0E6 6.0E5 1.0E3 3.0E9 0.0
0.0 0.0 -30.0 0.0 0.0
0 0 0 0 0 0
2.05E5 8.2E4 7.0E2 3.0E6 6.0E5 1.0E3 3.0E9 0.0
0.0 0.0 -30.0 0.0 0.0
0 0 0 0 0 0
2.05E5 8.2E4 7.0E2 3.0E6 6.0E5 1.0E3 3.0E9 0.0
0.0 0.0 -30.0 0.0 0.0
0 0 0 0 0 0
2.05E5 8.2E4 7.0E2 3.0E6 6.0E5 1.0E3 3.0E9 0.0
0.0 0.0 -30.0 0.0 0.0
0 0 0 0 0 0
0
0
2
3 0.0 3000.0 0.0 0.0 0.0 0.0 0.0
3 0.0 0.0 0.0
5 0.0 0.0 -6000.0 0.0 0.0 0.0 0.0
5 0.0 0.0 0.0
-1
```

```
C       PROGRAM FEETA
C
C       ELASTIC ANALYSIS OF 3D FRAMES OF GENERAL MEMBER SECTION GEOMETRY
C
C
C       SPECIFICATION OF ARRAY SIZES
C
      COMMON S(8,8),SDAT(200),AA(7,8),AB(7,8),SAT(8,7),
     +   ASAT(200,15),JTYPE(25,7),JNTDF(25),SKLOAD(7),
     +   SLOAD(175),SJLOAD(25,7),CORD(25,3),SR(200),
     +   AI(7,14),BTAI(7,7),B(7,7),SDATA(125),
     +   CALPHA(24,3),SALPHA(24,3),TT(3,3),TEM(3,6),
     +   DA(25,7),PIN(24,2,3),D(7),DEG(24),DE(7),
     +   IRJN(24),IRCN(24,2),COSIR(24),SINIR(24),
     +   ECC(25,3),ER(7,7),AAE(7,8),ABE(7,8)
C
      INTEGER PIN
      REAL NUM
C
C       INPUT THE FRAME NO.  EXIT IF NEGATIVE
C
   10 READ(5,*)JJ
   20 FORMAT(I5)
      IF(JJ) 30,40,40
   30 CONTINUE
      STOP
C
C       READ ELEMENT COUNT
C
   40 READ(5,*)NM
   50 FORMAT(I5)
      JCT=NM+1
C
C       READ JOINT COORDS AND TYPE OF DEFORMATION
C
      DO 200 N1=1,JCT
  200 READ(5,*)(CORD(N1,N2),N2=1,3),(JTYPE(N1,N2),N2=1,7)
  205 FORMAT(3F10.3,7I5)
C
C       READ ELEMENT PROPERTIES
C
      DO 210 N1=1,NM
      N2=8*N1-7
      N3=N2+6
      N5=5*N1-4
      N6=N5+4
      READ(5,*)(SDAT(N4),N4=N2,N3),ALPHA
      READ(5,*)(SDATA(N4),N4=N5,N6)
      READ(5,*)(PIN(N1,1,N4),N4=1,3),(PIN(N1,2,N4),N4=1,3)
  212 FORMAT(6I5)
```

```
      CALPHA(N1,3)=COS(3.1415926*ALPHA/180.0)
      SALPHA(N1,3)=SIN(3.1415926*ALPHA/180.0)
      DEG(N1)=SDATA(5*N1)/57.296
      TEMP=SDATA(5*N1-2)
      SDATA(5*N1-2)=SDATA(5*N1-2)*COS(DEG(N1))+SDATA(5*N1-1)
     +    *SIN(DEG(N1))
      SDATA(5*N1-1)=-TEMP*SIN(DEG(N1))+SDATA(5*N1-1)*COS(DEG(N1))
  210 CONTINUE
  215 FORMAT(7E10.3,F10.3)
  214 FORMAT(5F10.5)
C
C       READ INCLINED RESTRAINT DATA
C
      READ(5,*)IR
  216 FORMAT(I5)
      IF(IR) 213,213,221
  221 DO 217 N1=1,IR
  217 READ(5,*)IRJN(N1),IRCN(N1,1),IRCN(N1,2),COSIR(N1),SINIR(N1)
  218 FORMAT(3I5,2F10.8)
C
C       READ ECCENTRIC RESTRAINT DATA
C
  213 READ(5,*) NJER
  222 FORMAT(I5)
      IF(NJER) 219,219,223
  223 DO 226 N1=1,JCT
      DO 226 N2=1,3
  226 ECC(N1,N2)=0.0
      DO 228 N1=1,NJER
  228 READ(5,*) NNUM,(ECC(NNUM,N2),N2=1,3)
  229 FORMAT(I5,3F10.7)
C
C       CALCULATE DEGREES OF FREEDOM
C
  219 L=0
      DO 220 N1=1,JCT
      DO 220 N2=1,7
  220 L=L+JTYPE(N1,N2)
C
      KJ=L+1
C
C       CALCULATE MEMBER LENGTHS AND ORIENTATIONS
C
      DO 230 N1=1,NM
      OLX=CORD(N1+1,1)-CORD(N1,1)
      OLY=CORD(N1+1,2)-CORD(N1,2)
      OLZ=CORD(N1+1,3)-CORD(N1,3)
      SDAT(8*N1)=SQRT((OLX*OLX)+(OLY*OLY)+(OLZ*OLZ))
      OL1=SQRT((OLZ*OLZ)+(OLY*OLY))
      CALPHA(N1,2)=OL1/SDAT(8*N1)
```

```
      SALPHA(N1,2)=OLX/SDAT(8*N1)
C
      IF(OL1) 225,227,225
C
  225 CALPHA(N1,1)=OLZ/OL1
      SALPHA(N1,1)=OLY/OL1
      GO TO 230
  227 CALPHA(N1,1)=1.0
      SALPHA(N1,1)=0.0
  230 CONTINUE
C
C     PRINT GENERAL HEADINGS AND DATA FOR VERIFICATION
C
      WRITE(6,300) JJ
  300 FORMAT(30H ELASTIC ANALYSIS OF FRAME NO.,I5,1X,
     +  19HUSING PROGRAM FEETA)
      WRITE(6,301) NM
  301 FORMAT(/19H NUMBER OF ELEMENTS,I5)
      WRITE(6,303)
  303 FORMAT(/19H ELEMENT PROPERTIES)
      WRITE(6,302)
  302 FORMAT(/* ELEMENT    MOD E      MOD G      AREA        IXX*,
     +  *         IYY         J         IWW      LENGTH*)
      DO 305 N1=1,NM
      NN1=8*(N1-1)+1
      NN2=8*(N1-1)+8
      WRITE(6,304) N1,(SDAT(N2),N2=NN1,NN2)
  304 FORMAT(I5,3X,7E10.3,F10.3)
  305 CONTINUE
      WRITE(6,319)
  319 FORMAT(///' CENTROIDAL AND SHEAR AXIS ECCENTRICITIES')
      WRITE(6,320)
  320 FORMAT(/* ELEMENT     BX          BY          AX          AY*,
     +  *          ALPHA*)
      DO 321 N1=1,NM
      NN1=5*(N1-1)+1
      NN2=5*(N1-1)+5
      WRITE(6,322) N1,(SDATA(N2),N2=NN1,NN2)
  322 FORMAT(I5,2X,5F10.3)
  321 CONTINUE
C
      WRITE(6,316)
  316 FORMAT(///' ELEMENT ORIENTATIONS')
      WRITE(6,306)
  306 FORMAT(/* ELEMENT  COS ALPHAX   SIN ALPHAX   COS ALPHAY   SIN *,
     +  *ALPHAY   COS ALPHAZ   SIN ALPHAZ*)
      DO 307 N1=1,NM
      WRITE(6,308) N1,CALPHA(N1,1),SALPHA(N1,1),CALPHA(N1,2),
     +  SALPHA(N1,2),CALPHA(N1,3),SALPHA(N1,3)
  307 CONTINUE
```

```
  308 FORMAT(I5,1X,6F13.6)
C
      WRITE(6,311) JCT
  311 FORMAT(///17H NUMBER OF JOINTS,I5)
      WRITE(6,312)
  312 FORMAT(//* JOINT     X CORD    Y CORD    Z CORD      DEGREES OF*,
     +  * FREEDOM=1 CONSTRAINTS=0*)
      WRITE(6,313)
  313 FORMAT(/*                                              XD    YD    ZD*,
     +  *    XR    YR    ZR  WARP*)
      DO 315 N1=1,JCT
  315 WRITE(6,314) N1,(CORD(N1,N7),N7=1,3),(JTYPE(N1,N2),N2=1,7)
  314 FORMAT(I5,2X,3F9.1,2X,7I5)
      WRITE(6,380)
  380 FORMAT(//24H LOCATION OF MEMBER PINS)
      WRITE(6,381)
  381 FORMAT(/43H          PINS AT L.H. END  PINS AT R.H. END)
      WRITE(6,382)
  382 FORMAT(/42H ELEMENT   XP1  YP1  WP1      XP2  YP2  WP2)
      DO 384 I=1,NM
      WRITE(6,383) I,(PIN(I,1,J),J=1,3),(PIN(I,2,J),J=1,3)
  383 FORMAT(I5,3X,3I5,3X,3I5)
  384 CONTINUE
      IF(IR) 334,334,324
  324 WRITE(6,325)
  325 FORMAT(///20H INCLINED RESTRAINTS)
      WRITE(6,326)
  326 FORMAT(/50H   IRJN      IRCN1     IRCN2    COSIR     SINIR   )
      DO 327 N1=1,IR
      WRITE(6,218) IRJN(N1),IRCN(N1,1),IRCN(N1,2),COSIR(N1),SINIR(N1)
  327 CONTINUE
  334 IF(NJER) 323,323,335
  335 WRITE(6,336)
  336 FORMAT(///25H RESTRAINT ECCENTRICITIES)
      WRITE(6,337)
  337 FORMAT(/32H JOINT     X          Y          Z)
      DO 338 I=1,JCT
  338 WRITE(6,339) I,(ECC(I,J),J=1,3)
  339 FORMAT(I4,3F10.2)
  323 CONTINUE
C
C       READ LOAD SET DATA
C
      READ(5,*)NLJ
  245 FORMAT(I5)
      DO 247 N1=1,25
      DO 247 N2=1,7
  247 SJLOAD(N1,N2)=0.0
      DO 248 N1=1,25
      DO 248 N2=1,3
```

```
248 DA(N1,N2)=0.0
    WRITE(6,235)
235 FORMAT(///10H LOAD DATA)
    WRITE(6,237)
237 FORMAT(/* JOINT  X FORCE    Y FORCE    Z FORCE     X MOM     Y MOM *,
   + *    Z MOM    BIMOMENT*)
    DO 270 N1=1,NLJ
    READ(5,*) NNUM,(SJLOAD(NNUM,N2),N2=1,7)
255 FORMAT(I5,7F10.7)
270 READ(5,*) NNUM,(DA(NNUM,N2),N2=1,3)
256 FORMAT(I5,3F10.7)
    DO 271 N1=1,JCT
271 WRITE(6,257) N1,(SJLOAD(N1,N2),N2=1,7)
257 FORMAT(I5,F8.1,2F10.1,F11.1,3F9.1)
    WRITE(6,330)
330 FORMAT(///20H LOAD ECCENTRICITIES)
    WRITE(6,331)
331 FORMAT(/' JOINT      DX         DY         DZ')
    DO 332 N1=1,JCT
332 WRITE(6,333) N1,(DA(N1,N2),N2=1,3)
333 FORMAT(I5,3F10.2)
C
    GOTO 241
240 CONTINUE
    GO TO 10
241 CONTINUE
    NFLAG = 0
C
C       ADJUST LOAD VECTOR FOR ECCENTRIC LOADS
C
    LL=0
    DO 273 N1=1,JCT
    SKLOAD(1)=SJLOAD(N1,1)
    SKLOAD(2)=SJLOAD(N1,2)
    SKLOAD(3)=SJLOAD(N1,3)
    SKLOAD(4)=SJLOAD(N1,4)-SJLOAD(N1,2)*DA(N1,3)+SJLOAD(N1,3)*DA(N1,2)
    SKLOAD(5)=SJLOAD(N1,5)+SJLOAD(N1,1)*DA(N1,3)-SJLOAD(N1,3)*DA(N1,1)
    SKLOAD(6)=SJLOAD(N1,6)-SJLOAD(N1,1)*DA(N1,2)+SJLOAD(N1,2)*DA(N1,1)
C
C       COMPACT LOADS FOR FIXED DEGREES OF FREEDOM
C
    DO 273 N3=1,7
    IF(JTYPE(N1,N3)) 273,273,264
264 LL=LL+1
    SLOAD(LL)=SKLOAD(N3)
273 CONTINUE
C
C       GENERATE THE FRAME STATICS MATRIX FOR THE ITH MEMBER
C
417 DO 416 N1=1,NM
```

```
      DO 416 N2=1,8
      N3=8*(N1-1)+N2
  416 SR(N3)=0.0
      DO 410 N1=1,L
      DO 410 N2=1,15
  410 ASAT(N1,N2)=0.0
  420 CONTINUE
      I=0
      KK=1
      JNTDFT=0
  430 CONTINUE
      I=I+1
C
      DO 440 N1=1,7
      DO 440 N2=1,8
      AA(N1,N2)=0.0
  440 AB(N1,N2)=0.0
C
      TT(1,1)=CALPHA(I,2)*CALPHA(I,3)
      TT(1,2)=-CALPHA(I,2)*SALPHA(I,3)
      TT(1,3)=SALPHA(I,2)
      TT(2,1)=-SALPHA(I,1)*SALPHA(I,2)*CALPHA(I,3)
     +  +CALPHA(I,1)*SALPHA(I,3)
      TT(2,2)=CALPHA(I,1)*CALPHA(I,3)
     +  +SALPHA(I,1)*SALPHA(I,2)*SALPHA(I,3)
      TT(2,3)=SALPHA(I,1)*CALPHA(I,2)
      TT(3,1)=-CALPHA(I,1)*SALPHA(I,2)*CALPHA(I,3)
     +  -SALPHA(I,3)*SALPHA(I,1)
      TT(3,2)=-SALPHA(I,1)*CALPHA(I,3 )
     +  +CALPHA(I,1)*SALPHA(I,2)*SALPHA(I,3)
      TT(3,3)=CALPHA(I,1)*CALPHA(I,2)
C
      TEM(1,1)=0.0
      TEM(1,2)=SIN(DEG(I))/SDAT(8*I)
      TEM(1,3)=TEM(1,2)
      TEM(1,4)=COS(DEG(I))/SDAT(8*I)
      TEM(1,5)=TEM(1,4)
      TEM(1,6)=0.0
      TEM(2,1)=0.0
      TEM(2,2)=-TEM(1,4)
      TEM(2,3)=TEM(2,2)
      TEM(2,4)=TEM(1,2)
      TEM(2,5)=TEM(2,4)
      TEM(2,6)=0.0
      TEM(3,1)=-1.0
      TEM(3,2)=0.0
      TEM(3,3)=TEM(3,2)
      TEM(3,4)=0.0
      TEM(3,5)=TEM(3,4)
      TEM(3,6)=0.0
```

```
C
      DO 460 N1=1,3
      DO 460 N2=1,6
      DO 460 N3=1,3
  460 AA(N1,N2)=AA(N1,N2)+TT(N1,N3)*TEM(N3,N2)
      DO 461 N1=1,3
      DO 461 N2=1,6
  461 AB(N1,N2)=-AA(N1,N2)
C
      TEM(1,1)=-SDATA(5*I-3)
      TEM(1,2)=COS(DEG(I))
      TEM(1,3)=0.0
      TEM(1,4)=-SIN(DEG(I))
      TEM(1,5)=0.0
      TEM(1,6)=0.0
      TEM(2,1)=SDATA(5*I-4)
      TEM(2,2)=SIN(DEG(I))
      TEM(2,3)=0.0
      TEM(2,4)=COS(DEG(I))
      TEM(2,5)=0.0
      TEM(2,6)=0.0
      TEM(3,1)=0.0
      TEM(3,2)=-SDATA(5*I-2)/SDAT(8*I)
      TEM(3,3)=TEM(3,2)
      TEM(3,4)=-SDATA(5*I-1)/SDAT(8*I)
      TEM(3,5)=TEM(3,4)
      TEM(3,6)=-1.0
C
      DO 470 N1=1,3
      DO 470 N2=1,6
      DO 470 N3=1,3
      NN1=N1+3
  470 AA(NN1,N2)=AA(NN1,N2)+TT(N1,N3)*TEM(N3,N2)
C
      AA(7,2)=SDATA(5*I-2)
      AA(7,4)=SDATA(5*I-1)
      AA(7,7)=1.0
C
C       BUILD ECCENTRIC RESTRAINT MATRIX AND MODIFY
C       STATICS MATRIX FOR END A
C
      IF(NJER) 479,479,431
  431 IF(ECC(KK,1)) 442,432,442
  432 IF(ECC(KK,2)) 442,433,442
  433 IF(ECC(KK,3)) 442,479,442
  442 DO 444 N1=1,7
      DO 444 N2=1,7
  444 ER(N1,N2)=0.0
      DO 446 N1=1,7
      ER(N1,N1)=1.0
```

```
  446 CONTINUE
C
      ER(1,5)=-ECC(KK,3)
      ER(1,6)=ECC(KK,2)
      ER(2,4)=ECC(KK,3)
      ER(2,6)=-ECC(KK,1)
      ER(3,4)=-ECC(KK,2)
      ER(3,5)=ECC(KK,1)
C
      DO 474 N1=1,7
      DO 474 N2=1,8
      AAE(N1,N2)=0.0
      DO 474 N3=1,7
      AAE(N1,N2)=AAE(N1,N2)+ER(N3,N1)*AA(N3,N2)
  474 CONTINUE
      DO 4760 II=1,7
      DO 4760 JJ=1,8
      AA(II,JJ)=AAE(II,JJ)
 4760 CONTINUE
C
  479 TEM(1,1)=SDATA(5*I-3)
      TEM(1,2)=0.0
      TEM(1,3)=COS(DEG(I))
      TEM(1,4)=0.0
      TEM(1,5)=-SIN(DEG(I))
      TEM(1,6)=0.0
      TEM(2,1)=-SDATA(5*I-4)
      TEM(2,2)=0.0
      TEM(2,3)=SIN(DEG(I))
      TEM(2,4)=0.0
      TEM(2,5)=COS(DEG(I))
      TEM(2,6)=0.0
      TEM(3,1)=0.0
      TEM(3,2)=SDATA(5*I-2)/SDAT(8*I)
      TEM(3,3)=TEM(3,2)
      TEM(3,4)=SDATA(5*I-1)/SDAT(8*I)
      TEM(3,5)=TEM(3,4)
      TEM(3,6)=1.0
C
      DO 490 N1=1,3
      DO 490 N2=1,6
      DO 490 N3=1,3
      NN1=N1+3
  490 AB(NN1,N2)=AB(NN1,N2)+TT(N1,N3)*TEM(N3,N2)
C
      AB(7,3)=SDATA(5*I-2)
      AB(7,5)=SDATA(5*I-1)
      AB(7,8)=1.0
C
C       BUILD ECCENTRIC RESTRAINT MATRIX AND MODIFY
```

```
C       STATICS MATRIX FOR END B
C
      IF(NJER) 488,488,476
  476 KK=KK+1
      IF(ECC(KK,1)) 456,452,456
  452 IF(ECC(KK,2)) 456,454,456
  454 IF(ECC(KK,3)) 456,488,456
  456 DO 458 N1=1,7
      DO 458 N2=1,7
  458 ER(N1,N2)=0.0
      DO 462 N1=1,7
      ER(N1,N1)=1.0
  462 CONTINUE
C
      ER(1,5)=-ECC(KK,3)
      ER(1,6)=ECC(KK,2)
      ER(2,4)=ECC(KK,3)
      ER(2,6)=-ECC(KK,1)
      ER(3,4)=-ECC(KK,2)
      ER(3,5)=ECC(KK,1)
C
      DO 482 N1=1,7
      DO 482 N2=1,8
      ABE(N1,N2)=0.0
      DO 482 N3=1,7
  482 ABE(N1,N2)=ABE(N1,N2)+ER(N3,N1)*AB(N3,N2)
      DO 484 II=1,7
      DO 484 JJ=1,8
      AB(II,JJ)=ABE(II,JJ)
  484 CONTINUE
C
C       REDUCTION OF STATICS MATRIX FOR CONSTRAINTS AT END A
C
  488 IF(IR) 1491,1491,489
  489 DO 491 N1=1,IR
      IF(IRJN(N1)-I) 491,492,491
  492 N2=IRCN(N1,1)
      N3=IRCN(N1,2)
      DO 493 N4=1,8
  493 AA(N2,N4)=AA(N2,N4)*COSIR(N1)+AA(N3,N4)*SINIR(N1)
  491 CONTINUE
 1491 CONTINUE
C
      N1=0
      DO 510 N2=1,7
      IF(JTYPE(I,N2))510,510,500
  500 N1=N1+1
      DO 505 N3=1,8
  505 AA(N1,N3)=AA(N2,N3)
  510 CONTINUE
```

```
C
      JNTDF(I)=N1
C
C       REDUCTION OF STATICS MATRIX FOR CONSTRAINTS AT END B
C
      IF(IR) 1521,1521,519
  519 DO 521 N1=1,IR
      IF(IRJN(N1)-I-1) 521,522,521
  522 N2=IRCN(N1,1)
      N3=IRCN(N1,2)
      DO 523 N4=1,8
  523 AB(N2,N4)=AB(N2,N4)*COSIR(N1)+AB(N3,N4)*SINIR(N1)
  521 CONTINUE
 1521 CONTINUE
C
      N1=0
C
      DO 560 N2=1,7
      IF(JTYPE(I+1,N2)) 560,560,550
  550 N1=N1+1
      DO 555 N3=1,8
  555 AB(N1,N3)=AB(N2,N3)
  560 CONTINUE
C
      JNTDF(I+1)=N1
C
C       BUILD THE MEMBER STIFFNESS MATRIX FOR ITH MEMBER
C
      DO 600 N1=1,8
      DO 600 N2=1,8
  600 S(N1,N2)=0.0
C
      EIXXL=SDAT(8*I-7)*SDAT(8*I-4)/SDAT(8*I)
      EIYYL=SDAT(8*I-7)*SDAT(8*I-3)/SDAT(8*I)
      EIWW=SDAT(8*I-7)*SDAT(8*I-1)
      GJ=SDAT(8*I-6)*SDAT(8*I-2)
      EAL=SDAT(8*I-7)*SDAT(8*I-5)/SDAT(8*I)
      TLAM=SQRT(GJ/EIWW)
      TLAML=TLAM*SDAT(8*I)
      TG=2.*(COSH(TLAML)-1.)-(TLAML)*SINH(TLAML)
      TN=TLAML*COSH(TLAML)-SINH(TLAML)
C
      S(1,1)=EAL
      IF(PIN(I,1,1)-PIN(I,2,1)) 605,607,606
  605 S(2,2)=3.*EIXXL
      GO TO 609
  606 S(3,3)=3.*EIXXL
      GO TO 609
  607 IF(PIN(I,1,1)) 608,608,609
  608 S(2,2)=4.*EIXXL
```

```
      S(3,2)=2.*EIXXL
      S(2,3)=2.*EIXXL
      S(3,3)=4.*EIXXL
  609 CONTINUE
C
      IF(PIN(I,1,2)-PIN(I,2,2)) 610,612,611
  610 S(4,4)=3.*EIYYL
      GO TO 614
  611 S(5,5)=3.*EIYYL
      GO TO 614
  612 IF(PIN(I,1,2)) 613,613,614
  613 S(4,4)=4.*EIYYL
      S(4,5)=2.*EIYYL
      S(5,4)=2.*EIYYL
      S(5,5)=4.*EIYYL
  614 CONTINUE
C
      IF(PIN(I,1,3)-PIN(I,2,3)) 615,617,616
  615 S(6,6)=EIWW*(TLAM**3)*COSH(TLAML)/TN
      S(6,7)=EIWW*(TLAM**2)*SINH(TLAML)/TN
      S(7,6)=S(6,7)
      S(7,7)=S(6,7)*SDAT(8*I)
      GO TO 619
C
  616 S(6,6)=EIWW*(TLAM**3)*COSH(TLAML)/TN
      S(6,8)=EIWW*(TLAM**2)*SINH(TLAML)/TN
      S(8,6)=S(6,8)
      S(8,8)=S(6,8)*SDAT(8*I)
      GO TO 619
C
  617 IF(PIN(I,1,3)) 620,620,621
  620 S(6,6)=-EIWW*(TLAM**3)*SINH(TLAML)/TG
      S(6,7)=-EIWW*(TLAM**2)*(COSH(TLAML)-1.)/TG
      S(6,8)=S(6,7)
      S(7,6)=S(6,7)
      S(8,6)=S(6,7)
      S(7,7)=-EIWW*TN*TLAM/TG
      S(8,8)=S(7,7)
      S(7,8)=EIWW*TLAM*(TLAML-SINH(TLAML))/TG
      S(8,7)=S(7,8)
C
      GO TO 619
  621 S(6,6)=GJ/SDAT(8*I)
  619 CONTINUE
C
C      GENERATE THE FRAME STIFFNESS MATRIX AND STRESS RESULTANTS
C
      JNTDFI=JNTDF(I)
      JNTDIP=JNTDF(I+1)
C
```

```
      IF(JNTDFI) 725,725,699
  699 DO 700 N1=1,8
      DO 700 N2=1,JNTDFI
      SAT(N1,N2)=0.0
      DO 700 N3=1,8
  700 SAT(N1,N2)=SAT(N1,N2)+S(N1,N3)*AA(N2,N3)
C
      DO 710 N1=1,JNTDFI
      DO 710 N2=1,JNTDFI
      N1G=N1+JNTDFT
      DO 710 N3=1,8
  710 ASAT(N1G,N2 )=ASAT(N1G,N2 )+AA(N1,N3)*SAT(N3,N2)
C
      DO 720 N1=1,8
      N1G=N1+8*(I-1)
      SR(N1G)=0.0
      DO 720 N3=1,JNTDFI
      N3G=N3+JNTDFT
  720 SR(N1G)=SR(N1G)+SAT(N1,N3)*ASAT(N3G,15)
  725 CONTINUE
C
      JNTDFT=JNTDFT+JNTDF(I)
C
      JNTDIP=JNTDF(I+1)
      IF(JNTDIP) 765,765,727
C
  727 DO 730 N1=1,8
      DO 730 N2=1,JNTDIP
      SAT(N1,N2)=0.0
      DO 730 N3=1,8
  730 SAT(N1,N2)=SAT(N1,N2)+S(N1,N3)*AB(N2,N3)
C
      DO 740 N1=1,JNTDIP
      DO 740 N2=1,JNTDIP
      N1G=N1+JNTDFT
      DO 740 N3=1,8
  740 ASAT(N1G,N2)=ASAT(N1G,N2)+AB(N1,N3)*SAT(N3,N2)
      IF(JNTDFI) 755,755,747
C
  747 DO 750 N1=1,JNTDFI
      DO 750 N2=1,JNTDIP
      N1G=N1+JNTDFT -JNTDF(I)
      N2G=N2+7
      DO 750 N3=1,8
  750 ASAT(N1G,N2G)=ASAT(N1G,N2G)+AA(N1,N3)*SAT(N3,N2)
  755 CONTINUE
C
      DO 760 N1=1,8
      N1G=N1+8*(I-1)
      DO 760 N3=1,JNTDIP
```

```
      N3G=N3+JNTDFT
  760 SR(N1G)=SR(N1G)+SAT(N1,N3)*ASAT(N3G,15)
  765 CONTINUE
C
      IF (NM-I) 770,770,430
C
  770 IF(NFLAG) 800,800,980
C
C       SET UP AND SOLVE THE DEFORMATION EQUATIONS
C
  800 CONTINUE
      JNTDFT=0
      JCTM1=JCT-1
C
C       ELIMINATION
C
      DO 850 JJ1=1,JCTM1
      JNTDFI=JNTDF(JJ1)
      JNTDIP=JNTDF(JJ1+1)
C
      IF(JNTDFI) 850,850,808
  808 IF(JNTDIP) 850,850,809
  809 NFLAGB=0
      CALL INVERT(JNTDFI,JNTDFT,NFLAGB)
      IF(NFLAGB) 810,810,1370
C
  810 CONTINUE
C
      DO 820 N1=1,JNTDIP
      N1G=N1+7
      DO 820 N2=1,JNTDFI
      BTAI(N1,N2)=0.0
      DO 820 N3=1,JNTDFI
      N3G=N3+JNTDFT
      B(N3,N1)=ASAT(N3G,N1G)
  820 BTAI(N1,N2)=BTAI(N1,N2)+B(N3,N1)*AI(N3,N2)
C
      DO 830 N1=1,JNTDIP
      N1G=N1+JNTDFT+JNTDF(JJ1)
      DO 830 N2=1,JNTDIP
      N2G=N2+7
      DO 830 N3=1,JNTDFI
      N3G=N3+JNTDFT
  830 ASAT(N1G,N2)=ASAT(N1G,N2)-BTAI(N1,N3)*ASAT(N3G,N2G)
C
      DO 840 N1=1,JNTDIP
      N1G=N1+JNTDFT+JNTDFI
      DO 840 N3=1,JNTDFI
      N3G=N3+JNTDFT
  840 SLOAD(N1G)=SLOAD(N1G)--BTAI(N1,N3)*SLOAD(N3G)
```

```
      JNTDFT=JNTDFT+JNTDF(JJ1)
  850 CONTINUE
C
C       BACK SUBSTITUTION
C
      JNTDFT=L-JNTDF(JCT)
C
      DO 890 JJ1=1,JCT
      JJ2=JCT+1-JJ1
      JNTDFI=JNTDF(JJ2)
      IF(JNTDFI) 872,872,858
C
  858 NFLAGB=0
      CALL INVERT(JNTDFI,JNTDFT,NFLAGB)
      IF(NFLAGB) 860,860,1370
C
  860 CONTINUE
C
      DO 870 N1=1,JNTDFI
      N1G=N1+JNTDFT
      DO 870 N3=1,JNTDFI
      N3G=N3+JNTDFT
  870 ASAT(N1G,15)=ASAT(N1G,15)+AI(N1,N3)*SLOAD(N3G)
C
  872 IF(JJ1-JCT) 875,890,890
C
  875 CONTINUE
      JNTDIM=JNTDF(JJ2-1)
      IF(JNTDIM) 890,890,876
  876 IF(JNTDFI) 885,885,877
C
  877 DO 880 N1=1,JNTDIM
      N1G=N1+JNTDFT-JNTDIM
      DO 880 N3=1,JNTDFI
      N3G=N3+7
      N3H=N3+JNTDFT
  880 SLOAD(N1G)=SLOAD(N1G)-ASAT(N1G,N3G)*ASAT(N3H,15)
  885 CONTINUE
C
      JNTDFT=JNTDFT-JNTDF(JJ2-1)
C
  890 CONTINUE
C
C       CALCULATE THE STRESS RESULTANTS
C
  960 NFLAG=1
      GO TO 420
  980 CONTINUE
      NFLAG=0
C
```

```
C       OUTPUT STRESS RESULTANTS
C
  989 WRITE(6,990)
  990 FORMAT(///18H STRESS RESULTANTS)
      WRITE(6,9990)
 9990 FORMAT(18H ******************)
      WRITE(6,991)
  991 FORMAT(//45H APPLIED MOMENTS AT ENDS OF ELEMENT          )
      WRITE(6,992)
  992 FORMAT(/* ELEMENT   MOMENTS ABOUT X AXIS     MOMENTS ABOUT Y *,
     +  *AXIS*)
C
      DO 994 I=1,NM
      WRITE(6,993) I,SR(8*I-6),SR(8*I-5),SR(8*I-4),SR(8*I-3)
  993 FORMAT(I5,4X,E10.3,2X,E10.3,3X,E10.3,2X,E10.3)
  994 CONTINUE
      WRITE(6,995)
  995 FORMAT(//22H TORQUES AND BIMOMENTS)
      WRITE(6,996)
  996 FORMAT(/* ELEMENT  TORQUE  BIMOMENT AT L.H. END  BIMOMENT*,
     +  * AT R.H. END*)
      DO 999 I=1,NM
      WRITE(6,998) I,SR(8*I-2),SR(8*I-1),SR(8*I)
  998 FORMAT(I5,3X,E10.3,5X,E10.3,12X,E10.3)
  999 CONTINUE
      WRITE(6,1000)
 1000 FORMAT(//13H AXIAL FORCES)
      WRITE(6,2000)
 2000 FORMAT(/21H ELEMENT  AXIAL FORCE)
      DO 9002 I=1,NM
      WRITE(6,1001) I,SR(8*I-7)
 1001 FORMAT(I5,4X,E10.3)
 9002 CONTINUE
 1002 CONTINUE
C
C       OUTPUT THE JOINT DEFORMATIONS
C
 1004 WRITE(6,1005)
 1005 FORMAT(///19H JOINT DEFORMATIONS)
      WRITE(6,1007)
 1007 FORMAT(19H ******************)
      WRITE(6,1006)
 1006 FORMAT(//* JOINT  X DEFLN  Y DEFLN  Z DEFLN    X ROTN*
     +  *      Y ROTN      Z ROTN       WARP*)
C
 1010 CONTINUE
      LL=0
      DO 1230 J=1,JCT
      DO 1229 K=1,7
      IF(JTYPE(J,K)) 1030,1030,1020
```

```
 1020 LL=LL+1
      DE(K)=ASAT(LL,15)
      GO TO 1400
 1030 DE(K)=-0.0
 1400 CONTINUE
 1229 CONTINUE
C
      IF(NJER) 1233,1233,1228
 1228 KK=J
      IF(ECC(KK,1)) 1260,1261,1260
 1261 IF(ECC(KK,2)) 1260,1262,1260
 1262 IF(ECC(KK,3)) 1260,1233,1260
 1260 DO 1263 N1=1,7
      DO 1263 N2=1,7
 1263 ER(N1,N2)=0.0
      DO 1264 N1=1,7
 1264 ER(N1,N1)=1.0
      ER(1,5)=-ECC(KK,3)
      ER(1,6)=ECC(KK,2)
      ER(2,4)=ECC(KK,3)
      ER(2,6)=-ECC(KK,1)
      ER(3,4)=-ECC(KK,2)
      ER(3,5)=ECC(KK,1)
C
      DO 1240 L=1,7
      D(L)=-0.0
      DO 1240 K=1,7
      D(L)=D(L)+ER(L,K)*DE(K)
 1240 CONTINUE
      GO TO 1234
 1233 DO 1232 L=1,7
      D(L)=DE(L)
 1232 CONTINUE
 1234 WRITE(6,1221) J,(D(K),K=1,7)
 1230 CONTINUE
 1221 FORMAT(I5,3F9.3,1X,F10.6,1X,F10.6,1X,F10.6,1X,F11.7)
      GO TO 240
C
C       ERROR DESCRIPTIONS
C
 1370 WRITE(6,1380)
 1380 FORMAT(37H    ZERO DIVISION IN EQUATION SOLUTION)
      GOTO 10
C
C
C
      END
C
      FUNCTION SINH(X)
      SINH=(EXP(X)-EXP(-X))/2.0
```

```
      RETURN
      END
C
C
      FUNCTION COSH(X)
      COSH=(EXP(X)+EXP(-X))/2.0
      RETURN
      END
C
      SUBROUTINE INVERT(JNTDFI,JNTDFT,NFLAGB)
      COMMON S(8,8),SDAT(200),AA(7,8),AB(7,8),SAT(8,7),
     +   ASAT(200,15),JTYPE(25,7),JNTDF(25),SKLOAD(7),
     +   SLOAD(175),SJLOAD(25,7),CORD(25,3),SR(200),
     +   AI(7,14),BTAI(7,7),B(7,7),SDATA(125),
     +   CALPHA(24,3),SALPHA(24,3),TT(3,3),TEM(3,6),
     +   DA(25,7),PIN(24,2,3),D(7),DEG(24),DE(7),
     +   IRJN(24),IRCN(24,2),COSIR(24),SINIR(24),
     +   ECC(25,3),ER(7,7),AAE(7,8),ABE(7,8)
      DO 901 N1=1,JNTDFI
      DO 901 N2=1,JNTDFI
      N2G=N2+JNTDFI
  901 AI(N1,N2G)=0.0
      DO 902 N1=1,JNTDFI
      N1G=N1+JNTDFI
  902 AI(N1,N1G)=1.0
      KJ=2*JNTDFI
      DO 905 N1=1,JNTDFI
      N1G=N1+JNTDFT
      DO 905 N2=1,JNTDFI
  905 AI(N1,N2)=ASAT(N1G,N2)
C
      DO 9680 I=1,JNTDFI
      IP1=I+1
      TEMP=ABS(AI(I,I))
      K=I
      DO 9590 J=I,JNTDFI
      IF(ABS(AI(J,I))-TEMP)9590,9590,9585
 9585 K=J
      TEMP=ABS(AI(J,I))
 9590 CONTINUE
      IF(K-I)9600,9620,9600
 9600 DO 9610 J=I,KJ
      TEMP=AI(I,J)
      AI(I,J)=AI(K,J)
 9610 AI(K,J)=TEMP
 9620 IF(AI(I,I)) 9640,9685,9640
 9640 TEMP=1.0/AI(I,I)
      DO 9650 J=I,KJ
 9650 AI(I,J)=AI(I,J)*TEMP
      DO 9680 J=1,JNTDFI
```

```
      IF(I-J)9660,9680,9660
9660  TEMP=AI(J,I)
      DO 9670 K=IP1,KJ
9670  AI(J,K)=AI(J,K)-TEMP*AI(I,K)
9680  CONTINUE
      GOTO 9690
9685  NFLAGB=1
      GO TO 9695
9690  CONTINUE
      DO 959 N1=1,JNTDFI
      DO 959 N2=1,JNTDFI
      N2G=N2+JNTDFI
 959  AI(N1,N2)=AI(N1,N2G)
9695  RETURN
      END
```

APPENDIX VIII

PROGRAM LISTINGS AND SAMPLE DATA

b) Program CAFOP
(Inelastic cross-section analysis)

PROGRAM CAFOP

THIS PROGRAM ENABLES AN ELASTIC-PLASTIC ANALYSIS OF OPEN CROSS-SECTIONS OF GENERAL GEOMETRY. A SET OF STRESS RESULTANTS MAY BE APPLIED TO THE CROSS-SECTION TO ENABLE THE DETERMINATION OF FIRST YIELD , MOMENT-CURVATURE RELATIONSHIPS AND THE EXTENT OF YIELDING IN THE CROSS-SECTION. A RESIDUAL STRAIN PATTERN MAY ALSO BE APPLIED TO THE CROSS-SECTION.

DATA SPECIFICATION

DATA IS REQUIRED FOR THE MAIN PROGRAM AND THE SUBROUTINE.

MAIN PROGRAM

1. NUMBER OF NODES AND NUMBER OF ELEMENTS.

SUBROUTINE

1. CROSS-SECTION NUMBER , YOUNG'S MODULUS AND SHEAR MODULUS.

2. NUMBER OF NODES.

3. NODE NUMBER , X AND Y COORDINATES AND THE RESIDUAL STRAIN AT THE NODE. THIS IS REPEATED FOR EACH NODE.

4. NUMBER OF ELEMENTS.

5. ELEMENT NUMBER , CONNECTING NODES , THICKNESS , RATIOS OF INELASTIC TO ELASTIC VALUES OF YOUNG'S AND SHEAR MODULI AND THE YIELD STRAIN. THIS IS REPEATED FOR EACH ELEMENT.

6. STRESS RESULTANTS. THE STRESS RESULTANTS ARE THE SHEAR FORCES PARALLEL TO THE X AND Y AXES , AXIAL TENSION , MOMENTS ABOUT THE X AND Y AXES , WARPING TORQUE , SAINT VENANT TORQUE AND THE BIMOMENT.

7. LOAD FACTOR INCREMENT (0.01 TO 0.5).

SAMPLE DATA

THE DATA FOR THE CROSS-SECTION ANALYSIS OF THE STANCHION TOPS OF FRAME 7 IS GIVEN BELOW.

```
9 8
1
9
1 76.0 137.0 0.0
2 76.0 152.0 0.0
3 38.0 152.0 0.0
4 0.0 152.0 0.0
5 0.0 76.0 0.0
6 0.0 0.0 0.0
7 38.0 0.0 0.0
8 76.0 0.0 0.0
9 76.0 15.0 0.0
8
1 1 2 1.86 0.0303 0.25 0.001561
2 2 3 1.86 0.0303 0.25 0.001561
3 3 4 1.86 0.0303 0.25 0.001561
4 4 5 1.86 0.0303 0.25 0.001561
5 5 6 1.86 0.0303 0.25 0.001561
6 6 7 1.86 0.0303 0.25 0.001561
7 7 8 1.86 0.0303 0.25 0.001561
8 8 9 1.86 0.0303 0.25 0.001561
0.0 0.0 0.785 20.0 -0.02 0.0 0.0 -23.22
0.025
```

```
C     PROGRAM CAFOP
C
C     ELASTIC-PLASTIC OPEN CROSS-SECTION ANALYSIS
C
C
C     MAIN PROGRAM
C
      REAL CON(50,50),COM(50,50)
      READ(5,*) NODES,NELS
   15 FORMAT(2I5)
      NCONT=NODES*2+NELS*2-2
      CALL REST(CON,COM,NCONT)
      STOP
      END
C
      SUBROUTINE REST(CON,COM,NCONT)
C
      DIMENSION T(50),CORD(50,2),MCON(50,2),OLEN(50),ST(50)
     *,AREA(50),ANGLE(50),EN(50),GN(50),ENP(50),GNP(50),XP(50),YP(50)
     *,RHOL(50),KOUNT(50),W(100),GP(50,2),EPS(50),EPST(50),EPSR(50)
     *,EPSY(50),AN(50),WN(100),SF(100,3),RSS(50),WORK1(100),WORK2(100)
     *,PEF(50),STRESS(50,2),CORDS(50,2),ENS(50),GNS(50),WNS(100),XPS(50)
     *,YPS(50),PEFS(50),WNSS(100)
      REAL CON(NCONT,NCONT),COM(NCONT,NCONT)
C
      REAL MX,MY,MZX,MZY,MZW,KBAR
      INTEGER PEF,PEFS
C
      NFLAGE=0
      NFLAGG=0
C
C INPUT CROSS-SECTION NO. EXIT IF NEGATIVE
C
   10 READ(5,*) NCS,E,G
   20 FORMAT(I5,2F10.5)
      IF(NCS) 30,40,40
   30 STOP
C
C READ NODE DATA
C
   40 READ(5,*) NODES
   50 FORMAT(I5)
      DO 60 I=1,NODES
      READ(5,*) K,(CORD(K,J),J=1,2),EPSR(K)
   60 RSS(K)=E*EPSR(K)
   65 FORMAT(I5,2F10.5,F15.5)
C
C READ PANEL DATA
C
      READ(5,*) NELS
```

```
   70 FORMAT(I5)
      DO 80 I=1,NELS
   80 READ(5,*) K,(MCON(K,J),J=1,2),T(K),ENP(K),GNP(K),EPSY(K)
   85 FORMAT(3I5,4F10.5)
C
C GENERATE FLOATING NODES AND PANELS
C
      K=NODES
      J=NELS
      DO 90 I=1,NELS
      K=K+1
      J=J+1
      N1=MCON(I,1)
      N2=MCON(I,2)
      CORD(K,1)=(CORD(N1,1)+CORD(N2,1))/2.0
      CORD(K,2)=(CORD(N1,2)+CORD(N2,2))/2.0
      EPSR(K)=(EPSR(N1)+EPSR(N2))/2.0
      RSS(K)=E*EPSR(K)
      MCON(I,1)=N1
      MCON(I,2)=K
      MCON(J,1)=K
      MCON(J,2)=N2
      T(J)=T(I)
      ENP(J)=ENP(I)
      GNP(J)=GNP(I)
   90 EPSY(J)=EPSY(I)
C
      NODEST=K
      NELST=J
C
      DO 520 I=1,NELST
  520 PEF(I)=0
C
      DO 510 N1=1,NELST
      EN(N1)=1.0
  510 GN(N1)=1.0
C
      DO 515 I=1,NELS
      IF=NODES+I
      EPS(IF)=0.0
      RSS(IF)=0.0
  515 EPST(IF)=0.0
C
      XLF=1.0
      NFLAGA=0
      NFLAGD=0
C
C INPUT WORKING LOAD DATA
C
      READ(5,*) XXP,YYP,ZZP,XXM,YYM,ZZMJ,ZZMW,BIM
```

```
  820 FORMAT(8F10.5)
      READ(5,*) ZZ
  821 FORMAT(F10.5)
C
C FIND CENTROID AND MODIFY AXIS SYSTEM
C
      AT=0.0
      MX=0.0
      MY=0.0
      DO 133 I=1,NELST
      J1=MCON(I,1)
      J2=MCON(I,2)
      X=CORD(J2,1)-CORD(J1,1)
      Y=CORD(J2,2)-CORD(J1,2)
      OLEN(I)=SQRT(X*X+Y*Y)
      AREA(I)=OLEN(I)*T(I)
      AN(I)=AREA(I)*EN(I)
      AT=AT+AN(I)
      MX=MX+AN(I)*(CORD(J1,2)+CORD(J2,2))/2.0
      MY=MY+AN(I)*(CORD(J1,1)+CORD(J2,1))/2.0
  133 CONTINUE
C
      IF(AT-0.0001) 131,131,132
  131 XCEN=0.0
      YCEN=0.0
      GOTO 95
  132 XCEN=MY/AT
      YCEN=MX/AT
C
   95 WRITE(6,100) NCS
  100 FORMAT(46H1ELASTIC-PLASTIC ANALYSIS OF CROSS-SECTION NO.,I5)
      WRITE(6,180) E,G
  180 FORMAT(16H YOUNGS MODULUS=,F10.2,15H SHEAR MODULUS=,F10.2)
      WRITE(6,181)
  181 FORMAT(/14H WORKING LOADS)
      WRITE(6,190) XXM,YYM
  190 FORMAT(/29H MOMENTS ABOUT X AND Y AXES =,F10.3,2X,F10.3)
      WRITE(6,191) ZZP
  191 FORMAT(16H AXIAL TENSION =,F10.3)
      WRITE(6,194) BIM
  194 FORMAT(11H BIMOMENT =,F10.3)
      WRITE(6,192) XXP,YYP
  192 FORMAT(40H SHEAR FORCES PARALLEL TO X AND Y AXES =,F10.3,2X,F10.3)
      ZZMT=ZZMW+ZZMJ
      WRITE(6,193) ZZMT,ZZMW,ZZMJ
  193 FORMAT(15H TOTAL TORQUE =,F10.3,17H WARPING TORQUE =,F10.3,
     * 22H SAINT-VENANT TORQUE =,F10.3)
      WRITE(6,134)
  134 FORMAT(/62H COORDINATES HAVE NOW BEEN MODIFIED TO GIVE ORIGIN AT C
     *ENTROID)
```

```
      WRITE(6,130) XCEN
  130 FORMAT(27H X COORDINATE OF CENTROID =,F8.3)
      WRITE(6,140) YCEN
  140 FORMAT(27H Y COORDINATE OF CENTROID =,F8.3)
      DO 150 J1=1,NODEST
      CORD(J1,1)=CORD(J1,1)-XCEN
      CORD(J1,2)=CORD(J1,2)-YCEN
  150 CONTINUE
C
C SET-UP CONNECTIVITY(EQUILIBRIUM) MATRIX
C
      DO 205 N1=1,NCONT
      DO 205 N2=1,NCONT
  205 CON(N1,N2)=0.0
C
      DO 230 I=1,NELST
      J1=MCON(I,1)
      N1=2*I-1
      IF(J1-NODEST)200,210,210
  200 CON(J1,N1)=-1.0
  210 J2=MCON(I,2)
      N2=2*I
      IF(J2-NODEST) 220,230,230
  220 CON(J2,N2)=1.0
  230 CONTINUE
      DO 240 I=1,NELST
      NP=NODEST-1+I
      N1=2*I-1
      N2=2*I
      CON(NP,N1)=-1.0
  240 CON(NP,N2)=1.0
C
C SET UP COMPATIBILITY MATRIX
C
      DO 305 N1=1,NCONT
      DO 305 N2=1,NCONT
  305 COM(N1,N2)=0.0
C
      DO 300 I=1,NODEST
      KOUNT(I)=0
      DO 300 J=1,NELST
      DO 300 K=1,2
      IF(I-MCON(J,K)) 300,310,300
  310 KOUNT(I)=KOUNT(I)+1
  300 CONTINUE
C
      NP=0
      DO 320 I=1,NODEST
      LP=1
      J=0
```

```
      IF(KOUNT(I)-LP)320,320,325
  325 NP=NP+1
      LP=LP+1
  330 J=J+1
      IF(I-MCON(J,1)) 340,350,340
  340 IF(I-MCON(J,2)) 330,360,330
  350 N1=2*J-1
      GO TO 390
  360 N1=2*J
      GO TO 390
  380 NP=NP+1
      LP=LP+1
  390 J=J+1
      IF(I-MCON(J,1)) 400,410,400
  400 IF(I-MCON(J,2)) 390,420,390
  410 N2=2*J-1
      GO TO 430
  420 N2=2*J
  430 COM(NP,N1)=-1.0
      COM(NP,N2)=1.0
      IF(KOUNT(I)-LP)320,320,380
  320 CONTINUE
C
      DO 440 I=1,NELST
      NP=NP+1
      N1=2*I-1
      N2=2*I
      COM(NP,N1)=-1.0
  440 COM(NP,N2)=1.0
C
      NP=NP+1
      COM(NP,1)=1.0
C
C  INVERT COM AND CON
C
      CALL MINV(CON,NCONT,D1,WORK1,WORK2)
      CALL MINV(COM,NCONT,D2,WORK1,WORK2)
      WRITE(6,450) D1,D2
  450 FORMAT(/4H D1=,F16.5,4H D2=,F16.5)
C
C CALCULATE AREAS,AXES,MOMENTS OF INERTIA AND TORSION CONSTANT
C
  500 CONTINUE
      A=0.0
      AT=0.0
      MX=0.0
      MY=0.0
      MZX=0.0
      MZY=0.0
      MZW=0.0
```

```
      ZI=0.0
C
      DO 540 I=1,NELST
      J1=MCON(I,1)
      J2=MCON(I,2)
      X=CORD(J2,1)-CORD(J1,1)
      Y=CORD(J2,2)-CORD(J1,2)
      OLEN(I)=SQRT(X*X+Y*Y)
      ZI=ZI+(OLEN(I)*T(I)**3)*GN(I)/3.0
      AREA(I)=OLEN(I)*T(I)
      A=A+AREA(I)
      AN(I)=AREA(I)*EN(I)
      AT=AT+AN(I)
      MX=MX+AN(I)*(CORD(J1,2)+CORD(J2,2))/2.0
      MY=MY+AN(I)*(CORD(J1,1)+CORD(J2,1))/2.0
      IF (X) 536,534,536
  534 X=0.000001
  536 TANGLE=Y/X
      ANGLE(I)=ATAN(TANGLE)
  540 CONTINUE
C
      IF(AT-0.0001) 550,550,551
  550 XCENT=0
      YCENT=0
      GO TO 552
  551 XCENT=MY/AT
      YCENT=MX/AT
  552 UU=0.0
      VV=0.0
      UV=0.0
      AA=XCENT
      BB=YCENT
C
      DO 560 I=1,NELST
      XI=(OLEN(I)*T(I)**3)*EN(I)/12.0
      YI=(OLEN(I)**3*T(I)*EN(I))/12.0
      C=COS(ANGLE(I))
      S=SIN(ANGLE(I))
      C2=C*C
      S2=S*S
      S2A=2.0*S*C
      C2A=2.0*C*C-1.0
      J1=MCON(I,1)
      J2=MCON(I,2)
      XN=(CORD(J1,1)+CORD(J2,1))/2.0-AA
      YN=(CORD(J1,2)+CORD(J2,2))/2.0-BB
      XCENT=XN*C+YN*S
      YCENT=-XN*S+YN*C
      UU=UU+(XI+AN(I)*YCENT**2)*C2+(YI+AN(I)*XCENT**2)*S2+AN(I)*XCENT*
     *YCENT*S2A
```

```
      VV=VV+(YI+AN(I)*XCENT**2)*C2+(XI+AN(I)*YCENT**2)*S2-AN(I)*XCENT*
     *YCENT*S2A
      UV=UV+AN(I)*XCENT*YCENT*C2A-0.5*(XI-YI+AN(I)*(YCENT**2-XCENT**2))
     * *S2A
  560 CONTINUE
      TEST=VV-UU
      IF(TEST)596,594,596
  594 TEST=0.000001
  596 SLOPE=2.0*UV/TEST
      ALP2=ATAN(SLOPE)
      DEG=ALP2*90.0/3.14159265
      SALP2=SIN(ALP2)
      ALP=ALP2/2.0
      SALP=SIN(ALP)
      CALP=COS(ALP)
C
      UUP=UU*CALP**2+VV*SALP**2-UV*SALP2
      VVP=UU*SALP**2+VV*CALP**2+UV*SALP2
      AAP=AA*CALP+BB*SALP
      BBP=-AA*SALP+BB*CALP
C
C CALCULATE SHEAR CENTRE POSITION AND FLEXURAL SHEARS
C
      DO 650 I=1,NODEST
      XP(I)=(CORD(I,1)-AA)*CALP+(CORD(I,2)-BB)*SALP
  650 YP(I)=(CORD(I,1)-AA)*(-SALP)+(CORD(I,2)-BB)*CALP
C
      DO 660 I=1,NCONT
      DO 660 J=1,2
  660 GP(I,J)=0.0
C
      DO 680 I=1,NELST
      NP=NODEST-1+I
      J1=MCON(I,1)
      J2=MCON(I,2)
      GP(NP,1)=-AN(I)*(YP(J1)+YP(J2))/(2.0*UUP)
      GP(NP,2)=-AN(I)*(XP(J1)+XP(J2))/(2.0*VVP)
  680 CONTINUE
C
      DO 690 I=1,NCONT
      DO 690 J=1,2
      SF(I,J)=0.0
      DO 690 K=1,NCONT
  690 SF(I,J)=SF(I,J)+CON(I,K)*GP(K,J)
C
      DO 700 I=1,NELST
      J1=MCON(I,1)
      J2=MCON(I,2)
      N1=2*I-1
      N2=2*I
```

```
      FY=-AN(I)*(2.0*YP(J1)+YP(J2))/(6.0*UUP)+SF(N1,1)
      MZY=MZY+FY*(XP(J2)*YP(J1)-YP(J2)*XP(J1))
      FX=-AN(I)*(2.0*XP(J1)+XP(J2))/(6.0*VVP)+SF(N1,2)
  700 MZX=MZX+FX*(XP(J2)*YP(J1)-YP(J2)*XP(J1))
C
      XSP=-MZY
      YSP=MZX
      XS=XSP*CALP-YSP*SALP+AA
      YS=XSP*SALP+YSP*CALP+BB
C
      IF(NFLAGG) 702,702,704
  702 NFLAGG=1
      XSOLD=XS
      YSOLD=YS
  704 CONTINUE
C
C CALCULATE WARPING NORMAL STRESS AND DISPLACEMENT PATTERNS
C
      DO 710 I=1,NCONT
  710 GP(I,1)=0.0
C
      NP=NODEST-2
      DO 720 I=1,NELST
      NP=NP+1
      J1=MCON(I,1)
      J2=MCON(I,2)
      RHOL(I)=-(XP(J2)-XSP)*(YP(J1)-YSP)+(XP(J1)-XSP)*(YP(J2)-YSP)
  720 GP(NP,1)=RHOL(I)
C
      DO 730 I=1,NCONT
      W(I)=0.0
      DO 730 K=1,NCONT
  730 W(I)=W(I)+COM(I,K)*GP(K,1)
C
      TEMP4=0
      DO 735 I=1,NELST
      DO 735 J=1,2
      K=2*(I-1)+J
  735 TEMP4=TEMP4+W(K)*AN(I)/2.0
C
      TEMP4=TEMP4/AT
      DO 737 I=1,NELST
      DO 737 J=1,2
      K=2*(I-1)+J
  737 W(K)=W(K)-TEMP4
C
      DO 850 I=1,NELST
      J1=MCON(I,1)
      J2=MCON(I,2)
      WN(J1)=W(2*I-1)
```

```
  850 WN(J2)=W(2*I)
C
      IF(NFLAGD) 541,541,542
  541 NFLAGD=1
      DO 543 I=1,NELST
      J1=MCON(I,1)
      J2=MCON(I,2)
      WNSS(J1)=WN(J1)
  543 WNSS(J2)=WN(J2)
  542 CONTINUE
C
C CALCULATE WARPING SHEAR FLOWS AND WARPING RIGIDTY
C
      DO 740 I=1,NCONT
  740 GP(I,1)=0.0
C
      DO 750 I=1,NELST
      NP=NODEST-1+I
      N1=2*I-1
  750 GP(NP,1)=-AN(I)*RHOL(I)/2.0-AN(I)*W(N1)
C
      DO 760 I=1,NCONT
      SF(I,3)=0.0
      DO 760 K=1,NCONT
  760 SF(I,3)=SF(I,3)+CON(I,K)*GP(K,1)
C
      DO 770 I=1,NELST
      J1=MCON(I,1)
      J2=MCON(I,2)
      N1=2*I-1
      FW=-AN(I)*RHOL(I)/6.0+SF(N1,3)-W(N1)*AN(I)/2.0
  770 MZW=MZW-FW*(XP(J2)*YP(J1)-YP(J2)*XP(J1))
C
C
C ANALYSIS UNDER LOAD
C
C CALCULATE LONGITUDINAL STRAINS AT ENDS OF PANELS
C
      IF(NFLAGA) 830,830,840
  830 EPSA=ZZP/(E*AT)
      RHOX=XXM/(E*UUP)
      RHOY=YYM/(E*VVP)
      D2PHI=-BIM/(E*MZW)
C
      DO 860 I=1,NODEST
      EPS(I)=EPSA+RHOX*CORD(I,2)-RHOY*CORD(I,1)-D2PHI*WNSS(I)
      EPST(I)=EPSR(I)+EPS(1)
      IF(EPSY(I)-EPST(I)) 861,861,850
  861 WRITE(6,862) I
  862 FORMAT(14H YIELD AT NODE,I3)
```

```
  860 CONTINUE
C
C ADJUST LOADS TO FIND  LOAD FACTOR FOR FIRST YIELD
C
      TEMP1=100.0
      DO 1000 I=1,NELST
      DO 1000 K=1,2
      J=MCON(I,K)
      T3=ABS(EPS(J))
      IF(T3-0.00001) 1000,1000,990
  990 TEMP2=EPSY(I)/ABS(EPS(J))-EPSR(J)/EPS(J)
      IF(TEMP1-TEMP2) 1000,1000,1005
 1005 TEMP1=TEMP2
      JFY=J
 1000 CONTINUE
C
      EUUP=UUP
      EVVP=VVP
      EAT=AT
      EMZW=MZW
      NCYCL=0
      YLF=TEMP1
      XLF=YLF
      EPSA=EPSA*YLF
      RHOX=RHOX*YLF
      RHOY=RHOY*YLF
      D2PHI=D2PHI*YLF
      XXMY=XXM*YLF
      ZZPY=ZZP*YLF
      YYMY=YYM*YLF
      BIMY=BIM*YLF
      XXM=XXMY
      YYM=YYMY
      ZZP=ZZPY
      BIM=BIMY
      DO 1020 I=1,NODEST
      EPS(I)=EPSA+RHOX*CORD(I,2)-RHOY*CORD(I,1)-D2PHI*WNSS(I)
 1020 EPST(I)=EPSR(I)+EPS(I)
      NFLAGA=1
C
C CALCULATE LOADS FROM STRESSES
C
  840 XMOM=0.0
      YMOM=0.0
      ZP=0.0
      BIMOM=0.0
      KBAR=0.0
      DO 949 I=1,NELST
      J1=MCON(I,1)
      J2=MCON(I,2)
```

```
      STRESS1=EPST(J1)*E
      STRESS2=EPST(J2)*E
      YSS=EPSY(I)*E
      IF(STRESS1-YSS) 932,932,931
  931 STRESS1=YSS
  932 IF(STRESS1+YSS) 933,934,934
  933 STRESS1=-YSS
  934 IF(STRESS2-YSS) 936,936,935
  935 STRESS2=YSS
  936 IF(STRESS2+YSS) 937,938,938
  937 STRESS2=-YSS
  938 CONTINUE
      STRESS(I,1)=STRESS1
      STRESS(I,2)=STRESS2
C
      ZP=ZP+STRESS1*AREA(I)+(STRESS2-STRESS1)*AREA(I)/2.0
      XMOM=XMOM+STRESS1*AREA(I)*(CORD(J1,2)+CORD(J2,2))/2.0
     * +(STRESS2-STRESS1)*AREA(I)*(CORD(J1,2)+2.0*CORD(J2,2))/6.0
      YMOM=YMOM+STRESS1*AREA(I)*(CORD(J1,1)+CORD(J2,1))/2.0
     * +(STRESS2-STRESS1)*AREA(I)*(CORD(J1,1)+2.0*CORD(J2,1))/6.0
      BIMOM=BIMOM+STRESS1*AREA(I)*(WNSS(J1)+WNSS(J2))/2.0
     * +(STRESS2-STRESS1)*AREA(I)*(WNSS(J1)+2.0*WNSS(J2))/6.0
      DO 1949 N1=1,2
 1949 KBAR=KBAR+STRESS1*AREA(I)*(CORD(J1,N1)**2+CORD(J1,N1)*CORD(J2,N1)+
     * CORD(J2,N1)**2)/3.0 +(STRESS2-STRESS1)*AREA(I)*(CORD(J1,N1)**2+
     *  2.0*CORD(J1,N1)*CORD(J2,N1)+3.0*CORD(J2,N1)**2)/12.0
  949 CONTINUE
      YMOM=-YMOM
C
      AAS=AA
      BBS=BB
      ALPS=ALP
      XSS=XS
      YSS=YS
C
C OUTPUT ACTIONS
C
      WRITE(6,1999) XLF
 1999 FORMAT(13H LOAD FACTOR=,F10.5)
      WRITE(6,964) RHOX,RHOY,EPSA,D2PHI
  964 FORMAT(7H RHOX =,F13.10,7H RHOY =,F13.10,7H EPSA =,F13.10,
     *8H D2PHI =,F13.10)
      WRITE(6,961) XXM,YYM,ZZP,BIM,KBAR
  961 FORMAT(10H XMOMENT= ,F13.4,10H YMOMENT= ,F13.4,14H AXIAL FORCE= ,
     * F13.4,10H BIMOMENT=,F13.4,6H KBAR=,F15.5)
      WRITE(6,961) XMOM,YMOM,ZP,BIMOM,KBAR
C
C CORRECT ACTION ERRORS
C
      CONSTO=-BB*(XS-XSOLD)+AA*(YS-YSOLD)
```

```
      IF(ABS(VVP)-0.0001) 3001,3001,3002
 3001 VVP=EVVP
 3002 IF(ABS(UUP)-0.0001) 3003,3003,3004
 3003 UUP=EUUP
 3004 IF(ABS(AT)-0.0001) 3005,3005,3006
 3005 AT=EAT
 3006 IF(ABS(MZW)-0.0001) 3007,3007,3008
 3007 MZW=EMZW
 3008 CONTINUE
C
      DZP=ZP-ZZP
      DXMOM=XMOM-XXM
      DYMOM=YMOM-YYM
      DBIM=BIMOM-BIM
C
      DZPP=DZP
      DXMOMP=-DZP*BBP+DXMOM*CALP+DYMOM*SALP
      DYMOMP=DZP*AAP-DXMOM*SALP+DYMOM*CALP
      DBIMP=-DZP*CONSTO-(XS-XSOLD)*DXMOM-(YS-YSOLD)*DYMOM+DBIM
C
      DEPSAP=DZPP/(E*AT)
      DRHOXP=DXMOMP/(E*UUP)
      DRHOYP=DYMOMP/(E*VVP)
      DD2PHIP=-DBIMP/(E*MZW)
C
      DEPSA=DEPSAP-BBP*DRHOXP+AAP*DRHOYP+CONSTO*DD2PHIP
      DRHOX=DRHOXP*CALP-DRHOYP*SALP+(XS-XSOLD)*DD2PHIP
      DRHOY=DRHOXP*SALP+DRHOYP*CALP+(YS-YSOLD)*DD2PHIP
      DD2PHI=DD2PHIP
C
      EPSA=EPSA-DEPSA
      RHOX=RHOX-DRHOX
      RHOY=RHOY-DRHOY
      D2PHI=D2PHI-DD2PHI
C
C TEST CONVERGENCE
C
      IF(ABS(RHOX)-0.000010) 1501,1501,1500
 1500 TEST=ABS(DRHOX/RHOX)
      IF(TEST-0.001) 1501,1501,1550
 1501 IF(ABS(RHOY)-0.000010) 1503,1503,1502
 1502 TEST=ABS(DRHOY/RHOY)
      IF(TEST-0.001) 1503,1503,1550
 1503 IF(ABS(EPSA)-0.000010) 1505,1505,1504
 1504 TEST=ABS(DEPSA/EPSA)
      IF(TEST-0.001) 1505,1505,1550
 1505 IF(ABS(D2PHI)-0.000010) 1507,1507,1506
 1506 TEST=ABS(DD2PHI/D2PHI)
      IF(TEST-0.001) 1507,1507,1550
 1507 CONTINUE
```

```
      GOTO 1558
C
C DECREASE LOADS
C
 1550 PROPS=UUP+VVP+AT+MZW
      IF(PROPS-0.0003) 1552,1552,1551
 1551 IF(NCYCL-4) 1555,1555,1552
 1552 XXM=XXMS
      YYM=YYMS
      ZZP=ZZPS
      BIM=BIMS
      XLF=XLFS
      ZZ=0.4*ZZ
      IF(ZZ-0.001) 1110,1110,1553
 1553 RHOX=RHOXS
      RHOY=RHOYS
      EPSA=EPSAS
      D2PHI=D2PHIS
      DO 1554 I=1,NODEST
      CORD(I,1)=CORDS(I,1)
 1554 CORD(I,2)=CORDS(I,2)
      DO 3555 I=1,NELST
      EN(I)=ENS(I)
      GN(I)=GNS(I)
 3555 PEF(I)=PEFS(I)
      DO 1557 I=1,NODEST
      XP(I)=XPS(I)
      YP(I)=YPS(I)
 1557 WN(I)=WNS(I)
      CALP=CALPS
      SALP=SALPS
      BBP=BBPS
      AAP=AAPS
      GO TO 1560
 1558 CONTINUE
C
 1560 NCYCL=0
C
      XLFS=XLF
      XXMS=XXM
      YYMS=YYM
      ZZPS=ZZP
      BIMS=BIM
C
      DO 1561 I=1,NODEST
      CORDS(I,1)=CORD(I,1)
 1561 CORDS(I,2)=CORD(I,2)
      DO 1562 I=1,NELST
      ENS(I)=EN(I)
      GNS(I)=GN(I)
```

```
1562 PEFS(I)=PEF(I)
     DO 1563 I=1,NODEST
     XPS(I)=XP(I)
     YPS(I)=YP(I)
1563 WNS(I)=WN(I)
     CALPS=CALP
     SALPS=SALP
     BBPS=BBP
     AAPS=AAP
C
     RHOXS=RHOX
     RHOYS=RHOY
     EPSAS=EPSA
     D2PHIS=D2PHI
C
C INCREASE LOADS
C
     XLF=XLF+ZZ*YLF
     XXM=XXM+ZZ*XXMY
     YYM=YYM+ZZ*YYMY
     ZZP=ZZP+ZZ*ZZPY
     BIM=BIM+ZZ*BIMY
C
     DZP=ZP-ZZP
     DXMOM=XMOM-XXM
     DYMOM=YMOM-YYM
     DBIM=BIMOM-BIM
C
     DZPP=DZP
     DXMOMP=-DZP*BBP+DXMOM*CALP+DYMOM*SALP
     DYMOMP=DZP*AAP-DXMOM*SALP+DYMOM*CALP
     DBIMP=-DZP*CONSTO-(XS-XSOLD)*DXMOM-(YS-YSOLD)*DYMOM+DBIM
C
     DEPSAP=DZPP/(E*AT)
     DRHOXP=DXMOMP/(E*UUP)
     DRHOYP=DYMOMP/(E*VVP)
     DD2PHIP=-DBIMP/(E*MZW)
C
     DEPSA=DEPSAP-BBP*DRHOXP+AAP*DRHOYP+CONSTO*DD2PHIP
     DRHOX=DRHOXP*CALP-DRHOYP*SALP+(XS-XSOLD)*DD2PHIP
     DRHOY=DRHOXP*SALP+DRHOYP*CALP+(YS-YSOLD)*DD2PHIP
     DD2PHI=DD2PHIP
C
     RHOX=RHOX-DRHOX
     RHOY=RHOY-DRHOY
     EPSA=EPSA-DEPSA
     D2PHI=D2PHI-DD2PHI
C
C RECAPITULATE NODE AND ELEMENT DATA
C
```

```
      WRITE(6,101) NODEST
  101 FORMAT(//14H0NODE DATA FOR,I5,6H NODES)
      WRITE(6,102)
  102 FORMAT(66H NODE    X-CORDINATE  Y-CORDINATE  RESIDUAL STRAIN  RESID
     *UAL STRESS)
      WRITE(6,103)
  103 FORMAT(12H FIXED NODES)
      DO 104 I=1,NODES
  104 WRITE(6,105) I,CORD(I,1),CORD(I,2),EPSR(I),RSS(I)
  105 FORMAT(I5,2(2X,F10.5),2(4X,F10.5))
      WRITE(6,106)
  106 FORMAT(15H FLOATING NODES)
      NODESF=NODEST-NODES
      NELSF=NELST-NODES
      DO 108 I=1,NODESF
      J=NODES+I
  108 WRITE(6,107) J,CORD(J,1),CORD(J,2)
  107 FORMAT(I5,2(2X,F10.5))
      WRITE(6,109) NELST
  109 FORMAT(15H0PANEL DATA FOR,I5,7H PANELS)
      WRITE(6,110)
  110 FORMAT(63H PANEL   CONNECTION THICKNESS   ESH/E  GSH/G YIELD STRAI
     *N YIELD)
      DO 120 I=1,NELST
      WRITE(6,111) I,MCON(I,1),MCON(I,2),T(I),ENP(I),GNP(I),EPSY(I),
     *PEF(I)
  120 CONTINUE
  111 FORMAT(I5,2X,I5,3H TO,I5,3(1X,F7.4),1X,F9.6,4X,I5)
C OUTPUT PROPERTIES
C
      WRITE(6,800) AT
  800 FORMAT(29H TRANSFORMED AREA OF SECTION=,F16.3)
      WRITE(6,801) AA
  801 FORMAT(25H X-CORDINATE OF CENTROID=,F16.3)
      WRITE(6,802) BB
  802 FORMAT(25H Y-CORDINATE OF CENTROID=,F16.3)
      WRITE(6,803) XS
  803 FORMAT(30H X-CORDINATE OF SHEAR CENTRE =,F16.3)
      WRITE(6,804) YS
  804 FORMAT(30H Y-CORDINATE OF SHEAR CENTRE =,F16.3)
      WRITE(6,805) UU
  805 FORMAT(22H IXX THROUGH CENTROID=,F16.3)
      WRITE(6,806) VV
  806 FORMAT(22H IYY THROUGH CENTROID=,F16.3)
      WRITE(6,807) UV
  807 FORMAT(22H IXY THROUGH CENTROID=,F16.3)
      WRITE(6,808) UUP
  808 FORMAT(36H IXPXP (PRINCIPAL MOMENT OF INERTIA),F16.3)
      WRITE(6,809) VVP
  809 FORMAT(36H IYPYP (PRINCIPAL MOMENT OF INERTIA),F16.3)
```

```
      WRITE(6,810)DEG
  810 FORMAT(24H SLOPE OF NEUTRAL AXIS)=,F16.3)
      WRITE(6,811) ZI
  811 FORMAT(22H TORSION CONSTANT (J)=,F16.6)
      WRITE(6,812) MZW
  812 FORMAT(22H WARPING CONSTANT(IW)=,F16.3)
C
C OUTPUT STRESS AND STRAIN DISTRIBUTION
C
      WRITE(6,900)
  900 FORMAT(48H STRESS AND STRAIN DISTRIBUTION IN CROSS-SECTION)
      WRITE(6,910)
  910 FORMAT(117H PANEL    CONNECTION   RESIDUAL  RESIDUAL   LONG.      L
     *ONG.   WARPING     SHEAR       LONG.     LONG.    WARPING     SHEAR)
      WRITE(6,920)
  920 FORMAT(118H                                  STRESS    STRESS    STRESS     ST
     *RAIN     DISPL.     STRESS     STRESS    STRAIN     DISPL.     STRESS)
      WRITE(6,930)
  930 FORMAT(117H                                   END1      END2      END1       E
     *ND1       END1       END1       END2      END2       END2       END2)
      DO 950 I=1,NELST
      J1=MCON(I,1)
      J2=MCON(I,2)
      STRESS1=STRESS(I,1)
      STRESS2=STRESS(I,2)
      SF1=0
      SF2=0
  950 WRITE(6,940) I,J1,J2,RSS(J1),RSS(J2),STRESS1,EPST(J1),WN(J1),
     * SF1,STRESS2,EPST(J2),WN(J2),SF2
  940 FORMAT(1H ,I4,3X,I4,3H TO,I4,1X,F9.5,1X,F9.5,2X,F8.3,3(2X,F8.5),
     * 2X,F8.3,3(2X,F8.5))
      WRITE(6,941)
  941 FORMAT(1H1)
      GO TO 1555
C
C
C ADJUST FLOATING NODES FOR YIELDED REGIONS
C
 1555 NCYCL=NCYCL+1
      DO 1032 I=1,NODEST
      EPS(I)=EPSA+RHOX*CORD(I,2)-RHOY*CORD(I,1)-D2PHI*WNSS(I)
 1032 EPST(I)=EPSR(I)+EPS(I)
C
      DO 1090 I=1,NELS
      IPNELS=I+NELS
      IPNODES=I+NODES
      J1=MCON(I,1)
      J2=MCON(IPNELS,2)
      T1=ABS(EPST(J1))-EPSY(I)
      T2=ABS(EPST(J2))-EPSY(I)
```

```
C
      IF(T1) 1040,1050,1050
 1040 IF(T2) 1085,1085,1070
 1050 IF(T2) 1080,1060,1060
 1060 CORD(IPNODES,1)=(CORD(J1,1)+CORD(J2,1))/2.0
      CORD(IPNODES,2)=(CORD(J1,2)+CORD(J2,2))/2.0
      WNSS(IPNODES)=(WNSS(J1)+WNSS(J2))/2.0
      EPST(IPNODES)=EPST(J1)
      EN(I)=ENP(I)
      GN(I)=GNP(I)
      EN(IPNELS)=ENP(IPNELS)
      GN(IPNELS)=GNP(IPNELS)
      PEF(I)=1
      PEF(IPNELS)=1
      GOTO 1090
 1070 IF(EPST(J2)) 1071,1071,1072
 1071 EPSYI=-EPSY(I)
      GO TO 1073
 1072 EPSYI=EPSY(I)
 1073 CORD(IPNODES,1)=(CORD(J2,1)-CORD(J1,1))*(ABS(EPSYI-EPST(J1)))
     * /ABS(EPST(J2)-EPST(J1))+CORD(J1,1)
      CORD(IPNODES,2)=(CORD(J2,2)-CORD(J1,2))*(ABS(EPSYI-EPST(J1)))
     * /ABS(EPST(J2)-EPST(J1))+CORD(J1,2)
      WNSS(IPNODES)=(WNSS(J2)-WNSS(J1))*(ABS(EPSYI-EPST(J1)))
     * /ABS(EPST(J2)-EPST(J1))+WNSS(J1)
      EPST(IPNODES)=EPST(J2)
      EN(IPNELS)=ENP(IPNELS)
      GN(IPNELS)=GNP(IPNELS)
      PEF(IPNELS)=1
      GOTO 1090
 1080 IF(EPST(J1)) 1081,1081,1082
 1081 EPSYI=-EPSY(I)
      GO TO 1083
 1082 EPSYI=EPSY(I)
 1083 CORD(IPNODES,1)=(CORD(J1,1)-CORD(J2,1))*(ABS(EPSYI-EPST(J2)))
     * /ABS(EPST(J1)-EPST(J2))+CORD(J2,1)
      CORD(IPNODES,2)=(CORD(J1,2)-CORD(J2,2))*(ABS(EPSYI-EPST(J2)))
     * /ABS(EPST(J1)-EPST(J2))+CORD(J2,2)
      WNSS(IPNODES)=(WNSS(J1)-WNSS(J2))*(ABS(EPSYI-EPST(J2)))
     * /ABS(EPST(J1)-EPST(J2))+WNSS(J2)
      EPST(IPNODES)=EPST(J1)
      EN(I)=ENP(I)
      GN(I)=GNP(I)
      PEF(I)=1
      GOTO 1090
 1085 CORD(IPNODES,1)=(CORD(J1,1)+CORD(J2,1))/2.0
      CORD(IPNODES,2)=(CORD(J1,2)+CORD(J2,2))/2.0
      WNSS(IPNODES)=(WNSS(J1)+WNSS(J2))/2.0
      EPST(IPNODES)=(EPST(J1)+EPST(J2))/2.0
      EN(I)=1
```

```
      GN(I)=1
      EN(IPNELS)=1
      GN(IPNELS)=1
      PEF(I)=0
      PEF(IPNELS)=0
 1090 CONTINUE
C
 1100 GO TO 500
 1110 RETURN
      END
      SUBROUTINE MINV(A,N,D,L,M)                                    MINV 033
      DIMENSION A(N,N),L(N),M(N)
      D=1.0                                                         MINV 056
      NK=-N                                                         MINV 057
      DO 80 K=1,N                                                   MINV 058
      NK=NK+N                                                       MINV 059
      L(K)=K                                                        MINV 060
      M(K)=K                                                        MINV 061
      KK=NK+K                                                       MINV 062
      BIGA=A(KK)                                                    MINV 063
      DO 20 J=K,N                                                   MINV 064
      IZ=N*(J-1)                                                    MINV 065
      DO 20 I=K,N                                                   MINV 066
      IJ=IZ+I                                                       MINV 067
   10 IF( ABS(BIGA)- ABS(A(IJ))) 15,20,20                           MINV 068
   15 BIGA=A(IJ)                                                    MINV 069
      L(K)=I                                                        MINV 070
      M(K)=J                                                        MINV 071
   20 CONTINUE                                                      MINV 072
C                                                                   MINV 073
C         INTERCHANGE ROWS                                          MINV 074
C                                                                   MINV 075
      J=L(K)                                                        MINV 076
      IF(J-K) 35,35,25                                              MINV 077
   25 KI=K-N                                                        MINV 078
      DO 30 I=1,N                                                   MINV 079
      KI=KI+N                                                       MINV 080
      HOLD=-A(KI)                                                   MINV 081
      JI=KI-K+J                                                     MINV 082
      A(KI)=A(JI)                                                   MINV 083
   30 A(JI) =HOLD                                                   MINV 084
C                                                                   MINV 085
C         INTERCHANGE COLUMNS                                       MINV 086
C                                                                   MINV 087
   35 I=M(K)                                                        MINV 088
      IF(I-K) 45,45,38                                              MINV 089
   38 JP=N*(I-1)                                                    MINV 090
      DO 40 J=1,N                                                   MINV 091
      JK=NK+J                                                       MINV 092
      JI=JP+J                                                       MINV 093
```

```
      HOLD=-A(JK)                                                    MINV 094
      A(JK)=A(JI)                                                    MINV 095
   40 A(JI) =HOLD                                                    MINV 096
C                                                                    MINV 097
C        DIVIDE COLUMN BY MINUS PIVOT (VALUE OF PIVOT ELEMENT IS     MINV 098
C        CONTAINED IN BIGA)                                          MINV 099
C                                                                    MINV 100
   45 IF(BIGA) 48,46,48                                              MINV 101
   46 D=0.0                                                          MINV 102
      RETURN                                                         MINV 103
   48 DO 55 I=1,N                                                    MINV 104
      IF(I-K) 50,55,50                                               MINV 105
   50 IK=NK+I                                                        MINV 106
      A(IK)=A(IK)/(-BIGA)                                            MINV 107
   55 CONTINUE                                                       MINV 108
C                                                                    MINV 109
C        REDUCE MATRIX                                               MINV 110
C                                                                    MINV 111
      DO 65 I=1,N                                                    MINV 112
      IK=NK+I                                                        MINV 113
      HOLD=A(IK)                                                     MINV M01
      IJ=I-N                                                         MINV 114
      DO 65 J=1,N                                                    MINV 115
      IJ=IJ+N                                                        MINV 116
      IF(I-K) 60,65,60                                               MINV 117
   60 IF(J-K) 62,65,62                                               MINV 118
   62 KJ=IJ-I+K                                                      MINV 119
      A(IJ)=HOLD*A(KJ)+A(IJ)                                         MINV M02
   65 CONTINUE                                                       MINV 121
C                                                                    MINV 122
C        DIVIDE ROW BY PIVOT                                         MINV 123
C                                                                    MINV 124
      KJ=K-N                                                         MINV 125
      DO 75 J=1,N                                                    MINV 126
      KJ=KJ+N                                                        MINV 127
      IF(J-K) 70,75,70                                               MINV 128
   70 A(KJ)=A(KJ)/BIGA                                               MINV 129
   75 CONTINUE                                                       MINV 130
C                                                                    MINV 131
C        PRODUCT OF PIVOTS                                           MINV 132
C                                                                    MINV 133
      D=D*BIGA                                                       MINV 134
C                                                                    MINV 135
C        REPLACE PIVOT BY RECIPROCAL                                 MINV 136
C                                                                    MINV 137
      A(KK)=1.0/BIGA                                                 MINV 138
   80 CONTINUE                                                       MINV 139
C                                                                    MINV 140
C        FINAL ROW AND COLUMN INTERCHANGE                            MINV 141
C                                                                    MINV 142
```

```
      K=N                                                          MINV 143
  100 K=(K-1)                                                      MINV 144
      IF(K) 150,150,105                                            MINV 145
  105 I=L(K)                                                       MINV 146
      IF(I-K) 120,120,108                                          MINV 147
  108 JQ=N*(K-1)                                                   MINV 148
      JR=N*(I-1)                                                   MINV 149
      DO 110 J=1,N                                                 MINV 150
      JK=JQ+J                                                      MINV 151
      HOLD=A(JK)                                                   MINV 152
      JI=JR+J                                                      MINV 153
      A(JK)=-A(JI)                                                 MINV 154
  110 A(JI) =HOLD                                                  MINV 155
  120 J=M(K)                                                       MINV 156
      IF(J-K) 100,100,125                                          MINV 157
  125 KI=K-N                                                       MINV 158
      DO 130 I=1,N                                                 MINV 159
      KI=KI+N                                                      MINV 160
      HOLD=A(KI)                                                   MINV 161
      JI=KI-K+J                                                    MINV 162
      A(KI)=-A(JI)                                                 MINV 163
  130 A(JI) =HOLD                                                  MINV 164
      GO TO 100                                                    MINV 165
  150 RETURN                                                       MINV 166
      END
```

APPENDIX VIII

PROGRAM LISTINGS AND SAMPLE DATA

c) Program BFINST
(Inelastic buckling analysis)

PROGRAM BFINST

THIS PROGRAM ENABLES A FINITE STRIP BUCKLING ANALYSIS OF FOLDED PLATE STRUCTURES SUCH AS THIN-WALLED OPEN CROSS-SECTIONS. AN INELASTIC BUCKLING ANALYSIS MAY BE PERFORMED BY INSERTING THE YIELDED MATERIAL PROPERTIES IN THE YIELDED PANELS OF THE CROSS-SECTION. THE NODAL LINES OF THE CROSS-SECTION MAY BE RESTRAINED FROM DISPLACEMENT OR ROTATION. THE BUCKLING EIGENVALUE IS OBTAINED FROM THE LONGITUDINAL STRESS DISTRIBUTION WHICH IS APPLIED AT THE NODES.

DATA SPECIFICATION

THE DATA IS PREPARED SUCH THAT THE LONGITUDINAL AXIS OF THE MEMBER CORRESPONDS TO THE Z AXIS OF THE MEMBER AXIS SYSTEM.

1. MEMBER NUMBER.

2. NUMBER OF NODAL LINES , NUMBER OF ELEMENTS , BUCKLING MODE NUMBER , DUMMY VARIABLE (1) AND THE LENGTH.

3. NODE NUMBER , X AND Y COORDINATES , THE NODAL LINE RESTRAINTS WHICH MAY BE APPLIED (THE RESTRAINTS ARE THE DISPLACEMENTS IN THE X,Y AND Z DIRECTIONS AND ROTATION ABOUT THE Z AXIS) AND THE LONGITUDINAL STRESS AT THE NODE. THIS IS REPEATED FOR EACH NODE.

4. ELEMENT NUMBER , CONNECTING NODES , ELEMENT THICKNESS AND THE FOLLOWING MATERIAL PROPERTIES :-

   YOUNG'S MODULUS IN THE LONGITUDINAL DIRECTION
   YOUNG'S MODULUS IN THE TRANSVERSE DIRECTION
   POISSON'S RATIO IN THE LONGITUDINAL DIRECTION
   POISSON'S RATIO IN THE TRANSVERSE DIRECTION
   SHEAR MODULUS

   THIS IS REPEATED FOR EACH ELEMENT.

5. PROGRAM EXIT (-1).

SAMPLE DATA

THE DATA FOR A PARTICULAR BUCKLING ANALYSIS OF THE EXAMPLE PRESENTED IN SECTION 7.7.2 IS GIVEN BELOW.

```
1
10 9 1 1 150.0
1 76.0 137.0 1 1 1 1 231.9
2 76.0 152.0 1 1 1 1 42.5
3 23.01 152.0 1 1 1 1 -320.0
4 0.0 152.0 1 1 1 1 -320.0
5 0.0 126.53 1 1 1 1 -320.0
6 0.0 17.91 1 1 1 1 320.0
7 0.0 0.0 1 1 1 1 320.0
8 16.36 0.0 1 1 1 1 320.0
9 76.0 0.0 1 1 1 1 -67.7
10 76.0 15.0 1 1 1 1 -258.1
1 1 2 1.86 205000.0 205000.0 0.3 0.3 78800.0
2 2 3 1.86 205000.0 205000.0 0.3 0.3 78800.0
3 3 4 1.86 6212.1 6212.1 0.5 0.5 19700.0
4 4 5 1.86 6212.1 6212.1 0.5 0.5 19700.0
5 5 6 1.86 205000.0 205000.0 0.3 0.3 78800.0
6 6 7 1.86 6212.1 6212.1 0.5 0.5 19700.0
7 7 8 1.86 6212.1 6212.1 0.5 0.5 19700.0
8 8 9 1.86 205000.0 205000.0 0.3 0.3 78800.0
9 9 10 1.86 205000.0 205000.0 0.3 0.3 78800.0
-1
```

```
C      PROGRAM BFINST
C
C      FINITE STRIP BUCKLING ANALYSIS
C
C
       COMMON AGAT(60,60),ASAT(60,60),X(60)
      0DIMENSION  S(8,8) ,SDAT(40) ,AA(4,8) ,AB(4,8) ,SAT(8,4) ,
      1 JTYPE(20,4),JNTDF(20),
      2 CORD(20,2),CALPHA(20),SALPHA(20),JNTDFT(20),D(4),MCON(20,2),
      3 G(8,8),GAT(8,4),SIGMA(20),
      4 EX(20),EZ(20),PX(20),PZ(20),GP(20)
C
       DOUBLE PRECISION AGAT,ASAT,X,TEMPD,S,G,AA,AB,SAT,GAT
       INTEGER PIN,FNAM1(3),FNAM2(3)
       WRITE(1,9009)
 9009 FORMAT('FINITE STRIP BUCKLING ANALYSIS')
       WRITE(1,8)
    8 FORMAT('WHAT IS THE NAME OF YOUR DATA FILE')
       READ(1,7)(FNAM2(I),I=1,3)
    7 FORMAT(3A2)
       WRITE(1,11)
   11 FORMAT('DO YOU WANT OUTPUT ON FILE OR VDU')
       WRITE(1,12)
   12 FORMAT('TYPE 6 FOR FILE OR 1 FOR VDU')
       READ(1,13) NO
   13 FORMAT(I5)
       IF(NO-6) 9020,9014,9020
 9014 WRITE(1,9015)
 9015 FORMAT('WHAT IS THE NAME OF YOUR OUTPUT FILE')
       READ(1,9016) (FNAM1(I),I=1,3)
 9016 FORMAT(3A2)
 9020 CONTINUE
C
C      INPUT THE PLATE NO.  EXIT IF NEGATIVE
C
   10 READ(5,20) JJ
   20 FORMAT(I5)
       IF(JJ) 30,40,40
   30 CONTINUE
       STOP
C
C      INPUT NUMBER OF NODES,STRIPS,MODES,AND THE LENGTH
C
   40 READ(5,50) JCT,NM,NMOD,NSON,OLEN
   50 FORMAT(4I5,F10.3)
C
C      READ NODE COORDS AND RESTRAINTS
C
       DO 200 N1=1,JCT
  200 READ(5,205) NNUM,(CORD(NNUM,N2),N2=1,2),(JTYPE(NNUM,N2),N2=1,4)
```

```
     1 ,SIGMA(NNUM)
  205 FORMAT(I5,2F10.3,4I5,F10.3)
C
C     READ STRIP PROPERTIES
C
      DO 210 N1=1,NM
      N2=2*N1-1
  210 READ(5,215) NST,(MCON(NST,J),J=1,2),SDAT(N2),EX(N1),EZ(N1),PX(N1),
     1 PZ(N1),GP(N1)
  215 FORMAT(3I5,6F12.3)
C
C      CALCULATE DEGREES OF FREEDOM
C
      L1=0
      DO 220 N1=1,JCT
      L2=0
      JNTDFT(N1)=L1
      DO 225 N2=1,4
      L1=L1+JTYPE(N1,N2)
  225 L2=L2+JTYPE(N1,N2)
      JNTDF(N1)=L2
  220 CONTINUE
C
      KJ=L1+1
C
C     CALCULATE STRIP WIDTHS AND ORIENTATIONS
C
      DO 230 N1=1,NM
      J1=MCON(N1,1)
      J2=MCON(N1,2)
      OLX=CORD(J2,1)-CORD(J1,1)
      OLY=CORD(J2,2)-CORD(J1,2)
      SDAT(2*N1)=SQRT((OLX*OLX)+(OLY*OLY))
      CALPHA(N1)=OLX/SDAT(2*N1)
      SALPHA(N1)=OLY/SDAT(2*N1)
  230 CONTINUE
C
C     PRINT GENERAL HEADINGS AND DATA FOR VERIFICATION
C
      WRITE(NO,300) JJ
 3000FORMAT(30HBUCKLING ANALYSIS OF PLATE NO.,I5,X,
     120HUSING PROGRAM BFINST)
      WRITE(NO,301) NM
  301 FORMAT(/19H NUMBER OF ELEMENTS,I5)
      WRITE(NO,302) OLEN
  302 FORMAT(/14H MEMBER LENGTH,F10.3)
      WRITE(NO,303)
  303 FORMAT(//28H ELEMENT MATERIAL PROPERTIES)
      WRITE(NO,304)
  304 FORMAT(/47H ELEMENT      EX        EZ      PX     PZ      G)
```

```
      DO 305 I=1,NM
  305 WRITE(NO,306) I,EX(I),EZ(I),PX(I),PZ(I),GP(I)
  306 FORMAT(I5,4X,2E10.3,2F6.2,E10.3)
      WRITE(NO,307)
  307 FORMAT(//19H ELEMENT DIMENSIONS)
      WRITE(NO,308)
  308 FORMAT(/58H ELEMENT  J1   J2      T          B     COS ALPHA SIN AL
     1PHA)
      DO 321 N1=1,NM
      NN1=2*N1-1
      NN2=2*N1
      J1=MCON(N1,1)
      J2=MCON(N1,2)
      WRITE(NO,322) N1,(J1,J2,(SDAT(N2),N2=NN1,NN2),CALPHA(N1),SALPHA(N1
     1))
  322 FORMAT(I5,2X,2I5,4F10.3)
  321 CONTINUE
C
      WRITE(NO,311) JCT
  311 FORMAT(//16H NUMBER OF NODES,I5)
      WRITE(NO,312)
  312 FORMAT(/59H NODE  X CORD    Y CORD  DEGREES OF FREEDOM=1 CONSTRAIN
     1TS=0)
      WRITE(NO,313)
  313 FORMAT(59H                              XD   YD   ZD   ZR    LONG STR
     1ESS)
      DO 315 N1=1,JCT
  315 WRITE(NO,314) N1,(CORD(N1,N4),N4=1,2),(JTYPE(N1,N2),N2=1,4),
     1SIGMA(N1)
  314 FORMAT(I4,F8.1,F10.1,1X,4I5,4X,F10.3)
C
C     INITIALISE MATRICES
C
      II=1
      ZI=II
      PI=3.14159265
  417 CONTINUE
      DO 410 N1=1,L1
      DO 410 N2=1,L1
      AGAT(N1,N2)=0.0
  410 ASAT(N1,N2)=0.0
  420 CONTINUE
      I=0
  430 CONTINUE
      I=I+1
      DO 440 N1=1,4
      DO 440 N2=1,8
      AA(N1,N2)=0.0
  440 AB(N1,N2)=0.0
C
```

```
C     GENERATE THE [A] MATRIX FOR THE ITH STRIP
C
      NN1=2*I-1
      NN2=2*I
C
      AA(1,1)=-SALPHA(I)
      AA(1,3)=3.*SALPHA(I)
      AA(1,4)=-2.*SALPHA(I)
      AA(1,5)=CALPHA(I)
      AA(1,6)=-CALPHA(I)
      AA(2,1)=CALPHA(I)
      AA(2,3)=-3.*CALPHA(I)
      AA(2,4)=2.*CALPHA(I)
      AA(2,5)=SALPHA(I)
      AA(2,6)=-SALPHA(I)
      AA(3,7)=1.0
      AA(3,8)=-1.0
      AA(4,2)=SDAT(NN2)
      AA(4,3)=-2.*SDAT(NN2)
      AA(4,4)=SDAT(NN2)
      AB(1,3)=-AA(1,3)
      AB(1,4)=-AA(1,4)
      AB(1,6)=-AA(1,6)
      AB(2,3)=-AA(2,3)
      AB(2,4)=-AA(2,4)
      AB(2,6)=-AA(2,6)
      AB(3,8)=-AA(3,8)
      AB(4,3)=-SDAT(NN2)
      AB(4,4)=SDAT(NN2)
C
C     REDUCTION OF THE [A] MATRIX FOR CONSTRAINTS AT END A
C
      N1=0
      DO 510 N2=1,4
      J1=MCON(I,1)
      IF(JTYPE(J1,N2))510,510,500
  500 N1=N1+1
      DO 505 N3=1,8
  505 AA(N1,N3)=AA(N2,N3)
  510 CONTINUE
C
C     REDUCTION OF THE [A] MATRIX FOR CONSTRAINTS AT END B
C
      N1=0
      DO 560 N2=1,4
      J2=MCON(I,2)
      IF(JTYPE(J2,N2)) 560,560,550
  550 N1=N1+1
      DO 555 N3=1,8
  555 AB(N1,N3)=AB(N2,N3)
```

```
  560 CONTINUE
C
C     BUILD THE [S] MATRIX FOR THE ITH STRIP
C
      DO 600 N1=1,8
      DO 600 N2=1,8
      G(N1,N2)=0.0
  600 S(N1,N2)=0.0
C
      DZ=EZ(I)*SDAT(NN1)**3/(12.0*(1.0-PX(I)*PZ(I)))
      D1=PX(I)*EZ(I)*SDAT(NN1)**3/(12.0*(1.0-PX(I)*PZ(I)))
      DXZ=GP(I)*SDAT(NN1)**3/12.0
      DX=EX(I)*SDAT(NN1)**3/(12.0*(1.0-PX(I)*PZ(I)))
      DDZ=DZ*(ZI*PI/OLEN)**4
      DD1=D1*(ZI*PI/(OLEN*SDAT(NN2)))**2
      DDXZ=DXZ*(ZI*PI/(OLEN*SDAT(NN2)))**2
      DDX=DX/SDAT(NN2)**4
C
      ZKM=ZI*PI/OLEN
      E1=EX(I)/((1.0-PX(I)*PZ(I))*SDAT(NN2)**2)
      E2=EZ(I)*ZKM**2/(1.0-PX(I)*PZ(I))
      E12=PX(I)*EZ(I)*ZKM/((1.0-PX(I)*PZ(I))*SDAT(NN2))
      GG=GP(I)*ZKM**2
      BZKM=SDAT(NN2)*ZKM
C
  603 S(1,1)=DDZ/2.0
      S(1,2)=DDZ/4.0
      S(1,3)=DDZ/6.0-DD1
      S(1,4)=DDZ/8.0-3.*DD1/2.0
      S(2,1)=S(1,2)
      S(2,2)=DDZ/6.0+2.0*DDXZ
      S(2,3)=DDZ/8.0+2.0*DDXZ-DD1/2.0
      S(2,4)=DDZ/10.0+2.*DDXZ-DD1
      S(3,1)=S(1,3)
      S(3,2)=S(2,3)
      S(3,3)=DDZ/10.+8.*DDXZ/3.0-2.*DD1/3.+2.*DDX
      S(3,4)=DDZ/12.0+3.0*DDXZ-DD1+3.0*DDX
      S(4,1)=S(1,4)
      S(4,2)=S(2,4)
      S(4,3)=S(3,4)
      S(4,4)=DDZ/14.0+18.0*DDXZ/5.0-6.0*DD1/5.0+6.0*DDX
C
      S(5,5)=GG/2.0
      S(5,6)=GG/4.0
      S(5,8)=GG/(2.0*BZKM)
      S(6,5)=S(5,6)
      S(6,6)=GG/6.0+E1/2.0
      S(6,7)=-E12/2.0
      S(6,8)=-E12/4.0+GG/(4.0*BZKM)
      S(7,6)=S(6,7)
```

```
      S(7,7)=E2/2.0
      S(7,8)=E2/4.0
      S(8,5)=S(5,8)
      S(8,6)=S(6,8)
      S(8,7)=S(7,8)
      S(8,8)=E2/6.0+GG/(2.0*BZKM**2)
C
      DO 601 N1=1,8
      DO 601 N2=1,8
      TEMPD=SDAT(NN2)*OLEN
  601 S(N1,N2)=S(N1,N2)*TEMPD
C
      DO 602 N1=1,4
      DO 602 N2=1,4
      N3=N1+4
      N4=N2+4
      TEMPD=SDAT(NN1)
  602 S(N3,N4)=S(N3,N4)*TEMPD
C
      J1=MCON(I,1)
      J2=MCON(I,2)
      TEMP=((PI**2)*SDAT(NN1)*SDAT(NN2)/(2.0*OLEN))
      FAC1=TEMP*SIGMA(J1)
      FAC2=TEMP*(SIGMA(J2)-SIGMA(J1))
C
      G(1,1)=FAC1+FAC2/2.
      G(1,2)=FAC1/2.+FAC2/3.
      G(1,3)=FAC1/3.+FAC2/4.
      G(1,4)=FAC1/4.+FAC2/5.
      G(2,1)=G(1,2)
      G(3,1)=G(1,3)
      G(4,1)=G(1,4)
      G(2,2)=G(1,3)
      G(2,3)=G(1,4)
      G(2,4)=FAC1/5.+FAC2/6.
      G(3,2)=G(2,3)
      G(4,2)=G(2,4)
      G(3,3)=G(2,4)
      G(3,4)=FAC1/6.+FAC2/7.
      G(4,3)=G(3,4)
      G(4,4)=FAC1/7.+FAC2/8.
C
      G(5,5)=G(1,1)
      G(5,6)=G(1,2)
      G(6,5)=G(5,6)
      G(6,6)=G(2,2)
      G(7,7)=G(5,5)
      G(7,8)=G(5,6)
      G(8,7)=G(7,8)
      G(8,8)=G(6,6)
```

```
C
C     GENERATE THE GLOBAL STIFFNESS MATRIX
C
  605 CONTINUE
      WRITE(1,606) I
  606 FORMAT(37H FORMING STIFFNESS MATRIX FOR ELEMENT,I5)
      J1=MCON(I,1)
      J2=MCON(I,2)
      JNTDT1=JNTDFT(J1)
      JNTDT2=JNTDFT(J2)
      JNTDFI=JNTDF(J1)
      JNTDIP=JNTDF(J2)
      IF(JNTDFI) 725,725,699
  699 DO 700 N1=1,8
      DO 700 N2=1,JNTDFI
      SAT(N1,N2)=0.0
      GAT(N1,N2)=0.0
      DO 700 N3=1,8
      GAT(N1,N2)=GAT(N1,N2)+G(N1,N3)*AA(N2,N3)
  700 SAT(N1,N2)=SAT(N1,N2)+S(N1,N3)*AA(N2,N3)
      DO 710 N1=1,JNTDFI
      DO 710 N2=1,JNTDFI
      N1G=N1+JNTDT1
      N2G=N2+JNTDT1
      DO 710 N3=1,8
      AGAT(N1G,N2G)=AGAT(N1G,N2G)+AA(N1,N3)*GAT(N3,N2)
  710 ASAT(N1G,N2G)=ASAT(N1G,N2G)+AA(N1,N3)*SAT(N3,N2)
  725 CONTINUE
      IF(JNTDIP) 765,765,727
  727 DO 730 N1=1,8
      DO 730 N2=1,JNTDIP
      SAT(N1,N2)=0.0
      GAT(N1,N2)=0.0
      DO 730 N3=1,8
      GAT(N1,N2)=GAT(N1,N2)+G(N1,N3)*AB(N2,N3)
  730 SAT(N1,N2)=SAT(N1,N2)+S(N1,N3)*AB(N2,N3)
      DO 740 N1=1,JNTDIP
      DO 740 N2=1,JNTDIP
      N1G=N1+JNTDT2
      N2G=N2+JNTDT2
      DO 740 N3=1,8
      AGAT(N1G,N2G)=AGAT(N1G,N2G)+AB(N1,N3)*GAT(N3,N2)
  740 ASAT(N1G,N2G)=ASAT(N1G,N2G)+AB(N1,N3)*SAT(N3,N2)
      IF(JNTDFI) 755,755,747
  747 DO 750 N1=1,JNTDFI
      DO 750 N2=1,JNTDIP
      N1G=N1+JNTDT1
      N2G=N2+JNTDT2
      DO 750 N3=1,8
      AGAT(N1G,N2G)=AGAT(N1G,N2G)+AA(N1,N3)*GAT(N3,N2)
```

```
      ASAT(N1G,N2G)=ASAT(N1G,N2G)+AA(N1,N3)*SAT(N3,N2)
      AGAT(N2G,N1G)=AGAT(N1G,N2G)
  750 ASAT(N2G,N1G)=ASAT(N1G,N2G)
  755 CONTINUE
  765 CONTINUE
C
      IF (NM-I) 770,770,430
C
  770 CONTINUE
C
C     CALCULATE EIGENVALUE AND EIGENVECTOR
C
      DO 1231 I=1,NMOD
      CALL EIGEN(L1,I,0.0001,TLAM)
C
C     OUTPUT THE NODE DEFORMATIONS
C
      TLAM=1./TLAM
      LL=0
 1004 WRITE(NO,1005) TLAM
      WRITE(7,1223) TLAM,I
 1223 FORMAT(F10.6,I5)
 1005 FORMAT(/28H EIGENVECTOR FOR EIGENVALUE=,F10.6,I5)
      WRITE(NO,1006)
 1006 FORMAT('  X-DEFLN   Y-DEFLN   Z-DEFLN   Z-ROTN ')
      DO 1230 J=1,JCT
      DO 1229 K=1,4
      IF(JTYPE(J,K))1030,1030,1020
 1020 LL=LL+1
      IF(K-3) 1021,1022,1021
 1021 D(K)=X(LL)
      GOTO 1023
 1022 D(K)=X(LL)
 1023 CONTINUE
      GO TO 1040
 1030 D(K)=-0.0
 1040 CONTINUE
 1229 CONTINUE
      WRITE(NO,1221) (D(K),K=1,4)
 1230 WRITE(7,1222) (D(K),K=1,4)
 1221 FORMAT(4F10.3)
 1231 CONTINUE
 1222 FORMAT(4F12.5)
      GOTO 10
C
      END
C
C     DIRECT EIGENVALUE CALCULATOR
C
C
```

```
      SUBROUTINE EIGEN(L,NE,E,TLAM)
      COMMON C(60,60),A(60,60),P(60)
      DOUBLE PRECISION C,A,P,DTLAM,DIAG,SUM,XRP12,TEMP,XK,RS
C
C     SYMMETRIC FACTORISATION OF [A] MATRIX TO [L][L']
C
      IF(NE-1) 419,419,1012
  419 CONTINUE
      NFLAG=0
      WRITE(1,410)
  410 FORMAT('TRIANGULATION OF STIFFNESS MATRIX')
      DO 400 I=1,L
      IM1=I-1
      SUM=0.0
      IF(IM1) 402,402,401
  401 DO 403 N=1,IM1
  403 SUM=SUM+A(N,I)**2
  402 DIAG=A(I,I)-SUM
      IF(DIAG) 407,407,406
  406 A(I,I)=DSQRT(DIAG)
      IP1=I+1
      IF(IP1-L) 409,409,400
  409 DO 404 J=IP1,L
      SUM=0.0
      IF(IM1) 404,404,408
  408 DO 405 N=1,IM1
  405 SUM=SUM+A(N,I)*A(N,J)
  404 A(I,J)=(A(I,J)-SUM)/A(I,I)
      GOTO 400
  407 NFLAG=1
  400 CONTINUE
C
C     REDUCTION TO STANDARD FORM [B]=[L]-1[C][L']-1
C
      WRITE(1,510)
  510 FORMAT('REDUCTION TO STANDARD FORM')
      IF(NFLAG) 505,505,506
  506 WRITE(1,507)
  507 FORMAT('NON POSITIVE DEFINITE [A] MATRIX')
      RETURN
  505 DO 500 I=1,L
      DO 501 J=1,L
      IM1=I-1
      SUM=0.0
      IF(IM1) 503,503,502
  502 DO 504 N=1,IM1
  504 SUM=SUM+A(N,I)*C(N,J)
  503 C(I,J)=(C(I,J)-SUM)/A(I,I)
  501 CONTINUE
  500 CONTINUE
```

```
C
      DO 600 J=1,L
      DO 601 I=1,L
      JM1=J-1
      SUM=0.0
      IF(JM1) 603,603,602
  602 DO 604 N=1,JM1
  604 SUM=SUM+C(I,N)*A(N,J)
  603 C(I,J)=(C(I,J)-SUM)/A(J,J)
  601 CONTINUE
  600 CONTINUE
C
C     REDUCTION OF [B] MATRIX TO TRIDIAGONAL FORM
C     USING HOUSEHOLDERS METHOD
C
      WRITE(1,710)
  710 FORMAT('HOUSEHOLDERS TRIDIAGONALISATION')
      LM2=L-2
      DO 700 I=1,LM2
      IP1=I+1
      IP2=I+2
      SUM=0.
      DO 720 J=IP1,L
  720 SUM=SUM+C(I,J)**2
      RS=DSQRT(SUM)
      TEMP=DSIGN(1.0D00,C(I,IP1))/(2.0*RS)
      XRP12=0.5+C(I,IP1)*TEMP
      C(IP1,I)=DSQRT(XRP12)
      TEMP=TEMP/C(IP1,I)
      DO 730 J=IP2,L
  730 C(J,I)=C(I,J)*TEMP
      DO 745 K=IP1,L
      SUM=0.0
      DO 740 J=IP1,L
      KK=K-I+1
  740 SUM=SUM+C(J,K)*C(J,I)
  745 P(KK)=SUM
      TC=C(I,IP1)
      TEMP=SIGN(1.,TC)
      C(I,IP1)=-TEMP*RS
      SUM=0.0
      DO 760 J=IP1,L
      JJ=J-I+1
  760 SUM=SUM+C(J,I)*P(JJ)
      XK=SUM
      DO 765 J=IP1,L
      JJ=J-I+1
  765 P(JJ)=P(JJ)-XK*C(J,I)
      DO 775 K=IP1,L
      KK=K-I+1
```

```
      DO 770 J=K,L
      JJ=J-I+1
      C(K,J)=C(K,J)-2.0*C(K,I)*P(JJ)-2.0*C(J,I)*P(KK)
  770 C(J,K)=C(K,J)
  775 CONTINUE
  700 CONTINUE
C
 1012 CONTINUE
C
C     METHOD OF BISECTIONS EVALUATION OF CHOSEN EIGENVALUE
C
      TLAM=0.
      NS=0
      CALL STURM(NS,TLAM,L)
      IF(NS-L) 903,902,902
  903 WRITE(1,904)
  904 FORMAT('WARNING NEGATIVE EIGENVALUES')
  902 TLAM=1.0
  910 NS=0
      CALL STURM(NS,TLAM,L)
      IF(NS-NE) 900,901,901
  901 TLAM=TLAM*10.
      GOTO 910
  900 AA=0.
      B=TLAM
      TLAM=(AA+B)/2.0
  911 CALL STURM(NS,TLAM,L)
      IF(NS-NE) 905,906,906
  905 TLAM=0.75*AA+0.25*B
      B=(AA+B)/2.0
      GOTO 907
  906 TLAM=0.25*AA+0.75*B
      AA=(AA+B)/2.0
  907 RANGE=(B-AA)/B
      WRITE(1,909) TLAM
      IF(RANGE-E) 908,911,911
  908 CONTINUE
  909 FORMAT(21H   CHOSEN EIGENVALUE=,F12.8)
C
C     EIGENVECTOR CALCULATION BY BACKSUBSTITUTION
C     FOR UNIT VECTOR  (WILKINSONS METHOD)
C
      DTLAM=TLAM
      WRITE(1,1011)
 1011 FORMAT('BACKSUBSTITUTION FOR EIGENVECTOR')
      DO 1000 I=1,L
 1000 P(I)=1.0
      NCOUNT=0
 1003 CONTINUE
      DO 1001 I=1,L
```

```
 1001 C(I,I)=C(I,I)-DTLAM
      LM1=L-1
      LM2=L-2
      C(1,3)=C(2,2)-(C(1,2)**2)/C(1,1)
      P(2)=P(2)-(C(IM1,I)**2)/C(IM1,IM1)
      DO 1010 I=3,LM1
      IM1=I-1
      IM2=I-2
      IP1=I+1
      C(IM1,IP1)=C(I,I)-(C(IM1,I)**2)/C(IM2,I)
 1010 P(I)=P(I)-(C(IM1,I)*P(IM1))/C(IM2,I)
      TEMP=C(L,L)-(C(LM1,L)**2)/C(LM2,L)
      P(L)=P(L)/TEMP
      DO 1020 J=2,LM1
      I=L-J+1
      IP1=I+1
      IM1=I-1
 1020 P(I)=(P(I)/C(IM1,IP1))-(C(I,IP1)*P(IP1)/C(IM1,IP1))
      P(1)=P(1)/C(1,1)-(C(1,2)*P(2))/C(1,1)
      DO 1002 I=1,L
 1002 C(I,I)=C(I,I)+DTLAM
      NCOUNT=NCOUNT+1
      IF(NCOUNT-2) 1003,1004,1004
 1004 CONTINUE
C
C     REVERSING HOUSEHOLDERS PROCESS
C     TO CALCULATE EIGENVECTOR (V)
C
      DO 1100 J=3,L
      I=L-J+2
      SUM=0.0
      IM1=I-1
      DO 1110 M=I,L
 1110 SUM=SUM+C(M,IM1)*P(M)
      DO 1120 M=I,L
 1120 P(M)=P(M)-2.0*SUM*C(M,IM1)
 1100 CONTINUE
C
C     BACKSUBSTITUTION TO CALCULATE (X)=[L']-1(V)
C
      DO 1200 M=1,L
      I=L-M+1
      IP1=I+1
      SUM=0.0
      IF(IP1-L) 1220,1220,1230
 1220 DO 1210 J=IP1,L
 1210 SUM=(SUM+A(I,J)*P(J))
 1230 P(I)=(P(I)-SUM)/A(I,I)
 1200 CONTINUE
      TEMP=P(1)
```

```
      DO 1031 I=2,L
      IM1=I-1
      IF(DABS(P(I))-DABS(TEMP)) 1031,1031,1032
 1032 TEMP=P(I)
 1031 CONTINUE
      DO 1030 I=1,L
 1030 P(I)=P(I)/TEMP
C
      RETURN
      END
C
C     EVALUATION OF STURMS SEQUENCE
C
      SUBROUTINE STURM(NS,TLAM,L)
      COMMON C(60,60),A(60,60),P(60)
      DOUBLE PRECISION C,A,P,DTLAM,PR,PRM1,PRM2
      DTLAM=TLAM
      NS=0
      PRM2=1.0
      PRM1=C(1,1)-DTLAM
      IF(DSIGN(1.0D00,PRM2)-DSIGN(1.0D00,PRM1)) 801,800,801
  800 NS=1
  801 DO 820 J=2,L
      JM1=J-1
      PR=(C(J,J)-DTLAM)*PRM1-(C(JM1,J)**2)*PRM2
      IF(DSIGN(1.0D00,PRM1)-DSIGN(1.0D00,PR)) 803,802,803
  802 NS=NS+1
  803 PRM2=PRM1
  820 PRM1=PR
      WRITE(1,821) NS
  821 FORMAT(4H NS=,I5)
      RETURN
      END
```

International Conference On

THIN-WALLED STRUCTURES

3rd - 6th April 1979

THE BEHAVIOUR OF PORTAL FRAMES COMPOSED OF COLD-FORMED MEMBERS

by

A H Baigent and G J Hancock

University of Strathclyde

Organised in association with CONSTRADO and The Institution of Structural Engineers

THE BEHAVIOUR OF PORTAL FRAMES COMPOSED OF COLD-FORMED MEMBERS

A H Baigent and G J Hancock

Department of Civil Engineering, University of Sydney

Synopsis

An investigation into the behaviour of low rise structures composed of cold-formed members is described. An experimental study, in which seven pitched-roof portal frames were tested to destruction, is presented. The frames were subjected to three different loading patterns and supported by two different sets of lateral restraints. The elastic response of each frame is compared with a prediction from a matrix stiffness analysis which included thin-walled torsion theory and cross-section monosymmetry. Cross-sectional distortion was incorporated in the study using the finite strip method of analysis.

1 INTRODUCTION

One of the most interesting developments in structural steelwork during recent years has been the widespread and increasing use of cold-formed members. The designer of a structure composed of cold-formed members is interested in the way both the individual members and complete structure behave. If rigid joints are used to join the members, the structure will exhibit strength and stiffness characteristics different from those of the individual members. While many tests on isolated cold-formed members have been reported, relatively few fully instrumented tests on representative frame systems have been carried out.

In this paper, the results of an investigation into the behaviour of low rise structures composed of light-gauge members are presented. An experimental study was made with half scale models of a representative frame system constructed from cold-formed members. The stiffness characteristics of these structures are investigated in this paper. The measured in-plane and out-of-plane deformations of the test structures are compared with predictions produced using a linear elastic matrix stiffness analysis. This analysis included the effects which must be considered in structures of this type. These effects are warping torsion, cross-section monosymmetry and the specific nature of the joints connecting the members. Sectional distortion

also influences the stiffness of the structure and has been included in the study.

2 *EXPERIMENTAL INVESTIGATION*

A. Frame and Section Geometry

An experimental study of the behaviour of pitched-roof portal frames was made by testing a total of seven frames. Each frame was constructed from cold-formed channel sections bent about the major axis. The geometry of the channel is shown in Fig 1. The overall geometry of the test frames is shown in Fig 2. The positions of the lateral restraints are also shown in this figure. The restraints were attached to the outside flange of the members.

B. Joints

All members were bolted through their webs to joints which consisted of stiffened plates. Figure 3 shows the construction of an eave joint. A cross-section through the joint shown in this figure, demonstrates the method of attachment of the section to the joint. Four 19 mm diameter high tensile friction-grip bolts were used at the end of each member. The bolts passed through a cover plate, the web of the cold-formed channel and finally the stiffened joint-plate. Thus, the webs of each cold-formed member were rigidly attached to the joint. The apex joint was of a similar construction to the eave joint. The joints used for the frame retained the simplicity required for erection purposes and also allowed continuity of the forces and moments from one member to another. The lower end of each stanchion was bolted to a pinned base joint which was attached to a laboratory test floor.

C. Lateral Restraints

In conventional frames, the purlins and girts have two main functions. Firstly, they support the cladding and transmit the external forces applied to the cladding onto the frame. Secondly, they provide restraint to the frame in a number of ways. The most obvious form of restraint is the prevention of the displacement, at the points of attachment, normal to the plane of the frame. Depending on the nature of the purlin to frame or girt to frame connection, torsional restraint may also be applied to the members of the frame. However, to simplify the experimental apparatus and the analytical considerations, the lateral restraints were designed to provide no torsional restraint. A complex arrangement of linkages and spherical bearings enabled the restraint to carry out its design functions. The restraints were distributed around the frame in such a way so as to approximate the actual positions of purlins and girts in a conventional structure. The point of restraint was located 50 mm beyond the outside flange of each member.

Provision was also made for a second series of lateral restraints to be attached to the frame. These restraints were fixed to the internal

flange of the frame and were also located 50 mm beyond the flange plate. This additional restraint had the effect of eliminating the longitudinal rotation of the member at the point of attachment. In conventional structures, restraint of this type is achieved using fly bracing attached to the purlins and girts. Fly bracing provisions were made opposite the third lateral restraint position in each stanchion and opposite the first and third restraint positions in each rafter.

D. Loads

Vertical loads could be applied at each of the rafter restraint points and horizontal forces could be applied at each of the stanchion restraint points. An arrangement of rods and spherical bearings enabled the forces to be applied at the points of lateral restraint. For downward vertical loading, a set of platforms was suspended from the loading points. This system ensured that the load remained vertical when the frame deformed.

The uplift vertical loading used the same loading platforms as the downward loading; however the cables from the loading beams were suspended from a moveable pulley system mounted on a loading rig. The loading rig also permitted the application of horizontal forces to each of the stanchions. A system of pulleys was used to apply the horizontal loads by means of gravity loads. Lead ingots and lead shot were placed on the loading platforms to apply the loads to the frame.

Three different loading patterns were chosen for the tests. Loading Case 1, shown in Fig 4, simulated vertical dead and live loading. The second and third loading cases were chosen to simulate particular wind loading situations. When designing industrial buildings in Australia, wind forces specified by the S.A.A. Loading Code (Part 2 - Wind Forces) (1) form an important design consideration. Hence loading cases that represented the two major types of wind loading were chosen. They were transverse and longitudinal wind loadings.

E. Test Sequence

Two series of tests were performed. Each series used the three loading cases summarised in Fig 4. The first series (Frames numbered 1, 2, 3 and 4) consisted of frames having only the restraints along the outside flange of the members. The second series of tests (Frames numbered 5, 6 and 7) had the additional lateral restraints (simulating fly braces) attached to the inside flange of the members. A summary of the test sequence is shown in Table 1.

F. Experimental Results

Each frame was tested to collapse and the ultimate load was obtained. All frames failed when local buckling occurred in the channel section at points of high bending moment. The failure loads of all frames are summarised in Table 1.

The in-plane deformations for Frame 2 are shown in Fig 5. The vertical

apex and rafter mid-point deflections are compared as are the horizontal eave and stanchion mid-point deflections for the left hand side of the frame. The figure shows the observed load-deflection response which was similar for all frames tested. This behaviour consisted firstly of the frame undergoing a linear response. When the load reached a value of approximately two-thirds of the ultimate load, a non-linear response followed. The frame exhibited a non-linear response until the attainment of the collapse load. At this point large deformations took place and resulted in collapse of the frame. The collapse load for Frame 2 has been shown in Fig 5. From the strain gauges used to monitor the strains in the peak moment regions, a value of load was obtained for the commencement of yield in these regions. The load at which the observed first yield took place is shown in Fig 5.

The corresponding deformations associated with out-of-plane movement of Frame 2 are shown in Fig 6. The rotations about the longitudinal axis of the left hand stanchion are shown for the mid-point position and the eave joint. The rotations about the longitudinal axis of the left hand rafter at the mid-point and apex joint are also shown. The deformations shown in Fig 6 exhibit a similar response to those shown in Fig 5. However the non-linear response began at a lower load than that measured for the in-plane deformation. The eccentrically applied loads on the rafters caused large deformations. These large deformations most likely caused the non-linear out-of-plane response before yielding.

Figure 7 shows the out-of-plane deformations for Frame 5 which was subjected to the same loading pattern as Frame 2 but was restrained by both internal and external restraints. The rotation about the longitudinal axis of the left hand stanchion measured at the mid-point and eave, and of the left hand rafter measured at the mid-point and apex, have been plotted in Fig 7. The rotations have been significantly reduced at the rafter mid-point and apex joint and to a lesser extent at the eave joint. However the rotations of the unloaded stanchion have not been greatly affected.

The linear load-deflection response of all the frames tested has been given in Table 1. In Table 1, the deformations at one-third of the collapse load have been divided by this load value to give a tabulated stiffness. The stiffer response of the frames with internal restraints when compared with the frame externally braced only, can be observed in the table. This occurred not only for Frame 5 when compared with Frames 1 and 2 but also for Frame 6 when compared with Frame 3 and for Frame 7 when compared with Frame 4. Loading Case 3 simulated suction on all members of the frame. Hence the values for the stiffnesses shown in Table 1 for this load case, are of negative sign when compared with Frames 1, 2 and 5 since the members moved upwards and outwards.

The measured rotations about the longitudinal axis of each member resulted from two structural effects. These were firstly, the torsional rotation of the member which was quite large as a result of the eccentricity of the load from the section shear centre. Secondly,

cross-sectional distortion caused the loaded flange to rotate relative to the web of the section. Significant rotations were measured in the loaded flange of the members of each frame throughout the first series of tests. In the second series, the internal bracing restricted the out-of-plane movements of the internal flanges. As demonstrated in Table 1, this resulted in the torsional component of the deformation being significantly reduced. However, the eccentricity of the applied loads still caused the same amount of cross-sectional distortion.

A more detailed description of the test results is given in (2).

3 *ANALYTICAL MODELLING*

A. The Behaviour of Thin-Walled Frames

The elastic response of a pitched-roof portal frame having the same geometry as the test frames was studied with the use of a linear elastic matrix stiffness analysis. The method included the thin-walled non-uniform torsion theory derived by Vlasov (3) and thin-walled cross-section monosymmetry. However, one area of behaviour which was not included within the matrix stiffness analysis of the thin-walled frame was the influence of cross-sectional distortion of the members. This effect is concerned with the localised response in a member and is influenced by the nature of the applied forces.

In order to predict the elastic response of the pitched-roof portal frames, it was necessary to include the effects of sectional distortion in the analytical prediction. The simple approach adopted for this study was to superimpose the distortional deformations at points of concentrated load on the rigid body sectional deformations. The distortional deformations at points of concentrated load were derived using a separate analysis.

B. Stiffness Analysis of Thin-Walled Frames

The stiffness matrix for the thin-walled element shown in Fig 8(b) was developed by considering the stiffness relationships between the actions shown in Fig 8(a) which are aligned with the centroidal and shear centre axes and the corresponding displacements of these axes. The axial forces at ends A and B (F_{zA}, F_{zB} respectively) can be related to the displacements of the centroidal axis at A and B (δ_{zA}, δ_{zB} respectively) by the linear stiffness relationships developed by Turner, Clough, Martin and Topp (4). These relationships are simply based on the axial rigidity EA.

The forces and moments (F_{xA}, M_{yA}, F_{xB}, M_{yB}) associated with flexure of the shear centre axis about the y-axis can be related to the corresponding displacements and rotations (δ_{xA}, θ_{yA}, δ_{xB}, θ_{yB}) of the shear centre axis at ends A and B by the stiffness relationships developed by Clough (5). These relationships are simply based on the flexural rigidity EI_y. Similarly the actions (F_{yA}, M_{xA}, F_{yB}, M_{xB}) associated with flexure of the shear centre axis about the x-axis can be related to the corresponding displacements and rotations (δ_{yA}, θ_{xA},

δ_{yB}, θ_{xB}) of the shear centre axis at ends A and B by the stiffness relationships based on the flexural rigidity EI_w.

The torques and bimoments (M_{zA}, B_{zA}, M_{zB}, B_{zB}) associated with torsion about the shear centre axis can be related to the corresponding torsional rotations and twists of the shear centre axis (θ_{zA}, θ'_{zA}, θ_{zB}, θ'_{zB}) by the stiffness relationships developed by Krahula (6). These relationships are simply based upon the torsional rigidity (GJ) and warping rigidity (EI_ω).

The 14 end actions shown in Fig 8(a) which are aligned with the shear centre and centroidal axes can be transformed to the origin axes (X', Y', Z') located on the web of the channel shown in Fig 8(b) using eqns (1) to (7).

$$F_{X'} = F_x \qquad (1)$$
$$F_{Y'} = F_y \qquad (2)$$
$$F_{Z'} = F_z \qquad (3)$$
$$M_{X'} = M_x + F_z \cdot b_{Y'} \qquad (4)$$
$$M_{Y'} = M_y \qquad (5)$$
$$M_{Z'} = M_z + F_x \cdot a_{Y'} \qquad (6)$$
$$B_{Z'} = B_z - M_y \cdot a_{Y'} \qquad (7)$$

Equations (1) to (6) are simply based on moment and force equilibrium. Equation (7) was derived by Vlasov to transform a bimoment from one axis system to another. A physical interpretation of this transformation is given by Zbirohowski-Koscia (7). It represents a transformation of the plane of the moment from the shear centre to the web of the channel.

A corresponding set of displacement transformations can be derived to evaluate the end displacements associated with the shear centre and centroidal axes from those associated with the origin axes (X', Y', Z').

$$\delta_x = \delta_{X'} + a_y \cdot \theta_{Z'} \qquad (8)$$
$$\delta_y = \delta_{Y'} \qquad (9)$$
$$\delta_z = \delta_{Z'} + b_y \cdot \theta_{X'} \qquad (10)$$
$$\theta_x = \theta_{X'} \qquad (11)$$
$$\theta_y = \theta_{Y'} - a_{Y'} \cdot \theta'_{Z'} \qquad (12)$$
$$\theta_z = \theta_{Z'} \qquad (13)$$
$$\theta'_z = \theta'_{Z'} \qquad (14)$$

Equations (8) to (11) and (13), (14) are simply based on rigid body motion. Equation (12) is based on warping compatibility and was derived by Vlasov. Hence the stiffness relationships relating the end actions in Fig 8(b) to the corresponding displacements can be derived from the stiffness relationships for the actions and displacements shown in Fig 8(a) transformed by the relationships in eqns (1) to (14).

The stiffness matrix for the complete frame can be derived by summing the actions from all members or elements at each joint of the frame accounting for the orientation of the X', Y', Z' axes of each element relative to the global axis system (X, Y, Z). The resulting stiffness

matrix is then reduced to allow for joint restraints. Lateral restraints such as those used on the test frames are not located on the X', Y', Z' axes of the elements. Hence they cannot be accounted for by the normal process of equating the relevant joint displacements to zero. However they can be accounted for by taking linear combinations of the relevant stiffness equations.

C. *Analytical Representation of Joints*

The bolted joints shown in Fig. 3 were designed to transmit moments and forces from the web of one channel member to the web of another channel member without any slip occurring in the bolted connections. The analytical representation of the joints is shown in Fig 9. Since the plate thickness of the joints including the cover plate was 25 mm and the plate thickness of the channel section was 1.86 mm, the joints were regarded as effectively rigid bodies linking the webs of two adjacent channel sections. In the analysis, they were treated as prismatic members with their shear centre and centroidal axes along the centreline of the plate. They were considered as having no warping torsion capability but transmitted all torque by Saint-Venant torsion. Hence they could not transmit a bimoment. Consequently the bimoment ($B_{Z'}$) on the end of the channel (calculated with respect to the X', Y', Z' axes) was zero. However from eqn (7),

$$B_z = M_y \cdot a_{Y'} \qquad \text{(15)}$$

Therefore a bimoment (B_z) calculated with respect to the shear centre of the channel and equal to the major axis moment multiplied by the distance from the shear centre to the channel web was applied on the end of the channel.

D. *Cross-Sectional Distortion*

The problem of the cross-sectional distortion of the member was studied by means of the finite strip method of structural analysis (8). The cross-sectional distortion was determined for the stanchions and rafters of each frame. In order to carry out the analysis, the channel cross-section was subdivided into a number of longitudinal strips. The two flanges and the web were subdivided into two strips each and the reinforcing lip on each flange was represented by a further strip. Each member analysed was considered to be simply supported at each end. The loads which were applied to the stanchions and rafters of each frame, were applied to the particular member for analysis. Lateral restraint simulating the restraining action of the purlins and girts was applied to the member in the analysis.

The distortional rotation was calculated from the difference between the rotation of the loaded flange, measured at the top of the web and the rotation of the unloaded flange measured at the base of the web. The distortional rotation was divided by the ultimate load to determine the distortional stiffness. Assuming superposition, the distortional stiffness was added to the torsional stiffness to obtain a total stiffness for the rotation of the flange about the longitudinal axis of the member. A more detailed summary of the analytical methods

is given in (2).

4 *DISCUSSION*

The analytical model derived to study the behaviour of each frame was programmed on a digital computer. The deformations produced by the computer program have been shown as stiffnesses and appear in Table 2. A comparison can be made with the experimental stiffnesses shown in Table 1.

The in-plane stiffnesses have been shown for the apex and left-hand eave joint for each frame tested. The agreement between the experimental and analytical models was favourable in all frames. However, the experimental apex results indicated a slightly more flexible response from the frames. The discrepancy between the analytical model and the experimental stiffnesses was of the order of a few percent. The consistency of the difference in stiffness indicates an influence that was present in each of the test frames. An explanation for the greater flexibility could lie in the behaviour of the joint system used in the frame tests. The stiffened plate joint to which the web of the cold-formed channel members were attached could result in a more flexible connection than that modelled analytically, because of the presence of shear straining of the cold-formed channel at the member to joint interface.

The stiffening of the in-plane response due to the additional simulated fly braces has been highlighted in the experimental results. The analytical model accurately predicts this stiffer response. A comparison between the accuracy of the in-plane deformation prediction and the experimental response is shown in Fig. 10. The figure shows the response of the vertical apex deflection of Frame 2. Plotted on this figure is the linear elastic prediction for a frame composed of prismatic members with a major axis moment of inertia identical with the cold-formed channel. Also plotted is the prediction of the linear elastic behaviour including the effects of thin-walled torsion theory and cross-section monosymmetry. The effect of member type on the elastic prediction for the apex joint movement is clearly shown.

The experimental out-of-plane stiffnesses for the stanchion and rafter mid-points have been shown in Table 1. The analytical prediction for the rafter mid-point is shown in Table 2. The prediction shown in Table 2 is composed of the rigid body rotation about the longitudinal axis and the distortional rotation. The influence of the distortional rotation is very significant in each of the frames. For Frames 5, 6 and 7, the simulated fly bracing has almost eliminated the rigid body rotation and hence the total rotation is a measurement of the cross-sectional distortion. The out-of-plane distortional model is thus quite accurate in the prediction of the distortional rotation.

5 *CONCLUSION*

The tests described in this report provide useful information on the response of light-gauge cold-formed portal frames under static load.

Relevant deformations have been presented both in the elastic and inelastic regions of the frames' behaviour. The effect of lateral bracing on the elastic behaviour of the frame was also examined. Internal bracing was found to significantly affect the deformations of the frame, including the in-plane deflections. The restraint of the flange also resulted in a slight increase in ultimate load. The ultimate load of each frame has been tabulated.

The data from the tests have been compared with predictions produced using a linear elastic matrix stiffness analysis. The matrix stiffness analysis included the thin-walled torsion theory derived by Vlasov and cross-section monosymmetry. The analytical predictions were remarkably accurate for the in-plane response. The effect of torsional deformations on the in-plane deflections was accurately modelled. The importance of the precise modelling of joints in thin-walled structures was emphasised. However the nature of the problem presented difficulties for the accurate prediction of the out-of-plane response. It was discovered that an analysis assuming rigid body deformation of the members was insufficient to predict the elastic response of the structure at load points. It was found necessary to superimpose the distortional deformations derived from a finite strip analysis on the rigid body rotations. The distortional analysis highlighted the significant deformations that cross-sectional distortion can cause at points of concentrated load.

Acknowledgements

The work has been carried out in the School of Civil Engineering at the University of Sydney under the general direction of Professor J.W. Roderick as Head of the School. Calculations were performed in the C.A. Hawkins Computing Laboratory at a terminal to a multi-user, PRIME minicomputer. Funds to purchase this system were provided by members of the Civil Engineering Graduates' Association.

References

1. Standards Association of Australia, AS1170, Part 2-1973, SAA Loading Code, Part 2-Wind Forces, Sydney 1973.

2. Baigent, A.H. and Hancock, G.J. 'The behaviour of portal frames composed of cold-formed members.' University of Sydney, School of Civil Engineering, Research Report R327, September 1978.

3. Vlasov, V.Z. 'Thin-walled elastic beams.' Moscow 1959 (English Translation, Israel Program for Scientific Translations, Jerusalem, 1961).

4. Turner, M.J., Clough, R.W., Martin, H.C. and Topp, L.J. 'Stiffness and deflection analysis of complex structures.' Journal of the Aeronautical Sciences, Vol. 23, No. 9, September 1956.

5. Clough, R.W. 'Structural analysis by means of a matrix algebra program.' ASCE, 1st Conference on Electronic Computation, 1956.

6. Krahula, J.L. 'Analysis of bent and twisted bars using the finite element method.' Journal of AIAA, Vol. 5, No. 6, June 1967.

7. Zbirohowski-Koscia, K. 'Thin-walled beams.' Crosby Lockwood, London, 1967.

8. Cheung, Y.K. 'Finite strip method in structural analysis.' Pergamon Press, 1976.

TABLE 1 EXPERIMENTAL RESULTS

FRAME No.	RESTRAINTS	LOAD CASE	ULTIMATE LOAD (kN)	IN-PLANE STIFFNESS (mm/kN)		OUT-OF-PLANE STIFFNESS (rad/kN)	
				APEX	L.H. EAVE	L.H. RAFTER	L.H. STANCHION
1	External	1	15.00	-2.320	-0.653	0.00973	0.00093
2	External	1	15.00	-2.233	-0.627	0.00853	0.00080
3	External	2	19.00	4.342 (Horiz.)	4.447	0.00484	0.00279
4	External	3	36.33	1.453	0.418	-0.00556	-0.00149
5	External and Internal	1	17.00	-2.088	-0.600	0.00365	0.00065
6	External and Internal	2	23.00	3.435 (Horiz.)	3.370	0.00187	0.00196
7	External and Internal	3	38.67	1.236	0.372	-0.00186	-0.00168

TABLE 2 THEORETICAL RESULTS

FRAME No.	IN-PLANE STIFFNESS (mm/kN)		OUT-OF-PLANE STIFFNESS (rad/kN)		
	APEX	L.H. EAVE	L.H. RAFTER RIGID BODY ROTATION	L.H. RAFTER DISTORTIONAL ROTATION	L.H. RAFTER TOTAL ROTATION
1	-2.201	-0.743	0.00404	0.00340	0.00744
2	-2.201	-0.743	0.00404	0.00340	0.00744
3	4.273 (Horiz.)	4.386	0.00553	0.00168	0.00721
4	1.386	0.467	-0.00294	-0.00264	-0.00558
5	-1.861	-0.610	0.00011	0.00347	0.00358
6	3.198 (Horiz.)	3.320	0.00009	0.00170	0.00179
7	1.180	0.384	-0.00010	-0.00256	-0.00266

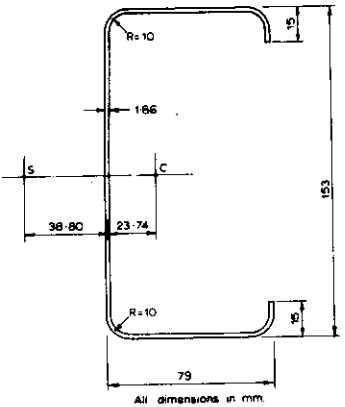

Fig 1. Cross-Section Geometry

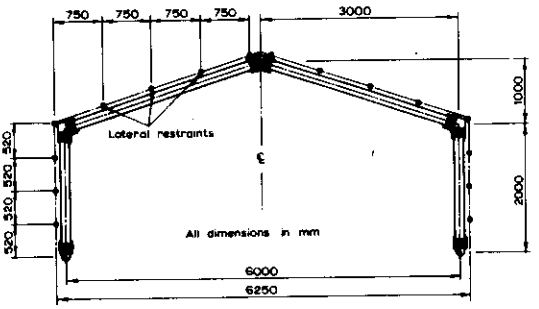

Fig 2. Frame Geometry

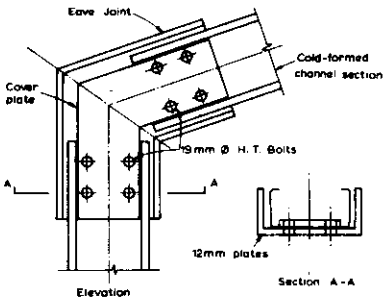

Fig 3. Joint Details

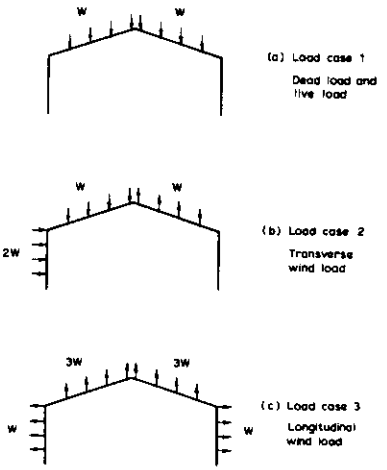

Fig 4. Loading Patterns

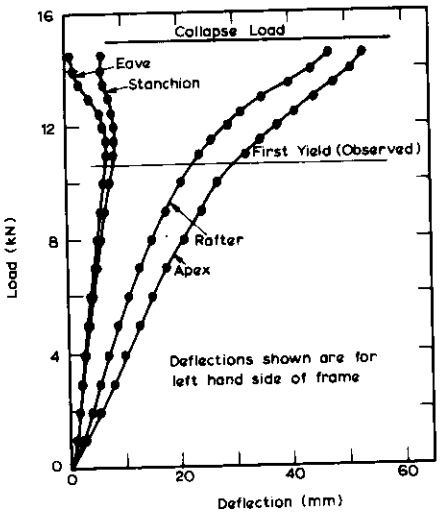

Fig 5. In-Plane Deformations for Frame 2

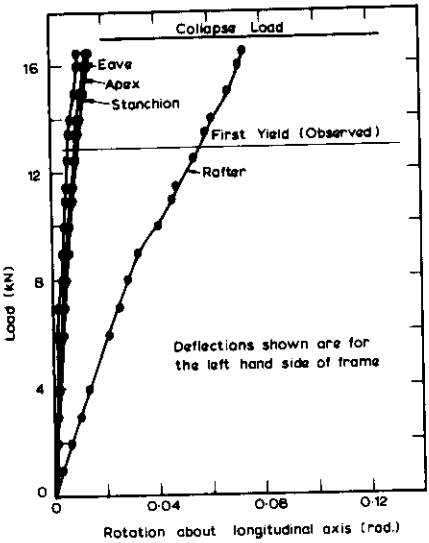

Fig 7. Out-of-Plane Deformations for Frame 5

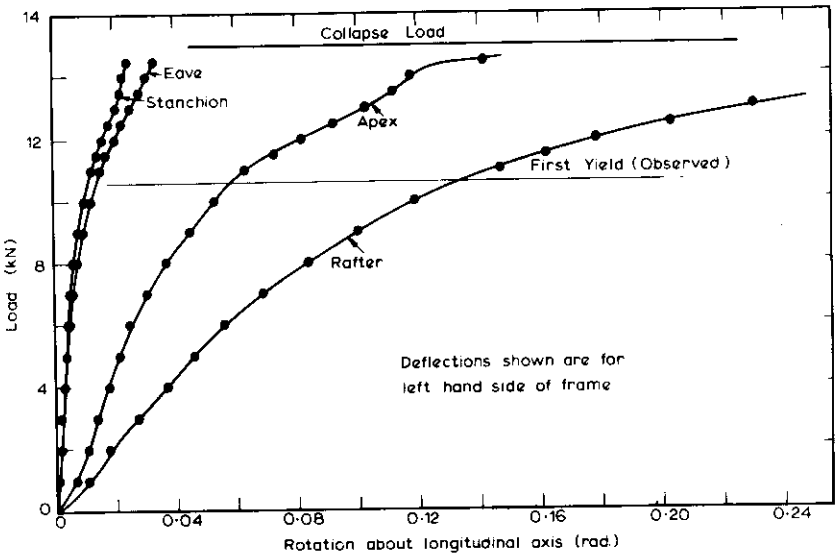

Fig 6. Out-of-Plane Deformations for Frame 2

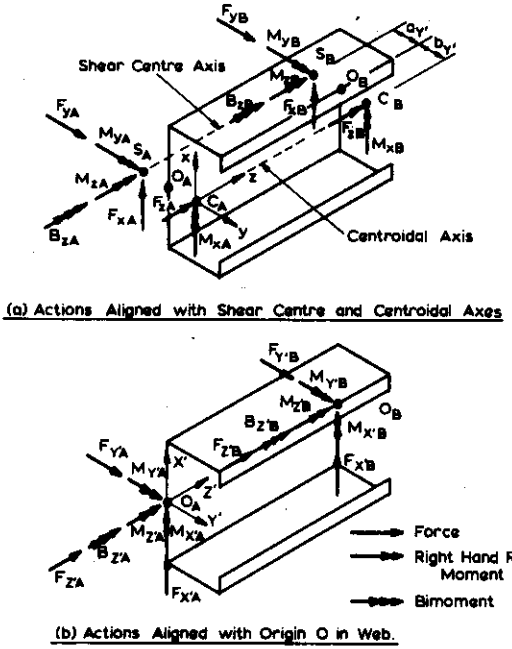

(a) Actions Aligned with Shear Centre and Centroidal Axes

(b) Actions Aligned with Origin O in Web.

Fig 8. Thin-Walled Element

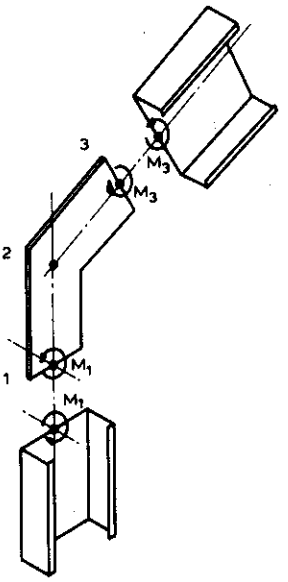

Fig 9. Transmission of Major Axis Moment Through Joint

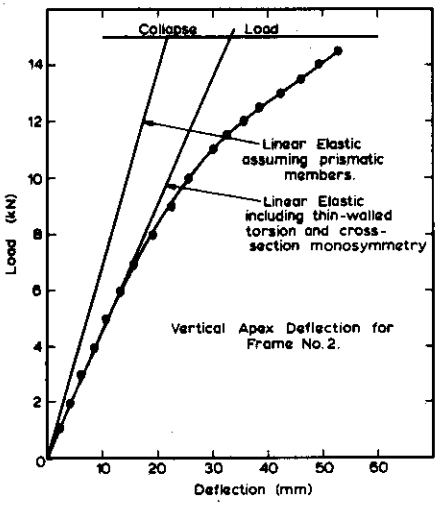

Fig 10. Comparison Between Theoretical Model and Frame Tests

UNIVERSITY OF SYDNEY LIBRARY
0000000604793193

Allbook Bindery
91 Ryedale Road
West Ryde. 2114
Phone: 807 6026